ASSESSMENT OF CLIMATE CHANGE AND DEVELOPMENT OF DATA BASED PREDICTION MODELS OF SEDIMENT YIELDS IN UPPER INDUS BASIN

Zur Erlangung des akademischen Grades eines

DOKTOR-INGENIEURS

von der KIT-Fakultät für
Bauingenieur-, Geo- und Umweltwissenschaften
des Karlsruher Instituts für Technologie (KIT)

genehmigte

DISSERTATION

Von

Waqas-Ul-Hussan, MSc.
aus Pakistan
Tag der mündlichen Prüfung

10/07/2020

Referent: Prof. Dr.-Ing. Dr. h.c. mult. Franz Nestmann
Korreferent: Ass.Prof. Dr.-Ing. Muhammad Khurram Shahzad

Karlsruhe 2020

Acknowledgement

All the praises are to the Almighty Allah, who blessed me with great motivation, dedication, strength and my special interest in the field of water sciences to complete this dissertation.

First of all, I owe a debt of gratitude to my reverend research supervisor, Prof. Dr.-Ing. Dr. h.c. mult. Franz Nestmann, head of the Chair of Water Resources Management and Hydraulic Engineering at Institute of Water and River Basin Management (IWG), for his unconditional and great support during the whole of my PhD research period. He has not only invited me to the Germany but also provided me the scientific freedom, confidence, believe and inspiration to complete a valuable research work to deal with the present challenges of Pakistan in the field of water, climate and sediment erosions. His great commitment, research cooperation and special interest for enhancing the research potential of Pakistan in the field of water resources will always be remembered in Pakistan. His firm confidence, significant support and continuous commitment during my research time enabled me to succeed in my PhD program.

I am also deeply thankful to my honourable, co-supervisor, Assc. Prof. Dr.-Ing. Muhammad Khurram Shahzad from Pakistan. It was him, who continuously supported me from the start of my PhD till the end of the results during the research work. He also provided me his unconditional help and valuable suggestions in improving the results during my research. I am also grateful for him to provide me the work space in his institution during my scientific visits to Pakistan in 2017 and 2018. As being his pioneer young PhD research student, I have learned a lot from his intellectual and conceptual approach during whole of my research period. Despite his remote access and quit busy hours, he always spared his maximum time and significant effort required during my research work.

I am grateful and also extend my special gratitude to the members of my doctoral examination, Prof. Dr.-Ing. Erwin Zehe (IWG) and apl. Prof. Dr. Stefan Norra, head of the chair of doctoral examination.

I also want to pay my special thanks to Dr.-Ing. Frank Seidel from the IWG, who has given me all the necessary work space, resources, freedom, believe and motivation during the four years of my PhD research work. He also provided me the useful suggestions in establishing the relationships with other scientific community outside of KIT for exchange of knowledge and improving the skills. I am also grateful to Dr.-Ing. Uwe Ehret and Prof. re. nat. Dr. Matthias Winiger for their useful technical suggestions in the early stage of my research work.

I also knowledge the special thanks to all my colleagues, Mrs. Dr.-Ing. Irina Klassen, Mrs. M.Sc. Wendy Gonzalez Otero, Ms. M.Sc. Phoebe Pauline Onjira, Ms. M.Sc. Christin Kannen, Dr. rer. nat. Moritz Zemann, M.Sc. Andreas Müller, M.Sc. Philipp Schultz, M.Sc. Mohamad Attieh and all those in the IWG who continuously supported me in different ways to complete my PhD dissertation. Without their moral supports and friendly environment, I would not have been able to deal with all the challenges faced during four years of research. I am also thankful to Dipl. -Ing. (FH). Hans Schleisiek, for providing me his support in necessary installations of software and IT related matters in the institution.

I would also like to mention my thanks for the supports of Mrs. Karin Krix, Mrs. Sandra Knoll, Mrs. Ilse Engelmann, Mrs. Bettina Waibel and Ms. Ines Ferring in all the necessary administrative matters and also providing me the uninterrupted access to the resources of library in IWG. I am also thankful to all the remaining technical staff working in IWG Theodor-Rehbock who were very friendly and spared their time to help me in my minor works.

I also acknowledge the financial support of HEC-DAAD PhD scholarship program, without their financial supports this research work would not have been able to be materialized. I also acknowledge the support by the KIT-Publication Fund of the Karlsruhe Institute of Technology in publishing my research articles.

I am also grateful to the Prof. Dr. Walter Immerzeel from the Department of Geosciences of Utrecht University, and Assc. Prof. Dr.-Ing. Adnan Ahmad Tahir Environmental Sciences, Comsats University, Abbottabad Pakistan and all of my friends for their different kind of support during my PhD research work.

Finally, last but never the less, I am deeply grateful to my beloved father, remaining family members, my wife and my kids (Mahnoor Fatima and Muhammad Qasim Hassan). Without their love, sacrifice, prayers, and encouragement none of my success could be accomplished.

Waqas Ul Hussan

Abstract

High rates of sediment fluxes and its estimations in fluvial river basins require the selection of efficient quantification approaches with better understanding of dominated factors controlling the erosion process on temporal and spatial scale. The prior assessment of influencing factors such as amount of river discharges, climate, landscape and flow process is helpful to develop the suitable modeling approach for quantification of sediment yields. One of the weakest aspects of the quantification of sediment load is the use of traditional sediment rating curves, which cannot account the hydrometeorological variation and flow generation processes such as snow cover, snow melts, ice melts etc. In such cases the use of empirical sediment rating curve gives un reasonable estimation of sediment loads, which represents to the poor generality.

Nowadays the data-based models using artificial intelligence can make it possible to precisely estimate the sediment loads. The data-based models learn from datasets presented to them by establishing the suitable functional relationship between the output and its inputs variables in the cases of complex phenomena like the sediment transport. In this context the data-based modelling algorithms in present research work were developed at the Chair of Water and River Basin Management, Karlsruhe Institute of Technology of Karlsruhe, which was used for prediction of sediments in upper lower catchments of Upper Indus Basin (UIB) of Pakistan.

The framework of the methodology is divided into four objectives: (1) Comparative Assessment of Spatial Variability and Trends of Flows and Sediments Under the Impact of Climate Change in The Upper Indus Basin (2) Application of soft computing models with input vectors of snow cover area in addition to hydro-climatic data to predict the sediment loads (3) Prediction of sediment yields by using the hydroclimate and normalized difference vegetation index (NDVI) datasets with soft computing models (4) Climate signaling in suspended sediment exports from Glacier and Snow Melts Sub-basins in the Upper Indus Basin (UIB).

This analysis carried out on UIB has enabled to understand the better assessment of climate and dominated parameters such snow cover and hydrological process useful for sediment predictions.

The analysis of assessment of climate change on flows and sediments in snow and glacier dominated UIB of 13 gauging stations reveals that the annual flows and suspended sediments are in the balanced state on main Indus River at Besham Qila upstream of Tarbela reservoir. However, the annual suspended sediment concentrations (SSC) were reduced significantly ranging from 18.56%–28.20% per decade in Gilgit at Alam Bridge (Snow & glacier dominated basin), Indus at Kachura and Brandu at Daggar (lower rainfall dominated basin). During summer period the SSC were significantly reduced ranging from 18.63%–27.79% per decade along with flows in the Hindukush and Western–Karakorum regions due to climate change anomaly, and in rainfed lower sub-basin due to the rainfall reductions. However, the SSC during winter season were significantly increased ranging from 20.08%–40.72% per decade due to significant warming of averaged air temperature.

Within this research data-based modelling in snow and glacier melts Gilgit sub-basin of UIB was carried using artificial neural network (ANN), adaptive neuro fuzzy logic inference system with grid partition (ANFIS-GP), adaptive neuro fuzzy logic inference system with subtractive clustering (ANFIS-SC), adaptive neuro fuzzy logic inference system with fuzzy c-means clustering, multiple adaptive regression splines (MARS) and sediment rating curves (SRC).

The results of machine learning algorithms shown that the input combination consisting of daily discharges (Q_t), snow cover area (SCA_t), temperature (T_{t-1}) and evapotranspiration ($Evap_{t-1}$) improved the performance of the sediment prediction models. From the comparison of overall performance of

the models the ANN model performed better than remaining models. During peak time prediction of sediment loads the prediction of ANN, ANIS-FCM and MARS models were closer to the measured sediment loads. The ANIS-FCM model with a relative accuracy of 81.31% performed better during the estimation of peak sediments compared to the ANN and MARS with 80.17% and 80.16% of relative accuracy respectively.

The data-based modelling of sediment yield in the rainfall dominated Brandu sub-basin of lower UIB was carried out using hydroclimate and biophysical inputs datasets, consisting of flows, rainfall, mean air temperature and Normalized Difference Vegetation Index (NDVI). The results of four Artificial Neural Networks (ANNs) and three Adaptive Neuro-Fuzzy Logic Inference System (ANFIS) algorithms for the Brandu River basin has revealed that the remotely sensed NDVI as biophysical parameters in addition to hydroclimate parameters does not improved the performance of the models. The ANFIS-GP performed better in testing phase than other models with input combination of flows and rainfall. However, ANN imbedded with Levenberg-Marquardt (ANN-LM) for the period 1981-2010 performed best with input combinations of flows, rainfall and mean air temperatures. The results accuracy of R^2 using ANN-LM algorithm improved up to 28% compared to sediment rating curve (SRC). Its demonstrated that for the lower part of UIB flows, rainfall and mean air temperature are more dominated factors than biophysical parameters of NDVI for prediction of sediment yields.

The modelling for assessing the changes in flow process to export the SSC in snow and glacier fed Gilgit and Astore sub-basins of UIB was carried out using Temp-Index degree day model. The results of Mann-Kendall Trend test in both Gilgit and Astore Rivers revealed that during winter season the increase of SSC is due to warming of mean air temperature, increase in winter precipitations and increase of winter snow melts. During spring season, the precipitation and snow cover fractions has increased in Gilgit sub-basin contrary to its reduction in the Astore sub-basin. In Gilgit sub-basin during summers the SSC were significantly reduced due to combined effect of Karakorum climate anomaly and increased snow cover area. Reduction of summer SSC in Gilgit River is due to the cooling of summer temperature and covering of the exposed proglacial landscape due to increased snows, reduced debris flows and reduced snow melts from debris glaciers.

Contrary to the Gilgit River the SSC in Astore River are increased during summer. The increase of SSC in Astore sub-basin is due to reduction of spring rainfall and snow cover, warming of summer mean air temperature and increased of effective rainfall. The results further reveal a shift in domination of glacier melts to snow melts in Gilgit sub-basin, and snow to the rainfall in Astore sub-basin in transports of the fine sediments in UIB.

The present research methodology for assessment of changes in SSC due to climate and its prediction in both upper as well as lower sub-basins will be useful for better understanding of sediment exports process, management of sediment and design of future planned water infrastructures in the UIB.

Zusammenfassung

Hohe Raten von Sedimentflüssen und ihre Schätzungen in Flusseinzugsgebieten erfordern die Auswahl effizienter Quantifizierungsansätze mit einem besseren Verständnis der dominierten Faktoren, die den Erosionsprozess auf zeitlicher und räumlicher Ebene steuern. Die vorherige Bewertung von Einflussfaktoren wie Abflussvariation, Klima, Landschaft und Fließprozess ist hilfreich, um den geeigneten Modellierungsansatz zur Quantifizierung der Sedimenterträge zu entwickeln. Einer der schwächsten Aspekte bei der Quantifizierung der Sedimentfracht ist die Verwendung traditioneller Beziehung zwischen Strömungsgeschwindigkeit und Bodensatzlöschung (SRC), bei denen die hydrometeorologischen Schwankungen, Abflusserzeugungsprozesse wie Schneedecke, Schneeschmelzen, Eisschmelzen usw. nicht berücksichtigt werden können. In vielen Fällen führt die empirische Q-SSC Beziehung daher zu ungenauen Prognosen

Heute können datenbasierte Modelle mit künstlicher Intelligenz die Sedimentfracht präziser abschätzen. Die datenbasierten Modelle lernen aus den eingespeisten Datensätzen, indem sie bei komplexen Phänomenen wie dem Sedimenttransport die geeignete funktionale Beziehung zwischen dem Output und seinen Input-Variablen herstellen. In diesem Zusammenhang wurden die datenbasierten Modellierungsalgorithmen in der vorliegenden Forschungsarbeit am Lehrstuhl für Wasser- und Flussgebietsmanagement des Karlsruher Instituts für Technologie in Karlsruhe entwickelt, die zur Vorhersage von Sedimenten in oberen unteren Einzugsgebieten des oberen Indusbeckens von Pakistan (UIB) verwendet wurden.

Die dieser Arbeit zugrunde liegende Methodik gliedert sich in vier Bearbeitungsschritte: (1) Vergleichende Bewertung der räumlichen Variabilität und der Trends von Abflüssen und Sedimentfrachten unter dem Einfluss des Klimawandels im oberen Indus-Becken (2) Anwendung von Soft-Computing-Modellen mit Eingabevektoren der schneedeckten Fläche zusätzlich zu hydro-klimatischen Daten zur Vorhersage der Sedimentfracht (3) Vorhersage der Sedimentfracht unter Verwendung der NDVI-Datensätze (Hydroclimate and Normalized Difference Vegetation Index) mit Soft-Computing-Modellen (4) Klimasignalisierung bei suspendierten Sedimentausträge aus Gletscher und Schnee dominierten Teileinzugsgebeiten im oberen Indus-Becken (UIB).

Diese im UIB durchgeführte Analyse hat es ermöglicht, die dominiertenden Parameter wie Schneedecke und hydrologischen Prozesses besser zu und in eine verbesserte Prognose der Sedimentfrachten einfließen zu lassen.

Die Analyse der Bewertung des Klimawandels von Flüssen und Sedimenten in schnee- und gletscherdominierten UIB von 13 Messstationen zeigt, dass sich die jährlichen Flüsse und suspendierten Sedimente am Hauptindus in Besham Qila stromaufwärts des Tarbela-Reservoirs im ausgeglichenen Zustand befinden. Jedoch, die jährlichen Konzentrationen suspendierter Sedimente (SSC) wurden signifikant gesenkt und lagen zwischen 18,56% und 28,20% pro Jahrzehnt in Gilgit an der Alam Bridge (von Schnee und Gletschern dominiertes Becken), Indus in Kachura und Brandu in Daggar (von weniger Niederschlag dominiertes Becken). Während der Sommerperiode war der SSC signifikant reduziert und lag zwischen 18,63% und 27,79% pro Jahrzehnt, zusammen mit den Flüssen in den Regionen Hindukush und West-Karakorum aufgrund von Anomalien des Klimawandels und im unteren Unterbecken mit Regen aufgrund der Niederschlagsreduzierung. Die SSC während der Wintersaison waren jedoch aufgrund der signifikanten Erwärmung der durchschnittlichen Lufttemperatur signifikant erhöht und lagen zwischen 20,08% und 40,72% pro Jahrzehnt.

Die datenbasierte Modellierung im schnee und gletscherdominierten Gilgit Teilbecken unter Verwendung eines künstlichen neuronalen Netzwerks (ANN), eines adaptiven Neuro-Fuzzy-Logik-Inferenzsystems mit Gitterpartition (ANFIS-GP) und eines adaptiven Neuro-Fuzzy-Logik-Inferenzsystems mit subtraktivem Clustering (ANFIS) -SC), ein adaptives Neuro-Fuzzy-Logik-

Inferenzsystem mit Fuzzy-C-Mittel-Clustering, multiplen adaptiven Regressionssplines (MARS) und Sedimentbewertungskurven (SRC) durchgeführt.

Die Ergebnisse von Algorithmen für maschinelles Lernen zeigen, dass die Eingabekombination aus täglichen Abflüssen (Q_t), Schneedeckenfläche (SCA_t), Temperatur (T_{t-1}) und Evapotranspiration ($Evap_{t-1}$) die Leistung der Sedimentvorhersagemodelle verbesserne. Nach dem Vergleich der Gesamtleistung der Modelle schnitt das ANN-Modell besser ab als die übrigen Modelle. Bei der Vorhersage der Sedimentfrachten in Spitzenzeiten lag die Vorhersage der ANN-, ANIS-FCM- und MARS-Modelle näher an den gemessenen Sedimentbelastungen. Das ANIS-FCM-Modell mit einem absoluten Gesamtfehler von 81,31% schnitt bei der Vorhersage der Spitzensedimente besser ab als ANN und MARS mit einem absoluten Gesamtfehler von 80,17% bzw. 80,16%.

Die datenbasierte Modellierung der Sedimentfrachten im von Regen dominierten Brandu-Teilbecken wurde unter Verwendung von Datensätzen für Hydroklima und biophysikalische Eingaben durchgeführt, die aus Strömungen, Niederschlag, mittlerer Lufttemperatur und normalisiertem Differenzvegetationsindex (NDVI) bestehen. Die Ergebnisse von vier ANNs (Artificial Neural Networks) und drei ANFIS-Algorithmen (Adaptive Neuro-Fuzzy Logic Inference System) für das Brandu Teilnbecken haben gezeigt, dass der mittels Fernerkundung bestimmte NDVI als biophysikalische Parameter zusätzlich zu den Hydroklima-Parametern die Leistung das Modell nicht verbessert. Der ANFIS-GP schnitt in der Testphase besser ab als andere Modelle mit einer Eingangskombination aus Durchfluss und Niederschlag. ANN, eingebettet in Levenberg-Marquardt (ANN-LM) für den Zeitraum 1981-2010, schnitt jedoch am besten mit Eingabekombinationen aus Strömungen, Niederschlag und mittleren Lufttemperaturen ab. Die Ergebnisgenauigkeit R^2 unter Verwendung des ANN-LM-Algorithmus verbesserte sich im Vergleich zur Sedimentbewertungskurve (SRC) um bis zu 28%. Es wurde gezeigt, dass für den unteren Teil der UIB-Flüsse Niederschlag und mittlere Lufttemperatur dominierende Faktoren für die Vorhersage von Sedimenterträgen sind und biophysikalische Parameter (NDVI) eine untergeordnete Rolle spielen.

Die Modellierung zur Bewertung der Änderungen des SSC in schnee- und gletschergespeiste Gilgit- und Astore-Teilbecken wurde unter Verwendung des Temp-Index degree day modell durchgeführt. Die Ergebnisse des Mann-Kendall-Trendtests in den Flüssen Gilgit und Astore zeigten, dass der Anstieg des SSC während der Wintersaison auf die Erwärmung der mittleren Lufttemperatur, die Zunahme der Winterniederschläge und die Zunahme der Schneeschmelzen im Winter zurückzuführen ist. Während der Frühjahrssaison haben die Niederschlags- und Schneedeckenanteile im Gilgit-Unterbecken zugenommen, im Gegensatz zu seiner Verringerung im Astore-Unterbecken. Im Gilgit-Unterbecken war der SSC im Sommer aufgrund des kombinierten Effekts der Karakorum-Klimaanomalie und der vergrößerten Schneedecke signifikant reduziert. Die Reduzierung des Sommer-SSC im Gilgit Fluss ist auf die Abkühlung der Sommertemperatur und die Bedeckung der exponierten proglazialen Landschaft zurückzuführen, die auf erhöhten Schnee, verringerte Trümmerflüsse Trümmerflüsse und verringerte Schneeschmelzen von Trümmergletschern zurückzuführen sind.

Im Gegensatz zum Gilgit River sind die SSC im Astore River im Sommer erhöht. Der Anstieg des SSC im Astore-Unterbecken ist auf die Verringerung des Frühlingsniederschlags und der Schneedecke, die Erwärmung der mittleren Sommerlufttemperatur und den Anstieg des effektiven Niederschlags zurückzuführen. Die Ergebnisse zeigen ferner eine Verschiebung der Dominanz von Gletscherschmelzen zu Schneeschmelzen im Gilgit-Unterbecken und von Schnee zu Niederschlägen im Astore-Unterbecken bei Sedimenteden Sedimentfrachten in UIB.

Die vorliegende Forschungsarbeit zur Bewertung der klimabedingten Veränderungen des SSC und seiner Vorhersage sowohl in den oberen als auch in den unteren Teilbecken des UIB wird nützlich sein, um den Sedimenttransportprozess besser zu verstehen und aufbauen auf dem verbesserten

Prozessverständnis ein angepasstes Sedimentmanagement und angepasste Planungen der zukünftigen Wasserinfrastrukturen im UIB ableiten zu können.

Contents

List of Figures XIV

List of Tables XVII

Chapter 1- Introduction 1

1.1 Research background 1

1.1.1 Assessment of sediment loads trends under climate changes 1

1.1.2 Prediction/Estimation of sediment loads 2

1.1.3 Modelling of snow and glacier melts in contrast to sediment exports 3

1.1.4 Need of research 4

1.2 Study area 5

1.3 Research objectives 8

1.5 Structure of Thesis 8

1.6 References 10

Chapter 2- Comparative Assessment of Spatial Variability and Trends of Flows and Sediments Under the Impact of Climate Change in The Upper Indus Basin 14

2.1 Abstract 14

2.2 Introduction 15

2.3 Materials 16

2.3.1 Study Area 16

2.3.2 Data Collection 21

2.4 Methods 25

2.4.1 Statistical Methods 25

2.4.2 Serial Correlation and Trend-Free Pre-Whitening (TFPW) 25

2.4.3 Mann–Kendall Test 26

2.4.4 Sen's Slope Estimator 27

2.5 Results 27

2.5.1 Preliminary Analysis 27

2.5.2 Monthly, Seasonal, and Annual Trends of Discharges 28

2.5.3 Monthly, Seasonal, and Annual Trends of Suspended Sediment Concentrations (SSC)……29
2.5.4 Mean Basin Precipitation Trends 36
2.5.5 Mean Monthly Average Temperature Trends 37
2.5.6 Pearson's Correlations between Flows, SSC and Gridded Climatic Variables 40
2.6 Discussion 40
2.7 Conclusions 42
2.8 References 42
Chapter 3- Application of soft computing models with input vectors of snow cover area in addition to hydro-climatic data to predict the sediment loads 46
3.1 Abstract 46
3.2 Introduction 47
3.1.1. Background 47
3.2 Data Collection and Methodology 49
3.2.1 Study area 49
3.2.2 Application of Temperature index-snow model for snow cover estimates 53
3.2.3 Artificial neural networks (ANN) 54
3.2.4 Adaptive neuro-fuzzy logic inference system (ANFIS) 55
3.2.5 Multivariate adaptive regression splines (MARS) 57
3.2.6 Sediment rating curve (SRC) 57
3.2.7 Performance measurement metrics for model evaluation 58
3.2.8 Application of ANN, ANFIS-GP, ANFIS-SC, ANFIS-FCM and MARS models 58
3.3 Results and Discussion 59
3.3.1 Simulation of snow melts and snow cover area 59
3.3.2 Comparison of the ANN, ANFIS-GP, ANFIS-SC, ANFIS-FCM, MARS and SRC models 67
3.3.3 Deveoplement of Multiple Linear Regression Equation 71
3.4 Conclusions 72
3.5 References 73
3.6 Supplementary Materials 78
Chapter 4- Prediction of sediment yields by using the hydroclimate and normalized difference vegetation index (NDVI) datasets with soft computing models 81

4.1 Abstract 81
4.2 Introduction 81
4.3 Material and Methodology 83
4.3.1 Data collection and study area 83
4.3.2 Artificial neural networks (ANN) 89
4.3.3 Adaptive neuro-fuzzy logic inference system (ANFIS) 90
4.3.4 Sediment rating curve (SRC) 93
4.3.5 Performance measurement metrics for model evaluation 93
4.4 Results and Discussions 94
4.4.1 Relationships of NDVI between SSY, runoff and rainfall 94
4.4.2 ANN and ANFIS model results 94
4.4.3 SRC model results 97
4.4.4 Discussion 97
4.5 Conclusion 99
4.6 References 100
Chapter 5- Climate signaling in suspended sediment exports from Glacier and Snow Melts Sub-basins in the Upper Indus Basin (UIB) 104
5.1 Abstract 104
5.2 Introduction 105
5.3 Data Collection and Methodology 107
5.3.1 Study area and data collections 107
5.3.2 Methodology 108
5.3.3 Temperature index-snow melt model 111
5.3.4 Temperature Index-Ice melt model 113
5.3.5 Performance measurement metrics for model evaluation 113
5.4 Results and Discussion 115
5.4.1 Simulation of snow melts and snow cover area 115
5.4.2 Effect of frequency of intermittent SSC Sampling 118
5.4.3 Hydroclimatic changes and activation of sediment sources 119
5.5 Conclusions 127
5.6 References 128
Chapter 6- Conclusion and Recommendations 134

6.1 Conclusions 134
6.2 Significance of the research 136
6.3 Recommendation of Future Work 137
List of Symbols 138

List of Figures

Figure 1.1 The map of the study area of Upper Indus River basin. 7

Figure 2. 1 The map of the study area shows the locations of stream gauges, climatic stations, and sub-basins contributing to the Upper Indus Basin (UIB). 18

Figure 2. 2 Seasonal flow trends spatially distributed over the basin with % of changes per decade in % of mean values for the whole period. (**a**) DJF (winter), (**b**) MAM (spring), (**c**) JJA (summer), (**d**) SON (autumn) seasons. 33

Figure 2. 3 Seasonal suspended sediment concentration (SSC) trends spatially distributed over the basin with % of changes per decade in % of mean values for the whole period. (a) DJF (winter), (b) MAM (spring), (c) JJA (summer), (d) SON (autumn) seasons. 34

Figure 2. 4 Annual flow and suspended sediment concentration (SSC) trends spatially distributed over the basin with % of changes per decade in % of mean values for the whole period. (**a**) Annual flows, (**b**) annual SSC..... 35

Figure 3. 1 The location map of Gilgit River in the Upper Indus Basin (UIB) of Pakistan. 50

Figure 3. 2 Graphical presentations of (a) mean basin temperature (T), discharges at Gilgit gauge (Q), and suspended sediment concentrations (SSC) at Gilgit gauge, (b) mean basin snow covered area (SCA), mean basin rainfall (R), and mean basin evapotranspiration (Evap) for the Gilgit basin during period 1981-2010. 51

Figure 3. 3 Time series plots between the MODIS-observed snow cover fractions and temp-index snow model- simulated snow cover fractions during calibration (2000-2007) and validation periods (2008-2010)..... 60

Figure 3. 4 Plot of the sediment rating curve (SRC) for the Gilgit basin. 66

Figure 3. 5 Plot of the best performance measures for predictions of SSY by using the ANN, ANFIS-GP, ANFIS-SC, ANFIS-FCM, MARS and SRC model during testing phase for Gilgit basin. 69

Figure 3. 6 Plot of the best performance measures for predictions of SSY by using the ANN, ANFIS-GP, ANFIS-SC, ANFIS-FCM, MARS and SRC model during testing phase for Gilgit basin. 70

Figure 3. 7 Overall Comparison of performance measures of coefficient of determination (R^2), Nash–Sutcliffe efficiency model performance coefficient (NSE) and root mean squared error (RMSE) with different input variable scenarios during testing phase from all the models. 70

Figure 3. 8 Plot of the SSY by using ensembled average equation during training and testing phase for Gilgit basin. 72

Figure A 1. Schematic diagram of the ANN model for prediction of sediment yields with one hidden layer. 78

Figure A 2. Schematic diagram of the ANFIS model for prediction of sediment yields with two inputs. 78

Figure 4. 1 Location of the Brandu River basin at the Daggar stream gauging station in the Upper Indus Basin (UIB) of Pakistan. 84
Figure 4. 2 Classification of the Landuse map of the Brandu River Basin for year 2010. 85
Figure 4. 3 Graphical presentations of (a) Discharges (Q), mean basin normalized difference vegetation index (NDVI) and suspended sediment concentrations (SSC) (b) mean basin rainfall (R) and mean basin average temperature (T) for Brand River basin.. 88
Figure 4. 4 Schematic diagram of ANN Model for prediction of sediment yields with one hidden layer. 90
Figure 4. 5 Schematic diagram of ANFIS Model for prediction of sediment yields with two inputs. 92
Figure 4. 6 Comparison among the annual flows (Q), suspended sediment yields (SSY), normalized difference vegetation Index (NDVI) and rainfall (mm) in the Brandu River basin. 94
Figure 4. 7 Comparison of ANN-LM, ANN- BR, ANN-GDS, ANN-SCG, ANFIS-GP, ANFIS-SC and ANFIS-FCM models by RMSE statistics during testing period in the Brandu River basin. 97
Figure 4. 8 Comparison of best performance of networks developed from the ANN, ANFIS and SRC models during testing period in the Brandu River basin. 98
Figure 4. 9 Overall Comparison of the monthly measured SSY with the best outputs of SRC, ANN and ANFIS models at Brandu River since 1981-2010 99
Figure 4. 10 Overall Comparison of the monthly measured SSY with the best outputs of SRC, ANN and ANFIS models at Brandu River since 1981-2010 99
Figure 5. 1 Map of the Gilgit and Astore sub-basins of UIB with topography (GDEM 30 m resolutions), river networks and glacierized areas. 109
Figure 5. 2 Graphical presentations of (a) discharges (Q) and mean basin rainfall (R) (b) mean basin snow covered area (SCA), and mean basin temperature (T) for Gilgit and Astore sub-basins of UIB. 110
Figure 5. 3 Comparison between the MODIS observed snow cover fractions and temp-index snow model simulated snow cover fractions for Gilgit and Astore basins. 116
Figure 5. 4 Comparison of mean monthly/annual observed and simulated flows with different flow process for the period 1981-2010: (a) Gilgit basin (monthly) (b) Astore basin (monthly) (a) Gilgit basin (Annual) (b) Astore basin (Annual). Simulated SM+R+IM are the sum of snow melts (SM), effective rainfall (R) and ice melts (IM). 117
Figure 5. 5 Plots of Cumulative distribution functions of (a) measured flows, (b) snow cover fractions (SCF), (c) snow melts (SM), (d) ice melts (IM), and (e) effective rainfall (ER) on continuous (all days) and intermittent (SSC daily measurements) frequency of the Gilgit basin. 118
Figure 5. 6 Plots of Cumulative distribution functions of (a) measured flows, (b) snow cover fractions (SCF), (c) snow melts (SM), (d) ice melts (IM), and (e) effective rainfall (ER) on continuous (all days) and intermittent (SSC daily measurements) frequency of the Gilgit basin. 120

Figure 5. 7 Observed (a) mean basin air temperature (b) mean basin precipitations (c) suspended sediment concentrations (SSC) (d) measured discharge for the period 1981-2010 of Gilgit basin. 120

Figure 5. 8 Observed (a) mean basin air temperature (b) mean basin precipitations (c) suspended sediment concentrations (SSC) (d) measured discharge for the period 1981-2010 of Gilgit basin. 121

Figure 5. 9 Monthly changes in (a) mean basin snow melts (SM) (b) mean basin snow cover fractions (SCF) (c) mean basin ice melts (IM) (d) mean basin effective rainfall (ER) for the period 1981-2010 of Gilgit basin..... 122

Figure 5. 10 Observed (a) basin mean temperature (b) mean basin precipitations (c) suspended sediment concentrations (SSC) (d) measured discharge for the period 1981-2010 of Astore basin..... 124

Figure 5. 11 Observed (a) mean basin air temperature (b) mean basin precipitations (c) suspended sediment concentrations (SSC) (d) measured discharge for the period 1981-2010 of Astore basin..... 125

Figure 5. 12 Monthly changes in (a) mean basin snow melts (SM) (b) mean basin snow cover fractions (SCF) (c) mean basin ice melts (IM) (d) mean basin effective rainfall (ER) for the period 1981-2010 of Astore basin. 126

List of Tables

Table 2. 1 Geographical characteristics of the stream gauging sites measuring flows and suspended sediment concentrations (SSC) in the Upper Indus Basin (UIB). 20

Table 2. 2 Hydrological characteristics of discharge gauging stations in the Upper Indus Basin (UIB). 23

Table 2. 3 Characteristics of climatic gauging stations in the Upper Indus Basin (UIB). 24

Table 2. 4 Characteristics of climatic gauging stations in the Upper Indus Basin (UIB). 25

Table 2. 5 Summary of descriptive statistics of the selected discharge and sediment gauging stations. 28

Table 2. 6 Mann–Kendall trends for monthly time series data and Sen's slope estimates. 31

Table 2. 7 Annual and seasonal percentage changes per decade for mean of data periods. 36

Table 2. 8 Total changes in monthly precipitation (mm) extracted from the grid data for the Upper Indus Basin (UIB) from 1981 to 2010. 38

Table 2. 9 Changes in mean monthly averaged temperatures (°C) from 1981 to 2010 for stations located at different altitudes in the Upper Indus Basin (UIB). 39

Table 2. 10 Pearson's correlations between daily flows, SSC and gridded climatic datasets since 1981–2010 in the Upper Indus Basin (UIB). 40

Table 3. 1 Data collected for prediction of suspended sediment yields for the Gilgit River basin. 51

Table 3. 2 Relationship of Gilgit basin input variables determined by using Pearson correlation coefficient. Log Q: logarithm of water discharges; Log SSY: logarithm of sediment yields; SCA: snow covers area: T_{avg}: mean temperature; P: basin averaged effective rainfall; Evap: evapotranspiration. 52

Table 3. 3 Results of performance measurement statistics during calibration (2000-2007) and validation (2008-2010) periods of the temperature-index snow model for simulations of snow melt and snow cover fractions. 59

Table 3. 4 Training and testing statistics of ANN model by using Levenberg-Marquardt algorithm using different input combinations for Gilgit basin. 61

Table 3. 5 Training and testing statistics of AFIS1 grid partition (GP) model by using different input combinations for Gilgit basin. 62

Table 3. 6 Training and testing statistics of AFIS2 subtractive clustering (SC) model by using different input combinations for Gilgit basin. 63

Table 3. 7 Training and testing statistics of AFIS3 FCM clustering model by using different input combinations for the Gilgit basin. 64

Table 3. 8 Training and testing statistics of MARS model by using different input combinations for the Gilgit basin. 65

Table 3. 9 Comparison of the performance measurements by using the SRC, ANFIS-GP, ANFIS-SC, ANFIS-SC, ANFIS-FCM and MARS models in predictions of sediment yields. . 67

Table 3. 10 Comparison of the ANFIS-GP, ANFIS-SC, ANFIS-SC, ANFIS-FCM, MARS and SRC models' absolute sediment fluxes (%) for peak estimations of SSY for Gilgit basin. . 71

Table A 1 Summary of the reviewed publications of data-based models sorted by year and input variables. 79
Table A 2 Characteristics of the Gilgit River basin in the Upper Indus River. 79
Table 4. 1 Characteristics of the Daggar River sub-basin of the Upper Indus River. 86
Table 4. 2 Collection of data used for prediction of suspended sediment yields of the Brandu River the Sub-basin of Upper Indus River. 87
Table 4. 3 Relationship by using Pearson correlation coefficient for input variables of Gilgit Basin. Log Q: logarithm of water discharges; Log SSY: logarithm of sediment yields; SCA: snow covers area: T_{avg}: mean temperature; P: basin averaged effective rainfall; Evap: evapotranspiration. 88
Table 4. 4 Training and testing statistics of ANN model embedded with Levenberg-Marquardt (LM), Bayesian Regularization (BR), Gradient Descent (GD) and Scaled Conjugate Gradient (SCG) algorithms for Brandu River. 95
Table 4. 5 Training and testing statistics of AFIS model embedded with grid partition (GP), subtractive clustering (SC), fuzzy c-means (FCM) clustering algorithms and SRC model for Brandu River. 96
Table 5. 1 Characteristics of the Gilgit River basin in the Upper Indus River. 110
Table 5. 2 List of variables data collected, analyzed and simulated for Gilgi and Astore Sub-basins in UIB. 111
Table 5. 3 Results of performance measurement statistics during calibration (2000-2007) and validation (2008-2010) period of Temperature-Index snow model for simulations of snow melt and snow cover fraction. 115
Table 5. 4 Results of goodness of fit measures: mass balance errors (MBE_S) computed during ablation period (June-October) and mass balance errors (MBE_A) during whole year for ice melt model calibrations. 117

Chapter 1- Introduction

1.1 Research background

High rates of erosion from the younger mountains of Himalayas in Indus River are due to high rates of denudation up to 6 mm/year like the Ganges-Brahmaputra River system [1]. Higher erosions rate due to complex phenomena of sediment generations in these River systems always present challenges to the assessment of changes in sediment yields, management of annual sediment loads, estimation/predictions of sediments, sustain able development of water structures and design & its operation in future. There are number of factors affecting the erosion rates which results in rapid depletion of reservoirs such as climate changes, land use changes, rapidly activation and deactivation of sediment sources, landslides, frequency of flash floods and hydrodynamic changes of river water regime etc. Assessment of climate changes with trends of sediment loads, accurate estimate of sediments and understanding of relevancy of flow generation process such as snow and glaciers melting have a significant importance due to following reasons in water resource engineering.

1.1.1 Assessment of sediment loads trends under climate changes

The assessment of spatial and temporal variability of flows and sediment due to climate changes is not only important for watershed management activities, tectonics/earthquakes activities, landslides, reservoir sediment management as well as for management of River eco-system. Although there are many research reports [1,2,3,4] have been reported from literature review regarding the assessment of climate changes on discharges in various sub-basins of Upper Indus basin (UIB) during past decades. However, the scientific contribution on spatio-temporal trend of suspended sediment concentrations (SSC) is scarce. Ali and De Boer [5] investigated the spatial patterns of sediment yields by dividing the UIB into three zones: upper snow- and glacial melts-dominated zone, middle snow-/glacial melts-, and rainfall-dominated mixed zone, and lower rainfall-dominated zone. Ali and De Boer [5] analyzed the spatial distribution of sediment in the UIB by dividing the region into three zones: upper snow- and glacial melt-dominated zone, middle snow-/glacial melt-, and rainfall-dominated mixed zone, and lower rainfall-dominated zone. Ateeq-Ur-Rehman et al. and Tarar et al. [6,7] explained the trends of SSC of Upper Indus at Besham Qila, Upper Indus at Bunji/Partab Bridge, Hunza basin at Danyor, and Shyok basin at Yogu, gauging stations of the UIB. The results of their research concluded the balanced state of annual SSC at Besham Qila the intake of Tarbela reservoir with significant inter-annual shift of sediment yields.

The investigations of recent researchers [6,7] used daily outputs of sediment computed from sediment rating curves (SRC) and artificial neural networks (ANN) to drive the conclusions of sediment trends on monthly, seasonal and annual basis in UIB. The sediments outputs derived from data-based models are most of the times are less reliable compared to the measured sediments. Therefore, this research investigated the trends of flows and sediments with measured SSC. This research work is also one of the pioneer researches in analyzing the trends of corrected estimates of rainfall and temperature for the assessment climate changes, flows and SSC in the UIB [8,9]. A

comprehensive assessment of spatio-temporal variation of SSC and flows in relation to relevant hydrometeorological parameters for all the 13 sub-basins of the entire UIB has not yet been made.

The process of sediment transport is highly non-linear and data of measured sediment loads are not normally distributed due to non-linearity nature of sediment erosion. In order to assess the dynamics of sediments and flows variation due to climate changes on spatial and temporal scale, the use of non-parametric tests is assumed to be the most suitable and robust approach. The results of numerous non-parametric trend tests may be distinct in quantifying the changes of SSC and flows. In the past the researchers [10,11,12] have widely used the non-parametric Mann-Kendall Trend test for detection of trends of flows, climate and SSC.

In the current research Mann-Kendall Trend test together with serial correlation [13] and Sen's slope estimator [14] is used to analyze how the changes in patterns of SSC and flows were affected due to changes in climate and transport capacity of River at 13 gauged sub-basins in UIB since 1981-2010. The comparative assessment of spatial variability and trends of flows and SSC due to climate changes in UIB includes; (1) the detection and assessment of on monthly to seasonal and annual basis for flows and SSC of the 13 hydrological stations in the UIB since 1980–2010; (2) development of seasonal and annual trend maps for representing the spatial changes in % for flows and SSC per decade in the UIB; (3) extracting the missing year's climatic information for sparsely gauged climatic stations using the linear scaling bias correction method along with the station-recorded data and satellite grid point data; (4) assessment of the impact of changes in the trends of mean monthly rainfalls of the basins and average monthly temperatures, adjusted for lapse rate per elevation zone, on the monthly flows and SSC of the UIB; (5) assessing the significant changes in monthly, seasonal, and annual flows and SSC, which are partly due to climate change, in past 30 years for selected catchments with major SSC contributions.

1.1.2 Prediction/Estimation of sediment loads

Estimation of suspended sediment loads (SSL) is a challenge particular in the catchments like UIB, where the role of hydrometeorological process like snow and ice melting, effective rainfall, snows accumulated in the form of snow cover and vegetations play a significant role in transport the suspended and bed loads. The bed loads are transported in coarse form due to its continuous in contact with the surface of river bed. The erodibility of soil, effective discharges, intensive rainfall and flows process are governing factors in sediment transports. The soil particles are detached from soil surface in the catchment due to intensive rainfall events, and are then transported in the river as long as shear stress of discharge is greater than its critical limit to transport the sediment. The suspended sediments in the form of fine particles are transported in suspension state with flows. Discharges of the rivers result in the transport of these fine sediment particulars due to sheet/gully erosion of catchment, river banks and bed erosion etc. The process of erosion from sub-basins somewhere deposits the sediments due to river morphology, slopes of streams in catchment and fluvial hydraulics and somewhere erode it. The variations of runoff in upper region of UIB due to rising precipitations, Karakorum Climate Anomaly [1,2,15], glacier ablation and snow melting due to depletion of catchment snow cover increase/decreases the amounts of SSL. Similarly, in lower region of UIB the increase of anthropogenic activities such as increase of population, rapid urbanization, deforestation, over grazing of animals, irrigation practices and rapidly increase in

human activities can affect the land cover. The changes in land cover affect the soil erodibility, land surface frictions/roughness, gradient of catchment surface which also affect the sediment generation phenomena [16]. All these factors pose the challenge for accurate estimations of SSL in UIB.

To estimate the suspended sediment concentrations (SSC) the conventional sediment rating curve (SRC) is commonly used. The SRC approach is simple methods based on the power law relationships between the flows and SSC [17]. However, for the large basins like UIB where sediments transport is a complex phenomenon due to multiple variables which control the erosion process, the use of simple SRC approach results in under/over estimation of the sediment loads. Practically the estimates of SSC based on SRC results in consequences of early depletion of water reservoir rapidly such as early siltation of Tarbela, Mangla and Warsak and Chashma reservoirs [18,19,20,21] in Pakistan. In addition to SRC approach the empirical derived universal soil loss equation (USLE) and modified universal soil loss equation (MUSLE) used for estimation of SSC is also not considered an applicable approach to provide spatial distributed output [22,23,24]. Moreover, the use of physical based models to estimate sediments also have not shown any significant outcome [25] beside its model complexity, data extensive and time-consuming simulations. To overcome these challenges during past few decades soft computing data-based models like artificial intelligence (AIs) have been widely used to capture the complex nature of sediment non-linear process with less data requirements and accurate predictions/estimates of SSC.

Many researchers have used the artificial neural networks (ANN), artificial neuro fuzzy logic inference system (ANFIS), support vector machine (SVM) and multiple adaptive regression splines (MARS) [26,27,28,29,30] etc. to predict the suspended sediment concentrations. Most often more than two data-based algorithms were used with input combinations of flows, rainfall and sediments to compare their results and check the applicability of suitable model for estimation of SSC. In this research the applicability of artificial neural networks (ANN), hybrid ANFIS embedded grid partition (GP), hybrid ANFIS embedded subtractive clustering (SC), hybrid ANFIS embedded FCM clustering (FCM) and MARS models is checked with inputs combinations of grid climatic data, snow cover fraction, flows and normalized difference vegetation index (NDVI) as biophysical factor of the land cover to predict the sediment yields. To the best of authors knowledge from literature review this is the first research which used the combination of spatial averaged grid effective rainfall, mean basin averaged temperature, averaged basin snow cover fractions and NDVI in combination with flows to predict the sediment yields.

Three sub-basins Gilgit (snow-glacier dominated), Astore (snow-rainfall dominated) and Brandu (rainfall and agriculture dominated) of UIB were selected to predict the SSC for the period 1981-2010.

1.1.3 Modelling of snow and glacier melts in contrast to sediment exports

Generation of sediment yields in the basins are controlled by four important factors as: (i) geology (ii) relief (iii) climate and (iv) land use [31]. The knowledge of geological forcing, glacier inheritance and crustal thickness of cluster facilitates in a way to easily understand the orogenic erosions due to landscape erosion process [32]. The relief of the basin and its catchment discharges are also important factors in generation of sediments [33,34,35]. The pattern of climate changes, earth evaluation process on its surface and land use changes are also helpful in assessment of the denudation rates of drainage basins [36,37,38]. Ul Hussan et al. concluded that the Karakorum Climate Anomaly in UIB is reducing

the sediment loads during summer season in glacier and snow dominated basin, whereas SSSC are increased during winters [15]. As result of the Karakorum Climate Anomaly [1,2] glaciers are retrieving the in UIB which are probably reducing the summer flows. Ateeq-Ur-Rehman et al. and Tarar et al. [6,7] also noticed the decrease of sediment concentration during summer period at downstream region of UIB at Partab Bridge with reduced trends of flows. Khawja F.A et al. [39] in his research analysis reported that percentage of snow cover/ice cover (LCs) solely can explain 73.4% of the variance in sediment yields in UIB. He further elaborated that percentage of snow cover/ice cover (LCs), climatic variables and relief can explain up to 98.5% variance of sediment yields in UIB. The glaciers lying in Himalayas mountains are covered with thick layer of debris materials. These glaciers evacuate from subglacial traction zone and are primary sources of sediment generation in Indus River [40,41].

The erosion of sediments depends upon the transport capacity of the river, supply of sediments and its sources. The transport capacity of the channel depends upon the discharges originating upstream of catchment. The supply of sediment is dependent upon spatial location of sediment sources from the main river and flow process such as snow melts, rainfall, glacier melts and snow cover variations involved in sediment transport. The alteration of discharges, rates of snow and glacier melts, snow cover variations and effective rainfalls alters the sediment concentrations measured at the outlet of the basin. The premise of present research work is to explain the climate changes in context of changes in flows, ice melt, glacier melts, snow cover and SSC of selected basins in UIB. To accomplish this study two sub-basins Gilgit (Glacier-snow melt dominated) and Astore (rainfall-snow melt dominated) in alpine environment of UIB were selected to explain the relevancy of climate and flow process in partially controlling the sediment yields.

The relative contribution of snow melts, ice melts, effective rainfall and fractions of snow-covered area triggers the sediment sources in the form of glacial erosion, hillslope/sheet erosion, river bank and bed erosion, and landslides/mass wasting due to rock falls and debris flows. The snow cover area also increases or decrease the ice melting rates from the debris covered proglacial area in the catchment.

In the Gilgit and Astore sub-basins to infer the changes of climate on dynamics of fine sediments the hydroclimatic forgings are conceptualized on spatial scale to activate/deactivate the spatially distributed sediments sources. For investigation of daily snow melt rates, glacial melts, snow cover depletion and effective rainfall the spatially distributed Temperature Index degree day model [42,43] is used for Gilgit and Astore Rivers. For trend analysis of flows, SSC, snow melts, ice melts, effective rainfall and snow cover fractions the Mann Kendall Trend [10,11] test along with serial correlation [13] and Sen's slope estimator [14] was used to explain the relevancy of changes in flows process due to climate changes in exports of sediments yields on monthly, seasonal and annual basis in Gilgit and Astore Rivers.

1.1.4 Need of research

Erosion of sediments and its transport is mainly influenced by hydrological and hydraulic parameters. The climate forces largely drive and alter the role of hydrological and hydraulic factors

in sediment generation phenomena. The Indus River on an average produce the sediment loads of 250 million tons per year by three mountain ranges Hindukush, Karakorum and Himalayas [44]. The knowledge about magnitude variation of sediment yields and distribution of hydrological characteristics of the catchment is crucial to verify the conclusion of impact of climate changes in Indus River. It is also important to understand the impact of climate variations on sediment generations and flows of UIB to formulate effective sediment management strategies, watershed management and sustainability of existing storages like Tarbela dam. Over the past few decades since 1974 Tarbela dam in UIB has lost 35% of its storage due to sedimentations in its reservoir storages [45]. Pakistan is in the list of top 10 countries of the world facing the challenges of water shortage, climate vulnerability, increasing water demands and depletion of its water storages [46,47]. As per review of the literature, in contrast to assessment of impact of climate changes on trends of the SSC much extensive research work is available on investigating the trends of flows due to climate change by many researchers [1,2,48,49]. Ateeq-Ur-Rehman et al. and Tarar et al. [6,7] analyzed the trends of SSC mainly on main Indus River by using the data of two and four gauging stations of the UIB, respectively. However, a comprehensive assessment of trends on SSC and flows due to hydrometeorological changes at 13 gauged sub-basins in UIB with correct information of rainfall and mean air temperature has not yet been studied.

For the correct budgeting/prediction of suspended sediment loads (SSL) the sufficient knowledge and understanding is required about the process of sediment erosion, depositions and its transports on spatial and temporal scale [50]. Water resource engineers, hydrologists and researchers uses the sediment rating curves and databased models to estimate the SSL using the inputs combinations of flows sediment concentrations and rainfall [26,27,28,29,30]. However, the input combination of spatial averaged grid means of basin air temperature, snow cover fractions, normalized difference vegetative index and effective rainfall in addition to the discharges have not been tested to check the applicability of data-based artificial intelligence algorithms.

Another aspect of the need of present research was to explore the contribution and patterns of the flows process such as snow melts, ice melts, rainfall and snow cover depletions in exports of sediments yields in glacier and snow dominated sub-basins of UIB. This can help to better understand the sediments trends and its generation during the period 1981-2010 partially due to climate changes.

1.2 Study area

The Indus River is the longest is river of the south Asia, with its length of 2880 km and drainage basin are of 912,200 km^2 lying in Pakistan, China, India and Afghanistan [51,52]. The Indus is an oldest river in Himalayan mountain region which has not changed its course like the Ganges-Brahmaputra River basins in the region [53]. The Indus River consist of world's largest irrigation networks with total length of its total length of main canal of 58,500 km. Its irrigation system feeds an agriculture area of 181,000 km^2 [54,55]. The Indus River is also as source of an inexpensive energy. Presently, its hydropower potential has a share of 29% in total national energy generation capacity of Pakistan [55]. Indus River basin comprises of five main rivers as main Indus River, Jhelum River, Chenab River, Ravi River and Sutlej river as shown in Figure 1.1. Three main storages in Pakistan namely; Mangla dam on Jehlum River, Tarbela dam and Chashma reservoirs on main Indus River.

The Upper Indus Basin (UIB) lies upstream of Tarbela reservoir in north region of the Pakistan. The UIB comprises total catchment area of 172,000 km^2 and total river length of 1125 km [56,57]. The watershed elevation upstream of Tarbela dam in UIB ranges from 360 to 8572 m above mean sea level of [57]. The catchment area of the UIB upstream of the Tarbela dam is situated at 31°–37° E and 72°–82° N. The Tarbela Dam is among world's largest earth fill-rock fill multipurpose dams lying UIB.

The UIB starts from frozen place of Tibetan Plateau at an elevation of 5486 m on Mount Kailash in China [58]. Then it drains from south eastern direction parallel to the geological strike through a well-defined valley. Throughout of its river length it flows in a defined valley parallel to the fault zone and then it ends at Arabian sea. Most of its flows comes from three mountain ranges Hindukush, Karakorum and Himalayas. The major tributaries of UIB are Gilgit, Hunza, Shyok and Shigar i.e. upper region of glacier and snow dominated UIB; Kharmong and Astore i.e middle snow and rainfall dominated UIB; and lower Brandu and Gorband rainfall dominated UIB. During mid Eocene period has shaped the UIB in a complex geologic structure with its high relief due to tectonic activities and culminating of Himalayan orogenic process [59,60]. The young rugged and high elevated mountains were rapidly degraded due to combination of various process [61,62]. The UIB is also high source of sediment yields due its tectonic instability, rapidly weathering with severe climatic conditions, mass movements spread over the wide basin area, heavy snowfalls and its melting during spring season, dominancy of glacial melts, landslides and mass wasting, glacial dammed lakes, glacial lakes outburst, moraines and catastrophic flood events [63,64,65,66]. The lower region of UIB is dominated with heavy rainfall events during spring and summer seasons and generation of sediments results due to flash floods and extensive rainfall intensity.

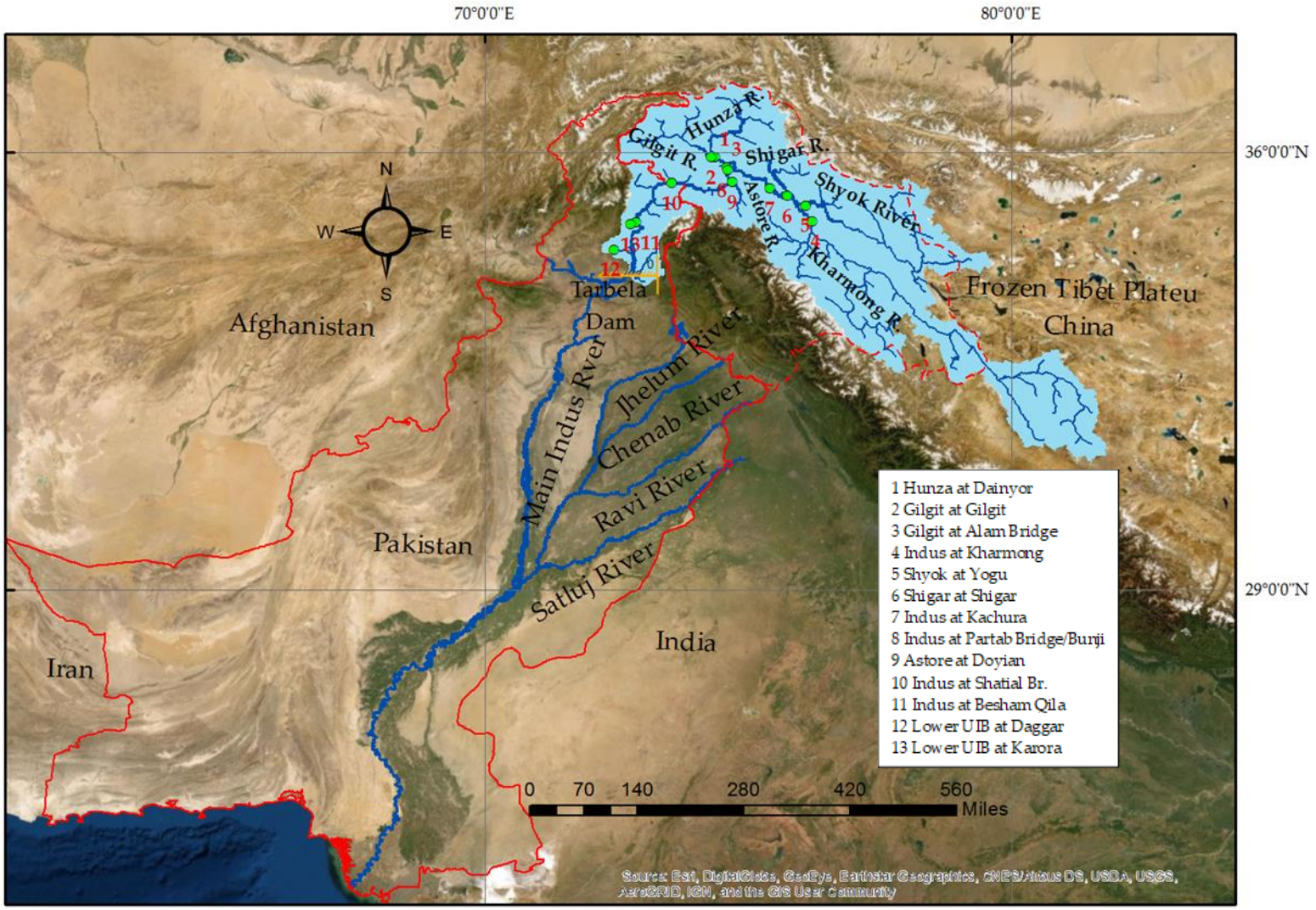

Figure 1.1 The map of the study area of Upper Indus River basin.

1.3 Research objectives

The main objective of this study was to assess the impact of climate changes on sediments yields and develop a framework for prediction of suspended sediments in data-sparse and data scarce Upper Indus River basin. The upper Indus basin consist of famous mountains of world like K2 peak due to its unique topography and existence of its three young mountain ranges Hindukush, Karakorum and Himalayas in the basin. with sparsely distributed large river networks. It still exists in its natural condition due to less anthropogenic activities in the basin. In view of water scarcity and economical energy demands of Pakistan where 30,000 MW of hydropower projects and water reservoirs are planned, a better understanding about sediment yields generation process and its accurate estimation seems timely and desirable. In order to address the need of research in estimations of sediment yields of UIB raised in section 1.1.4. these were the objectives of this study.

- To assess the spatial variability and trends of flows and sediments in the Upper Indus River basin due to climate changes.
- Estimation of accurate suspended sediment concentrations (SSC) in the upper Indus basin using the conceptualized artificial intelligence approach.
- Assessment of signaling of climate changes in exports of SSC from glacierized and snow melt dominated sub-basins of UIB.

1.5 Structure of Thesis

Chapter 1 is the introduction covers the literature review relevant to the research, need of research, study area and objectives of research. The literature review overviews the pervious studies related to assessment of climate changes on SSC of UIB, estimations/predictions of SSC and signaling of climate changes on exports of sediments. The need of research discusses the usefulness of research, inclusion of remote sensing land cover i.e. snow cover and NDVI in addition to hydroclimatic information as inputs of soft computing models to improve the predictions of sediments. It offers a feasible robust approach to accurately estimate the suspended sediments. It also discusses the importance of erosion and flows process for exports of SSC in snow and glacier dominated sub-basins of UIB.

Chapter 2 discusses the first objective of research with detailed methodology focusing on investigation of trends on SSC and flows using Mann-Kendall trend test. It further addressed the comparative assessment of trends of SSC and flows due to climate changes in sparsely distributed UIB. In this chapter corrected grid basin rainfall and corrected mean air temperature on different altitudes were used to assess the trends of SSC and flows. Per decade changes of seasonal/annual SSC and flows for each gauging station were calculated and spatial maps of their trends on seasonal and annual basis were plotted to assess the changes on spatial scale. Moreover, it has also analyzed the Pearson's correlation among flows, SSC, mean air temperature and rainfall. It discusses the role of changes in seasonal basin precipitations and mean air temperature at different altitudes in UIB, which were partially responsible for the trends of SSC and flows during period 1981-2010.

Chapter 3 focuses on the second objective of the study to check the applicability of conceptualized data-driven models with their detailed methodology to predict the SSC in glacier and snow dominated Gilgit sub-basin of UIB. It explained the methodology related to neural network (ANN), adaptive neuro fuzzy logic inference system with grid partition (ANFIS-GP), adaptive neuro fuzzy

logic inference system with subtractive clustering (ANFIS-SC), adaptive neuro fuzzy logic inference system with fuzzy c-means clustering, multiple adaptive regression splines (MARS) and sediment rating curves (SRC) models used during this research objective. It integrated the concept of simulated snow cover fractions estimated from Temperature index snow model as the input vector of data-based models in addition to the discharges, effective rainfalls, evapotranspiration and mean air temperature to predict the SSL. It discussed the results of best performing input combinations with best performing data-based models for prediction of daily SSC during regular period as well against the peak events of SSC. In this chapter the total absolute accuracies from the comparison between the estimated data-based peak sediment values and measured peak sediments were calculated. Moreover, an ensembled averaged equation from the outputs of all the models against the measured sediments was also developed and tested in this section.

Chapter 4 describes the detailed methodology and results of second objective in rainfall dominated Brandu River in Lower UIB for estimation of SSC. It described the methodology related to four neural network (ANN), adaptive neuro fuzzy logic inference system with grid partition (ANFIS-GP), adaptive neuro fuzzy logic inference system with subtractive clustering (ANFIS-SC), adaptive neuro fuzzy logic inference system with fuzzy c-means clustering and sediment rating curves (SRC) models used to predict the SSC. This section describes the relationships between SSC, flows, rainfall and normalized vegetative index (NDVI) parameters of the Brandu River basin. It also introduced the remotely sensed bio physical parameters of NDVI as land cover factor with hydroclimatic input vectors during prediction of SSC using data-base algorithms. In the results using the data-based modelling approach the comparison between the input combinations consisting of hydroclimatic datasets with and without NDVI was also discussed. The accuracy of best performing data-based model was also calculated with the objective that the conclusion can help in the projects of the watershed managements, sediment management, design and operation of existing/future planned hydropower's and water reservoirs in the study area.

Chapter 5 analyzed the different flow process such as snow melts, ice melts, effective rainfall and snow cover depletions in contrast to climate changes for exports of sediment yields in Gilgit (glacier-snow dominated) and Astore (snow-rainfall dominated) sub-basins of UIB. It also describes the detailed methodology of Temperature index snow and ice models to estimate the flow processes. Mann-Kendall trend test and Sen 's slope estimator discussed in chapter 2 was used to detect the trends of flows process, discharges and SSC. Here, the cumulative frequency analysis of flow process responsible for transport of SSC in the basins during intermittent samplings days and regular days was also carried out in order to check whether or not the intermittent sampling significantly influenced the results of monthly/seasonal trends.

Chapter 6, Summarized the results and made the conclusion from the results of each objective with limitation of the current research outcome, discussed the significant of the results of current research and future recommendations to improve the modelling approach for future researchers.

1.6 References

1. Hewitt, K. The Karakorum Anomaly? Glacier Expansion and the 'Elevation Effect,' Karakorum Himalaya. Mt. Res. Dev. 2005, 25, 332–340, doi:10.1659/0276-4741(2005)025[0332:TKAGEA]2.0.CO;2.
2. Lutz, A.F.; Immerzeel, W.W.; Kraaijenbrink, P.D.A.; Shrestha, A.B.; Bierkens, M.F.P. Climate Change Impacts on the Upper Indus Hydrology: Sources, Shifts and Extremes. PLoS ONE 2016, 11, e0165630, doi:10.1371/journal.pone.0165630.
3. Arfan, M.; Lund, J.; Hassan, D.; Saleem, M.; Ahmad, A. Assessment of Spatial and Temporal Flow Variability of the Indus River. Resources 2019, 8, 103, doi:10.3390/resources8020103.
4. Hasson, S.U.; Böhner, J.; Lucarini, V. Prevailing climatic trends and runoff response from Hindukush-Karakorum-Himalaya, upper Indus Basin. Earth Syst. Dyn. 2017, 8, 337–355, doi:10.5194/esd-8-337-2017.
5. Ali, K.F.; De Boer, D.H. Spatial patterns and variation of suspended sediment yield in the upper Indus River basin, northern Pakistan. J. Hydrol. 2007, 334, 368–387, doi:10.1016/j.jhydrol.2006.10.013.
6. Ateeq-Ur-Rehman, S.; Bui, M.; Rutschmann, P. Variability and Trend Detection in the Sediment Load of the Upper Indus River. Water 2018, 10, 16, doi:10.3390/w10010016.
7. Tarar, Z.; Ahmad, S.; Ahmad, I.; Majid, Z. Detection of Sediment Trends Using Wavelet Transforms in the Upper Indus River. Water 2018, 10, 918, doi:10.3390/w10070918.
8. Immerzeel, W.W.; Wanders, N.; Lutz, A.F.; Shea, J.M.; Bierkens, M.F.P. Reconciling high-altitude precipitation in the upper Indus basin with glacier mass balances and runoff. Hydrol. Earth Syst. Sci. 2015, 19, 4673–4687, doi:10.5194/hess-19-4673-2015.
9. Lutz, A.F.; Immerzeel, W.W. HI-AWARE Reference Component 1. Climate Dataset for the Indus, Ganges and Brahmaputra River Basins. *FutureWater Rep.* **2015**, *146*. Available online: https://www.futurewater.eu/wpcontent/uploads/2015/10/Report_IGB_historical_climate_dataset.pdf (accessed on 06.03.2018).
10. Mann, H.B. Nonparametric Tests Against Trend. Econometrica 1945, 13, 245, doi:10.2307/1907187.
11. Kendall, M.G. Rank Correlation Methods, 4th ed.; Griffin: London, UK, 1970; ISBN 978-0-85-264199-6.
12. Gao, P.; Geissen, V.; Ritsema, C.J.; Mu, X.-M.; Wang, F. Impact of climate change and anthropogenic activities on stream flow and sediment discharge in the Wei River basin, China. Hydrol. Earth Syst. Sci. 2013, 17, 961–972, doi:10.5194/hess-17-961-2013.
13. Sinha, T.; Cherkauer, K.A. Time Series Analysis of Soil Freeze and Thaw Processes in Indiana. J. Hydrometeorol. 2008, 9, 936–950, doi:10.1175/2008JHM934.1.
14. Sen, P.K. Estimates of the Regression Coefficient Based on Kendall's Tau. J. Am. Stat. Assoc. 1968, 63, 1379, doi:10.2307/2285891.
15. Ul Hussan, W.; Khurram Shahzad, M.; Seidel, F.; Costa, A.; Nestmann, F. Comparative Assessment of Spatial Variability and Trends of Flows and Sediments under the Impact of Climate Change in the Upper Indus Basin. Water 2020, 12, 730, doi:10.3390/w12030730.
16. Wardrop, D.H.; Brooks, R.P. The Occurrence and Impact of Sedimentation in Central Pennsylvania Wetlands. Environmental Monitoring and Assessment 1998, 51, 119–130, doi:10.1023/A:1005958429834.
17. McBean, E.A.; Al-Nassri, S. Uncertainty in Suspended Sediment Transport Curves. Journal of Hydraulic Engineering 1988, 114, 63–74, doi:10.1061/(ASCE)0733-9429(1988)114:1(63).
18. Khan, N.M.; Tingsanchali, T. Optimization and simulation of reservoir operation with sediment evacuation: a case study of the Tarbela Dam, Pakistan. Hydrol. Process. 2009, 23, 730–747, doi:10.1002/hyp.7173.

19. Ackers, J.; Hieatt, M.; Molyneux, J.D. Mangla reservoir, Pakistan – approaching 50 years of service. Dams and Reservoirs 2016, 26, 68–83, doi:10.1680/jdare.16.00036.
20. Pakistan Water and Power Development Authority (WAPDA). 5th Hydrographic survey of Chashma Reservoir. International Sedimentation Research Institute, Pakistan (ISRIP) 2012.
21. King, R.; Stevens, M. Sediment management at Warsak, Pakistan. Int. J. Hydropower Dams 2001, 8, 61–68.
22. Jakeman, A.J.; Green, T.R.; Beavis, S.G.; Zhang, L.; Dietrich, C.R.; Crapper, P.F. Modelling upland and instream erosion, sediment and phosphorus transport in a large catchment. Hydrol. Process. 1999, 13, 745–752, doi:10.1002/(SICI)1099-1085(19990415)13:5<745: AID-HYP777>3.0.CO;2-E.
23. Wasson, R. What approach to the modelling of catchment scale erosion and sediment transport should be adopted. Modelling Erosion, Sediment Transport and Sediment. IHP-VI Technical Documents in Hydrology 2002, 1–11.
24. Vente, J. de; Poesen, J.; Verstraeten, G. The application of semi-quantitative methods and reservoir sedimentation rates for the prediction of basin sediment yield in Spain. Journal of Hydrology 2005, 305, 63–86, doi: 10.1016/j.jhydrol.2004.08.030.
25. Vente, J. de; Poesen, J.; Bazzoffi, P.; van Rompaey, A.; Verstraeten, G. Predicting catchment sediment yield in Mediterranean environments: the importance of sediment sources and connectivity in Italian drainage basins. Earth Surf. Process. Landforms 2006, 31, 1017–1034, doi:10.1002/esp.1305.
26. Jain, S.K. Development of Integrated Sediment Rating Curves Using ANNs. J. Hydraul. Eng. 2001, 127, 30–37, doi:10.1061/(ASCE)0733-9429(2001)127:1(30).
27. Kerem Cigizoglu, H.; Kisi, Ö. Methods to improve the neural network performance in suspended sediment estimation. Journal of Hydrology 2006, 317, 221–238, doi: 10.1016/j.jhydrol.2005.05.019.
28. Emamgholizadeh, S.; Demneh, R. The comparison of artificial intelligence models for the estimation of daily suspended sediment load: a case study on Telar and Kasilian Rivers in Iran. Water Science and Technology: Water Supply 2018, 19, ws2018062, doi:10.2166/ws.2018.062.
29. Kakaei Lafdani, E.; Moghaddam Nia, A.; Ahmadi, A. Daily suspended sediment load prediction using artificial neural networks and support vector machines. Journal of Hydrology 2013, 478, 50–62, doi: 10.1016/j.jhydrol.2012.11.048.
30. Adnan, R.M.; Liang, Z.; El-Shafie, A.; Zounemat-Kermani, M.; Kisi, O. Prediction of Suspended Sediment Load Using Data-Driven Models. Water 2019, 11, doi:10.3390/w11102060.
31. Meade, R.H. Suspended sediment in the Amazon River and its tributaries in Brazil during 1982-84; Open-File Report 85-492, 1985. http://pubs.er.usgs.gov/publication/ofr85492
32. Molnar, P.; England, P. Late Cenozoic uplift of mountain ranges and global climate change: chicken or egg? Nature 1990, 346, 29–34, doi:10.1038/346029a0.
33. Jansen, I.M.L.; Painter, R.B. Predicting sediment yield from climate and topography. Journal of Hydrology 1974, 21, 371–380, doi:10.1016/S0022-1694(74)80006-5.
34. Ludwig, W.; Probst, J.-L. River sediment discharge to the oceans; present-day controls and global budgets. American Journal of Science 1998, 298, 265–295, doi:10.2475/ajs.298.4.265.
35. Milliman, J.D.; Syvitski, J.P.M. Geomorphic/Tectonic Control of Sediment Discharge to the Ocean: The Importance of Small Mountainous Rivers. The Journal of Geology 1992, 100, 525–544, doi:10.1086/629606.
36. Glazyrin, G.; Tashmetov, H.K. Sediment yield alteration of mountain rivers and climate change in central Asia. Effects of Scale on Interpretation and Management of Sediment and Water Quality, Osterkamp WR (ed). 1995, IAHS Publication No. 226. IAHS Press: Wallingford; 187–190
37. Walling, D.E. Linking land use, erosion and sediment yields in river basins. Hydrobiologia 1999, 410, 223–240, doi:10.1023/A:1003825813091.

38. Church, M.; Slaymaker, O. Disequilibrium of Holocene sediment yield in glaciated British Columbia. Nature 1989, 337, 452–454, doi:10.1038/337452a0.
39. Faran Ali, K.; Boer, D.H. de. Factors controlling specific sediment yield in the upper Indus River basin, northern Pakistan. Hydrol. Process. 2008, 22, 3102–3114, doi:10.1002/hyp.6896.
40. Arora, M.; Kumar, R.; Kumar, N.; Malhotra, J. Assessment of suspended sediment concentration and load from a large Himalayan glacier. Hydrology Research 2014, 45, 292–306, doi:10.2166/nh.2013.129.
41. Haritashya, U.K.; Singh, P.; Kumar, N.; Gupta, R.P. Suspended sediment from the Gangotri Glacier: Quantification, variability and associations with discharge and air temperature. Journal of Hydrology 2006, 321, 116–130, doi:10.1016/j.jhydrol.2005.07.037.
42. Hock, R. Temperature index melt modelling in mountain areas. Journal of Hydrology 2003, 282, 104–115, doi:10.1016/S0022-1694(03)00257-9.
43. Costa, A.; Molnar, P.; Stutenbecker, L.; Bakker, M.; Silva, T.A.; Schlunegger, F.; Lane, S.N.; Loizeau, J.-L.; Girardclos, S. Temperature signal in suspended sediment export from an Alpine catchment. Hydrol. Earth Syst. Sci. 2018, 22, 509–528, doi:10.5194/hess-22-509-2018.
44. Milliman, J.D.; Syvitski, J.P.M. Geomorphic/Tectonic Control of Sediment Discharge to the Ocean: The Importance of Small Mountainous Rivers. J. Geol. 1992, 100, 525–544, doi:10.1086/629606.
45. Khan, N.M.; Tingsanchali, T. Optimization and simulation of reservoir operation with sediment evacuation: A case study of the Tarbela Dam, Pakistan. Hydrol. Process. 2009, 23, 730–747, doi:10.1002/hyp.7173.
46. Babur, M. Assessment of Climate Change Impact on Reservoir Inflows Using Multi Climate Models under RCPs—The Case of Mangla Dam in Pakistan. Water 2016, 8, 389.
47. Kreft, S.; Eckstein, D.; Melchior, I. Global Climate Risk Index 2017: Who Suffers Most From Extreme Weather Events? Weather-related Loss Events in 2015 and 1996 to 2015; Germanwatch Nord-Süd Initiative e V: Bonn, Germany, 2016; ISBN 978-3-943704-49-5.
48. Arfan, M.; Lund, J.; Hassan, D.; Saleem, M.; Ahmad, A. Assessment of Spatial and Temporal Flow Variability of the Indus River. Resources 2019, 8, 103, doi:10.3390/resources8020103.
49. Hasson, S.U.; Böhner, J.; Lucarini, V. Prevailing climatic trends and runoff response from Hindukush-Karakorum-Himalaya, upper Indus Basin. Earth Syst. Dyn. 2017, 8, 337–355, doi:10.5194/esd-8-337-2017.
50. Ali, K.F. Construction of Sediment Budgets in Large Scale Drainage Basins: The Case of the Upper Indus River. Ph.D. Thesis, Department of Geography and Planning, University of Saskatchewan, Saskatoon, SK, Canada, 2009.
51. Meadows, A.; Meadows, P.S. The Indus River. Biodiversity, Resources, Humankind; Azra. M., Peter, S., Eds.; Oxford University Press for the Linnean Society of London: Oxford, UK, 1999; ISBN 0195779053.
52. Ahmad, N. Water Resources of Pakistan and Their Utilization; Nazir Ahmad; Shahzad Nazir: Lahore Pakistan, Pakistan, 1993.
53. Clift, P.D. A brief history of the Indus River. Geological Society, London, Special Publications 2002, 195, 237–258, doi:10.1144/GSL.SP.2002.195.01.13.
54. Pakistan Water Sector Strategy. Executive Summary; Report; Ministry of Water and Power, Office of the Chief Engineering Advisor/Chairman Federal Flood Commission; Govt of Pakistan: Islamabad, Pakistan, 2002; Volume 1.
55. Pakistan Water Gateway. The Pakistan Water Situational Analysis; Report; Consultative Process in Pakistan (WCD CPP) Project; Pakistan Water Gateway; Islamabad, Pakistan: 2005.
56. Ali, K.F.; De Boer, D.H. Spatial patterns and variation of suspended sediment yield in the upper Indus River basin, northern Pakistan. J. Hydrol. 2007, 334, 368–387, doi:10.1016/j.jhydrol.2006.10.013.
57. Khan, A.; Richards, K.; Parker, G.; Mcrobie, F.; Mukhopadhyay, B. How large is the Upper Indus Basin? The pitfalls of auto-delineation using DEMs. J. Hydrol. 2014, 509, 442–453, doi:10.1016/j.jhydrol.2013.11.028.
58. Jain, S.K.; Agarwal, P.K.; Singh, V.P. Hydrology and water resources of India; Springer: Dordrecht, 2007, ISBN 1402051794.

59. Molnar, P.; Tapponnier, P. Cenozoic Tectonics of Asia: Effects of a Continental Collision: Features of recent continental tectonics in Asia can be interpreted as results of the India-Eurasia collision. Science 1975, 189, 419–426, doi:10.1126/science.189.4201.419.
60. Miller, K.J. The International Karakoram Project; Cambridge University Press: Cambridge, New York, 1984, ISBN 0521263409.
61. Searle, M.P. Geology and tectonics of the Karakoram Mountains; Wiley: Chichester West Sussex England, New York, 1991, ISBN 0471927732.
62. Shroder, J.F. Himalaya to the sea. Geology, geomorphology, and the Quaternary / edited by John F. Shroder, Jr; Routledge: London, 1993, ISBN 0415066484.
63. Ferguson, R.I. Sediment Load of the Hunza River; Mill, K.J., Ed.; International Karakoram Project Cambridge University Press: Cambridge, UK, 1984, Volume 2, pp. 580–598.
64. Hewitt, K. Catastrophic landslides and their effects on the Upper Indus streams, Karakoram Himalaya, northern Pakistan. Geomorphology 1998, 26, 47–80, doi:10.1016/S0169-555X(98)00051-8.
65. Hewitt, K. Catastrophic rock slope failures and late Quaternary developments in the Nanga Parbat–Haramosh Massif, Upper Indus basin, northern Pakistan. Quaternary Science Reviews 2009, 28, 1055–1069, doi:10.1016/j.quascirev.2008.12.019.
66. Shroder, J.F.; Bishop, M.P. Mass movement in the Himalaya: new insights and research directions. Geomorphology 1998, 26, 13–35, doi:10.1016/S0169-555X(98)00049-X.

Chapter 2- Comparative Assessment of Spatial Variability and Trends of Flows and Sediments Under the Impact of Climate Change in The Upper Indus Basin

This Chapter is published as:

Ul-Hussan, W.; Shahzad M.K.; Seidel F.; Costa A.; Nestmann F.; Comparative Assessment of Spatial Variability and Trends of Flows and Sediments under the Impact of Climate Change in the Upper Indus Basin. *Water (MDPI) Switzerland*, 2020, doi.org/10.3390/w12030730

2.1 Abstract

Extensive research of the variability of flows under the impact of climate change has been conducted for the Upper Indus Basin (UIB). However, limited literature is available on the spatial distribution and trends of suspended sediment concentrations (SSC) in the sub-basins of UIB. This study covers the comparative assessment of flows and SSC trends measured at 13 stations in the UIB along with the variability of precipitation and temperatures possibly due to climate change for the past three decades. In the course of this period, the country's largest reservoir, Tarbela, on the Indus River was depleted rapidly due to heavy sediment influx from the UIB. Sediment management of existing storage and future planned hydraulic structures (to tap 30,000 MW in the region) depends on the correct assessment of SSC, their variation patterns, and trends. In this study, the SSC trends are determined along with trends of discharges, precipitation, and temperatures using the non-parametric Mann–Kendall test and Sen's slope estimator. The results reveal that the annual flows and SSC are in a balanced state for the Indus River at Besham Qila, whereas the SSC are significantly reduced ranging from 18.56%–28.20% per decade in the rivers of Gilgit at Alam Bridge, Indus at Kachura, and Brandu at Daggar. The SSC significantly increase ranging from 20.08%–40.72% per decade in the winter together with a significant increase of average air temperature. During summers, the SSC are decreased significantly ranging from 18.63%–27.79% per decade along with flows in the Hindukush and Western–Karakorum regions, which is partly due to the Karakorum climate anomaly, and in rainfall-dominated basins due to rainfall reduction. In Himalayan regions, the SSC are generally increased slightly during summers. These findings will be helpful for understanding the sediment trends associated with flow, precipitation, and temperature variations, and may be used for the operational management of current reservoirs and the design of several hydroelectric power plants that are planned for construction in the UIB.

Keywords: suspended sediment concentrations; Upper Indus Basin; Mann–Kendall trend test; Sen's slope estimator; Gilgit basin; Karakorum climate anomaly; Karakorum-Hindukush-Himalaya

2.2 Introduction

Erosion from the relatively younger mountain ranges of the Hindukush, Karakorum, and Himalaya yield a huge amount of sediment that enters the Upper Indus Basin (UIB) and its storage reservoirs, such as the Tarbela reservoir. Average sediment loads of 250 million tons per year are produced in the Indus River by these three mountain ranges, making it one of the world's largest sediment-laden rivers [1]. Sediment erosion is a rather complex phenomenon that primarily requires determination of parameters contained in universal soil loss equation. Recent research has covered the impacts of temperature-driven snow melt processes and patterns and climate change scenarios on the erosion rate in various catchments [2,3]. Erosion and sediment transport largely depend on hydrological and hydraulic parameters that are largely driven and/or altered by climate forces. Knowledge about the distribution of hydro-meteorological parameters and sediment yields and their magnitude variations over time is crucial to the partial validation of the impacts of climate change. The assessment and quantification of variations of fluvial sediment fluxes and their spatiotemporal patterns are important for a better understanding of river geomorphology as well as the planning, design, and operation of hydraulic structures on the river. The variation of sediment fluxes affects the depletion of reservoirs, channel erosion and deposition, abrasion of hydropower turbines, pollution of river ecosystems, and the operation and management of hydropower as well as storage reservoirs. Assessment of spatio-temporal variation of suspended sediment concentrations (SSC) or yields due to precipitation, temperature, and flow process variations are vital to adapt watershed management practices and to better understand the landslide activities in the basin.

Pakistan's economy is based on agriculture. Agricultural production contributes 18.9% of the gross domestic product (GDP) in Pakistan and makes up the major part of the country's annual exports. Pakistan is among the top ten world water stressed countries due to the vulnerability of climate changes, reduction of storages, increase of its population, and increase of water demands [4,5]. The Tarbela reservoir, which lies in the UIB, has lost 35% of its capacity since 1974 due to reservoir sedimentations [6]. This rapid depletion of storage reservoirs due to siltation not only affects the country's economy, but also endangers food security and leads to cross-border water conflicts. Post construction measures against siltation in reservoirs are indispensable, but sometimes neither technically nor financially feasible. Sedimentation also adversely affects the ecosystems of both rivers and reservoirs. To enhance the sustainability and environmental compatibility of existing reservoirs and hydropower projects planned in the UIB, the impact of climate change on both flows and suspended sediments concentrations (SSC) has to be assessed. This assessment may improve the understanding of the effects of the Karakorum climate anomaly [7,8] on the seasonal and annual trends of flows and sediment yields in the UIB. This could also be beneficial for the management of sediments. This study will also help to understand the effect of different hydrological processes, such as snow cover, snow melt, ice melt, and rainfall, on erosion and sediment yield in sub-basins of the UIB dominated by snow and ice melting.

Many techniques, statistical methods, and approaches have been used by a lot of researchers for assessing changes in climate, flows, and SSC. The moving *t*-test, Yamonato method, Carner method, order clustering approach, and filter test method were used in the past [9,10]. The parametric regression approach was applied to determine the discharge–total suspended solids relationships (Q–TSS)/SSC vs. time–discharge (T–Q) for the trend analysis of sediments [11]. In 1945, Mann and Kendall suggested the nonparametric test method for time series analysis [12]. Gerstengarbe and Werner developed the Mann–Kendall test to analyze and detect trends [13]. Furthermore, the rank sum test [14], two-sample *t*-test [15], and Pettit test [16] were used for trend analysis in many studies. In a recent study for the Loess Plateau [17], trend analysis was carried out as well, because the plateau contributes 80% of the sediment belonging to the Yellow River. For large basins like the Indus basin,

the analysis and budgeting of sediments and their patterns require huge resources and a large data collection expenditure. A few years ago, sediment studies were carried out [18–20] on the UIB. These studies covered the sediment patterns, sediment distribution, and sediment budgeting on the basin scale. Sediment transport is a highly nonlinear and complex phenomenon due to multiple factors controlling and affecting the erosion process, such as channel erosion, gully erosion, snow and glacier melts erosion etc. To characterize the highly nonlinear processes of sediment erosion, flow, and climate change, most researchers have used the non-parametric test. It is the most powerful tool to assess the temporal and spatial dynamics of sediment fluxes, hydrological variables, and climate. For the trends of nonlinear processes, such as flows, climate, and sediment yields, the Mann–Kendall trend test is used for this study. It is a robust method and has the capacity to detect the trends of time series without considering the normal distribution of the input datasets. In a regional study [21], the non-parametric Mann–Kendall test was used to detect the trends of flows and sediment discharges in the Yellow River. Similarly, the non-parametric Mann–Kendall test was applied for the trend analysis of sediment yields based on data from a few stations in the UIB in two recent studies [22,23].

According to the experience gained by many researchers, however, the Mann–Kendall test alone, and without considering the serial/auto correlations, is insufficient to detect trends. Therefore, the trend-free pre-whitening (TFPW) approach, along with the Mann–Kendall trend test, is used here to detect the trends of flows, SSC, and climatic parameters. To further quantify the magnitudes of the trends of hydro-climatic time series, Sen's slope estimator is used after the trend-free pre-whitening (TFPW) and Mann–Kendall trend analysis. Several hydropower stations and storage reservoirs are planned to be constructed in the UIB according to the 2025–2030 vision of the Water and Power Development Authority (WAPDA). The comprehensive assessment of the trends of flows and suspended sediment concentrations (SSC) under the impact of climate change for all 13 gauging stations in the Hindukush, Karakorum, and Himalaya mountain ranges presented in this study will be particularly helpful for policymakers, hydraulic engineers, and water resources managers. Therefore, the objectives of this study are: (1) the detection and assessment of trends in different temporal intervals ranging from monthly to seasonal and annual basis for flows and SSC of the 13 hydrological stations in the UIB since 1980–2010; (2) development of seasonal and annual trend maps for representing the spatial changes in % for flows and SSC per decade in the UIB; (3) extracting the missing year's climatic information for sparsely gauged climatic stations using the linear scaling bias correction method along with the station-recorded data and satellite grid point data; (4) assessment of the impact of changes in the trends of mean monthly rainfalls of the basins and average monthly temperatures, adjusted for lapse rate per elevation zone, on the monthly flows and SSC of the UIB; (5) assessing the significant changes in monthly, seasonal, and annual flows and SSC, which are partly due to climate change, in past 30 years for selected catchments with major SSC contributions.

2.3 Materials

2.3.1 Study Area

The Indus River is among the largest rivers in South Asia with its total length of 2880 km [24,25]. It has a total catchment area of 970,468 km^2 with about 56% (529,134 km^2) of its area lying within the territory of Pakistan. The remaining catchment area is distributed between China, India, and Afghanistan. It also has the world's largest irrigation networks covering an irrigated agricultural area of 181,000 km^2 [26,27]. Moreover, the Indus basin is an economic source of energy. Hydropower produced here has a share of 29% in the total national power generation capacity of Pakistan [27].

This study focuses on the Upper Indus Basin (UIB) upstream of the Tarbela dam with a total catchment area of 172,000 km^2 and a length of 1125 km [18,28]. The watershed area of the UIB upstream of the Tarbela reservoir is situated at 31°–37° E and 72°–82° N. The watershed elevation of the UIB above the Tarbela dam ranges from 360 to 8572 m above mean sea level [28]. The detailed characteristics of the gauging stations measuring flows and SSC at 13 locations in the UIB are given

in the Table 2.1. Four gauging stations are located on the main arm of the Upper Indus, eight on the tributaries, and one station, Alam Bridge, at the confluence of two tributaries.

Figure 2.1 shows the details of the catchment area, the sub-basins, and the tributaries of the UIB. It starts from the frozen planes of the Tibetan Plateau in China. Then, it enters from the south eastern direction in a well-defined valley and flows parallel to the geological fault line. After crossing the fluvial plains 45 km upstream of Skardu town at an altitude of 2469 m, it joins Shyok River with 30% of glacier drainage area. Here, the valley widens and mostly consists of sediments in the form of glacial deposits down to Skardu town. Upstream of Skardu in the Deosai plains, the Kharmong River from the central Himalayas lying in Pakistan joins the main (Indus) River with a total glacier-covered area of 4%. Kharmong River is dominated by a snow and rainfall flow regime.

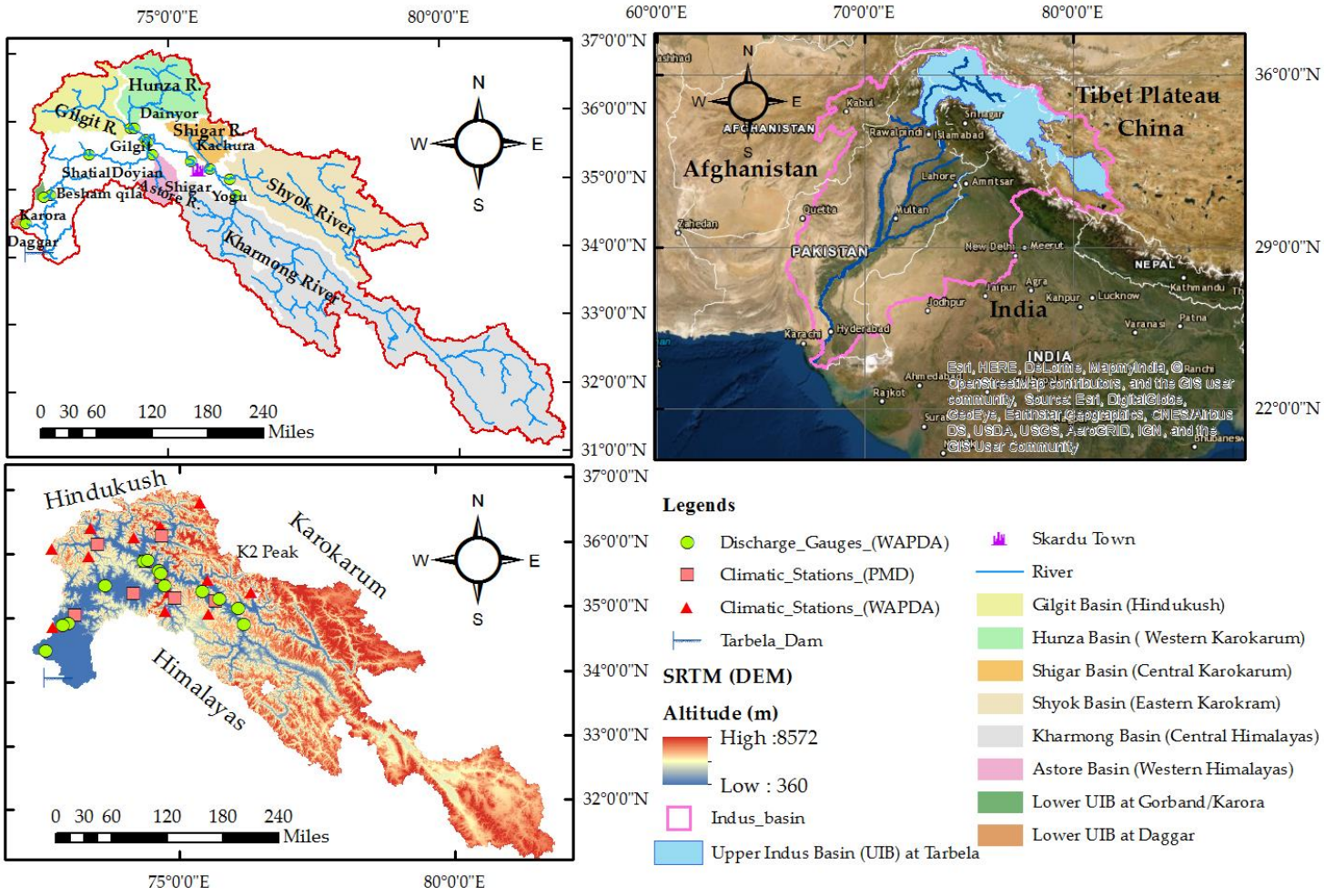

Figure 2. 1 The map of the study area shows the locations of stream gauges, climatic stations, and sub-basins contributing to the Upper Indus Basin (UIB).

Near the town of Skardu, the Shigar River with 39% of glacier-covered area from the Himalayas drains into the main (Indus) River at an altitude of 2438 m. Downstream of Skardu town, the main River flows towards the Northwest up to Kachura Lake along the steep and narrow valley of the main River. The Hunza River runs from North to South and Gilgit River runs from the Northwest to Southeast before confluence at Alam Bridge just downstream of Gilgit town. Hunza Basin borders with Shigar Basin on the right side in the direction of flow. Hunza and Gilgit Rivers are snow- and glacier-dominated basins lying in the Western Karakorum and Hindukush mountain ranges with 39% and 10% of glacier-covered area, respectively. Astore River also joins the main River. It comes from the western Himalayas with 8% of glacier-covered area north of the Nanga Parbat massif. Downstream of Alam Bridge, the confluence of Gilgit and Hunza Rivers join the main Indus River at Bunji/Partab Bridge in Jaglot town. Jaglot is a monumental place, where all three great mountain ranges, the Himalayas, Karakorum, and Hindukush, meet. The lower part of the UIB starts at Bunji and extends up to Tarbela dam. The main river widens between Alam Bridge and Chillas and contains sediments in the form of glacier deposits. The Indus River continues its journey towards Shatial Bridge. From Shatial Bridge, the main river flows further towards the South in a steep and narrow cross section and joins Besham Qila, approx. 45 km upstream of the Tarbela reservoir. Near Besham Qila, some small and large rivers also join the Indus from both the left and the right side. The right tributaries joining the main Indus River near Besham Qila are Brandu, Gorband, Khan Khawar, Duber Khwar, Keyal Khwar, Kandia, and Tangir. The left tributaries joining the main Indus River near Besham Qila are Siran, Chor Nullah, Spat Gah, Allai Khwar, Gunar Gah, Thor Gah, and Butto Gah.

The climate of the UIB comprises two climatic fronts. One is the monsoon pattern of rainfall that originates from the Bay of Bengal and Arabian Sea. The second is the westerlies climatic front originating from the Caspian Sea and Mediterranean region during winters and springs. Most of the annual precipitation in the UIB falls in the form of snow during the winter and spring season due to westerlies [29,30]. Mean annual precipitation in Gilgit ranges from 150 mm at lower elevations to 1800 mm in the snow accumulation zone in Bagrot valley [31]. In the Western Karakorum over the Batura glaciers, annual precipitation accounts for more than 1000 mm [32]. In the Central Karakorum, annual precipitation ranges from 1000 mm to more than 2000 mm over the Hispar and Biafo glaciers [33]. In the Central Karakorum, 67% of annual precipitation fall during winter is due to the westerly front, with the remaining 33% of annual rainfall during the summer season [7,34,35]. In the lower UIB, annual rainfall ranges from 1000 mm to 1500 mm between Dasu and Besham Qila [23]. In the UIB, the maximum mean basin rainfall occurs during the spring season, with April being the month of highest rainfall [36].

In the UIB the upper glaciered has very low population density (<50 people km^2) in comparison to the lower monsoon dominated region. The upper region of UIB has an estimated population of 1.5 Million. The lower region of UIB is vice versa. The upper region of UIB also has high percent of snow/ice cover, at up to 40% in Hunza, Gilgit, Shigar, and Shyok river basins. This snow/ice cover emerges as a single dominated land cover factor which explains 73.4% of the variance in sediment yields for whole UIB [37].

Table 2. 1 Geographical characteristics of the stream gauging sites measuring flows and suspended sediment concentrations (SSC) in the Upper Indus Basin (UIB).

Ser #	Discharge Gauging Stations	Region	Catchment Area km²	Elevation (m)	Elevation Range (m)	% of Glacier Cover
1	Hunza at Dainyor	Western Karakorum	13,157	1350	1426–7860	35
2	Gilgit at Gilgit	Hindukush	12,095	1430	1454–7048	10
3	Gilgit at Alam Bridge	Hunza + Gilgit	26,159	1280	1266–7843	25
4	Indus at Kharmong	Central Himalayas	67,858	2542	2478–7036	4
5	Shyok at Yogu	Eastern Karakorum	33,670	2469	2397–7553	30
6	Shigar at Shigar	Central Karakorum	6610	2438	2191–7793	39
7	Indus at Kachura	Main River UIB	112,665	2341	2107–7801	12
8	Astore at Doyian	Northwestern Himalayas	4040	1583	1580–8058	8
9	Indus at Partab Bridge/Bunji	Main River UIB	142,709	1228	1242–7889	11
10	Indus at Shatial Br.	Main River UIB	150,220	1040	906–8118	12
11	Indus at Besham Qila	Main River UIB	162,393	580	561–8118	13
12	Lower UIB at Daggar	Lower western UIB	598	700	685–2801	0
13	Lower UIB at Karora	Lower western UIB	635	880	893–4439	1

The trends induced by climate change on the discharges of various sub-catchments have been widely reported by many researchers [7,8,38,39], however, scientific literature on the spatio-temporal variation of SSC is far less extensive. Ali and De Boer [18] analyzed the spatial distribution of sediment in the UIB by dividing the region into three zones: upper snow- and glacial melt-dominated zone, middle snow-/glacial melt-, and rainfall-dominated mixed zone, and lower rainfall-dominated zone. Ateeq-Ur-Rehman et al. and Tarar et al. [22,23] identified the trends of SSC by using the data of two and four gauging stations of the UIB, respectively. Meanwhile, the former used the SSC of Hunza basin at Danyor, Shyok basin at Yogu, Upper Indus at Bunji/Partab Bridge, and Upper Indus at Besham Qila. They have used data from the gauge of Partab Bridge for the melt portion of the UIB and from Besham Qila to represent the load of the entire UIB. These studies found a significant inter-annual shift of SSC with the balanced annual sediment yield. However, an assessment of the spatio-temporal variation of SSC and discharges in relation to relevant hydrometeorological parameters and variables for all the sub-basins of the entire UIB has not yet been made. This study therefore covers the trends of spatial variability of SSC and discharges in the UIB using the data of 13 gauging stations located in the Karakorum, Himalayan, and Hindukush regions that represent almost the entire UIB with its eight sub-catchments (Table 2.1). Moreover, the previous studies used daily sediment values derived from discharge-sediment rating curves (SRC) and artificial neural networks (ANN) [22,23]. The SRC and databased models give highly overestimated and underestimated values and sometimes negative values, which are physically not possible. Especially, for the highly glacier and snow melt basins, the SRC are not reliable. In comparison to previous researches in the region that mainly relied on discharge-sediment rating curves (SRC) and artificial neural networks (ANN) for SSC, the mean of monthly sediments was taken by averaging the daily SSC gauged data. Thereby, SRC values were only used in those months where no information of sediment concentrations was available. This study is also one of the pioneer researches that used corrected estimates of rainfall and temperature for the assessment of comparative trends of precipitation, temperature, and SSC in the UIB [40,41].

2.3.2 Data Collection

For the present study, the data of 13 stream gauges in the UIB for the period 1981–2010 were collected within the Surface Water Hydrology Project (SWHP) of the Water and Power Development Authority (WAPDA). These stations measure flows on a daily basis and SSC on intermittent days. A rating curve was used to find the missing values of SSC for monthly, seasonal, and annual trend analysis. The list and characteristics of these stations are given in Table 2.2.

Hunza is second largest glacier-dominated basin of the UIB in the Western Karakorum. Here, data are available for the period of 1981–2010. The Hunza River generates 12% and 12.5% of the Besham Qila flows and suspended sediment loads (SSL), respectively. The Gilgit station at Gilgit lies in the Hindukush mountain range draining the Gilgit river basin. Here, data are available for 1981–2010. Its flows and SSL are 12% and 3.9% of the Besham Qila flows and SSL, respectively. Gilgit station is important due to the contribution of snow melt, ice melt, and rainfall to flows and SSL. The Alam Bridge station is located at the confluence of Gilgit River and Hunza River, generating 26% and 18.2% of Besham Qila flows and SSL, respectively. The major influx of sediment from the Hunza River raises the SSL in the combined flow of Gilgit and Hunza at Alam Bridge.

The gauge at Kharmong in the Central Himalayas was installed in 1982. For this reason, data of flows and SSC are available for the period 1983–2010. The main River comes from the Deosai plain and is dominated by snow melt and rainfall. Its flows and SSL are 18% and 7% of the Besham Qila flows and SSL, respectively. The Yogo station on Shyok River lies in the eastern Karakorum. Shyok River originates from the Tibetan Plateau in China and has the third largest glacier dominance in the UIB. Data are available for the period 1981–2010. The station measures 16% and 20.6% of flows and SSL, respectively, of Besham Qila. The Shigar station in the Central Karakorum generates most of the flows and SSL due to largest glacier dominance in the UIB. The station was installed in 1982, but data are

available from 1985–1998 only. After 1998, Shigar station was not in operation. Its flows and SSL are 9% and 15.4% of the Besham Qila flows and SSL, respectively.

The Indus at Kachura contributes 48% and 52.1% to the Besham Qila flows and SSL, respectively. Data are available for the long term from 1981–2010. The Bunji/Partab Bridge station on the main River has data from 1981 to June 2010. Due to the 2010 flood, the gauging site was destroyed, and the data of the remaining six months of 2010 are lacking. The Bunji station generates 71% and 97.6% of the flows and SSL, respectively, of Besham Qila. The river here contains the water and sediments from glacier- and snow-dominated upstream basins, i.e., Hunza and Gilgit on upper Northeastern side and from the parallel basins of Shigar, Shyok, and Kharmong on the lower Northeastern end. The Doyian station on Astore River also is located in a snow melt- and rainfall-dominated basin in the Western Himalayas. It generates 6% and 1.2% of the flows and SSL, respectively, of Besham Qila. Again, data are available for the entire period of 1981–2010.

The station Shatial Bridge was installed in 1983 and measures 87% of flows and surprisingly 70.0% of SSL of Besham Qila despite its location downstream of the Bunji station. Hydrological data of Shatial are available from 1983–2010. The Daggar station on Brandu River is the right tributary of the Lower UIB near Besham Qila. It is a rainfall-dominated basin contributing 0.4% and 0.4% of discharges and SSL, respectively, of Besham Qila. The Karora station of the Gorband basin is also is located on a right tributary near Besham Qila and contributes 0.7% and 0.2% of flows and SSC, respectively, of Besham Qila. Both Daggar and Karora measured data in the period from 1981–2010.

The SSC data given in % of Besham Qila benchmarks do not only reflect the availability of suspended sediment, but also indicate the transport capacity. For example, Shigar at Shigar, Shyok at Yogu, and Hunza at Dainyor report 2.75, 1.50, and 1.25 times the suspended sediment concentration of Besham Qila, respectively. Similarly, the Indus at Kachura (134%), Partab Bridge (117%), and Shatial Bridge (106%) is found to contain more suspended sediment than recorded at Besham Qila, which indicates that with the increasing flows from Kachura to Besham Qila, the suspended sediment does not match with the increasing rate of discharges. However, the SSL data reveal that from Kachura to Bunji, the sediment increases from 137 to 257 million tons, but decreases to 185 million tons at Shatial, and again rises to 263 Million tons at Besham Qila. Provided that the data are correct, the decrease of sediment load from Bunji to Shatial despite the increasing discharges means that sediment is being deposited between Bunji and Shatial and there may be either channel bed erosion or an addition of suspended sediments from the lateral tributaries between Shatial and Besham Qila, which makes the SSL more than double at the tail end.

The daily climatic data of rainfall and temperatures from 18 meteorological stations in the UIB were also collected in this study. The meteorological stations of Skardu, Gilgit, Gupis, Astore, Bunji, and Chillas are operated by the Pakistan Meteorological Department (PMD).

The remaining climatic stations under the supervision of the Water and Power Development Authority (WAPDA) have been recording data since 1995. Table 2.3 presents the details of these climatic stations. In addition, the grid data of precipitation and temperature of 5 × 5 km resolution determined in the HI-AWARE project for the Indus, Ganges, and Brahmaputra river basins were collected [40,41]. The Shuttle Radar Topography Mission's (SRTM) digital elevation model (DEM) data of 30-m resolution were applied as well. The mean basin precipitation data were extracted from the corrected rainfall data of the HI-AWARE project using DEM. The temperature data of higher elevated gauges for the missing period from 1981–1994 were extracted from grid data and corrected with station observations by using the linear biased scaling method. Estimation of glacier areas was based on the glacier polygons of the Global Land Ice Measurement (GLIMS) database. In this study, DEM is used to estimate the glacier area for each sub-basin from downloaded GLIMS polygons [42].

Table 2. 2 Hydrological characteristics of discharge gauging stations in the Upper Indus Basin (UIB).

Ser #	Discharge Gauging Stations	Region	Lat. (°)	Long. (°)	Period	Flows (m^3/sec)	SSC (mg/L)	% of UIB Flows	% of UIB SSC	SSL (Million Tons/Year)	% of UIB SSL
1	Hunza at Dainyor	Western Karakorum	35.92	74.37	1981–2010	297	1091	12	125	33	12.5
2	Gilgit at Gilgit	Hindukush	35.92	74.3	1981–2010	293	442	12	51	10	3.9
3	Gilgit at Alam Bridge	Hunza + Gilgit	35.76	74.59	1981–2010	632	795	26	91	48	18.2
4	Indus at Kharmong	Central Himalayas	34.93	76.21	1983–2010	453	669	18	76	19	7.0
5	Shyok at Yogu	Eastern Karakorum	35.18	76.1	1981–2010	390	1305	16	150	54	20.6
6	Shigar at Shigar	Central Karakorum	35.33	75.75	1985–1998	223	2395	9	275	40	15.4
7	Indus at Kachura	Main River UIB	35.45	75.41	1981–2010	1192	1171	48	134	137	52.1
8	Astore at Doyian	North Western Himalayas	35.54	74.7	1981–2010	140	295	6	34	3	1.2
9	Indus at Partab Bridge/Bunji	Main River UIB	35.73	74.62	1981–2010	1757	1019	71	117	257	97.6
10	Indus at Shatial Br.	Main River UIB	35.53	73.56	1983–2010	2167	919	87	106	185	0.70
11	Indus at Besham Qila	Main River UIB	34.92	72.88	1981–2010	2479	870	100	100	263	100.0
12	Lower UIB at Daggar	Lower western UIB	34.49	75.46	1981–2010	9.9	547	0.4	63	1	0.4
13	Lower UIB at Karora	Lower western UIB	34.89	72.76	1981–2010	18	355	0.7	41	0.4	0.2

Note: The flows and SSC are instantaneous values for the time the water samples are taken by sediment sampler

Table 2. 3 Characteristics of climatic gauging stations in the Upper Indus Basin (UIB).

Discharge Outlet	Region	Climatic Stations	Lat. (°)	Long. (°)	Average Altitude (m)	Period
Hunza at Dainyor	Western Karakorum (WK)	Naltar	36.29	74.12	2898	1995–2010
		Ziarat	36.47	74.62	3020	1995–2010
		Khunjrab	36.83	75.4	4440	1995–2010
Gilgit at Gilgit	Hindukush (HK)	Gilgit	34.92	73.34	1460	1981–2010
		Gupis	36.17	73.4	2156	1981–2010
		Ushkore	35.99	73.25	3051	1995–2010
		Yasin	36.43	73.27	3280	1995–2010
		Shendure	36.09	72.54	3712	1995–2010
Gilgit at Alam Bridge	Hunza + Gilgit	HK + WK	-	-	-	1981–2010
Indus at Kharmong	Central Himalayas (CH)	Desosai	35.09	75.54	4149	1995–2010
Shyok at Yogu	Eastern Karakorum (EK)	Hushey	35.42	76.37	3075	1995–2010
Shigar at Shigar	Central Karakorum (CK)	Shigar	35.63	75.53	2325	1995–2010
		Skardu	35.3	75.68	2210	1981–2010
Indus at Kachura	Main River UIB	EK + CH	-	-	-	1981–2010
Indus at Partab Bridge/Bunji	Main River UIB (HK + WK + CK + EK + CH)	Bunji	35.67	74.64	1372	1981–2010
Astore at Doyian	North Western Himalayas (NWH)	Astore	35.34	74.9	2168	1981–2010
		Raitu	35.14	74.73	2718	1995–2010
		Rama	35.43	74.79	3179	1995–2010
Indus at Shatial Br.	Main River UIB (HK + WK + CK + EK + CH)	Chillas	35.42	74.1	1250	1981–2010
Indus at Besham Qila	Main River UIB (HK + WK + CK + EK + CH)	Chillas	35.67	74.64	1250	1981–2010
Lower UIB at Daggar	Lower western UIB	Shangla	34.87	72.6	1960	1995–2010
Lower UIB at Karora	Lower western UIB	Shangla	34.87	72.6	1960	1995–2010

2.4 Methods

The data outliers in this study do not affect the analysis, as the Mann–Kendall test used for trend analysis is non-parametric. The homogeneity of the mean annual flows and SSC was checked using the standard normal homogeneity test (SNHT) and Buishand's range (BR) test at 5% significance level for each station. The flows and suspended sediments are considered homogeneous when the critical values of SNHT and BR are $T_0 < 9.17$, $Q\sqrt{n} < 1.27$, and $R\sqrt{n} < 1.55$. T_0 is SNHT test statistics. Similarly, $Q\sqrt{n}$ and $R\sqrt{n}$ are BR test statistics. Table 2.4 shows the results of the SNHT and BR tests.

2.4.1 Statistical Methods

The Mann–Kendall trend test is applied to detect the trends for mean values of flow, SSC, precipitation, and average temperatures on a monthly, seasonal, and annual basis. Before applying the Mann–Kendall test, the time series data were analyzed to check serial correlation. The serial correlations were eliminated from the series using the trend-free pre-whitening (TFPW) approach.

Table 2. 4 Characteristics of climatic gauging stations in the Upper Indus Basin (UIB).

Sr #	Station	Stream Flows (m^3/sec)			Suspended Sediments (mg/L)		
		SNHT	Buishand's Range (BR) Test		SNHT	Buishand's Range (BR) Test	
		T_0	$Q/\sqrt{n}$	$R/\sqrt{n}$	T_0	$Q/\sqrt{n}$	$R/\sqrt{n}$
1	Hunza at Dainyor	4.37	0.1	1.33	4.98	0.09	1.04
2	Gilgit at Gilgit	4.32	0.08	0.85	2.19	0.05	1.13
3	Gilgit at Alam Bridge	3.29	0.06	0.98	4.36	0.08	0.98
4	Indus at Kharmong	3.55	0.10	1.5	3.51	0.10	1.42
5	Shyok at Yogu	2.42	0.06	0.97	5.68	0.10	1.91
6	Shigar at Shigar	4.50	0.13	0.99	3.00	0.12	1.18
7	Indus at Kachura	1.97	0.06	1.16	7.09	0.11	1.25
8	Indus at Partab Bridge/Bunji	4.37	0.07	0.85	3.07	0.06	1.05
9	Astore at Doyian	5.92	0.07	0.85	3.83	0.08	1.08
10	Indus at Shatial Br.	1.33	0.05	0.74	5.01	0.11	1.34
11	Indus at Besham Qila	1.23	0.05	0.83	3.31	0.06	1.14
12	Lower UIB at Daggar	1.58	0.06	0.96	5.98	0.11	1.28
13	Lower UIB at Karora	12.59	0.17	1.8	11.39	0.05	0.97

Note: For homogeneous data series $T_0 < 9.17$, $Q/\sqrt{n} < 1.27$, and $R/\sqrt{n} < 1.55$.

2.4.2 Serial Correlation and Trend-Free Pre-Whitening (TFPW)

Serial correlation in time series is defined as correlation of a variable with itself over successive time intervals. This correlation must be removed before trend analysis [43]. Removal of this correlation is important, because it significantly affects the results of the non-parametric test during trend analysis. Using the two-tailed test of autocorrelation coefficient (r_1) at a 5% significance level, the time series of flows, SSC, rainfall, and temperatures were checked for serial correlation as:

$$r_1 = \frac{\sum_{i=1}^{n-1}(X_i - X^-)(X_{j+1} - X^-)}{\sum_{i=1}^{n}(X_i - X^-)^2} \quad (1)$$

where X_i is the value of suspended sediments at ith time interval and X^- is the mean value of sediments. n is the number of years.

The value of the autocorrelation coefficient r_1 at 95% of confidence interval in the two-tailed test is given as:

$$r_1 \text{ Suspended Sediments (95\%)} = \frac{-1 \pm 1.96\sqrt{(n-2)}}{n-1} \quad (2)$$

The trend-free pre-whitening (TFPW) approach is proposed when the r1 value of the time series lies between the upper and lower limits of the confidence interval [44].

2.4.3 Mann–Kendall Test

The Mann–Kendall test is most widely used for the trend analysis of hydro-climatic data in various studies [12,45–47]. To detect the statistically significant trends in the time series, the Mann–Kendall test uses two hypotheses. The null hypothesis (H_0) is that there is no trend overtime in flows and suspended sediment data. The (H_1) hypothesis is that the trend in the time series is increasing or decreasing.

For the Mann–Kendall test [12,45,47], S has been computed as given below:

$$S = \sum_{i=1}^{n-1}\sum_{j=i+1}^{n} \text{sig}\left(X_j - X_i\right) \quad (3)$$

As X_i and X_j are the data values at times i and j, while n is the length of the dataset.

$$\text{Sgn}\left(X_j - X_i\right) = \begin{cases} +1 \text{ if } \left(X_j - X_i\right) > 0 \\ 0 \text{ if } \left(X_j - X_i\right) = 0 \\ -1 \text{ if } \left(X_j - X_i\right) < 0\,, \end{cases} \quad (4)$$

The positive values of the calculated S indicate the positive trend and vice versa.

The variance S of data series is computed by the equation given below:

$$\text{Var (S)} = \frac{1}{18}\left[n\,(n-1)(2n+5) - \sum_{p=1}^{q} t_p\,(t_p-1)(2t_p+5)\right] \quad (5)$$

where t_p is the number of ties for pth values with q being the number of tied values. After calculating the variance Var (S) of data time series, the standard Z value is calculated as

$$Z = \begin{cases} \frac{s-1}{\sqrt{\text{Var (S)}}} \text{ if } S > 0 \\ 0 \text{ if } S = 0 \\ \frac{s+1}{\sqrt{\text{Var (S)}}} \text{ if } S < 0 \end{cases} \quad (6)$$

The calculated positive value of Z indicates an increasing trend, while a negative value of Z reflects a decreasing trend.

The Z value is compared at a significant level of α = 1%, 5%, and 10% with the normal distribution table value. The null hypothesis (H_0) is rejected, if the Z value is greater than $\left|Z_{1-\alpha/2}\right|$, $|z| > \left|Z_{1-\alpha/2}\right|$, where $\left|Z_{1-\alpha/2}\right|$ was obtained from the standard normal distribution table. The other hypothesis H_1 is accepted.

2.4.4 Sen's Slope Estimator

To quantify the magnitude of change of the trend in time series data, the Sen's slope estimation method [48] was used.

$$Qi = \frac{X_j - X_k}{j - k} \tag{7}$$

where Q_i is the slope of the ith paired of data, for i = 1, …, N

X_j and X_k are the data values at the time of j and k [j > k], respectively. The median of N values of Q_i values is the Sen's slope estimator given as

$$Q_i = \begin{cases} T_{(N+1)/2} & N \text{ is odd} \\ \frac{1}{2}\left(T_{N/2} + T_{(N+1)/2}\right) & N \text{ is even} \end{cases} \tag{8}$$

2.5 Results

2.5.1 Preliminary Analysis

The preliminary descriptive statistics for discharge and SSC are given in Table 2.5. Besham Qila station that represents the snow- and ice melt-dominated and partly rainfall-dependent basins shows the highest values of mean (Mean), minimum (Min), and maximum (Max) flows due to the fact it is the last gauging station of the UIB that is located just upstream of the Tarbela reservoir. Shatial Bridge just upstream of Besham Qila shows the highest standard deviation (Std.) of discharges, which means that the flow pattern is more erratic than at both neighboring upstream and downstream stations. Daggar, the basin dominated by high-intensity rainfall in spring and summer, is comparatively small and reports the highest values for the coefficient of variations (Cv (%)), coefficient of skewness (Cs), and coefficient of kurtosis (Ck) for discharges partly because of the low mean magnitude and high discharge variations because of rainfall storms. Daggar basin also shows the lowest minimum and maximum flows due to rainfall contribution only and the small catchment area. Gorband at Karora shows the lowest standard deviation. Besham Qila, Partab Bridge, and Kachura on the main Indus River are found to have the lowest coefficient of variations, coefficient of skewness, and coefficient of skewness, respectively. This is due to the fact that they represent very large catchments (Table 2.1).

Shigar, the glacier-dominated basin, shows the highest values of mean, maximum, and standard deviation of SSC, followed by Shyok, Kachura, and Hunza. The Indus at Shatial Bridge reaches the highest values of minimum of SSC, which may possibly be due to heterogeneous spells of channel erosion of glacier deposits. During low flow season these glacier deposits might be transported by increase of winter discharges in channel. The Gorband at Karora is found to have the highest coefficient of variations, which could be probably due to the operation of a lot of upstream micro hydropower stations installed by the community. Gilgit, the snow melt-, ice melt-, and rainfall-dominated basin, reaches the highest coefficient of skewness and coefficient of kurtosis of SSC, which may probably be due to dominant snow melts in the basin and increased sediment transport from the upstream catchment. Astore at Doyian, a snowfall-dominated basin, is found to have the lowest SSC in terms of mean, maximum, and standard deviation. Besham Qila shows the lowest coefficient of variations, which is attributed to the fact that it is last downstream station of the UIB, where river hydraulics is the predominant factor rather than upstream catchment erosions. Moreover, the representation of a larger catchment is less prone to variations by short-term local forcings. Hunza at Dainyor shows the lowest value of coefficient of skewness. Probably, more sediments are deposited in the upstream valley and hydraulics of the river with effective discharges from the glacier melts is more dominant, which ensures steady sediment transport. The Indus at Kachura shows the lowest

coefficient of skewness, probably due to high flows and steady SSC contribution along narrow river valleys with less glacier deposits in the channel. It must be noted that flow doubles and SSC is reduced by almost a quarter from Kachura to Besham Qila along the main arm of the Indus River, which means that either the lateral sub-basin downstream of Kachura yields less suspended sediment in comparison to discharges or there is an issue of sediment transport capacity in a reach between these stations.

Table 2. 5 Summary of descriptive statistics of the selected discharge and sediment gauging stations.

Sr #	Gauging Stations	Mean	Min	Max	Std.	Cv (%)	Cs	Ck
				Discharge m³/sec				
1	Hunza at Dainyor	296.75	50.73	508.21	96.59	32.55	−0.37	1.58
2	Gilgit at Gilgit	293.21	83.14	867.86	122.76	41.87	3.42	16.67
3	Gilgit at Alam Bridge	632.39	217.61	1215.64	185.44	29.32	0.58	3.12
4	Indus at Kharmong	452.78	118.94	782.45	140.29	30.98	0.17	1.09
5	Shyok at Yogu	390.07	180.28	545.96	89.29	22.89	−0.15	−0.36
6	Shigar at Shigar	223.25	142.06	330.64	57.44	25.73	0.29	−0.65
7	Indus at Kachura	1192.19	860.16	1547.26	197.44	16.56	0.09	−0.77
8	Indus at Partab Bridge/Bunji	1756.94	865.51	2256.72	369.38	21.02	−0.81	0.3
9	Astore at Doyian	139.9	37.52	232.24	38.58	27.58	−0.22	0.94
10	Indus at Shatial	2167.32	915.99	2981.57	499.73	23.06	−0.58	0.28
11	Indus Besham Qila	2479.37	1858.22	3304.93	378.85	15.28	0.37	−0.55
12	Lower UIB at Daggar	13.84	3.81	129.3	21.85	157.9	5.23	28.41
13	Lower UIB at Karora	18.1	5.89	37.36	7.24	40	0.97	1.26
				Suspended Sediments mg/l				
1	Hunza at Dainyor	1091.44	53.75	2244.65	568.27	52.07	0.03	−0.04
2	Gilgit at Gilgit	441.98	76.82	2169.5	410.59	92.9	2.78	9.94
3	Gilgit at Alam Bridge	795.32	114.47	1971.58	439.5	55.26	0.86	0.53
4	Indus at Kharmong	668.9	138.28	2150.42	537.79	80.4	1.37	1.21
5	Shyok at Yogu	1305.08	128.78	5219.85	1208.13	92.57	1.79	2.96
6	Shigar at Shigar	2395.08	257.48	7571.67	1883.03	78.62	1.6	3.64
7	Indus at Kachura	1171.27	131.29	2390.97	554.23	47.32	0.36	−0.16
8	Indus at Partab Bridge/Bunji	1019.35	306.92	3294.93	658.31	64.58	1.79	4.21
9	Astore at Doyian	295.27	96.8	675.68	164.53	55.72	0.94	0.04
10	Indus at Shatial	919	352.8	1993.22	355.1	38.64	1.32	2.34
11	Indus at Besham Qila	870.71	322.08	1584.57	286.96	32.97	0.43	0.63
12	Lower UIB at Daggar	546.85	76.8	1649.01	401.73	73.46	1.43	1.85
13	Lower UIB at Karora	355.03	48	1739.6	417.81	117.68	2.17	4.54

Note: **Red** color shows highest values and **blue** color indicates the lowest values for both flows and SSC.

2.5.2 Monthly, Seasonal, and Annual Trends of Discharges

Using longer time steps, such as decadal accumulative discharges, means to avoid inter-annual fluctuations when determining long-term trends for the Indus basin [22,49]. In this study, monthly trends of discharges (m³/sec) with 90% confidence interval are determined per decade by using the Sens's slope estimator after the Mann–Kendall trend test, as shown in Table 2.6. For the flows, most

of the stations show increasing trends of discharges in snow- and glacier-dominated basins in the months of from December to June but decreasing discharges in July-August on higher altitudes like Hunza and Kharmong. The Indus at Besham Qila (main UIB), Shatial Bridge (main UIB), Partab Bridge (main UIB), and Kachura (main UIB) and the Astore at Doyian (Western Himalayas) reveal increasing trends of flows per decade in most of the months between November and April. Most of the remaining glacier- and snow-dominated basins, such as Gilgit (Hindukush), Hunza (Western Karakorum), Shigar (Central Karakorum), and Shyok (Western Karakorum), show a significant increase of flows between October and March. However, the Kharmong (Central Himalayas) exhibits a mixed trend in these months.

The Kharmong (Central Himalayas) station shows a significant decrease of flows during the months of December, January, May, and June. In the Lower UIB, the rainfall-dominated Brandu basin at Daggar and Gorband basin at Karora (both in the Lower UIB in the West) mostly show significantly decreasing trends of discharges in the months between December and June. During the months of July, August, and September, an insignificant weak increase or decrease in flows is observed in most of the snow- and glacier-dominated basin. The Hunza at Dainyor (Western Karakorum) and Indus at Kachura (main UIB), however, show significantly decreasing trends of flows in the months of August and September. The lower UIB basins exhibit decreasing trends of flow during the months from July to September. The Gorband basin at Karora (Lower UIB in the West) shows a significant decrease of flows in the months from July to September. In the months of October and November, flows are generally increasing in all the basins except for the Shigar basin.

Table 2.7, Figure 2.2, and Figure 2.4a show the percentage of seasonal and annual changes in mean values of flows on a temporal and spatial basis in the UIB. The winter discharges of the Indus River at Besham Qila (main UIB), Shatial Bridge (main UIB), Partab Bridge (main UIB), and Kachura (main UIB) and of the Astore River at Doyian (Western Himalayas) increase significantly by 3.3–8.5% per decade. The spring discharges of the main (Indus) River at Shatial Bridge (main UIB) and Partab Bridge (main UIB) and of Astore River at Doyian (Western Himalayas) are also significantly increased by 3.3–8.5% per decade. In the Lower UIB, however, the spring discharges of Gorband at Karora (Lower UIB in the West) are reduced significantly by up to 20% of the mean values contrary to the basins containing water from glacier and snow melting. During the summers, there are no significant changes in flows of snow- and glacier-dominated basins except for the Shigar basin. In the Brandu at Daggar and Gorband at Karora (both Lower UIB in the West) the summer flows decrease significantly by up to 23% per decade in both basins. During the autumns, the flows at Besham Qila (main UIB) increase significantly by up to 7.27% per decade, whereas the autumn discharges are reduced significantly in Brandu River at Daggar.

On an annual basis, flows of glacier- and snow-dominated basins do not change significantly, except for the Shigar basin. However, the annual discharges of the rainfall-dominated Brandu at Daggar and Gorband at Karora are reduced significantly by up to 20% per decade.

2.5.3 Monthly, Seasonal, and Annual Trends of Suspended Sediment Concentrations (SSC)

Table 2.6 shows the monthly trends of suspended sediment concentrations (SSC) (mg/L) with 90% significance level, which have been obtained by using the Sens's slope estimation method. In the months from December to May the trends of SSC are mixed in upper sub-basins of the UIB. However, most of the stations located on snow- and glacier-dominated basins show an increase of the SSC from December to May along with, though disproportionate, positive discharge trends. The Indus at Partab Bridge (main UIB) and Shatial Bridge (main UIB), Astore River at Doyian (Western Himalayas), and Gilgit at Alam Bridge (Gilgit + Hunza) show significantly increasing trends of SSC (mg/L) and discharges per decade in the months between December and June. Similarly, Gilgit River at Gilgit (Hindukush) exhibits a major increase of SSC in the months of December, February, and

March. The Indus at Besham Qila shows a significant increase of SSC per decade in the months of December and May. In contrast to this, the Indus at Kharmong (Central Karakorum) and Kachura (main UIB) shows an insignificant reduction of SSC in the months of December, January, and February. Contrary to the upper sub-basins of the UIB, where the SSC is increased in the months from December to May, the Lower UIB exhibits decreased SSC and discharges in the same period. The Lower UIB at Daggar and Karora is found to have a significantly reduced SSC in the months between March and May. During the months from June to October and especially from July to September, most of the glacier- and snow-fed basins show a decrease in SSC. The Gilgit at Gilgit (Hindukush) and Alam Bridge (Gilgit + Hunza), Shoyk River at Yogo (Western Karakorum), and the Indus at Shatial Bridge (main UIB), Kachura (main UIB), and Kharmong (Central Karakorum) show a significant reduction of SSC in the months between June and September with no significant trend in discharges in the same period. In the month of November, the upper glacier- and snow melt-dominated basins of Gilgit at Gilgit (Hindukush), Gilgit at Alam Bridge (Gilgit + Hunza), and Astore at Doyian (Western Himalayas) show a significant increase of SSC. The SSC in the Lower UIB, i.e., in Brandu River at Daggar (Lower UIB in the West) is found to be reduced significantly per decade with an insignificant reduction of discharges during the months of July and August.

The seasonal and annual percentage changes per decade in mean values of SSC on a temporal and spatial basis in the UIB are presented in Table 2.7, Figure 2.3, and Figure 2.4b. Table 2.7 and Figure 2.3 show that during the winter season, SSC values increase significantly by 20%–40% for the basins of Gilgit at Gilgit (Hindukush), Hunza at Dainyor (Western Karakorum), Gilgit at Alam Bridge (Gilgit+Hunza), Astore at Doyian (Western Himalayas), and the Indus at Shatial Bridge (main UIB) and Partab Bridge (main UIB) in the UIB. During the spring season, the basins of Astore at Doyian (Western Himalayas) and Indus at Shatial Bridge (main UIB) and Partab Bridge (main UIB) also show a significant increase in SSC in the range of 14%–33% per decade in mean values. In the rainfall-dominated lower basin of Brandu at Daggar (Lower UIB in the West), however, the SSC decreases by up to 16.8% of its mean value per decade. During the summer season, the SSC levels in the UIB decrease significantly at most of the stations, such as Gilgit at Gilgit, Hunza at Dainyor, Gilgit at Alam Bridge, Shigar at Shigar, Shyok at Yogo, Indus at Kachura, and Brandu at Daggar. In this period, the SSC values of Gilgit at Gilgit (Hindukush), Gilgit at Alam Bridge (Gilgit + Hunza), Kachura (main UIB), and Brandu at Daggar are reduced by 18 to 28% of their mean values per decade. In the autumns, the SSC trends for Gilgit at Alam Bridge (Gilgit + Hunza), Kachura (main UIB), and Brandu at Daggar are also significantly reduced by 15%–28%. As obvious from Figure 2.4b, the annual SSC trends at most of the stations in the UIB decrease except for Astore at Doyian (Western Himalayas), Kharmong (Central Himalayas), and Indus at Shatial Bridge (main UIB). Figure 2.4b and Table 2.7 show that the annual SSC trends of Gilgit at Alam Bridge (Gilgit + Hunza), Indus at Kachura, and Brandu at Daggar) decrease significantly by 18%–28% per decade with no significant reduction of discharges except for Brandu at Daggar.

Table 2. 6 Mann–Kendall trends for monthly time series data and Sen's slope estimates.

Discharge Gauging Stations	January	February	March	April	May	June	July	August	September	October	November	December
Change in Discharge m³/sec per Decade												
Hunza at Dainyor	0.87	0.89	0.66	6.35	**−2.27**	12.13	**−28.64**	**−174.58 ***	5.17	1.71	5.11*	**−1.68**
Gilgit at Gilgit	0.29	0.09	0.9	5.36	55.82*	33.09	53.44	2.22	13.32	19.44 *	5.6	7.39 *
Gilgit at Alam Bridge	1.1	1.3	2.74	19.82 *	19.47	109.07*	21.57	9.62	71.52	31.03 *	18.9 *	12.44
Indus at Kharmong	**−1.44**	0.34	4.88	5.49	**−20.82**	**−3.24**	**−167.82**	**−7.03**	**−41.29**	16.33	7.74	**−1.58**
Shyok at Yogu	2.13 *	2.25 *	0.09	**−1.59**	6.41	58.34	78.54	88.74	12.55	31.21 *	10.3 *	2.01
Shigar at Shigar	1.76	2.98	8.74*	9.58	**−13.7**	176.1	432.67	376.17 *	33.78	−2.54	−1.43	**−1.24**
Indus at Kachura	4.9	10.55 *	10.42 *	2.74	43.95	78.62	279.97	78.77	**−175.18 ***	11.71	4.69	7.43
Indus at Partab Bridge/Bunji	13.8	20.27 *	24.19 *	46.93 *	149.07*	323.34	425.22	135.27	27.06	7.72	27.44 *	14.59
Astore at Doyian	2.62 *	2.76 *	3.93 *	13.86 *	39.44 *	22.06	**−6.72**	7.77	2.01	2.66	3.57	3.57 *
Indus at Shatial Br.	44.17 *	35.96 *	36.19 *	88.64 *	239.08	174.8	173.35	234	71.2	63.88	37.11 *	43.67 *
Indus at Besham Qila	36.31 *	41.08 *	30.48 *	6.96	170.34	16.31	214.18	125	163.75	95.17 *	57.61 *	35.84 *
Lower UIB at Daggar	0.33	0.55 *	**−4.31 ***	**−0.2**	0.1	0.4 *	**−1.45**	**−3.25**	0.01	0.15	0.07	0.2
Lower UIB at Karora	**−0.04**	1.51	**−2.81**	**−7.01 ***	**−7.88 ***	**−3.77 ***	**−5.73 ***	**−4.88 ***	**−2.77***	**−0.78**	**−0.52**	**−1.44**
Change in Suspended Sediments mg/l per Decade												
Hunza at Dainyor	24.03	8.34	42.5	−91.58	3.67	738.07	**−765**	**−1181.35**	**−12.73**	**−35.72**	15	8.67 *
Gilgit at Gilgit	15	15.89 *	17.5 *	18.86	45.53	**−68.77**	**−245.43**	**−472.47 ***	**−24.57**	**−0.21**	15.38 *	17.82 *
Gilgit at Alam Bridge	25 *	16.65 *	32.81	**−9.45**	−31.76	68.82	**−591.67 ***	**−858.57 ***	**−115 ***	**−9.05**	46.82 *	36.75 *
Indus at Kharmong	**−56.95**	**−22.21**	23.93	86.05*	62.67	376.84	**−110.4 ***	**−15.11**	**−167.62**	**−14.53**	2.09	**−5.62**
Shyok at Yogu	8.49	**−16.34**	33.98	108.57 *	43.86	**−458.54 ***	**−34.56**	**−385.34**	**−63.93**	5.21	13.84	32.15
Shigar at Shigar	34.3	74.56	13.89	96.5	201.25	1104.17	**−2175.64**	58.3	712.78	198.34	625.42	87.68
Indus at Kachura	**−42.86**	**−52.18**	71.56	**−156.76 ***	−179.95	39.87	**−699.07 ***	**−667.87**	**−462.05**	**−103.08**	**−103.85**	**−75.11**
Indus at Partab Bridge/Bunji	25.61 *	42.75 *	28.52 *	37.15 *	−108.62	154.05	137.87	**−201.63**	**−230.23**	14.17	2.55	20.53*
Astore at Doyian	21.09 *	32.34 *	8.69	45.49 *	60.98 *	13.55	**−41.11**	**−13.91**	54.9 *	19.53	22.15 *	17.5
Indus at Shatial Br.	50 *	38.61 *	95 *	146.1 *	117.97 *	−141.98	174.12	411.86	**−11.62 ***	**−0.96**	23.22	24.88

Indus at Besham Qila	9.01 *	4.56	6.07	13.04	182.16 *	142.51	**−34.44**	**−222.47**	26.9	**−18.22**	0.32	1.28
Lower UIB at Daggar	3.58	**−8.16**	**−64.75 ***	**−54.38 ***	−16.14 *	**−21.98**	**−544.84 ***	**−219.64 ***	**−67.85**	0.87	1	12.6
Lower UIB at Karora	5.79	7.54	**−34.13 ***	**−31.57**	−5.66	2.25	**−57.05**	11.96	6.71	**−4.07**	3.45	16.6

Note: * significant level 90%, negative values are in bold.

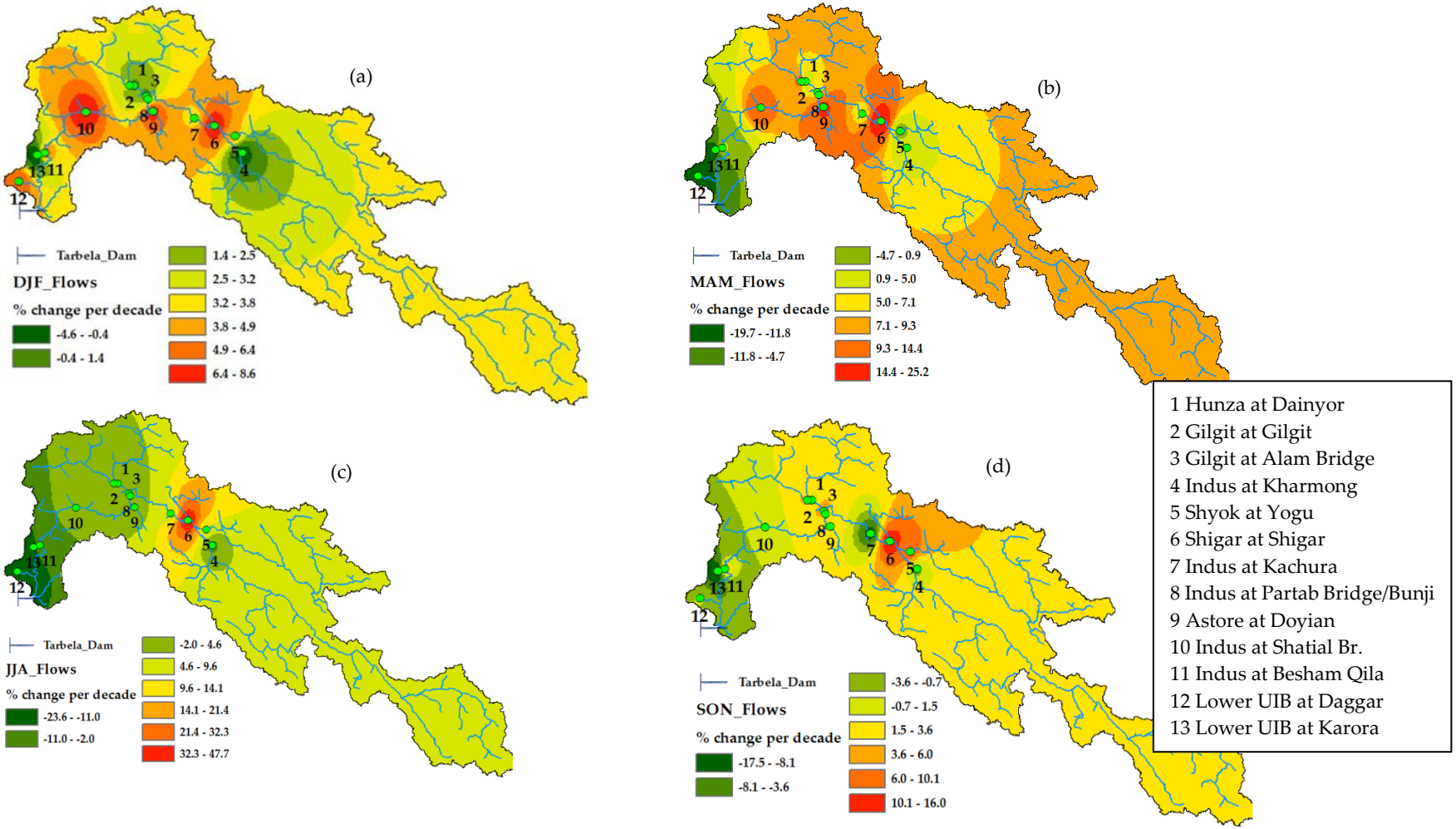

Figure 2. 2 Seasonal flow trends spatially distributed over the basin with % of changes per decade in % of mean values for the whole period. (**a**) DJF (winter), (**b**) MAM (spring), (**c**) JJA (summer), (**d**) SON (autumn) seasons.

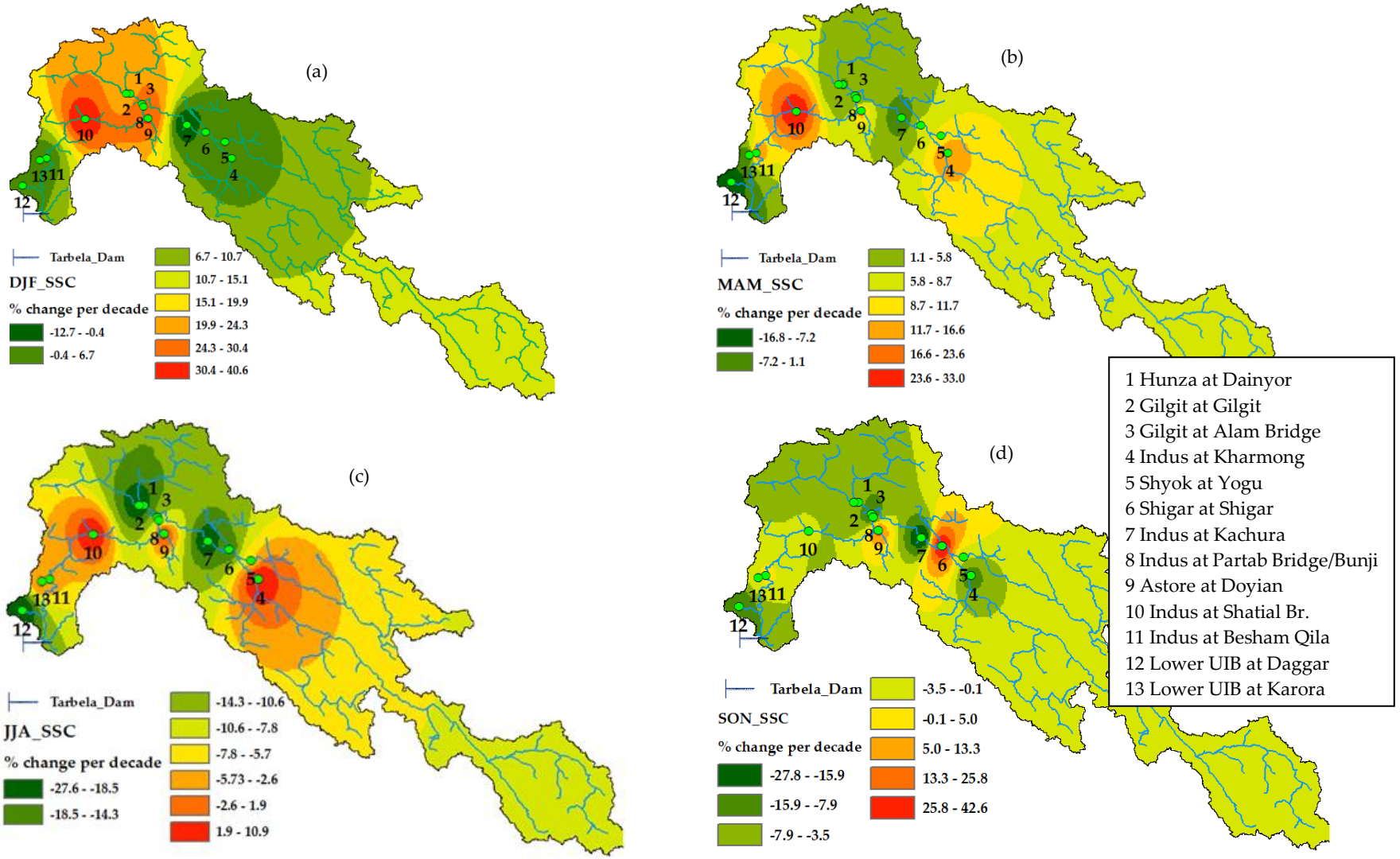

Figure 2. 3 Seasonal suspended sediment concentration (SSC) trends spatially distributed over the basin with % of changes per decade in % of mean values for the whole period. (a) DJF (winter), (b) MAM (spring), (c) JJA (summer), (d) SON (autumn) seasons.

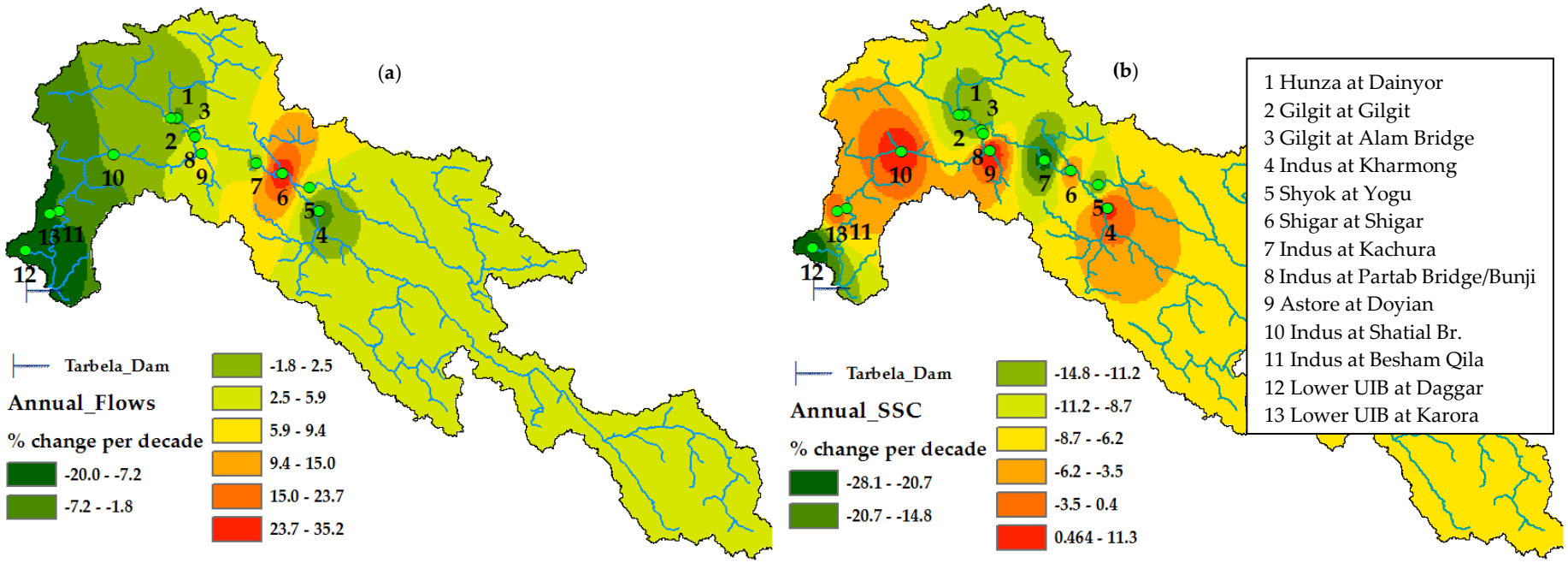

Figure 2. 4 Annual flow and suspended sediment concentration (SSC) trends spatially distributed over the basin with % of changes per decade in % of mean values for the whole period. (**a**) Annual flows, (**b**) annual SSC.

Table 2. 7 Annual and seasonal percentage changes per decade for mean of data periods.

Sr #	Discharge Gauging Stations	DJF (%)	MAM (%)	JJA (%)	SON (%)	Annual (%)
Per Decade % of Change in Discharge for Average Data Periods						
1	Hunza at Dainyor	0.41	**−2.74**	**−4.25**	**−1.26**	**−7.64**
2	Gilgit at Gilgit	3.27	14.16	4.18	5.66	5.85
3	Gilgit at Alam Bridge	**−0.46**	3.33*	4.13	7.93	4.29
4	Indus at Kharmong	**−1.95**	2.41	**−4.42**	**−1.55**	**−5.37**
5	Shyok at Yogu	4.36	**−1.88**	9.1	8.67	3.35
6	Shigar at Shigar	8.74	25.52	47.88 *	16.11	35.38 *
7	Indus at Kachura	3.32*	4.3	5.28	**−10.37 ***	0.6
8	Indus at Partab Bridge/Bunji	3.51*	9.6 *	3.18	0.44	1.14
9	Astore at Doyian	8.22 *	18.59 *	0.96	2.1	8.84
10	Indus at Shatial Br.	8.49 *	13.58 *	3.96	**−0.42**	**−1.49**
11	Indus at Besham Qila	6.95 *	5.82	0.42	7.27 *	**−0.71**
12	Lower UIB at Daggar	6.62	**−19.8**	**−23.61 ***	**−0.65**	**−18.30 ***
13	Lower UIB at Karora	**−4.84**	**−19.82 ***	**−22.92 ***	**−17.89 ***	**−20.34 ***
Per Decade % of Change in Suspended Sediments for Average Data Periods						
1	Hunza at Dainyor	20.08 *	**−0.84**	**−18.53**	**−7.6**	**−17.66**
2	Gilgit at Gilgit	20.27 *	3.98	**−27.79 ***	**−2.52**	**−10.28**
3	Gilgit at Alam Bridge	29.03 *	2.57	**−18.63 ***	**−21.37 ***	**−18.56 ***
4	Indus at Kharmong	3.39	16.49	10.91	**−11.73**	2.46
5	Shyok at Yogu	2.52	8.85	**−6.59**	**−3.68**	**−14.29**
6	Shigar at Shigar	1.89	6.55	**−17.3**	42.87	**−2.2**
7	Indus at Kachura	**−12.77**	**−5.96**	**−23.84 ***	**−27.87 ***	**−24.06 ***
8	Indus at Partab Bridge/Bunji	28.76 *	**−2.01**	**−3.97**	**−6.57**	**−9.43**
9	Astore at Doyian	31.86 *	14.6 *	4.93	18.19	11.87
10	Indus at Shatial Br.	40.72 *	33.11 *	7.68	**−2.84**	5.75
11	Indus at Besham Qila	2.68	19.9 *	−5.75	1.8	**−4.51**
12	Lower UIB at Daggar	0.84	**−16.88 ***	**−24.85 ***	**−15.56 ***	**−28.2 ***
13	Lower UIB at Karora	5.05	**−5.73**	**−1.38**	**−2.44**	**−0.74**

Note: * significant level 90%, negative values are in bold.

2.5.4 Mean Basin Precipitation Trends

Total changes in the basin's monthly precipitation (mm) for three decades (1981–2010) are shown in Table 2.8. In the winter months from December to January, there is an increase of precipitation in most of the basins probably due to increase of westerlies rainfall. In the month of February, Gilgit at Alam Bridge (Gilgit + Hunza) shows a significant increase in the basin-averaged precipitation, which is probably due to the effect of the Western front of the Hindukush during winters. During the spring months of March and April, precipitation is lowest, except in the Gilgit (Hindukush) basin. The month of March is the driest period in all basins.

In the springs, the basins of Gilgit at Gilgit (Hindukush) and Gilgit at Alam Bridge (Gilgit + Hunza) show a very wet period in the month of April. However, the Shyok at Yogo (Easter Karakorum), Astore at Doyian (Northwestern Himalayas), Brandu at Daggar (Lower UIB in the West), and Gorband at Karora (Lower UIB in the West) exhibit the driest trends in March. Drying in March can be found at almost all stations, except for Shigar. During the summer seasons, most of the stations show an increase in rainfall. The stations of Gilgit at Gilgit (Hindukush) and Gilgit at Alam Bridge (Gilgit + Hunza) record a significant increase in rainfall in the months of June and July. During the summer months, however, the rainfall-dominated basins of Brandu at Daggar (Lower UIB in the

West) and Gorband at Karora (Lower UIB in the West) show reduced rainfall, except for the month of June. In the autumns, from September to November, there is an increase of precipitation in the UIB. In the month of October, however, precipitation generally is reduced in the UIB.

2.5.5 Mean Monthly Average Temperature Trends

Table 2.9 shows the change in mean monthly average temperature (°C) between 1981 and 2010. The temperature trends of 18 meteorological stations located at different altitudes in UIB are shown with ascending altitude. Generally, most of the stations at higher and lower altitudes of the UIB show warming trends during the months of February and March. The Gilgit station at 1460 m altitude shows a significant increase in average temperature in the range of 1.23–3.02 °C during the months of January, February, and March. During the months of February, March, and April, the average temperature increases by 0.58–4 °C at altitudes from 1250 m to 4440 m. In the late springs and early summers, i.e., in the months of May and June, there is an insignificant increase of average temperature at most of the higher and lower altitudes of the UIB. During summers and early autumns, i.e., in the months of July, August, and September, however, there is generally a cooling trend ranging from 0.03–1.87 °C. The stations of Gilgit in Giglit (Hindukush), Gupis in Gilgit (Hindukush), Chillas (Main UIB), and Skradu (Main UIB) show a significant decrease of average temperature by 1.34–1.87 °C during summers and early autumns. In the late autumns, average temperature increases again. In the months of October and November, temperatures at higher altitudes increase at higher rates (0.97–2.38 °C) than valley stations (Table 2.9).

Table 2. 8 Total changes in monthly precipitation (mm) extracted from the grid data for the Upper Indus Basin (UIB) from 1981 to 2010.

Ser #	Basin	Region	Elevation (m)	January	February	March	April	May	June	July	August	September	October	November	December
1	Hunza	Western Karakorum	3996	0.0	0.0	0.0	0.3	0.0	0.9	−0.1	0.5	0.2	0.0	0.0	0.0
2	Gilgit	Hindukush	4053	27.6	38.8	−5.4	**122.6**	12.1	**44.6**	**29.2**	17.2	11.9	−0.8	11.8	−4.4
3	Alam Br.	Hunza + Gilgit	4550	39.4	**49.5**	−21.4	**96.7**	6.3	**41.4**	17.8	14.0	8.0	−3.0	6.9	−5.5
4	Kharmong	Central Himalayas	4798	8.7	−28.8	−95.4	−23.1	0.1	14.3	−21.4	5.9	3.9	−0.8	6.8	−1.1
5	Shyok	Eastern Karakorum	5094	4.7	−16.3	**−103.0**	5.6	−3.4	1.0	−20.8	17.6	13.3	−2.3	2.3	−11.6
6	Shigar	Central Karakorum	4497	241.3	256.7	104.5	88.3	84.4	44.1	41.0	−26.5	**49.2**	−13.1	−1.3	−38.9
7	Kachura	Main River UIB	4922	27.8	47.8	−86.2	32.0	−1.9	9.9	−1.6	16.8	9.3	−2.0	5.0	−1.8
8	Bunji	Main River UIB	4541	24.7	61.0	−81.2	50.2	−2.1	9.4	1.8	14.6	8.1	−1.0	4.9	0.3
9	Astore	North Western Himalayas	3996	48.9	57.1	**−174.3**	45.6	−10.7	11.5	1.2	−10.3	−1.7	−13.8	0.2	−11.9
10	Shatial	Main River UIB	4488	26.3	56.0	−83.1	46.8	−2.7	8.7	0.9	15.2	8.5	−1.7	5.1	−0.9
11	Besham Qila	Main River UIB	4312	26.2	56.3	−83.1	47.0	−2.8	8.8	0.9	14.9	8.5	−1.7	5.1	−0.5
12	Daggar	Lower Western UIB	1111	5.9	25.2	**−178.1**	−48.6	−19.5	**35.4**	−7.1	−50.5	12.1	−23.4	8.5	−19.6
13	Gorband	Lower Western UIB	2257	21.9	6.9	**−217.1**	−45.1	−22.4	**43.9**	−20.1	−42.3	11.5	−25.3	12.8	−25.1
14	Tarbela	UIB	4421	25.7	29.7	**−107.9**	27.2	−19.7	14.8	−8.5	2.2	2.2	−6.1	2.7	−9.2

Note: Values in a box and written in bold represent the highest values of rainfall in mm with 90% significant level. Red color reflects the months of reduced precipitation (driest), blue color indicates the months with highest increased of precipitations (wettest).

Table 2. 9 Changes in mean monthly averaged temperatures (°C) from 1981 to 2010 for stations located at different altitudes in the Upper Indus Basin (UIB).

Ser #	Station	Sub-Basin	Elevation (m)	January	February	March	April	May	June	July	August	September	October	November	December
1	Chilas	Besham Qila	1250	0.54	0.72	**2.35**	−0.13	0.24	−28	−1.12	**−1.68**	−1.16	0.77	0.24	−0.06
2	Bunji	Partab Br.	1372	1.08	1.46	**3.23**	**0.52**	0.98	0.31	−1.05	−1.21	−0.13	0.99	**1.12**	0.58
3	Gilgit	Gilgit	1460	**1.23**	**1.89**	**3.02**	0.23	0.92	0.64	−1.11	**−1.34**	−0.50	0.61	**0.97**	0.76
4	Shangla	Gorband	1960	0.99	1.52	3.24	**1.63**	**1.51**	0.21	0.31	0.18	−0.08	1.08	0.82	0.68
5	Gupis	Gilgit	2156	−0.26	−0.14	1.79	−0.35	−0.28	−0.01	**−1.87**	−1.29	−0.53	**2.44**	0.98	−0.47
6	Astore	Astore	2168	0.98	**2.43**	**3.13**	1.30	0.94	**1.48**	0.00	−0.51	0.27	1.01	**1.67**	0.61
7	Skardu	Shigar	2210	−0.69	−1.03	−0.26	0.36	0.83	0.92	0.08	−0.68	−0.43	0.69	0.58	−0.05
8	Skardu	Main Kachura	2210	1.11	1.63	1.87	0.29	−0.21	−0.01	−0.80	−0.92	**−1.60**	−0.35	0.83	−0.23
9	Raitu	Astore	2718	1.17	**2.61**	**3.19**	**2.07**	1.37	0.91	0.55	0.23	−0.07	**1.94**	**1.03**	0.23
10	Naltar	Hunza	2898	1.16	**1.74**	**2.86**	1.29	0.66	1.26	0.16	0.32	0.36	**1.86**	**1.63**	0.60
11	Ziarat	Hunza	3020	1.18	**1.99**	**3.05**	**1.46**	0.69	1.21	0.37	0.46	0.49	**1.85**	**2.16**	1.25
12	Ushkore	Gilgit	3051	1.07	**2.20**	**2.68**	1.43	0.66	0.95	−0.27	−0.06	−0.16	**1.95**	1.19	0.34
13	Hushey	Shyok	3075	0.81	**1.77**	**3.54**	1.47	1.12	0.82	0.70	0.56	0.74	**1.67**	**1.80**	1.27
14	Rama	Astore	3179	1.02	**1.88**	**3.17**	**1.58**	0.93	0.60	0.46	0.30	0.18	**1.60**	0.99	0.50
15	Yasin	Gilgit	3280	1.13	**1.56**	**2.81**	1.20	0.69	1.47	−0.23	0.04	−0.20	1.47	−0.02	**−1.44**
16	Shendure	Gilgit	3712	1.20	**1.98**	**2.17**	1.23	0.80	0.95	−0.03	0.03	−0.21	**2.07**	0.59	0.20
17	Desosai	Kharmong	4149	1.00	**1.53**	**3.15**	**1.56**	1.23	1.35	1.06	0.24	0.44	**1.86**	1.20	0.71
18	Khunjrab	Hunza	4440	1.38	**1.87**	**4.00**	**1.79**	1.56	**1.37**	0.22	0.44	0.66	**2.01**	**2.38**	1.01

Note: Values in a box and written in bold represent the highest values of average temperature (°C) at station altitudes with 90% significant level. Red color reflects an increase in monthly temperature (warming), blue color indicates decrease in monthly temperature (cooling).

2.5.6 Pearson's Correlations between Flows, SSC and Gridded Climatic Variables

To evaluate the dominancy of different hydro-climatic variable in flows and sediment generation process the correlation between these variables was find out. The Table 2.10 shows the results of Pearson's correlations coefficients between the daily flows, SSC and gridded basin averaged rainfall and basin averaged mean air temperature. The Table 2.10 describes that correlation coefficient between flows and SSC is more significant on main Indus River for example; Indus at Shatial Bridge and Indus at Besham Qila. However, in the glacier and snow dominated basins, the correlation between flows and SSC is less significant in most of the sub basins compared to the main Indus River. Similarly, in lower UIB sub basins, the correlation between flows and SSC is least significant.

The correlation coefficient between flows/SSC and gridded basin averaged rainfall is non-significant on main Indus River as well as at glacierized snow and ice melted dominated sub basins. However, in lower UIB at Daggar the gridded basin averaged rainfall is better correlated than temperature. The gauging stations lying on the main Indus River as well in snow and ice melted sub basins showed significant correlations between flows/SSC and gridded basin averaged mean air temperature. Ali K.F et al. [37] found that the percent of snow/ice cover (LCs) is major land cover controlling parameter along with temperature and seasonal rainfall. Ali K.F et al. [37] also found that the combination of snow/ice cover (LCs) and climatic variables explain 98.5% of variance in sediment yield in UIB. Similarly, for the lower monsoon dominated UIB, the mean annual rainfall explains the 99.4% of variance in sediment yields.

Table 2. 10 Pearson's correlations between daily flows, SSC and gridded climatic datasets since 1981–2010 in the Upper Indus Basin (UIB).

Ser #	Discharge Gauging Stations	Region	Pearson Correlations		
			Q vs. SSC	Q vs. R	Q vs. Tavg
1	Hunza at Dainyor	Western Karakorum	0.51	−0.01	0.77
2	Gilgit at Gilgit	Hindukush	0.73	0.04	0.82
3	Gilgit at Alam Bridge	Hunza + Gilgit	0.64	−0.06	0.80
4	Indus at Kharmong	Central Himalayas	0.23	0.14	0.79
5	Shyok at Yogu	Eastern Karakorum	0.46	0.06	0.74
6	Shigar at Shigar	Central Karakorum	0.49	−0.02	0.72
7	Indus at Kachura	Main River UIB	0.68	−0.14	0.79
8	Astore at Doyian	North Western Himalayas	0.27	0.04	0.71
9	Indus at Partab Bridge/Bunji	Main River UIB	0.62	0.03	0.77
10	Indus at Shatial Br.	Main River UIB	0.75	0.03	0.80
11	Indus at Besham Qila	Main River UIB	0.73	0.01	0.80
12	Lower UIB at Daggar	Lower western UIB	0.47	0.37	0.05
13	Lower UIB at Karora	Lower western UIB	0.11	0.13	0.11

2.6 Discussion

Except for Kharmong and Astore, the annual trends of the SSC in the glacier- and snow-dominated basins of the UIB decrease in the months of July, August, and September, which is due to less snow/glacial melt in the cooler summer, as was reported by researchers [7,8,38,39]. In contrast to the SSC trend, an insignificant increase or no change in annual flows is detected, as is shown in Tables 2.6 and 2.7. Despite the cooler summer that leads to fewer discharges in glacierized upper basins like Hunza, Kharmong, and

Astore, the absence of a significantly negative trend at Besham Qila indicates that this decrease is compensated by increased discharges from other sub-basins of the UIB.

During the winter season, Gilgit (Hindukush) and Hunza (Western Karakorum) show a significant increase of SSC along with discharges. This might be associated partly with a significant increase in the average winter temperature and an insignificant increase of precipitation due to westerlies in winter. Increasing temperature increases the snow melting rates and reduces seasonal precipitation in the form of snow during winters, which may lead to increased erosions in the catchment. A similar trend of an increase in SSC during the winter is observed for the basins of Astore (Northwestern Himalayas), Gilgit at Alam Bridge (Hunza + Gilgit), Indus at Partab Bridge (Main UIB), and Indus at Shatial Bridge (Main UIB), along with a significant increase of average temperature in the UIB.

During the spring season, the Astore at Doyian (Northwestern Himalayas), Indus at Shatial Bridge (Main UIB), Indus at Besham Qila (UIB), as well as Gilgit at Alam Bridge show a significant increase of SSC with a major increase in flows. The Indus at Kharmong and Shigar at Yogo show an insignificant increase of SSC and discharges. The increased flows in the river might result in an increase in effective discharges and erosion of the deposited sediments. Moreover, the sources of sediments in the glacial and snow melt-dominated catchments might be activated by rapid melting of snow accumulated in winter because of increasing temperatures in February and March. In the lower rainfall-dominated Daggar basin (Lower UIB), however, the SSC in springs decreases significantly with decreasing flows, which could probably be due to a reduction of spring rainfall. Table 2.8 shows that the rainfall at Daggar, Gorband, and Besham Qila in the Lower UIB decreases significantly in March, April, and May.

During the summer season, the SSC decreases in glacier-dominated basins, such as Gilgit (Hindukush), Hunza (Western Karakorum), Shigar (Central Karakorum), and Shyok at Yogo. This reduction of SSC in the summer at Gilgit (Hindukush) could be due to significant cooling of the summer temperature (Indus climate anomaly). Cooling of the summer temperature can be observed up to 3000 m altitude in the Gilgit basin. As in the UIB, many glaciers are located at elevations from 2500 to 7000 m. Seasonal snow accumulates in the elevation zone from 3000 m to 7000 m. Furguson [50] describes that in UIB the mass movement, supraglacial and sub glacial sediments transport supply large amount sediments in valley. These sediments are stored in alluvial fans, outwash trains and moraines. The sediment is mainly transported by snow and ice melt process. Collins [51] estimated that for Hunza basin and Indus at Bashem Qila drives 60% and 40% of sediment loads annually from glacier melting. Own et al. [52] concluded that debris transport is an important contributor in glacierized regions of the UIB. Glacier debris transport yields a large amount of coarse rock debris and sediments from the basal traction zone. The debris-covered glacier in the UIB lies below 3000 m [36,40]. This debris cover accelerates/deaccelerates melting [53,54]. This significant cooling of summer temperature up to 3000 m altitude probably reduces the supply of snow water from debris-covered glaciers and may increase the snow cover at lower and middle altitudes. This might result in a reduced SSC at the outlet. The Indus at Kachura also shows a decreasing trend of SSC over the entire year with a significant reduction in summers and autumns, which is probably also due to reduced temperatures and, hence, smaller snow water discharge rates in these months. In the Daggar (Lower UIB) basin, the SSC and flows are reduced significantly during summer, which is probably caused by a smaller rainfall intensity leading to smaller flows, sediment yields, and catchment erosion in the months of July and August.

In the autumn season, mixed trends of SSC are observed. Table 2.8 shows no significate change in precipitation during autumns. During the month of October, however, precipitation amounts generally are reduced in comparison to the precipitations of September and November. Moreover, as shown in Table 2.9, the month of September shows a lower average temperature at lower altitudes. So, the reduction of summer

SSC from the UIB could probably be due to an increase in precipitation in the form of snow and a decrease of rainfall amount.

2.7 Conclusions

It may be concluded that the annual flows and SSC in the upper Indus Basin at Besham Qila are in a balanced state with a small reduction during the analysis period of three decades. However, the annual SSC values in the upper snow- and glacier-dominated Hindukush and Karakorum basins decrease, whereas the values of the mixed snow melt- and rainfall-dominated Western and Central Himalayan basins increase. The significant SSC reduction in the Hindukush and Western Karakorum basins during summers could be attributed to the Karakorum climate anomaly [7,8]. During winters, SSC values increase along with flows due to increasing temperatures in the glacier- and snow-dominated basins. In the lower basins of Daggar and Gorband near Besham Qila, the SSC and flows decrease significantly during the spring, autumn, and summer seasons when rainfalls decrease. Contrary to the summer's SSC pattern, the reduced SSC at Kachura, coupled with increasing trends of SSC at Partab Bridge and Shatial Bridge on the main River during winter and spring, confirming the findings of [55] that sediments are deposited in the summer and erosion takes place in winter and spring between Kachura and Besham Qila. Moreover, winter erosion might cause increasing trends of discharges in this area, which may enhance the capacity of the river to erode and transport the suspended sediment. Summer sediment deposition in this area in the absence of any significant discharge trends might be due to natural morpho-dynamic processes to compensate winter erosion and maintain the balanced flow regime. These findings improve understanding of the erosion process in different sub-basins of the UIB and, sediment erosion/deposition and transport in the Indus River. Now, sediment budgets can be determined in the light of climate change. Moreover, the analysis of altering patterns of precipitation, temperature, and flow and their impacts on the SSC values of different sub-basins of the UIB will be important for the management of existing (by developing appropriate reservoir operation scenarios), and the design of future hydraulic structures on the Indus and its tributaries in the UIB. This study will also help investigate the changing patterns of water quality, ecosystems, and geomorphology of the rivers of the UIB.

2.8 References

1. Milliman, J.D.; Syvitski, J.P.M. Geomorphic/Tectonic Control of Sediment Discharge to the Ocean: The Importance of Small Mountainous Rivers. *J. Geol.* **1992**, *100*, 525–544, doi:10.1086/629606.
2. Costa, A.; Molnar, P.; Stutenbecker, L.; Bakker, M.; Silva, T.A.; Schlunegger, F.; Lane, S.N.; Loizeau, J.L.; Girardclos, S. Temperature signal in suspended sediment export from an Alpine catchment. *Hydrol. Earth Syst. Sci.* **2018**, *22*, 509–528, doi:10.5194/hess-22-509-2018.
3. Costa, A.; Anghileri, D.; Molnar, P. Hydroclimatic control on suspended sediment dynamics of a regulated Alpine catchment: A conceptual approach. *Hydrol. Earth Syst. Sci*. **2018**, *22*, 3421–3434, doi:10.5194/hess-22-3421-2018.
4. Babur, M. Assessment of Climate Change Impact on Reservoir Inflows Using Multi Climate Models under RCPs—The Case of Mangla Dam in Pakistan. *Water* **2016**, *8*, 389.
5. Kreft, S.; Eckstein, D.; Melchior, I. *Global Climate Risk Index 2017: Who Suffers Most From Extreme Weather Events? Weather-related Loss Events in 2015 and 1996 to 2015*; Germanwatch Nord-Süd Initiative e V: Bonn, Germany, 2016; ISBN 978-3-943704-49-5.
6. Khan, N.M.; Tingsanchali, T. Optimization and simulation of reservoir operation with sediment evacuation: A case study of the Tarbela Dam, Pakistan. *Hydrol. Process.* **2009**, *23*, 730–747, doi:10.1002/hyp.7173.
7. Hewitt, K. The Karakorum Anomaly? Glacier Expansion and the 'Elevation Effect,' Karakorum Himalaya. *Mt. Res. Dev.* **2005**, *25*, 332–340, doi:10.1659/0276-4741(2005)025[0332:TKAGEA]2.0.CO;2.

8. Lutz, A.F.; Immerzeel, W.W.; Kraaijenbrink, P.D.A.; Shrestha, A.B.; Bierkens, M.F.P. Climate Change Impacts on the Upper Indus Hydrology: Sources, Shifts and Extremes. *PLoS ONE* **2016**, *11*, e0165630, doi:10.1371/journal.pone.0165630.
9. Yamamoto, R.; Iwashima, T.; Sanga, N.K.; Hoshiai, M. An Analysis of Climatic Jump. *J. Meteorol. Soc. Jpn.* **1986**, *64*, 273–281, doi:10.2151/jmsj1965.64.2_273.
10. Fu, C.B.; Wang, Q. The Definition and Detection of the Abrupt Climatic Change. *Chin. J. Atmos. Sci.* **1992**, *16*, 482–493.
11. Montgomery, D.C.; Peck, E.A. *Introduction to Linear Regression Analysis*; Wiley: New York, NY, USA; Chichester, UK, 1982; ISBN 0471058505.
12. Mann, H.B. Nonparametric Tests Against Trend. *Econometrica* **1945**, *13*, 245, doi:10.2307/1907187.
13. Gerstengarbe, F.W.; Werner, P.C. Estimation of the beginning and end of recurrent events within a climate regime. *Clim. Res.* **1999**, *11*, 97–107, doi:10.3354/cr011097.
14. Bradley, J.V. *Distribution-Free Statistical Tests*; Prentice-Hall: Englewood Cliffs, NJ, USA, 1968.
15. Iman, R.L. *Modern Approach to Statistics*; Wiley: New York, USA, 1983; ISBN 978-0471096672.
16. Pettitt, A.N. A Non-Parametric Approach to the Change-Point Problem. *Appl. Stat.* **1979**, *28*, 126–135, doi:10.2307/2346729.
17. Shen, D.; Bao, W.; Ni, P. A Method for Detecting Abrupt Change of Sediment Discharge in the Loess Plateau, China. *Water* **2018**, *10*, 1183, doi:10.3390/w10091183.
18. Ali, K.F.; De Boer, D.H. Spatial patterns and variation of suspended sediment yield in the upper Indus River basin, northern Pakistan. *J. Hydrol.* **2007**, *334*, 368–387, doi:10.1016/j.jhydrol.2006.10.013.
19. Ali, K.F.; De Boer, D.H. Construction of sediment budgets in large-scale drainage basins: The case of the upper Indus River. *Iahs-Aish Publ.* **2003**, *279*, 206–215.
20. Ali, K.F.; De Boer, D.H. Spatially distributed erosion and sediment yield modeling in the upper Indus River basin. *Water Resour. Res. Water Resour. Res* **2010**, *46*, doi:10.1029/2009WR008762.
21. Gao, P.; Zhang, X.; Mu, X.; Wang, F.; Li, R.; Zhang, X. Trend and change-point analyses of streamflow and sediment discharge in the Yellow River during 1950–2005. *Hydrol. Sci. J.* **2010**, *55*, 275–285, doi:10.1080/02626660903546191.
22. Ateeq-Ur-Rehman, S.; Bui, M.; Rutschmann, P. Variability and Trend Detection in the Sediment Load of the Upper Indus River. *Water* **2018**, *10*, 16, doi:10.3390/w10010016.
23. Tarar, Z.; Ahmad, S.; Ahmad, I.; Majid, Z. Detection of Sediment Trends Using Wavelet Transforms in the Upper Indus River. *Water* **2018**, *10*, 918, doi:10.3390/w10070918.
24. Meadows, A.; Meadows, P.S. *The Indus River*. *Biodiversity, Resources, Humankind*; Azra. M., Peter, S., Eds.; Oxford University Press for the Linnean Society of London: Oxford, UK, 1999; ISBN 0195779053.
25. Ahmad, N. *Water Resources of Pakistan and Their Utilization*; Nazir Ahmad; Shahzad Nazir: Lahore Pakistan, *Pakistan*, 1993.
26. Pakistan Water Sector Strategy. *Executive Summary; Report; Ministry of Water and Power, Office of the Chief Engineering Advisor/Chairman Federal Flood Commission*; Govt of Pakistan: Islamabad, Pakistan, 2002; Volume 1.
27. Pakistan Water Gateway. *The Pakistan Water Situational Analysis; Report; Consultative Process in Pakistan (WCD CPP) Project*; Pakistan Water Gateway; Islamabad, Pakistan: 2005.
28. Khan, A.; Richards, K.; Parker, G.; Mcrobie, F.; Mukhopadhyay, B. How large is the Upper Indus Basin? The pitfalls of auto-delineation using DEMs. *J. Hydrol.* **2014**, *509*, 442–453, doi:10.1016/j.jhydrol.2013.11.028.
29. Ali, G.; Hasson, S.u.; Khan, A. *Climate Change: Implications and Adaptation of Water Resources in Pakistan, GCISC-RR-13, Global Change Impact Studies Centre (GCISC)*; Global Change Impact Studies Centre: Islamabad, Pakistan, 2009, doi:10.13140/RG.2.1.4533.9689.
30. Hewitt, K. Glacier Change, Concentration, and Elevation Effects in the Karakorum Himalaya, Upper Indus Basin. *Mt. Res. Dev.* **2011**, *31*, 188–200, doi:10.1659/MRD-JOURNAL-D-11-00020.1.

31. Winiger, M.; Gumpert, M.; Yamout, H. Karakorum-Hindukush-western Himalaya: Assessing high-altitude water resources. *Hydrol. Process.* **2005**, *19*, 2329–2338, doi:10.1002/hyp.5887.
32. Batura Investigations Group: The Batura Glacier in the Karakorum Mountains and its variations. *Sci. Sin*. **1979**, *22*, 958–974.
33. Wake, C.P. Snow accumulation studies in the central Karakorum. In Proceedinds of the Eastern Snow Conference 44th Annual Meeting Fredericton, New Brunswick, Canada, 3–4 June 1987; pp. 19–33.
34. Hewitt, K. Tributary glacier surges: An exceptional concentration at Panmah Glacier, Karakorum Himalaya. *J. Glaciol.* **2007**, *53*, 181–188, doi:10.3189/172756507782202829.
35. Young, G.J.; Hewitt, K. Glaciohydrological features of the Karakorum Himalaya: Measurements possibilities and constraints. *IAHS Publ.* **1993**, *218*, 273–283.
36. Khan, A.; Naz, B.; Bowling, L. Separating snow, clean and debris covered ice in the Upper Indus Basin, Hindukush-Karakorum-Himalayas, using Landsat images between 1998–2002. *J. Hydrol.* **2014**, *521*, doi:10.1016/j.jhydrol.2014.11.048.
37. Ali, K.F.; De Boer, D.H. Factors controlling specific sediment yield in the upper Indus River basin, northern Pakistan. *Hydrol. Process* **2008**, *22*, 3102–114, doi:10.1002/hyp.6896.
38. Arfan, M.; Lund, J.; Hassan, D.; Saleem, M.; Ahmad, A. Assessment of Spatial and Temporal Flow Variability of the Indus River. *Resources* **2019**, *8*, 103, doi:10.3390/resources8020103.
39. Hasson, S.U.; Böhner, J.; Lucarini, V. Prevailing climatic trends and runoff response from Hindukush-Karakorum-Himalaya, upper Indus Basin. *Earth Syst. Dyn.* **2017**, *8*, 337–355, doi:10.5194/esd-8-337-2017.
40. Immerzeel, W.W.; Wanders, N.; Lutz, A.F.; Shea, J.M.; Bierkens, M.F.P. Reconciling high-altitude precipitation in the upper Indus basin with glacier mass balances and runoff. *Hydrol. Earth Syst. Sci.* **2015**, *19*, 4673–4687, doi:10.5194/hess-19-4673-2015.
41. Lutz, A.F.; Immerzeel, W.W. HI-AWARE Reference Component 1. Climate Dataset for the Indus, Ganges and Brahmaputra River Basins. *FutureWater Rep.* **2015**, *146*. Available online: https://www.futurewater.eu/wpcontent/uploads/2015/10/Report_IGB_historical_climate_dataset.pdf (accessed on 06.03.2018).
42. GLIMS, and National Snow and Ice Data Center. *GLIMS Glacier Database. Glaciers in the Karakorum Mountain Region*; National Snow and Ice Data Center: Boulder, CO, USA, 2012, doi:10.7265/N5V98602.
43. Sinha, T.; Cherkauer, K.A. Time Series Analysis of Soil Freeze and Thaw Processes in Indiana. *J. Hydrometeorol.* **2008**, *9*, 936–950, doi:10.1175/2008JHM934.1.
44. Hamed, K.H.; Ramachandra Rao, A. A modified Mann-Kendall trend test for autocorrelated data. *J. Hydrol.* **1998**, *204*, 182–196, doi:10.1016/S0022-1694(97)00125-X.
45. Kendall, M.G. *Rank Correlation Methods*, 4th ed.; Griffin: London, UK, 1970; ISBN 978-0-85-264199-6.
46. Ahmed, K.; Shahid, S.; Wang, X.; Nawaz, N.; Khan, N. Spatiotemporal changes in aridity of Pakistan during 1901–2016. *Hydrol. Earth Syst. Sci.* **2019**, *23*, 3081–3096, doi:10.5194/hess-23-3081-2019.
47. Gao, P.; Geissen, V.; Ritsema, C.J.; Mu, X.-M.; Wang, F. Impact of climate change and anthropogenic activities on stream flow and sediment discharge in the Wei River basin, China. *Hydrol. Earth Syst. Sci.* **2013**, *17*, 961–972, doi:10.5194/hess-17-961-2013.
48. Sen, P.K. Estimates of the Regression Coefficient Based on Kendall's Tau. *J. Am. Stat. Assoc.* **1968**, *63*, 1379, doi:10.2307/2285891.
49. Shahzad, M.K. Statistical Analysis of Inflows of River Indus at Tarbela in the Wake of Climate Change. In Proceedings of the International Conference on HYDROPOWER-A Vital Source of Sustainable Energy for Pakistan 2017, UET Lahore, Pakistan, 19–20 December 2017; pp. 19–27, ISBN:978-969-8670-06-01.
50. Ferguson, R.I. *Sediment Load of the Hunza River*; Mill, K.J., Ed.; International Karakoram Project Cambridge University Press: Cambridge, UK, 1984, Volume 2, pp. 580–598.

51. Collins, D.N. Sediment transport from glacierized basins in the Karakoram mountains. In Proceedings of the International Symposium, Exeter, UK, 15–19 July 1996; Volume 236, pp. 85–96, ISBN 0-947571-89-2.
52. Owen, L.A.; Edward, D.; Christine, H.S. Contemporary sediment production and transfer in high-altitude glaciers. *Sediment. Geol.* **2003**, *155*, 13–36, doi:10.1016/S0037-0738(02)00156-2.
53. Kääb, A.; Berthier, E.; Nuth, C.; Gardelle, J.; Arnaud, Y. Contrasting patterns of early twenty-first-century glacier mass change in the Himalayas. *Nature* **2012**, *488*, 495–498, doi:10.1038/nature11324.
54. Nuimura, T.; Fujita, K.; Fukui, K.; Asahi, K.; Aryal, R.; Ageta, Y. Temporal Changes in Elevation of the Debris-Covered Ablation Area of Khumbu Glacier in the Nepal Himalaya since 1978. *Arct. Antarct. Alp. Res.* **2011**, *43*, 246–255, doi:10.1657/1938-4246-43.2.246.
55. Ali, K.F. Construction of Sediment Budgets in Large Scale Drainage Basins: The Case of the Upper Indus River. Ph.D. Thesis, Department of Geography and Planning, University of Saskatchewan, Saskatoon, SK, Canada, 2009.

Chapter 3- Application of soft computing models with input vectors of snow cover area in addition to hydro-climatic data to predict the sediment loads

This Chapter is published as:

Ul-Hussan, W.; Shahzad M.K.; Seidel F.; Nestmann F.; Application of soft computing models with input vectors of snow cover area in addition to hydro-climatic data to predict the sediment loads. *Water (MDPI) Switzerland*, 2020, doi.org/10.3390/w12051481

3.1 Abstract

The accurate estimate of sediment load is important for management of the river ecosystem, designing of water infrastructures and planning of reservoir operations. The direct measurement of sediment is the most credible method to estimate the sediments. However, this requires a lot of time and resources. Due to these two constraints, most often, it is not possible to continuously measure the daily sediments for most of the gauging sites. Nowadays, data-based sediment prediction models are famous for bridging the data gaps in the estimation of sediment loads. In data-driven sediment predictions models, the selection of input vectors is critical in determining the best structure of models for the accurate estimation of sediment yields. In this study, time series inputs of snow cover area, basin effective rainfall, mean basin average temperature, and mean basin evapotranspiration in addition to the flows were assessed for the prediction of sediment loads. The input vectors were assessed with artificial neural network (ANN), adaptive neuro-fuzzy logic inference system with grid partition (ANFIS-GP), adaptive neuro-fuzzy logic inference system with subtractive clustering (ANFIS-SC), adaptive neuro-fuzzy logic inference system with fuzzy c-means clustering (ANFIS-FCM), multiple adaptive regression splines (MARS), and sediment rating curve (SRC) models for the Gilgit River, the tributary of the Indus River in Pakistan. The comparison of different input vectors showed improvements in the prediction of sediments by using the snow cover area in addition to flows, effective rainfall, temperature, and evapotranspiration. Overall, the ANN model performed better than all other models. However, as regards sediment load peak time series, the sediment loads predicted using the ANN, ANFIS-FCM, and MARS models were found to be closer to the measured sediment loads. The ANFIS-FCM performed better in the estimation of peak sediment yields with a relative accuracy of 81.31% in comparison to the ANN and MARS models with 80.17% and 80.16% of relative accuracies, respectively. The developed multiple linear regression equation of all models show an R^2 value of 0.85 and 0.74 during the training and testing period, respectively.

Keywords: suspended sediment concentrations; Gilgit Basin; snow cover fraction; artificial neural network; MARS model; Hindukush

3.2 Introduction

Eroded sediment originating from drainage basins due to hydrometeorological processes like rainfall, snow melt, and ice melting, etc. is transported in the form of suspended loads and bed loads [1,2,3]. The bed loads are transported in the form of coarse particles with of different shapes and sizes continuously in contact with the river bed [4]. The suspended load, transports in suspension state formed due to the erosion of fine particles from the sheet and gully, runoff in the catchment, river banks, and channel beds [5]. The increased runoff due to rising rainfall, snow cover depletion, or glacier ablation, etc. often leads to an increase in flood events, increase in suspended sediments, channel bed erosion, pollutants in river ecosystem, and depletion of water storages, and damages or affects hydropower operations [6].

Sediment deposition in rivers and reservoirs is a very serious challenge worldwide. It leads to rapid depletion of water storage capacities which ultimately affects the supply of irrigation as well as power generation. It also affects the operation of water reservoirs to mitigate floods, polluting river ecosystem and recreational sites [7,8]. In Asia, during the period 1990-2010 the net reservoir storages has been lost by 6.5% which is due to higher rate of sedimentations in the world [9]. In Pakistan, a number of water storages, for example the Tarbela, Mangla, Warsak, and Chashma storages, have lost considerable storage volumes earlier than expected [10,11,12,13] during the past three decades. The cause of this earlier-than-expected depletion of storages might be the high variance and incorrect estimation of sediment yields.

The Indus River in Pakistan with its total length of 2880 km supports the major storages and hydropower generations [14,15]. It is an economical source of hydropower generation having a 29% share in the country's total national power generation capacity [16]. The Indus river has the world's largest irrigation network, having an irrigated agricultural area of 181,000 km^2 [16,17]. Hydropower projects generating more than 30,000 MW are planned on the Indus River for the future. Therefore, estimation of sediment yields for reaches in the Upper Indus Basin (UIB) is important for the design and operation of existing and new water infrastructures.

The erosion and transport of sediments are the outcome of complex physical processes. Their estimation is a difficult challenge due to the non-linearity of multiple factors controlling the sediment yield. Many factors including, among others, the amount of flows, sediment supplies, sources of sediments, catchment gully and channel erosion, river bed configuration, bed form resistance and slope, forces and moments controlling the incipient motion, and types and properties of sediment particles, control the amounts of sediments in rivers [18,19]. To overcome the challenges of sediment yield estimations, soft computing artificial intelligence methods have been developed over the past few decades. These soft computing machine learning techniques have replaced the traditional sediment rating curve (SRC), and multiple and auto-regressive models for estimation of sediment yields. The soft computing algorithms have proven a powerful tool for estimation of sediment yield from highly nonlinear processes of erosion and sediment transport.

3.1.1. Background

In the recent few decades, many researchers have used several black-box models for the prediction of sediment yield. The most widely used models among these black-box models include artificial neural networks (ANN), support vector machines (SVM), artificial neuro-fuzzy logic inference systems (ANFIS), and genetic programming (GP). Mostly, more than two models were used to compare the results for finding the best model for the prediction of sediment yields along with the rating curve (RC) model. For example, in some studies [20,21,22], ANN was found to be better for the prediction of sediment yields than the sediment rating curve (SRC) model. Similarly, ANN and multiple linear regression (MLR) models were used in some studies [23,24] for estimation of sediment yields. In these studies, the sediment prediction

results of ANN were found to be better than the sediment prediction results obtained by MLR. In yet another study [25], the grid rainfall and measured flows are used to predict sediment yields with ANNs by Levenberg-Marquardt (LM), scaled conjugated gradient (SCG), and Bayesian regulation (BR) algorithms. It was concluded that ANN with Levenberg-Marquardt algorithm performed fairly better than the other two ANN algorithms for sparsely distributed catchments with limited climatic recorded data. The results of ANN and ANFIS were compared by [26,27] for the prediction of sediment yield. In these studies, researchers found that ANFIS models show a higher accuracy than the ANN and SRC models. It was found in studies by [28,29] that gene expression algorithms are better than ANN and ANFIS models for predictions of sediment loads.

The studies [30,31] used the SVM along with ANFIS and ANN algorithms. The results obtained by SVM showed less erroring in comparison to those of the ANFIS and ANN models. The researchers referred to in [32] employed the ANN and SVM models using discharge and rainfall as input data to predict the sediment yields. They found that ANN is better than SVM for the prediction of sediments. The studies [33,34] used the wavelet artificial neural network (WANN) to compare their results with SRC, MLR, and ANN. They found that the WANN model is better than all other models used in the study. The study [35] used wavelet-based least-squares support vector machines (WLSSVM) along with WANN to compare the results for finding the better model for sediment predictions. The study revealed that WLSVM is more robust and better than WANN for estimation of sediment yields.

Heuristic regression models such as multiple adaptive regression splines (MARS), M5 decision tree regression learner, and support vector regression (SVR) have also been used in the recent decade for nonlinear modeling in water resources. In linear modeling, to capture the nonlinear behavior of the process involved in engineering specifically for flows and sediments, some improvements had been made by introducing methods like polynomial regression. In this regard, the multivariate regression spline (MARS) has been developed to detect the nonlinear relationship of inputs and outputs like discharge sediment yields [36, 37]. MARS is a nonparametric regression model that identifies the desired pattern between inputs and desired output in the form of piecewise cubical or linear splines.

MARS, M5 model tree, and SVR are models for the prediction of flows and sediment yields in water resources [38,39,40]. However, the use of MARS is comparatively rare for sediment yield predictions. The researchers referred to in [41,42] found that the performance of MARS is poor in comparison to that of dynamic evolving neural-fuzzy inference system (DENFIS) and ANN models. The study [43] compared the results of hybrid MARS fuzzy regression (HMARS-FR), fuzzy least squares regression (FLSR), and fuzzy least absolute regression (FLAR) for estimation of sediment yields. The hybrid MARS fuzzy regression was found to be better than the other two models for predictions of sediment loads. In another study [44] performed to predict sediment yields, the M5 model tree, SRC, GEP, and MLR models were used. The M5 model tree performed better than the SRC, GEP, and MLR models in this study. In yet another study [45] ANN, wavelet regression (WR), and M5 tree models were used for modeling the sediment yield using the inputs of flows and rainfall. In this study, the M5 model tree performed better than the ANN and wavelet regression models. Similarly, it was found in a study [46] carried out to predict sediments that the M5 tree model is better than ANN and fuzzy logic models. The study used hydro-climatic data for predictions of sediments using five different algorithms namely, ANN Levenberg-Marquardt, ANN scaled conjugate gradient, SVR, M5 model tree, and REPTree model. In this study, the researchers found that ANN using the Levenberg-Marquardt algorithm performed better than other models. Table A1 in section of supplementary materials presents the summary of the literature discussed above.

The study presented in this paper checks the applicability of ANN Levenberg-Marquardt, hybrid ANFIS embedded grid partition (GP), hybrid ANFIS embedded subtractive clustering (SC), hybrid ANFIS embedded FCM clustering (FCM), and MARS models with inputs of grid climatic data, snow cover

fraction, and flows to predict the sediment yields for sparsely distributed basins. These models were selected because, during the past three decades, the ANN and ANFIS data-driven models have been identified as being robust, powerful tools with a great ability of solving the complex nonlinear process-like prediction of sediment yields. As a result of the above discussions and scrutiny of literature review, and to the best knowledge of the authors, no study in artificial intelligence (AI) has used the combination of spatially averaged grid effective rainfall, mean basin-averaged temperature, and averaged basin snow cover fractions in combination with flows to predict the sediment yields.

3.2 Data Collection and Methodology

3.2.1 Study area

The present study was carried out in the Gilgit River basin situated in the Hindukush Mountains of the Upper Indus Basin (UIB). The Gilgit River originates from Shandoor Lake north of the Gilgit-Baltistan region in Pakistan. The Baha Lake is the right tributary of the Gilgit River with small tributaries being e.g., Yasin, Ishkoman, and Phandar. The Phandar Lake is located in Ghizer. The Yasin tributary joins the main Giglit River near Gupis. Figures 3.1 & 3.2 show the hydrological characteristics of the Gilgit basin that has a drainage area of 12095 km^2. The geographical location of the Gilgit basin is between latitude 35°55′35 N and 36°52′20′′N and longitude 72°26′04′′E and 74°18′25 E. The elevation of catchment ranges from 1454-7048 m a.s.l. Table A2 in supplementary materials shows the key features of the Gilgit basin. About 10% of the total catchment area is covered with glaciers and lies above an elevation of 5000 m. During the winter season, approximately 87% of the catchment area is covered with snow cover which reduces to 11% during the ablation period in summer. The mean annual discharge and suspended sediment concentrations (SSC) of the Gilgit basin are 291 m^3/sec and 448 mg/l, respectively. The ablation period starts in July after seasonal snow melts. The melting of the glacier is slow and continues until the month of October. Then, the accumulation period of snow starts at the end of October. The Gilgit basin receives 75% of its rainfall starting from the mid of spring (April) to the end of summer (October). The mean annual basin rainfall from grid data in the Gilgit basin is approximately 670 mm. The mean monthly basin average temperature for the Gilgit basin ranges from -19.8 to 7.20 ºC.

The Water and Development Authority (WAPDA) of Pakistan had also installed stream gauging stations at an altitude of 1430 m a.m. sea level for measuring flows and suspended sediment concentrations (SSC). The climatic stations installed in the Gilgit basin are sparsely distributed in the catchment. The climatic stations installed in the valley by the Pakistan Meteorological Department (PMD) at Gilgit and Gupis have at their disposal long-term daily climatic data collected from 1981-2010. However, the climatic stations of Uskhkore, Yasin, and Shendure located on higher altitudes are sparsely distributed and have short-term recorded data accumulated from 1996-2010 which are available from WAPDA. However, the suspended sediment concentrations (SSC) are recorded on intermittent days per week. Table 3.1 shows detailed information on the data used in this study. The flows, temperature, and rainfall are recorded on a daily basis. Due to scarcity of climatic information and the sparse distribution of climatic stations in the Gilgit catchment (see Figures 3.1 & 3.2), the information of grid climatic, snow cover fractions and grid evapotranspiration datasets of Table 3.1 were used for the period 1981-2010 during analysis of this research work. These grid datasets were extracted using the Shuttle Radar Topography Mission's (SRTM) Digital elevation model (DEM) of 30 m for Gilgit catchment.

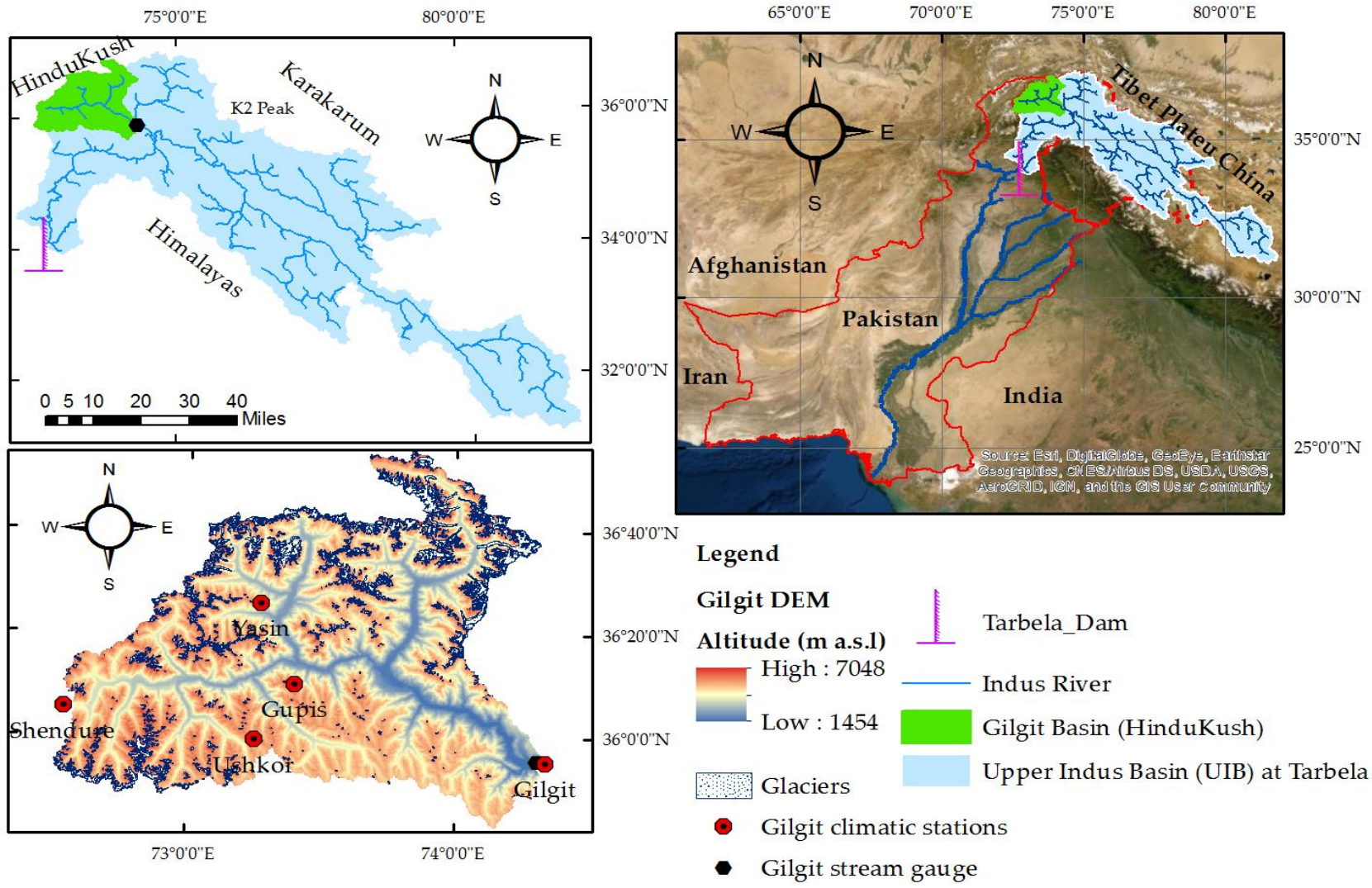

Figure 3. 1 The location map of Gilgit River in the Upper Indus Basin (UIB) of Pakistan.

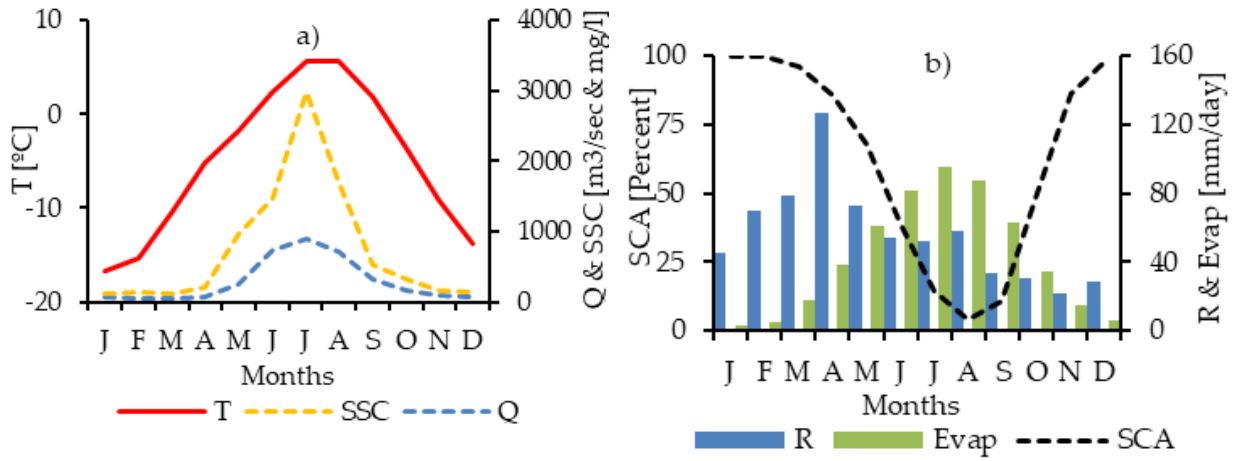

Figure 3. 2 Graphical presentations of (a) mean basin temperature (T), discharges at Gilgit gauge (Q), and suspended sediment concentrations (SSC) at Gilgit gauge, (b) mean basin snow covered area (SCA), mean basin rainfall (R), and mean basin evapotranspiration (Evap) for the Gilgit basin during period 1981-2010.

Table 3. 1 Data collected for prediction of suspended sediment yields for the Gilgit River basin.

Variable	Data Source	Period	Source
Q*	Daily mean discharge [m^3/sec]	Daily, 1981–2010	Water and Power Development Authority (WAPDA), Pakistan
SSC*	Suspended sediment concentration [mg/l]	Intermittent days per week 1981–2010	Water and Power Development Authority (WAPDA), Pakistan
SCF	Snow cover fractions ranging [0–1] extracted from MODIS satellite data	Weekly, basin avg. 2000–2010	https://nsidc.org/data/MOD10A2
T	Daily mean, maximum & minimum air temperature [° C] on a 5x5 km grid	Daily, basin avg. 1981–2010	HI-AWARE project [47, 48]
P	Daily mean rainfall [mm day–1] on a 5x5 km grid	Daily, basin avg. 1981–2010	HI-AWARE project [47, 48]
Evap	Daily mean Evapotranspiration [mm day–1] on a 5x5 km grid	Daily, basin avg. 1981–2010	HI-AWARE project [47, 48]

Note * The variable of discharge (Q) and suspended sediment concentrations (SSC) are measured at Gilgit gauging station and variables of SCF, T, P and Evap are basin averages grid datasets.

The Moderate Resolution Imaging Spectroradiometer (MODIS) MOD10A2 product was downloaded on a weekly basis for the period of 2000-2010 from the National Snow and Ice Data Center (NSIDC) online server. The MODIS data with 500 m resolution was used for estimating the snow cover area and snow melt runoff [49,50]. The same procedure was adopted in other studies to estimate and linearly interpolate the snow cover fractions for daily snow cover fractions of the Gilgit basin for the period of 2000-2010 [49,50]. The temperature-index snow model was further used to estimate the snow cover fraction for the period of 1981-2010 after calibration and validation of the snow model with MODIS snow cover.

Table 3.2 shows the Pearson's correlations of input variables used in this study. Generally, correlation analysis such as cross correlation, auto-correlation, and partial auto-correlation are also used to determine the input combinations of various variables with lag times. However, the main deficiency of these methods is the inability to cover the nonlinear relationship between the input and output variables like discharge sediment, etc. For this reason, in the current study, the various input combinations were identified by examining the test accuracy of the model output.

In general, the discharges trigger the channel erosion. However, in addition to discharges, the temperature and snow cover area of the snow- and ice-dominated basin also triggers hillslope erosion, snow melt erosion and glacier melt erosion. The evapotranspiration also has an indirect relationship with erosion processes in the form of the vegetative cover of the plants and forests. Keeping in view the importance of direct and indirect factors controlling the erosion of catchments, different variables other than discharges such as snow cover area, effective rainfall, and evapotranspiration were also chosen in this study for the prediction of sediment yields. Prior to the analysis for prediction of sediment yields, the flows and suspended sediment load (SSL) were transferred into a log transformation form to compensate the biases and very high values in datasets. The datasets were divided into 70% and 30% for training and testing of the model, respectively. Shahin et al. [51] suggested that for optimum performance of soft computing methods datasets should be divided into training (i.e. 70%) and testing (i.e. 30%) phases. The daily datasets of measured SSC were not available for continuous days. The measured SSC values were available for total 767 days during the period 1981-2010. For the sediment rating curve (SRC) the flows and SSC values for the period 1981-2003 (i.e. 1-537 days) and 2003-2010 (i.e. 538-6767 days) were used for training and testing respectively. However, the random sampling [52] of whole datasets for training (70%) and remainder datasets as testing (30%) was conducted in MATLAB to reduce over and under fitting of network. Then ANN, ANFIS and MARS models were trained and tested in MATLAB with various input combinations.

Table 3. 2 Relationship of Gilgit basin input variables determined by using Pearson correlation coefficient. Log Q: logarithm of water discharges; Log SSY: logarithm of sediment yields; SCA: snow covers area: T_{avg}: mean temperature; P: basin averaged effective rainfall; Evap: evapotranspiration.

	log Q [m^3/day]	log SS_Y [tons/day]	SCA [fractions]	T_{avg} [° C]	P [mm]	Evap [mm/day]
log Q [m^3/day]	1					
log SS_Y [tons/day]	0.87	1				

SCA [fractions]	-0.85	-0.74	1			
$T_{avg.}$ [° C]	0.87	0.79	-0.88	1		
P [mm]	0.16	0.15	0.09	0.10	1	
Evap. [mm/day]	0.86	0.81	-0.82	0.93	0.06	1

3.2.2 Application of Temperature index-snow model for snow cover estimates

The climatic stations in the Gilgit basin have less availability of long-term climatic records for the catchment. Previous studies [53,54,55] reported that the rainfall on higher elevations starting above 5000 m in the Upper Indus Basin (UIB) is 5-10 times higher than the rainfall recorded in the valley. For this reason, the grid data for rainfall and temperature from the HI-AWARE project [47,48] was used in this study. Keeping in view the above-mentioned constraints, the temperature-index snow model is used in this study. The temperature-index snow model is a simple and spatially distributed model which, in addition, has less data requirements. In this study, this method is used to simulate the long-term snow melts and snow cover fractions after calibration and validation of the simulated snow cover fraction with the MODIS snow cover fractions for the period of 2000-2010.

In the temp-index snow melt model [56,57], precipitation P is first separated into snow and liquid rain on a daily time scale. The threshold temperature TRS [°C], daily maximum temperature [°C], and daily minimum temperature [°C] separate the snow and liquid rainfall as:

$$\begin{cases} Rain = R = C_p P \\ Snow = S = (1 - C_p) P \end{cases} \quad (1)$$

Where,
Precipitation factor Cp proportionate to temperature difference is calculated as:

$$\begin{cases} C_p = 1 \; if \; T_{min} > T_{RS} \\ C_p = 0 \; if \; T_{max} \leq T_{RS} \\ C_p = \dfrac{T_{max} - T_{RS}}{T_{max} - T_{min}} \; if \; T_{min} \leq T_{RS} < T_{max} \end{cases} \quad (2)$$

The threshold temperature TRS is used to define the type of precipitation into rain/snow and the threshold temperature TSM for the snow melt process which depends on numerous factors like the boundary layer condition of atmosphere, temperature, and air humidity, etc.

Then, daily rates of snow melt, i.e. M_{snow} [mm/day] are estimated as:

$$\begin{cases} M_{snow} = K_{snow}(T_{mean} - T_{SM}) \;\; if \; T_{mean} > T_{SM} \\ M_{snow} = 0 \;\; if \; T_{mean} > T_{SM} \end{cases} \quad (3)$$

Here, the Ksnow [mm/day °C] is the degree day factor for snow melts, Tmean [°C] is the mean daily air temperature, and TSM [°C] is the threshold temperature.

After this, the snow model simulates the snow water equivalent or snow depth SD [mm] for each grid number of i as:

$$SD_i(t) = \quad SD_i(t-1) + S_i(t) - \ M_{snow_i}(t) \qquad (4)$$

Finally the snow cover fraction SCF for i = 1, 2, 3, 4,…., N number of grids for the whole basin is estimated for calibration and validation with the MODIS snow cover fraction as:

$$SCF\ (t) = \frac{1}{N}\sum_{i=1}^{N} H\ [SD_i(t)] \qquad (5)$$

Here, H = unit step function; when H = 0, SD = 0 and H = 1 then SD > 0. The area of integration N is the entire basin, sub-basins and elevation bands etc.

3.2.3 Artificial neural networks (ANN)

Artificial neural networks (ANNs) are data-based black box models primarily inspired by the concept of functioning of the biological nervous system. ANNs consist of a set of processing elements referred to as neurons. These neurons work in the parallel systems for acquiring the information and storing the knowledge for computational use. ANNs consist of three layers as their basic structure. These layers are the input layer, the hidden layer (processed layer), and the output layer. Each layer is connected by networks of neurons with preceding layers. This system of networks connected with neurons is called Multilayer Perceptron (MLP). There are various types of ANNs that perform various assignments in science and engineering. Among these ANNs of MLP, feed-forward back propagation FFBP-ANN is most popular. The literature [58,59,60,61,62,63,64] explains the details of the ANN model and its application to water resources with FFBP-MLP algorithm. In FFBP-MLP, the input data is learned in forward direction of network from input nodes to the hidden nodes with some transfer functions in the hidden layer. Then, the information is forwarded from the hidden layer to the output nodes. Figure A1 in supplementary materials explains the architectures of the FFBP ANN. In the output layer, an output is generated by the network, and the error between predicted and model output is computed. This output error of the network is back-propagated through the network to correct the connection weights of neurons in the hidden layer. This learning process of the network is performed until the minimum error is optimized to avoid overfitting as well underfitting of the network.

A neural network is described with 1) architectures of layers connected with networks of neurons, 2) transfer functions, and 3) training methods for estimation of weights in nodes. In general, the performance of ANN depends on its model network, learning complexity, and problem complexity. The performance of ANN depends on the number of neurons in hidden layers and the number of hidden layers to avoid the over- and underfittings of the network. The literature suggests the optimum neurons to be in the range of $2\sqrt{N_1} + \ N_0$, where N1 and N0 are the number of input and output neurons, respectively.

For this study, ANN with FFNN-MLP with Levenberg-Marquardt has been used with one hidden layer as more than one hidden layer increases the complexity of the network and does not improve the results, either. The FFNN-MLP with Levenberg-Marquardt is a robust and powerful tool. It has a high and fast ability of data convergence, and produces more accurate results than other ANN algorithms.

3.2.4 Adaptive neuro-fuzzy logic inference system (ANFIS)

The adaptive neuro-fuzzy logic inference system (ANFIS) is a novel architecture with combinations of neural networks and fuzzy inference systems (FIS). A basic ANFIS [65] structure is shown in Figure A2 in section of supplementary materials. The ANFIS works by tuning the parameters of FIS applying the neural network learning method. The ANFIS builds a network structure connected with a number of nodes. These nodes are characterized by fixed or adjustable parameters. The ANFIS uses neural networks with fuzzy logic if-then rules with appropriate membership functions to translate the input parameters into output values. Three inference systems are classified as Tsukamoto's, Mamdani's, and Sugenos's systems. The Mamdani's system [66] was mostly used in the past. The Sugeno's system [67] is more efficient than other systems. In this study, Sugeno's fuzzy logic structures were used.

As an example, it is assumed that a FIS has two inputs x1 and x2 with target values of z. Here, input of discharge and snow cover can be supposed as x1 and x2 with output z as sediment yield for a particular time t. Then, in Sugeno's fuzzy logic structures, typical rule sets with two IF/THEN rules are expressed as:

Rule 1: IF x1 is A1 and x2 is B1, THEN $z_1 = f_1 = p_1\, x_1 + q_1\, x_{2+} r_1$ (6)

Rule2: IF x1 is A2 and x2 is B2, THEN $z_2 = f_2 = p_2\, x_1 + q_2\, x_{2+} r_2$ (7)

Where pi, qi and ri are parameters corresponding to Rule 1, Rule 2… Rule n.

The ANFIS consist of five layers.

Layer 1 In first layer each node generates a membership grade for each input's variable. The output of ith node with generalized bell membership function in first layer is expressed as:

$$Oi^1 = \mu_{Ai^{(x1)}} = \frac{1}{1+((x_1-c_i))/a_i)^{2Ni}} \quad (8)$$

Where, {ai, ci, Ni} are the parameter sets for x1 input in ith node. These parameters change the shape of bell function in the range of 0-1.

Layer 2 The layer 2 is labeled with II in each node. In this layer every node multiplies the incoming signals coming from layer 1 as:

$$Oi^2 = wi = \mu_{Ai^{(x1)}} \times \mu_{Bi^{(x2)}}, \qquad i = 1, 2 \quad (9)$$

Layer 3 In layer 3 every node calculates the normalized firing strength as its relationship between firing strength of i^{th} rule to the sum of all rules:

$$Oi^3 = \overline{w} = \frac{w}{w_1+w_2} \qquad i = 1, 2 \quad (10)$$

Layer 4 In layer 4 the sum of signals from second- and third-layers networks are calculated for each ith node towards the model output as:

$$Oi^4 = \bar{w}_i f_i = \bar{w}_i(p_i\, x_1 + q_i\, x_{2+} r_i) \qquad \text{i = 1, 2} \qquad (11)$$

Here, $\bar{w}$ is the output from layer 3 in this equation.

Layer 5 Layer 5 calculates the overall output in the form of single node as the ANIFS model output against each target value as:

$$Oi^5 = \Sigma \bar{w}_i f_i = \frac{\Sigma \bar{w}_i f_i}{\Sigma \bar{w}_i} \qquad \text{i = 1, 2} \qquad (12)$$

In the ANFIS model, to obtain the model parameters, a hybrid learning method is used for this study. Further details about the ANFIS model are found in [68].

In this study, three strategies are used to produce the initial fuzzy inference system for the ANFIS model. These strategies are grid partition (ANFIS-GP), subtractive clustering (ANFIS-SC), and fuzzy c-means clustering (ANFIS-FCM). The ANFIS-GP is a combination of ANFIS and grid partition. In grid partition, the input linguistic variables are partitioned by fuzzy numbers and their membership functions (MFs). The grid partition uses predefined numbers of MFs to optimize the MFs according to input-output datasets. The quantitative characteristics of datasets are separated into n partitions (n = 2, 3, 4…). In this study, eight MFs were used such as gaussmf, gauss2mf, trimf, trapmf, gbellmf, pimf, dsig,mf, and psigmf. In the AFNIS-GP model, the number of rules increases exponentially with the increase in the number of input variables. For details about the ANFIS-GP, see [65].

The ANFIS-SC model is the extended model derived from the mountain clustering model [69] with combination of the ANFIS model by using the subtractive clustering strategy. This model was modified by Chiu [70]. This method has an advantage over the mountain clustering method. It eliminates the grid resolution to reduce the complex computations in the mountain clustering method. In the ANFIS-SC model, each dataset is considered as potential cluster. Then, the potential of each data point of a given dataset is calculated by its distance from all other data points. These data points having many neighboring data points show a high potential value. The influential radius decides the number of clusters in the ANFIS-SC model. The small value of influential radius has many numbers of clusters with more rules in comparison to its large value [71]. Using a hit-and-trial procedure, the suitable critical value of influential radius is sorted out during the data space clustering procedure. [72,70] further explain the detailed procedure of the ANFIS-SC model.

The ANFIS-FCM model was proposed in the literature [73,74,75,76,77] and enhanced by Zhang and Chen [78]. The ANFIS-FCM minimizes the errors by partitioning the X datasets into C clusters. This method reduces the errors regarding the weighted distance of each data point xi towards all centroids of the C clusters. After this, the ANFIS-FCM model minimizes the objective function as:

$$Min\, J_{FCM} = \sum_{c=1}^{C}\sum_{i=1}^{N} {w^p}_{ic} \left\| x_{i-\, v_c} \right\|^2 \quad s.t. \sum_{c=1}^{C} w_{ic} = 1, i = 1, 2, \ldots, N \qquad (13)$$

Where C, N, wic, v and x are number of clusters, number of data points, degree belongs to ith data point of Cith clusters data points and inputs data sets. The p (p > 1) entitles to the fuzzifier exponent. In ANFIS-FCM wic is calculated as:

$$w_{ic} = \frac{1}{\sum_{i=1}^{c} \left({d_{ic}}^2 / {d_{ij}}^2 \right)^{1/(p-1)}} \quad for\ i = 1, 2, \ldots N\ and\ c = 1,2, \ldots C \tag{14}$$

In FCM model after initialization of center vectors, centers are recomputed as:

$$v_c = \frac{\sum_{j=1}^{N} {w^p}_{Jc}\, x_j}{\sum_{j=1}^{N} {w^p}_{Jc}} \quad for\ c = 1, 2, \ldots N\ and\ 1 < p > N \tag{15}$$

The algorithm is run until convergence condition is completed.

3.2.5 Multivariate adaptive regression splines (MARS)

MARS is a non-parametric technique for the prediction of nonlinear processes developed in 1991 by Friedman [79]. The MARS model is a flexible and precise prediction model. It has been successfully applied in different studies [80,81,82] for prediction and forecasting purposes. In the MARS Model, the MARS function develops a series of linear segments having different slopes from the input-output relationships of given datasets. Each linear segment of MARS is then fitted with a linear basis function. For this study, the datasets were separated into break values between different regions or segments referred to as knots. Each region has its own regressions line. The shape of a piecewise linear basis function is expressed as:

$$[\max(0, x - k)]\ OR\ [\max(0, k - x)] \tag{16}$$

Here x represents the predictor variable and k explains about the threshold value of knots. In general MARS consists of combinations of basis-functions (BFs) given as:

$$y = f(x) + \varepsilon \tag{17}$$

$$f(x) = \beta_o + \beta_m BF_m(x) \tag{18}$$

In the above Equation 12, the variable y is dependent on estimated values of function f(x) with the error ε. In Equation 13, β_o is a constant value, BF_m is the basis function, and β_m represents the coefficient for the maximum number of basis functions (BFs) depending on the input's datasets.

In the MARS model with polynomial knots, there exist two phases called forward step phase and backward step phase. The forward step phase generates all possible BFs. And after generation of the BFs, the generalized cross validation criterion (GCV) is used for determining the BFs and appropriate nodes. After this forward step phase, the backward step phase of the MARS model works to reduce the number of BFs for improving the predictions and avoiding overfitting of the model. [79] gives detailed information about the MARS model.

3.2.6 Sediment rating curve (SRC)

The sediment rating curve is an empirical relationship of flows and sediment load or concentrations described as:

$$SSL_{(t)} = a \times {Q^b}_{(t)} \tag{19}$$

Where Q [m^3/day] is discharge, SSL [tons/day] both in log transformation form and a & b are the constants depends upon the characteristics of river and its catchments.

3.2.7 Performance measurement metrics for model evaluation

The performance of models was measured and assed using following statistics:

Root mean square error (RMSE)

$$RMSE = \sqrt{\frac{1}{N}\sum_{i=1}^{N}((S_{io}) - (S_{is}))^{2}} \quad (20)$$

Nash-Sutcliffe efficiency (NSE)

$$NSE = 1 - \frac{\sum_{t=1}^{N}(S_{io} - S_{is})^2}{\sum_{t=1}^{N}(S_{is} - \overline{S_{is}})^2} \quad -\infty \leq NSE \leq 1 \quad (21)$$

Pearson's correlation coefficient (R^2)

$$R^2 = \left(\frac{\sum_{i=1}^{N}(S_{i0} - \overline{S_{io}})(S_{is} - \overline{S_{is}})}{\sqrt{\sum_{i=1}^{N}(S_{i0} - \overline{S_{io}})^2 \sum_{i=1}^{N}(S_{is} - \overline{S_{is}})^2}} \right)^2 \quad (22)$$

Where N refers the data quantity, S_{io} is observed sediment and Sis is the simulated sediments and $\overline{S_{is}}$ is mean of simulated sediments.

Relative Accuracy

The relative accuracy is the % of accuracy expressed as:

$$\text{Relative Accuracy (\%)} = \left(1 - \left|\frac{S_{po} - S_{ps}}{S_{po}}\right|\right) \times 100 \quad (23)$$

where S_{po} is the observed peak value of SSY, S_{ps} is the simulated peak value of SSY.

3.2.8 Application of ANN, ANFIS-GP, ANFIS-SC, ANFIS-FCM and MARS models

For the application of ANN, ANFIS-GP, ANFIS-SC, ANFIS-FCM and MARS model various input combinations with daily lag time were examined with scenarios starting from S_1-S_{15} by testing the accuracy of the network using minimum RMSE and maximum value of R^2 and NSE as performance criteria. The inputs scenarios developed in this study for predictions of sediment yield are mentioned here:

a) Flows
   - $S_1 = SSC_t = f(Q_t, \beta_1) + e_i$
   - $S_2 = SSC_t = f(Q_t, Q_{t-1}, \beta_1, \beta_2) + e_i$
   - $S_3 = SSC_t = f(Q_t, Q_{t-1}, Q_{t-2}, \beta_1, \beta_2, \beta_3) + e_i$
   - $S_4 = SSC_t = f(Q_t, Q_{t-1}, Q_{t-2}, Q_{t-3}, \beta_1, \beta_2, \beta_3, \beta_4) + e_i$
   - $S_5 = SSC_t = f(Q_t, Q_{t-1}, Q_{t-2}, Q_{t-3}, Q_{t-4}, \beta_1, \beta_2, \beta_3, \beta_4, \beta_5) + e_i$

b) Flows and snow cover area
   - $S_6 = SSC_t = f(Q_t, SCA_t, \beta_1, \beta_6) + e_i$
   - $S_7 = SSC_t = f(Q_t, SCA_t, SCA_{t-1}, \beta_1, \beta_6, \beta_7) + e_i$
   - $S_8 = SSC_t = f(Q_t, SCA_t, SCA_{t-1}, SCA_{t-2}, \beta_1, \beta_6, \beta_7, \beta_8) + e_i$

c) Flow, snow cover area and effective rainfall

$S_9 = SSC_t = f(Q_t, R_{t-1}, SCA_t, SCA_{t-4}, \beta_1, \beta_9, \beta_6, \beta_{10}) + e_i$

a. Flow, snow cover area, temperature and evapotranspiration

$S_{10} = SSC_t = f(Q_t, T_{t-1}, Evap_{t-1}, SCA_t, SCA_{t-4}, \beta_1, \beta_{11}, \beta_{12}, \beta_6, \beta_{10}) + e_i$

e) Average mean basin air temperature

$S_{11} = SSC_t = f(T_t, \beta_{13}) + e_i$

$S_{12} = SSC_t = f(T_t, T_{t-1}, \beta_{13}, \beta_{11}) + e_i$

$S_{13} = SSC_t = f(T_t, T_{t-1}, T_{t-2}, \beta_{13}, \beta_{11}, \beta_{14}) + e_i$

$S_{14} = SSC_t = f(T_t, T_{t-1}, T_{t-2}, T_{t-3}, \beta_{13}, \beta_{11}, \beta_{14}, \beta_{15}) + e_i$

$S_{15} = SSC_t = f(T_t, T_{t-1}, T_{t-2}, T_{t-3}, T_{t-4}, \beta_{13}, \beta_{11}, \beta_{14}, \beta_{15}, \beta_{16}) + e_i$

In the combinations above β1- β16 represents the membership functions of layers in ANN, ANIFS and MARS models.

3.3 Results and Discussion

3.3.1 Simulation of snow melts and snow cover area

The results of the calibrated temperature-index snow melt model are shown in Table 3.3. The model was calibrated and validated to simulate the snow cover by using the degree day factor for the snow model. Table 3 shows the value of the degree day factor ksnow = 4.2 [mm day−1 °C−1] for the Gilgit basin. The literature review [83,84,85,86,87,50] for the regional case studies shows that the value of Ksnow ranges from 3-7 [mm/day/°C] in the Upper Indus Basin (UIB). Thus, during calibration and validation of the temperature-index snow model for this study, the value of ksnow = 4.2 [mm/day/°C] lies within the range of the values of previous studies carried out for snow melt runoff modeling in the UIB. The difference between the Ksnow value in the current study and that of previous studies is probably due to the use of different resolutions of input datasets, lengths of calibration datasets, threshold temperatures for separating rainfall and snow, threshold temperatures for snow melts, and characteristics of the catchment.

Table 3. 3 Results of performance measurement statistics during calibration (2000-2007) and validation (2008-2010) periods of the temperature-index snow model for simulations of snow melt and snow cover fractions.

	k_{snow} = 4.2 [mm/day/°C]	
	Calibration Period (2000-2007)	Validation Period (2008-2010)
R^2	0.90	0.90
NSE	0.72	0.70
RMSE	0.15	0.15

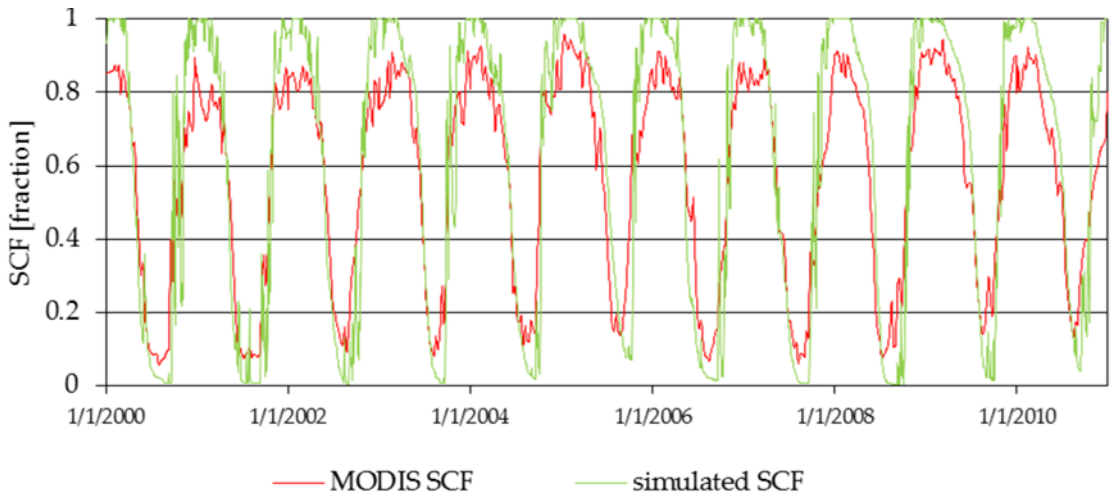

Figure 3. 3 Time series plots between the MODIS-observed snow cover fractions and temp-index snow model-simulated snow cover fractions during calibration (2000-2007) and validation periods (2008-2010).

Table 3.3, also shows the performance measurement statistics for the snow model during the calibration and validation periods. The value of R^2 is found at 0.90 between the MODIS-observed snow-covered area and model simulated snow cover area both during the calibration and validation periods. The performance evaluation criteria using the three criteria of R^2, NSE, and RMSE show that goodness of fit between the model and observed MODIS snow cover maps is more than 70% which is satisfactory in estimation of both the snow melts and snow cover area. Figure 3.3 also shows the time series plot between model snow cover area and MODIS-observed snow cover area during the calibration (2000-2007) and validation (2008-2010) period, respectively.

Table 3. 4 Training and testing statistics of ANN model by using Levenberg-Marquardt algorithm using different input combinations for Gilgit basin.

Scenarios	Model inputs	Neurons	Transfer function		R^2		RMSE		NSE	
			Input	Output	Training	Testing	Training	Testing	Training	testing
S_1	Q_t	3	logsig	purelin	0.76	0.81	0.48	0.42	0.76	0.8
S_2	Q_t, Q_{t-1}	3	logsig	purelin	0.77	0.79	0.48	0.44	0.77	0.79
S_3	Q_t, Q_{t-1}, Q_{t-2}	5	radbas	purlin	0.78	0.79	0.46	0.45	0.78	0.79
S_4	Q_t, Q_{t-1}, Q_{t-2}, Q_{t-3}	5	tansig	purelin	0.80	0.80	0.44	0.47	0.80	0.79
S_5	Q_t, Q_{t-1}, Q_{t-2}, Q_{t-3}, Q_{t-4}	7	logsig	purelin	0.81	0.80	0.43	0.44	0.81	0.80
S_6	Q_t, SCA_t	5	tansig	purelin	0.79	0.82	0.45	0.44	0.79	0.81
S_7	Q_t, SCA_t, SCA_{t-1}	7	tansig	tansig	0.80	0.80	0.44	0.43	0.80	0.8
S_8	Q_t, SCA_t, SCA_{t-1}, SCA_{t-2}	8	tansig	tansig	0.80	0.81	0.44	0.43	0.80	0.81
S_9	Q_t, R_{t-1}, SCA_t, SCA_{t-4}	7	logsig	purelin	0.80	0.82	0.44	0.42	0.80	0.82
S_{10}	**Q_t, T_{t-1}, $Evap_{t-1}$, SCA_t, SCA_{t-4}**	**5**	**radbas**	**tansig**	**0.81**	**0.82**	**0.42**	**0.43**	**0.81**	**0.81**
S_{11}	T_t	3	logsig	purelin	0.69	0.73	0.55	0.50	0.69	0.73
S_{12}	T_t, T_{t-1}	3	logsig	tansig	0.69	0.74	0.54	0.51	0.69	0.73
S_{13}	T_t, T_{t-1}, T_{t-2}	6	tansig	tansig	0.74	0.73	0.51	0.51	0.74	0.72
S_{14}	Tt, Tt-1, T_{t-2}, T_{t-3}	8	tansig	tansig	0.75	0.74	0.49	0.51	0.75	0.74
S_{15}	T_t, T_{t-1}, T_{t-2}, T_{t-3}, T_{t-4}	7	radbas	tansig	0.74	0.76	0.49	0.51	0.74	0.76

Table 3. 5 Training and testing statistics of AFIS1 grid partition (GP) model by using different input combinations for Gilgit basin.

Scenarios	Model inputs	Membership functions	No of Function	R^2		RMSE		NSE	
				Training	Testing	Training	Testing	Training	testing
S_1	Q_t	pimf	4	0.77	0.78	0.46	0.47	0.77	0.78
S_2	Q_t, Q_{t-1}	pimf	2	0.78	0.78	0.46	0.47	0.78	0.78
S_3	Q_t, Q_{t-1}, Q_{t-2}	gauss2mf	2	0.79	0.77	0.45	0.49	0.79	0.77
S_4	Q_t, Q_{t-1}, Q_{t-2}, Q_{t-3}	gbellmf	2	0.81	0.75	0.43	0.50	0.81	0.75
S_5	Q_t, Q_{t-1}, Q_{t-2}, Q_{t-3}, Q_{t-4}	trimf	2	0.81	0.71	0.43	0.53	0.81	0.69
S_6	Q_t, SCA_t	trimf	2	0.79	0.77	0.45	0.45	0.79	0.77
S_7	**Q_t, SCA_t, SCA_{t-1}**	**trimf**	**2**	**0.79**	**0.78**	**0.44**	**0.47**	**0.79**	**0.78**
S_8	Q_t, SCA_t, SCA_{t-1}, SCA_{t-2}	trimf	2	0.82	0.76	0.42	0.47	0.82	0.75
S_9	Q_t, R_{t-1}, SCA_t, SCA_{t-4}	trimf	2	0.82	0.76	0.41	0.49	0.82	0.76
S_{10}	Q_t, T_{t-1}, $Evap_{t-1}$, SCA_t, SCA_{t-4}	trimf	2	0.85	0.72	0.38	0.52	0.85	0.72
S_{11}	T_t	psigmf	2	0.70	0.70	0.55	0.52	0.70	0.70
S_{12}	T_t, T_{t-1}	pimf	2	0.71	0.71	0.54	0.51	0.71	0.71
S_{13}	T_t, T_{t-1}, T_{t-2}	trimf	2	0.71	0.73	0.52	0.52	0.71	0.73
S_{14}	Tt, Tt-1, T_{t-2}, T_{t-3}	trapmf	2	0.72	0.72	0.51	0.53	0.72	0.72
S_{15}	T_t, T_{t-1}, T_{t-2}, T_{t-3}, T_{t-4}	trimf	2	0.77	0.60	0.46	0.65	0.77	0.59

Table 3. 6 Training and testing statistics of AFIS2 subtractive clustering (SC) model by using different input combinations for Gilgit basin.

Scenarios	Model inputs	Radii	R^2		RMSE		NSE	
			Training	Testing	Training	Testing	Training	testing
S_1	Q_t	0.50	0.77	0.78	0.46	0.47	0.77	0.78
S_2	Q_t, Q_{t-1}	0.70	0.77	0.78	0.46	0.47	0.77	0.78
S_3	Q_t, Q_{t-1}, Q_{t-2}	0.70	0.77	0.78	0.46	0.47	0.77	0.78
S_4	Q_t, Q_{t-1}, Q_{t-2}, Q_{t-3}	0.70	0.78	0.78	0.45	0.47	0.78	0.78
S_5	Q_t, Q_{t-1}, Q_{t-2}, Q_{t-3}, Q_{t-4}	0.80	0.78	0.78	0.45	0.47	0.78	0.78
S_6	Q_t, SCA_t	0.60	0.78	0.78	0.45	0.47	0.78	0.78
S_7	Q_t, SCA_t, SCA_{t-1}	0.80	0.78	0.78	0.45	0.47	0.78	0.78
S_8	Q_t, SCA_t, SCA_{t-1}, SCA_{t-2}	0.70	0.79	0.77	0.44	0.48	0.79	0.77
S_9	Q_t, R_{t-1}, SCA_t, SCA_{t-4}	0.60	0.79	0.78	0.45	0.47	0.79	0.78
S_{10}	**Q_t, T_{t-1}, $Evap_{t-1}$, SCA_t, SCA_{t-4}**	**0.90**	**0.80**	**0.79**	**0.43**	**0.46**	**0.80**	**0.79**
S_{11}	T_t	0.50	0.70	0.70	0.53	0.55	0.70	0.70
S_{12}	T_t, T_{t-1}	0.60	0.71	0.70	0.52	0.55	0.71	0.70
S_{13}	T_t, T_{t-1}, T_{t-2}	0.80	0.72	0.72	0.51	0.53	0.72	0.72
S_{14}	Tt, Tt-1, T_{t-2}, T_{t-3}	0.80	0.72	0.71	0.51	0.54	0.72	0.71
S_{15}	T_t, T_{t-1}, T_{t-2}, T_{t-3}, T_{t-4}	0.70	0.72	0.73	0.51	0.52	0.72	0.73

Table 3. 7 Training and testing statistics of AFIS3 FCM clustering model by using different input combinations for the Gilgit basin.

Scenarios	Model inputs	No of Clusters	R^2		RMSE		NSE	
			Training	Testing	Training	Testing	Training	testing
S_1	Q_t	2	0.77	0.78	0.46	0.47	0.77	0.78
S_2	Q_t, Q_{t-1}	4	0.77	0.78	0.46	0.47	0.77	0.78
S_3	Q_t, Q_{t-1}, Q_{t-2}	2	0.77	0.78	0.46	0.47	0.78	0.78
S_4	Q_t, Q_{t-1}, Q_{t-2}, Q_{t-3}	2	0.77	0.78	0.46	0.48	0.77	0.78
S_5	Q_t, Q_{t-1}, Q_{t-2}, Q_{t-3}, Q_{t-4}	2	0.77	0.78	0.46	0.48	0.77	0.77
S_6	Q_t, SCA_t	2	0.78	0.78	0.45	0.47	0.78	0.78
S_7	Q_t, SCA_t, SCA_{t-1}	2	0.78	0.78	0.45	0.47	0.78	0.78
S_8	Q_t, SCA_t, SCA_{t-1}, SCA_{t-2}	2	0.78	0.77	0.45	0.48	0.80	0.78
S_9	Q_t, R_{t-1}, SCA_t, SCA_{t-4}	2	0.79	0.78	0.44	0.47	0.79	0.78
S_{10}	**Q_t, T_{t-1}, $Evap_{t-1}$, SCA_t, SCA_{t-4}**	**2**	**0.80**	**0.78**	**0.43**	**0.47**	**0.80**	**0.78**
S_{11}	T_t	3	0.70	0.70	0.53	0.55	0.70	0.70
S_{12}	T_t, T_{t-1}	2	0.71	0.70	0.53	0.55	0.71	0.70
S_{13}	T_t, T_{t-1}, T_{t-2}	4	0.72	0.71	0.51	0.54	0.72	0.71
S_{14}	Tt, Tt-1, T_{t-2}, T_{t-3}	6	0.76	0.72	0.48	0.53	0.76	0.72
S_{15}	T_t, T_{t-1}, T_{t-2}, T_{t-3}, T_{t-4}	2	0.72	0.70	0.51	0.55	0.72	0.70

Table 3. 8 Training and testing statistics of MARS model by using different input combinations for the Gilgit basin.

Scenarios	Model inputs	Basis Function	R^2		RMSE		NSE	
			Training	Testing	Training	Testing	Training	testing
S_1	Q_t	5	0.77	0.78	0.47	0.47	0.77	0.78
S_2	Q_t, Q_{t-1}	15	0.77	0.78	0.47	0.47	0.77	0.78
S_3	Q_t, Q_{t-1}, Q_{t-2}	15	0.77	0.78	0.47	0.47	0.77	0.78
S_4	Q_t, Q_{t-1}, Q_{t-2}, Q_{t-3}	15	*0.77*	*0.78*	*0.47*	*0.47*	*0.77*	*0.78*
S_5	Q_t, Q_{t-1}, Q_{t-2}, Q_{t-3}, Q_{t-4}	15	0.78	0.78	0.47	0.47	0.77	0.78
S_6	Q_t, SCA_t	15	0.77	0.78	0.46	0.48	0.78	0.77
S_7	Q_t, SCA_t, SCA_{t-1}	20	0.77	0.77	0.46	0.48	0.77	0.77
S_8	Q_t, SCA_t, SCA_{t-1}, SCA_{t-2}	15	0.77	0.77	0.46	0.48	0.77	0.77
S_9	Q_t, R_{t-1}, SCA_t, SCA_{t-4}	25	0.78	0.77	0.45	0.48	0.78	0.77
S_{10}	**Q_t, T_{t-1}, $Evap_{t-1}$, SCA_t, SCA_{t-4}**	**10**	**0.79**	**0.79**	**0.45**	**0.46**	**0.79**	**0.79**
S_{11}	T_t	20	0.69	0.70	0.54	0.55	0.69	0.70
S_{12}	T_t, T_{t-1}	15	0.70	0.70	0.53	0.55	0.70	0.70
S_{13}	T_t, T_{t-1}, T_{t-2}	10	0.71	0.71	0.52	0.55	0.71	0.70
S_{14}	Tt, Tt-1, T_{t-2}, T_{t-3}	10	0.72	0.71	0.52	0.54	0.72	0.71
S_{15}	T_t, T_{t-1}, T_{t-2}, T_{t-3}, T_{t-4}	20	0.72	0.71	0.51	0.54	0.72	0.71

For application of the ANN model, the transfer functions logsig, purelin, tansig, and radbas were used in the hidden layers. The network was trained by using 16 combinations of four transfer functions for input and output layers. The optimum number of neurons was determined ranging from 3-8 in single hidden layers for overall input scenarios giving best results at the end. Table 3.4 shows the results of various input combinations using ANN model. For the ANFIS-GP, ANFIS-SC, and ANFIS-FCM models, the hybrid algorithm was used in this study.

For the ANFIS-GP model application, the gaussmf, gauss2mf, trimf, trapmf, gbellmf, pimf, dsigmf, and psigmf membership functions were used. In ANFIS-GP, the type of membership functions and number of member functions are important for training the network. Table 3.5 shows the results of all scenarios using the ANFIS-GP model with optimal number and type of membership functions. The optimal number of functions ranges between 2 to 4 for all scenarios.

For application of the ANFIS-SC model, the network is trained with an optimal range of the radius of clusters which give a minimum value of RMSE and highest values of R^2 and NSE. The optimal value of the cluster radius represents the influence of the cluster radius on the dataset clusters. If the cluster radius is small, then there are numerous small cluster datasets.

On the other hand, a large value of the cluster radius means that there are few large cluster datasets for training the network. During training of the network, the hit-and-trial method was used to find out the optimum value of the cluster radius with the smallest value of RMSE for all scenarios during the testing period. Table 3.6 shows the results of the ANFIS-SC model for all scenarios. It was found that the optimal range of the cluster radius is from 0.5-0.9 for all scenarios.

For application of the ANFIS-FCM model, the various numbers of clusters were used to train and test the network for all scenarios. Table 3.7 shows the results of the ANFIS-FCM model for all input combinations. The optimal number of clusters ranges between 2 to 6 for this study with the lowest value of RMSE and highest value of R^2 during testing of the network for all input combinations.

For application of the MARS model, the controlling parameters generally include the maximum basis functions, maximum interaction, speed factor, minimum number of observations between knots, penalty of variable, and degree of freedom. However, for this study, the hit-and-trial method was used to train the model with an optimal number of maximum basis functions ranging from 5 to 25 for all input scenarios with the remaining parameters being default values in the model. Table 3.8 shows the results of the MARS model for various input scenarios used in this study.

For application of the sediment rating curve (SRC) model, the power law function was used to train the model with 70% of the datasets after transformation of flows and sediment yields into logarithm form.

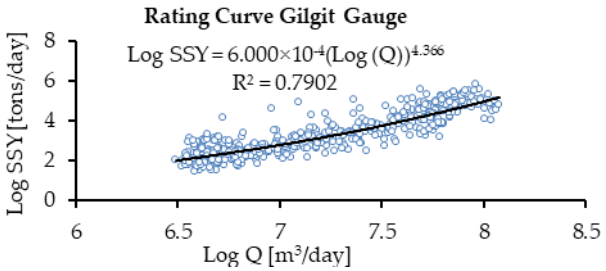

Figure 3. 4 Plot of the sediment rating curve (SRC) for the Gilgit basin.

After training of SRC with 70% of data sets the model was tested with 30% of the remaining data. The Figure 3.4 shows the plot of the sediment rating curve by using the power law functions. The Table 3.9 also shows the results of training and testing of sediment rating curve (SRC) model and compares its model performance statistics with other model used for predictions of sediment yields used in this study.

Table 3. 9 Comparison of the performance measurements by using the SRC, ANFIS-GP, ANFIS-SC, ANFIS-SC, ANFIS-FCM and MARS models in predictions of sediment yields.

Models	Training period			Testing period		
	R^2	RMSE	NSE	R^2	RMSE	NSE
SRC	0.81	0.49	0.75	0.71	0.60	0.66
ANN	**0.81**	**0.42**	**0.81**	**0.82**	**0.43**	**0.81**
ANFIS-GP	0.79	0.44	0.79	0.78	0.47	0.78
ANFIS-SC	0.80	0.43	0.80	0.79	0.46	0.79
ANFIS-FCM	0.80	0.43	0.80	0.78	0.47	0.78
MARS	0.79	0.45	0.79	0.79	0.46	0.79

3.3.2 Comparison of the ANN, ANFIS-GP, ANFIS-SC, ANFIS-FCM, MARS and SRC models

The results of the training and validation of the various scenarios are shown in Tables 3.4-3.9 for the ANN, ANFIS-GP, ANFIS-SC, ANFIS-FCM, MARS, and SRC models for predictions of the sediment yields for the Gilgit basin. In Table 3.4, the ANN shows the best performance of S10 scenarios with model inputs of Qt, Tt-1, Evapt-1, SCAt, and SCAt-4. In the ANN, the model parameters having radbas and tansig as input and output transfer functions along with five numbers of neurons performed best with S10 input scenarios during the training and validation phases. Table 3.5 shows the results of the ANFIS-GP for all input scenarios. Here, the ANFIS-GP shows the best performance of the model with S7 scenarios consisting of inputs of Qt, SCAt, and SCAt-1. The ANFIS-GP model performs best with model parameters consisting of triangular (trimf) membership functions along with two numbers of membership functions (MFs). The results of the ANFIS-SC model are shown in Table 3.6.

From Table 3.6, the input scenario S10 involving the inputs of Qt, Tt-1, Evapt-1, SCAt, and SCAt-4 gives the best performance of the ANFIS-SC model. The ANFIS-SC uses the model parameters having the value of a cluster radius of 0.90 to perform best with S10 input combinations. Table 3.7 shows the results of input scenarios by using the ANFIS-FCM model. It is evident that the best performance of the ANFIS-FCM model, too, was obtained with S10 scenarios having inputs of Qt, Tt-1, Evapt-1, SCAt, and SCAt-4. In the ANFIS-FCM model, the best network was developed by using the model parameter having two numbers of clusters with S10 input scenario.

Table 3.8 represents the results of the MARS model used in this study for prediction of the sediment yield of the Gilgit River basin. As shown in Table 3.8, again the input scenario S10 involving the inputs of Qt, Tt-1, Evapt-1, SCAt, and SCAt-4 developed the best-performing network in the MARS model. The MARS model performed best with its basis function (BF) parameter having the value of 10 with the S10 scenario.

Table 3.9 shows the overall results of the best networks of the ANN, ANFIS-GP, ANFIS-SC, ANFIS-FCM, and MARS models compared with the sediment rating curve performance for the Gilgit basin. Table 3.8

shows that the ANN model performs better than all other models with the least values of the RMSE errors of 0.42 and 0.43 during the training and testing phase.

Similarly, Figure 3.5 shows the scatter plot between the observed and predicted SSY by using ANN, ANFIS-GP, ANFIS-SC, ANFIS-FCM, MARS, and SRC during the testing phase for overall best input scenarios. From the scatter plot graphs, it can be observed that the ANN-based model has the least scatters with the highest value of R^2 during the testing phase. The ANN has improved the results of the scatter plot of the R^2 value to up to 0.82 in comparison to the rating curve R^2 value of 0.71 during the testing period.

Figure 3.6 shows the annual time series variation graphs of the observed and estimated SSY by using the ANN, ANFIS-GP, ANFIS-SC, ANFIS-FCM, MARS, and SRC models with best- performed input combinations. This Figure also includes the one detailed graph derived from the main time series plot to compare all model performances during the peak annual suspended sediment yields (SSY) period of the year 2005.

It is illustrated in Figure 3.6 that during the peak SSY period of the year 2005, the estimated SSY of the models ANN, MARS, and ANFIS-FCM are relatively closer to the observed SSY than those of the other models. However, the models ANFIS-GP and ANFIS-SC significantly underestimated the SSY during this peak year period of 2005. Similarly, the SRC model significantly overestimated the SSY during that period.

Figure 3.7 shows an overall comparison of different input variable scenarios developed from flows Q [m^3/day], snow cover area SCA [fractions], effective mean basin rainfall R [mm/day], mean basin average temperatures T [ºC/day], and mean basin evapotranspiration Evap [mm/day] for predictions of SSY during the testing period in the Gilgit basin. The model performance of R^2 was improved up to the value of 0.82 by introducing the combinations of the snow cover area along with flows, effective rainfall, temperatures, and evapotranspiration. The input combinations consisting of only the mean basin average temperature T perform less than other combinations consisting of flows, snow covers, effective rainfall etc. However, the mean basin average temperature T variable scenarios' performance with an R^2 value of 0.76 is better than the rating curve with an R^2 value of 0.71.

Rajaee et al. [22] applied artificial neural networks (ANNs), neuro-fuzzy (NF), multiple linear regression (MLR) and sediment rating curve (SRC) for prediction of suspended sediment concentrations (SSC) for Little Black River and Salt River in United states of America (USA). For example, in Little Black River gauging station, the value of R^2 was 0.69 for NF model, while it was 0.45, 0.25 and 0.23 for ANN, MLR and SRC models respectively. In the present study, the value of R^2 ranges from 0.78-0.82 using ANN and ANFIS models. It suggests that the soft computing models could be successfully applied for daily prediction sediment yields.

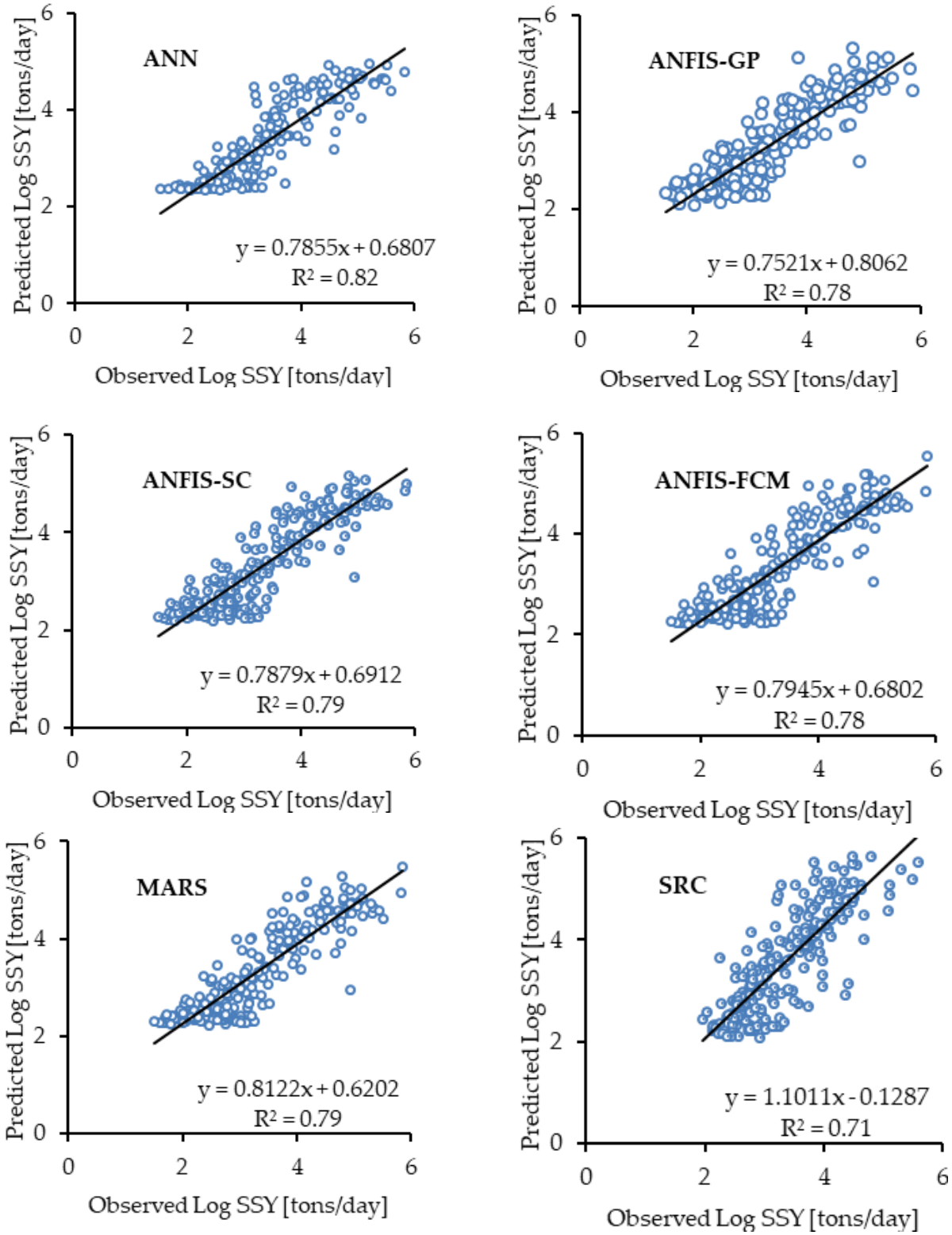

Figure 3. 5 Plot of the best performance measures for predictions of SSY by using the ANN, ANFIS-GP, ANFIS-SC, ANFIS-FCM, MARS and SRC model during testing phase for Gilgit basin.

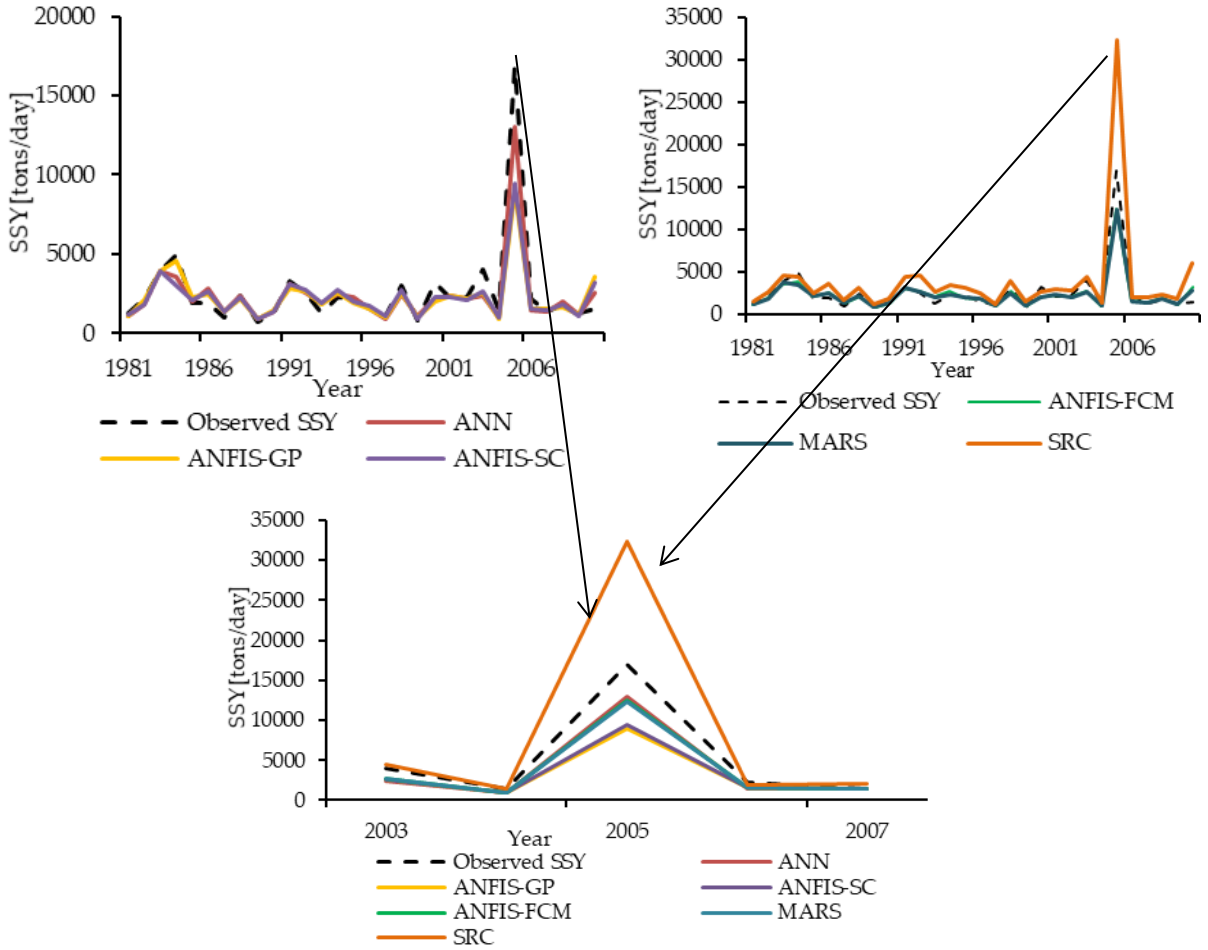

Figure 3. 6 Plot of the best performance measures for predictions of SSY by using the ANN, ANFIS-GP, ANFIS-SC, ANFIS-FCM, MARS and SRC model during testing phase for Gilgit basin.

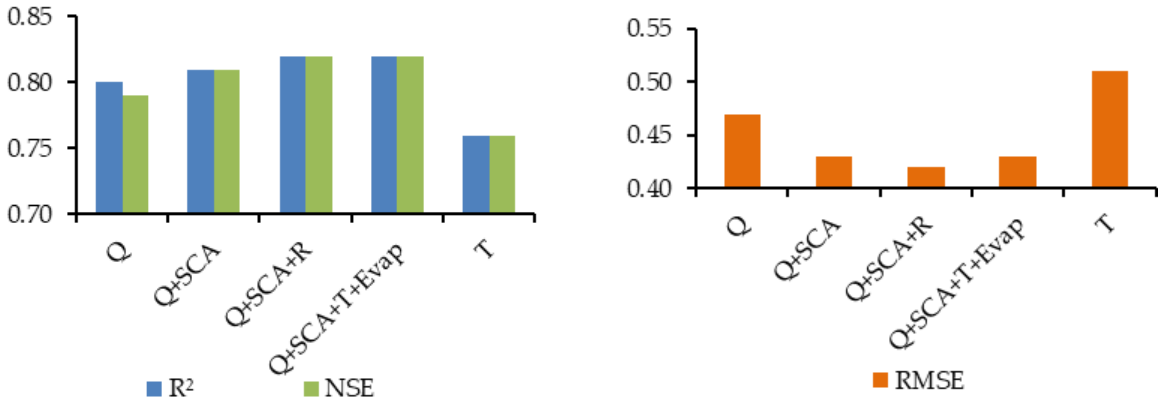

Figure 3. 7 Overall Comparison of performance measures of coefficient of determination (R^2), Nash–Sutcliffe efficiency model performance coefficient (NSE) and root mean squared error (RMSE) with different input variable scenarios during testing phase from all the models.

Table 3. 10 Comparison of the ANFIS-GP, ANFIS-SC, ANFIS-SC, ANFIS-FCM, MARS and SRC models' absolute sediment fluxes (%) for peak estimations of SSY for Gilgit basin.

Year	Peaks> 3200 [tons/day]	ANN [tons/day]	ANFIS-GP [tons/day]	ANFIS-SC [tons/day]	ANFIS-FCM [tons/day]	MARS [tons/day]	SRC [tons/day]
1983	3901	3934 (99.15)	3884 (99.56)	3886 (99.62)	3613 (92.62)	3826 (98.07)	4654 (80.69)
1984	4955	3542 (71.48)	4543 (91.68)	3033 (61.21)	3789 (76.46)	3385 (68.31)	4375 (88.29)
1991	3256	3088 (94.84)	2804 (86.11)	3128 (96.06)	3093 (94.99)	3105 (95.36)	4468 (62.77)
2003	4057	2372 (58.46)	2514 (61.96)	2616 (64.48)	2790 (68.77)	2674 (65.91)	4400 (91.54)
2005	16898	12993 (76.89)	8949 (52.95)	9480 (56.10)	12458 (73.72)	12365 (73.17)	32385 (8.35)
Mean (Relative Accuracy %)	**6613**	**5186 (80.17)**	**4539 (78.45)**	**4429 (75.49)**	**5149 (81.31)**	**5071 (80.16)**	**10056 (66.33)**

The mean values and absolute accuracy of predictions of SSY by using the ANFIS-GP, ANFIS-SC, ANFIS-SC, ANFIS-FCM, MARS and SRC models for Gilgit basin are shown in the Table 3.10. From Table 3.10 the ANN model predicted the mean of sediment peaks, 6613 [tons/day] as 5186 [tons/day] while the ANFIS-GP, ANFIS-SC, ANFIS-FCM, MARS and SRC resulted in less accurate outcomes than ANN model. However, Table 3.10 shows also that the model ANFIS-FCM with a relative accuracy of 81.31 % has superior accuracy in predicting the peak values of sediment yields compared to the ANN (80.17 %), ANFIS-GP (78.45 %), ANFIS-SC (75.49 %), MARS (80.16%) and SRC (66.33%) models respectively.

3.3.3 Deveoplement of Multiple Linear Regression Equation

The relationships between the measured sediment yields and the best-performing scenarios of the ANN, ANFIS-GP, ANFIS-SC, ANFIS-FCM, and MARS models have been developed using 70% of the data. The remaining 30% of the data was used to test the equation of multiple linear regression developed between the measured sediments and data-based model outputs. Equation 23 represents the relation between log-transferred measured sediments loads and data-based log-transferred modeled sediment loads as:

$$y = 0.60x_1 + 0.45x_2 + 0.11x_3 + 0.20x_4 - 0.05x_5 - 0.19x_6 - 0.39 \qquad (23)$$

where y = observed/measured sediment load in log form (tons/day), x1 = ANN model outputs of sediment load in log form (tons/day), x2 = ANFIS-GP model outputs of sediment load in log form (tons/day), x3 = ANFIS-SC model outputs of sediment load in log form (tons/day), x4 = ANFIS-FCM model outputs of sediment load in log form (tons/day), x5 = MARS model outputs of sediment load in log form (tons/day), and x6 = SRC model outputs of sediment load in log form (tons/day). Figure 3.8 shows the results of the multiple linear regression Equation 23 during the training and testing periods.

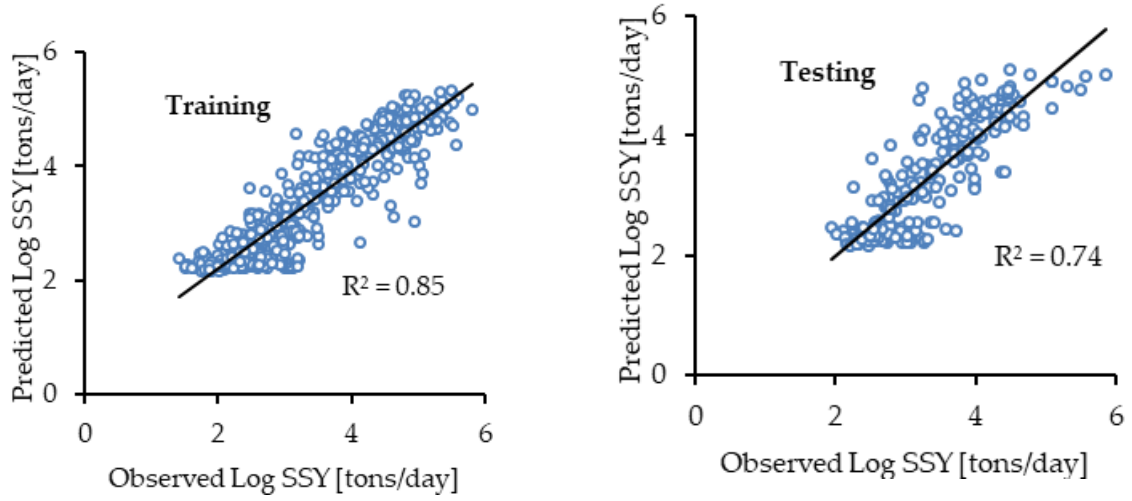

Figure 3. 8 Plot of the SSY by using ensembled average equation during training and testing phase for Gilgit basin.

3.4 Conclusions

This study was designed to improve the predictions of sediment yields by using different input variables applying the ANN, ANFIS-GP, ANFIS-SC, ANFIS-FCM, and MARS models in addition to the SRC model to the snow- and ice melt-dominated Gilgit basin. The objective of the study was to compare and examine the appropriate input variables based on the knowledge of hydrological process- and snow- and ice melt-dominated factors controlling erosion and sediment transport for predictions of sediment yields. To accomplish this objective, we investigated the input such as flows affecting channel erosion; temperature and snow cover area as snow melt erosion, glacier melt erosion and hillslope erosions; effective rainfall as mass wasting erosion, hillslope erosions and channel erosion; and evapotranspiration as effect of vegetation cover controlling catchment erosion for the prediction of sediment yields. It was concluded that for the prediction of sediment yields, the inputs of snow cover area, effective rainfall, and evapotranspiration significantly improve the accuracy of the ANN model when used in addition to flows and temperature as inputs. Combining the snow cover maps, effective rainfall, temperature, and evapotranspiration as inputs slightly increased the model performance (0.80 and 0.82) of R^2 when using the ANN model during the testing phase for the Gilgit River basin. It was concluded that the estimated snow cover area on land use maps and spatially distributed climatic information can improve the prediction of sediment yields when using data-based models.

It was also concluded that predictions of the peak values of sediment yields by means of the ANN, ANFIS-FCM, and MARS models are relatively closer to the values of the observed sediments than when using the SRC, ANFIS-GP, and ANFIS-SC models. The ANFIS-FCM, ANN, and MARS models predicted the sediment with relative accuracies of 81.31%, 80.17%, and 80.16%, respectively, against the peak values of

the observed time series. Overall, the ANFIS-FCM model was found to be more successful than the other models for predicting the peak values of sediments in the Gilgit basin.

Author Contributions: W.U.H. designed the work, highlighted the problem, formulated the work plan, analyzed the data and write up the paper. M.K.S. assisted in improving the work methodology and in writing up and reviewing the paper. A.C. coordinated the grid data and extracted it. F.S. and F.N assisted with practical knowledge and correction of the methodology.

Acknowledgments:
German Academic Exchange Service (DAAD) and the Higher Education Commission (HEC) of Pakistan. The Surface Water Hydrology Project (SWHP) of WAPDA and the Pakistan Meteorological Department (PMD) provided the hydro-climatic data. The Karlsruhe Institute of Technology (KIT) supported this work in the framework of the Open Access Publishing Program. We greatly appreciate all of the excellent support and help we received. The first author is also thankful to Prof Dr Immerzeel and his team from the Department of Geosciences at Utrecht University for providing the corrected grid rainfall data for the Upper Indus Basin (UIB).

Conflicts of Interest:
The Authors declare their no conflict of interests.

3.5 References

1. Foster, G.R.; Meyer, L.D. A Closed-Form Soil Erosion Equation for Upland Areas. In Sedimentation Symposium in Honor Prof. H.A. Einstein; Shen, H.W., Ed.; Colorado State University: Fort Collins, CO, USA, 1972; pp. 12.1–12.19.
2. Knack, I.M.; Shen, H.T. A numerical model for sediment transport and bed change with river ice. J. Hydraul. Res. 2018, 56, 844–856.
3. Burrell, B.C.; Beltaos, S. Effects and implications of river ice breakup on suspended-sediment concentrations: A synthesis. In Proceedings of the CGU HS Committee on River Ice Processes and the Environment 20th Workshop on the Hydraulics of Ice-Covered Rivers, Ottawa, ON, Canada, 14–16 May 2019.
4. Gomez, B. Bedload transport. Earth-Sci. Rev. 1991, 31, 89–132. doi.org/10.1016/0012-8252(91)90017-A
5. Kemp, P.; Sear, D.; Collins, A.; Naden, P.; Jones, I. The impacts of fine sediment on riverine fish. Hydrol. Process. 2011, 25, 1800–1821.
6. Yang, C.T.; Marsooli, R.; Aalami, M. T. Evaluation of total load sediment transport formulas using ANN. International Journal of Sediment Research 2009, 24, 274–286, doi:10.1016/S1001-6279(10)60003-0.
7. Bashar, K.E.; ElTahir, E.O.; Fattah, S.A.; Ali, A.S.; Osman, M. Nile Basin Reservoir Sedimentation Prediction and Mitigation. Nile Basin Capacity Building Network, Cairo, Egypt 2010. https://www.nbcbn.com/ctrl/images/img/uploads/4427_31104551.pdf.
8. Ghernaout, R.; Remini, B. Impact of suspended sediment load on the silting of SMBA reservoir (Algeria). Environ Earth Sci 2014, 72, 915–929, doi:10.1007/s12665-014-3125-9.
9. Wisser, D.; Frolking, S.; Hagen, S.; Bierkens, M.F.P. Beyond peak reservoir storage? A global estimate of declining water storage capacity in large reservoirs. Water Resour. Res. 2013, 49, 5732–5739, doi:10.1002/wrcr.20452.
10. Khan, N.M.; Tingsanchali, T. Optimization and simulation of reservoir operation with sediment evacuation: a case study of the Tarbela Dam, Pakistan. Hydrol. Process. 2009, 23, 730–747, doi:10.1002/hyp.7173.
11. Ackers, J.; Hieatt, M.; Molyneux, J.D. Mangla reservoir, Pakistan – approaching 50 years of service. Dams and Reservoirs 2016, 26, 68–83, doi:10.1680/jdare.16.00036.
12. Pakistan Water and Power Development Authority (WAPDA). 5th Hydrographic survey of Chashma Reservoir. International Sedimentation Research Institute, Pakistan (ISRIP) 2012.

13. King, R.; Stevens, M. Sediment management at Warsak, Pakistan. Int. J. Hydropower Dams 2001, 8, 61–68.
14. Meadows, .; Meadows, P.S. The Indus River. Biodiversity, resources, humankind / edited by Azra Meadows and Peter S. Meadows; Oxford University Press for the Linnean Society of London: Oxford, 1999, ISBN 0195779053.
15. Ahmad, N. Water Resources of Pakistan and Their Utilization, Shahid Nazir, Lahore, Pakistan. 1993. http://catalogue.nust.edu.pk/cgi-bin/koha/opac-detail.pl?biblionumber=695.
16. Pakistan Water Sector Strategy. Executive Summary; Report; Ministry of Water and Power, Office of the Chief Engineering Advisor/Chairman Federal Flood Commission, Govt of Pakistan: Islamabad, Pakistan 2002, Volume 1.
17. Pakistan Water Gateway. The Pakistan Water Situational Analysis; Report; Consultative Process in Pakistan (WCD CPP) Project; Pakistan Water Gateway 2005, https://de.scribd.com/document/334572557/Pakistan-Water-Situation-Analysis.
18. Faran Ali, K.; Boer, D.H. de. Factors controlling specific sediment yield in the upper Indus River basin, northern Pakistan. Hydrol. Process. 2008, 22, 3102–3114, doi:10.1002/hyp.6896
19. Chen, X.Y.; Chau, K.W. A Hybrid Double Feedforward Neural Network for Suspended Sediment Load Estimation. Water Resour Manage 2016, 30, 2179–2194, doi:10.1007/s11269-016-1281-2.
20. Jain, S.K. Development of Integrated Sediment Rating Curves Using ANNs. J. Hydraul. Eng. 2001, 127, 30–37, doi:10.1061/(ASCE)0733-9429(2001)127:1(30).
21. Kerem Cigizoglu, H.; Kisi, Ö. Methods to improve the neural network performance in suspended sediment estimation. Journal of Hydrology 2006, 317, 221–238, doi: 10.1016/j.jhydrol.2005.05.019.
22. Rajaee, T.; Mirbagheri, S.A.; Zounemat-Kermani, M.; Nourani, V. Daily suspended sediment concentration simulation using ANN and neuro-fuzzy models. Sci. Total Environ. 2009, 407, 4916–4927, doi: 10.1016/j.scitotenv.2009.05.016.
23. Melesse, A.M.; Ahmad, S.; McClain, M.E.; Wang, X.; Lim, Y.H. Suspended sediment load prediction of river systems: An artificial neural network approach. Agricultural Water Management 2011, 98, 855–866, doi: 10.1016/j.agwat.2010.12.012.
24. Taşar, B.; Kaya, Y.; Varçin, H.; Üneş, F.; Demirci, M. Forecasting of Suspended Sediment in Rivers Using Artificial Neural Networks Approach. International Journal of Advanced Engineering Research and Science 2017, 4, 79–84, doi:10.22161/ijaers.4.12.14.
25. Kumar, D.; Pandey, A.; Sharma, N.; Flügel, W.-A. Modeling Suspended Sediment Using Artificial Neural Networks and TRMM-3B42 Version 7 Rainfall Dataset. J. Hydrol. Eng. 2015, 20, doi:10.1061/(ASCE)HE.1943-5584.0001082.
26. Cobaner, M.; Unal, B.; Kisi, O. Suspended sediment concentration estimation by an adaptive neuro-fuzzy and neural network approaches using hydro-meteorological data. Journal of Hydrology 2009, 367, 52–61, doi: 10.1016/j.jhydrol.2008.12.024.
27. Kisi, O.; Haktanir, T.; Ardiclioglu, M.; Ozturk, O.; Yalcin, E.; Uludag, S. Adaptive neuro-fuzzy computing technique for suspended sediment estimation. Advances in Engineering Software 2009, 40, 438–444, doi: 10.1016/j.advengsoft.2008.06.004.
28. Kisi, O.; Shiri, J. River suspended sediment estimation by climatic variables implication: Comparative study among soft computing techniques. Computers & Geosciences 2012, 43, 73–82, doi: 10.1016/j.cageo.2012.02.007.
29. Emamgholizadeh, S.; Demneh, R. The comparison of artificial intelligence models for the estimation of daily suspended sediment load: a case study on Telar and Kasilian Rivers in Iran. Water Science and Technology: Water Supply 2018, 19, ws2018062, doi:10.2166/ws.2018.062.
30. Cimen, M. Estimation of daily suspended sediments using support vector machines. Hydrological Sciences Journal 2008, 53, 656–666, doi:10.1623/hysj.53.3.656.

31. Buyukyildiz, M.; Kumcu, S.Y. An Estimation of the Suspended Sediment Load Using Adaptive Network Based Fuzzy Inference System, Support Vector Machine and Artificial Neural Network Models. Water Resour Manage 2017, 31, 1343–1359, doi:10.1007/s11269-017-1581-1.
32. Kakaei Lafdani, E.; Moghaddam Nia, A.; Ahmadi, A. Daily suspended sediment load prediction using artificial neural networks and support vector machines. Journal of Hydrology 2013, 478, 50–62, doi: 10.1016/j.jhydrol.2012.11.048.
33. Rajaee, T. Wavelet and ANN combination model for prediction of daily suspended sediment load in rivers. Sci. Total Environ. 2011, 409, 2917–2928, doi: 10.1016/j.scitotenv.2010.11.028.
34. Olyaie, E.; Banejad, H.; Chau, K.-W.; Melesse, A.M. A comparison of various artificial intelligence approaches performance for estimating suspended sediment load of river systems: a case study in United States. Environ. Monit. Assess. 2015, 187, 189, doi:10.1007/s10661-015-4381-1.
35. Nourani, V.; Andalib, G. Daily and Monthly Suspended Sediment Load Predictions Using Wavelet Based Artificial Intelligence Approaches. Journal of Mountain Science 2015, 12, 85–100, doi:10.1007/s11629-014-3121-2.
36. Hild, C.; Bozdogan, H. The use of information-based model evaluation criteria in the GMDH algorithm. Systems Analysis Modelling Simulation 1995, 20, 29–50.
37. Ivakhnenko, A.G. The Group Method of Data of Handling; A rival of the method of stochastic approximation. Soviet Automatic Control 1968, vol.1, 3, 43-55.
38. Rahgoshay, M.; Feiznia, S.; Arian, M.; Hashemi, S.A.A. Simulation of daily suspended sediment load using an improved model of support vector machine and genetic algorithms and particle swarm. Arab J Geosci 2019, 12, 447, doi:10.1007/s12517-019-4444-7.
39. Malik, A.; Kumar, A.; Kisi, O.; Shiri, J. Evaluating the performance of four different heuristic approaches with Gamma test for daily suspended sediment concentration modeling. Environ. Sci. Pollut. Res. Int. 2019, 26, 22670–22687, doi:10.1007/s11356-019-05553-9.
40. Adnan, R.M.; Liang, Z.; Trajkovic, S.; Zounemat-Kermani, M.; Li, B.; Kisi, O. Daily streamflow prediction using optimally pruned extreme learning machine. Journal of Hydrology 2019, 577, 123981, doi: 10.1016/j.jhydrol.2019.123981.
41. Adnan, R.M.; Liang, Z.; El-Shafie, A.; Zounemat-Kermani, M.; Kisi, O. Prediction of Suspended Sediment Load Using Data-Driven Models. Water 2019, 11, doi:10.3390/w11102060
42. Vali, A.A.; Moayeri, M.; Ramesht, M.H.; Movahedinia, N. A. comparative performance analysis of artificial neural networks and regression models for suspended sediment prediction (case study: Eskandari cachment in Zayande Roud basin, Iran). Physical Geography Research Quarterly 2010, 42, 71, 21–30, https://www.sid.ir/en/Journal/ViewPaper.aspx?ID=173113.
43. Chachi, J.; Taheri, S.M.; Pazhand, H.R. Suspended load estimation using L1 -fuzzy regression, L2 -fuzzy regression and MARS-fuzzy regression models. Hydrological Sciences Journal 2016, 61, 1489–1502, doi:10.1080/02626667.2015.1016946.
44. Janga Reddy, M.; Ghimire, B. Use of Model Tree and Gene Expression Programming to Predict the Suspended Sediment Load in Rivers. Journal of Intelligent Systems 2009, 18, doi:10.1515/JISYS.2009.18.3.211.
45. Goyal, M.K. Modeling of Sediment Yield Prediction Using M5 Model Tree Algorithm and Wavelet Regression. Water Resour Manage 2014, 28, 1991–2003, doi:10.1007/s11269-014-0590-6.
46. Senthil Kumar, A.R.; Ojha, C.S.P.; Goyal, M.K.; Singh, R.D.; Swamee, P.K. Modeling of Suspended Sediment Concentration at Kasol in India Using ANN, Fuzzy Logic, and Decision Tree Algorithms. J. Hydrol. Eng. 2012, 17, 394–404, doi:10.1061/(ASCE)HE.1943-5584.0000445.
47. Immerzeel, W.W.; Wanders, N.; Lutz, A.F.; Shea, J.M.; Bierkens, M.F.P. Reconciling high-altitude precipitation in the upper Indus basin with glacier mass balances and runoff. Hydrol. Earth Syst. Sci. 2015, 19, 4673–4687, doi:10.5194/hess-19-4673-2015.

48. Lutz, A.F.; Immerzeel, W.W. HI-AWARE Reference Climate Dataset for the Indus, Ganges and Brahmaputra River Basins. FutureWater report 146. Wageningen, The Netherlands; 2015.
49. Tahir, A.A.; Chevallier, P.; Arnaud, Y.; Neppel, L.; Ahmad, B. Modeling snowmelt-runoff under climate scenarios in the Hunza River basin, Karakoram Range, Northern Pakistan. Journal of Hydrology 2011, 409, 104–117, doi: 10.1016/j.jhydrol.2011.08.035.
50. Adnan, M.; Nabi, G.; Saleem Poomee, M.; Ashraf, A. Snowmelt runoff prediction under changing climate in the Himalayan cryosphere: A case of Gilgit River Basin. Geoscience Frontiers 2017, 8, 941–949, doi: 10.1016/j.gsf.2016.08.008.
51. Shahin, M.A.; Maier, H.R.; Jaksa, M.B. Data Division for Developing Neural Networks Applied to Geotechnical Engineering. J. Comput. Civ. Eng. 2004, 18, 105–114, doi:10.1061/(ASCE)0887-3801(2004)18:2(105).
52. Pham, B.T.; van Phong, T.; Nguyen, H.D.; Qi, C.; Al-Ansari, N.; Amini, A.; Ho, L.S.; Tuyen, T.T.; Yen, H.P.H.; Ly, H.-B.; et al. A Comparative Study of Kernel Logistic Regression, Radial Basis Function Classifier, Multinomial Naïve Bayes, and Logistic Model Tree for Flash Flood Susceptibility Mapping. Water 2020, 12, 239, doi:10.3390/w12010239.
53. Hewitt, K. The Karakoram Anomaly? Glacier Expansion and the 'Elevation Effect,' Karakoram Himalaya. Mountain Research and Development 2005, 25, 332–340, doi:10.1659/0276-4741(2005)025[0332: TKAGEA]2.0.CO;2.
54. Hewitt, K. Tributary glacier surges: an exceptional concentration at Panmah Glacier, Karakoram Himalaya. J. Glaciol. 2007, 53, 181–188, doi:10.3189/172756507782202829.
55. Winiger, M.; Gumpert, M.; Yamout, H. Karakorum-Hindukush-western Himalaya: assessing high-altitude water resources. Hydrol. Process. 2005, 19, 2329–2338, doi:10.1002/hyp.5887.
56. Hock, R. Temperature index melt modelling in mountain areas. Journal of Hydrology 2003, 282, 104–115, doi:10.1016/S0022-1694(03)00257-9.
57. Costa, A.; Molnar, P.; Stutenbecker, L.; Bakker, M.; Silva, T.A.; Schlunegger, F.; Lane, S.N.; Loizeau, J.-L.; Girardclos, S. Temperature signal in suspended sediment export from an Alpine catchment. Hydrol. Earth Syst. Sci. 2018, 22, 509–528, doi:10.5194/hess-22-509-2018.
58. Artificial Neural Networks in Hydrology. I: Preliminary Concepts. J. Hydrol. Eng. 2000, 5, 115–123, doi:10.1061/(ASCE)1084-0699(2000)5:2(115).
59. Artificial Neural Networks in Hydrology. II: Hydrologic Applications. J. Hydrol. Eng. 2000, 5, 124–137, doi:10.1061/(ASCE)1084-0699(2000)5:2(124).
60. Haykin, S.S. Neural networks. A comprehensive foundation / Simon Haykin, 2nd ed.; Prentice Hall; London: Prentice-Hall International: Upper Saddle River, N.J., 1999, ISBN 0132733501.
61. Marquardt, D.W. An Algorithm for Least-Squares Estimation of Nonlinear Parameters. Journal of the Society for Industrial and Applied Mathematics 1963, 11, 431–441, doi:10.1137/0111030.
62. Rumelhart, D.E.; Hinton, G.E.; Williams, R.J. Learning Internal Representations by Error Propagation: Parallel Distributed Processing: Explorations in the Microstructure of Cognition, Vol. 1. In; Rumelhart, D.E., McClelland, J.L., PDP Research Group, C., Eds.; MIT Press: Cambridge, MA, USA, 1986; pp 318–362, ISBN 0-262-68053-X.
63. Minns, A.W.; Hall, M.J. Artificial neural networks as rainfall-runoff models. Hydrological Sciences Journal 1996, 41, 399–417, doi:10.1080/02626669609491511.
64. Nourani, V.; Baghanam, A.H.; Adamowski, J.; Gebremichael, M. Using self-organizing maps and wavelet transforms for space–time pre-processing of satellite precipitation and runoff data in neural network-based rainfall–runoff modeling. Journal of Hydrology 2013, 476, 228–243, doi: 10.1016/j.jhydrol.2012.10.054.
65. Jang, J.-S.R. ANFIS: adaptive-network-based fuzzy inference system. IEEE Trans. Syst., Man, Cybern. 1993, 23, 665–685, doi:10.1109/21.256541.

66. Mamdani, E.H.; Assilian, S. An experiment in linguistic synthesis with a fuzzy logic controller. International Journal of Man-Machine Studies 1975, 7, 1–13, doi:10.1016/S0020-7373(75)80002-2.
67. Takagi, T.; Sugeno, M. Fuzzy identification of systems and its applications to modeling and control. IEEE Trans. Syst., Man, Cybern. 1985, SMC-15, 116–132, doi:10.1109/TSMC.1985.6313399.
68. Abonyi, J.; Andersen, H.; Nagy, L.; Szeifert, F. Inverse fuzzy-process-model based direct adaptive control. Mathematics and Computers in Simulation 1999, 51, 119–132, doi:10.1016/S0378-4754(99)00142-1.
69. Yager, R.R.; Filev, D.P. Approximate clustering via the mountain method. IEEE Trans. Syst., Man, Cybern. 1994, 24, 1279–1284, doi:10.1109/21.299710.
70. Chiu, S. Extracting Fuzzy rules from Data for Function Approximation and Pattern Classification. Fuzzy Information Engineering: A Guided Tour of Applications; John Wiley & Sons: Hoboken, NJm USA, 1997, 1-10.
71. Chiu, S. Extracting fuzzy rules for pattern classification by cluster estimation. Proceedings of the Sixth International Fuzzy Systems Association World Congress, Sao Paulo, Brazl July 1995, 1-4.
72. Chiu, S. Fuzzy Model Identification Based on Cluster Estimation. Journal of the Intelligent and Fuzzy Systems 1994, 2, 267–278, doi:10.3233/IFS-1994-2306.
73. Cobaner, M. Evapotranspiration estimation by two different neuro-fuzzy inference systems. Journal of Hydrology 2011, 398, 292–302, doi: 10.1016/j.jhydrol.2010.12.030.
74. Bezdek, J.C.; Ehrlich, R.; Full, W. FCM: The fuzzy c-means clustering algorithm. Computers & Geosciences 1984, 10, 191–203, doi:10.1016/0098-3004(84)90020-7.
75. Jain, A.K.; Dubes, R.C. Algorithms for Clustering Data; Prentice-Hall, Inc: Upper Saddle River, NJ, USA, 1988, ISBN 0-13-022278-X.
76. Tsai, D.-M.; Lin, C.-C. Fuzzy C-means based clustering for linearly and nonlinearly separable data. Pattern Recognition 2011, 44, 1750–1760, doi: 10.1016/j.patcog.2011.02.009.
77. Taherdangkoo, M.; Bagheri, M.H. A powerful hybrid clustering method based on modified stem cells and Fuzzy C-means algorithms. Engineering Applications of Artificial Intelligence 2013, 26, 1493–1502, doi: 10.1016/j.engappai.2013.03.002.
78. Zhang, D.-Q.; Chen, S.-C. A novel kernelized fuzzy C-means algorithm with application in medical image segmentation. Artif. Intell. Med. 2004, 32, 37–50, doi: 10.1016/j.artmed.2004.01.012.
79. Friedman, J.H. Multivariate Adaptive Regression Splines. Ann. Statist. 1991, 19, 1–67, doi:10.1214/aos/1176347963.
80. Kisi, O.; Parmar, K.S. Application of least square support vector machine and multivariate adaptive regression spline models in long term prediction of river water pollution. Journal of Hydrology 2016, 534, 104–112, doi: 10.1016/j.jhydrol.2015.12.014.
81. Wang, L.; Kisi, O.; Zounemat-Kermani, M.; Gan, Y. Comparison of six different soft computing methods in modeling evaporation in different climates. Hydrol. Earth Syst. Sci. Discuss. 2016, 1–51, doi:10.5194/hess-2016-247.
82. Yilmaz, B.; Aras, E.; Nacar, S.; Kankal, M. Estimating suspended sediment load with multivariate adaptive regression spline, teaching-learning based optimization, and artificial bee colony models. Sci. Total Environ. 2018, 639, 826–840, doi: 10.1016/j.scitotenv.2018.05.153.
83. Tahir, A.A.; Chevallier, P.; Arnaud, Y.; Neppel, L.; Ahmad, B. Modeling snowmelt-runoff under climate scenarios in the Hunza River basin, Karakoram Range, Northern Pakistan. Journal of Hydrology 2011, 409, 104–117, doi: 10.1016/j.jhydrol.2011.08.035.
84. Tahir, A.A.; Hakeem, S.A.; Hu, T.; Hayat, H.; Yasir, M. Simulation of snowmelt-runoff under climate change scenarios in a data-scarce mountain environment. International Journal of Digital Earth 2019, 12, 910–930, doi:10.1080/17538947.2017.1371254.

85. Hayat, H.; Akbar, T.; Tahir, A.; Hassan, Q.; Dewan, A.; Irshad, M. Simulating Current and Future River-Flows in the Karakoram and Himalayan Regions of Pakistan Using Snowmelt-Runoff Model and RCP Scenarios. Water 2019, 11, 761, doi:10.3390/w11040761.
86. Lutz, A.F.; Immerzeel, W.W.; Kraaijenbrink, P.D.A.; Shrestha, A.B.; Bierkens, M.F.P. Climate Change Impacts on the Upper Indus Hydrology: Sources, Shifts and Extremes. PLoS ONE 2016, 11, e0165630, doi: 10.1371/journal.pone.0165630.
87. Adnan, M.; Nabi, G.; Kang, S.; Zhang, G.; Adnan, R.M.; Anjum, M.N.; Iqbal, M.; Ali, A.F. Snowmelt Runoff Modelling under Projected Climate Change Patterns in the Gilgit River Basin of Northern Pakistan. Pol. J. Environ. Stud. 2017, 26, 525–542, doi:10.15244/pjoes/66719.

3.6 Supplementary Materials

Supplementary Figures:

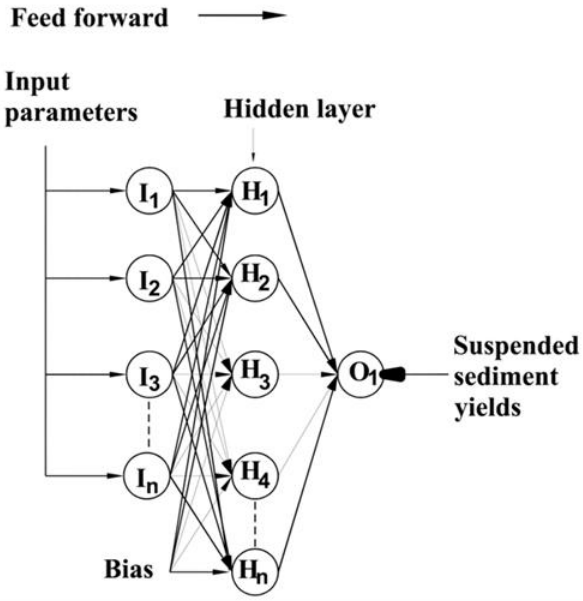

Figure A 1. Schematic diagram of the ANN model for prediction of sediment yields with one hidden layer.

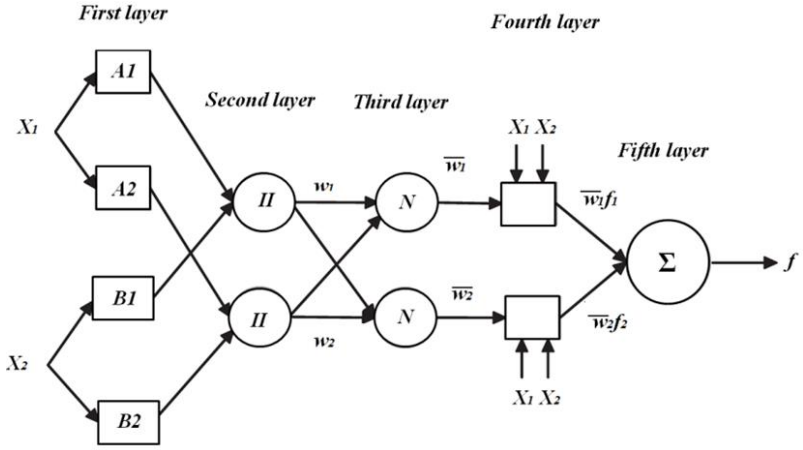

Figure A 2. Schematic diagram of the ANFIS model for prediction of sediment yields with two inputs.

Supplementary Tables:

Table A 1 Summary of the reviewed publications of data-based models sorted by year and input variables.

Serial #	Year	Authors	Input variables	Soft computing models
1	2001	Jain S.K [23]	Stage, Flows, Sediment	SRC, ANN
2	2006	Kerem et al. [24]	Flows, Sediment	SRC, ANN
3	2008	Cimen M. [33]	Flows, Sediment	ANN, SVM
4	2009	Rajaee et al. [25]	Flows, Sediment	SRC, ANN, ANFIS, MLR
5	2009	Cobaner et al. [29]	Flows, Sediment, Rainfall	SRC, ANN, ANFIS
6	2009	Kisi et al. [30]	Flows, Sediment	SRC, ANN, ANFIS
7	2010	Vali et al. [45]	Flows, Sediment	SRC, ANN, MARS
8	2011	Melesse et al. [26]	Flows, Sediment, Rainfall	ANN, MLR
9	2011	Rajaee T. [36]	Flows, Sediment	SRC, ANN, WANN
10	2012	Kisi et al. [31]	Flows, Sediment, Rainfall	ANN, ANFIS, GEP
11	2012	Senthil Kumar et al. [49]	Flows, Sediment, Rainfall	ANN, ANFIS, M5 tree
12	2013	Kakaei Lafdani et al. [35]	Flows, Sediment, Rainfall	ANN, SVM
13	2014	Goyal M.K [48]	Flows, Sediment, Rainfall	ANN, M5 tree, WR
14	2015	Kumar et al. [28]	Flows, Sediment, Rainfall	ANNs (LM, SCG, BR)
15	2015	Olyaie et al. [37]	Flows, Sediment	SRC, ANN, ANFIS, WANN
16	2015	Nourani et al. [38]	Flows, Sediment	ANN, WLSSVM, WANN
17	2016	Chachi et al. [46]	Flows	HMARS-FR, FLSR, FLAR
18	2017	Tsar et al. [27]	Flows, Sediment, Water Temperature	SRC, ANN, M5 tree, MLR
19	2017	Buyukyildiz et al. [34]	Flows, Sediment	ANN, SVM, ANFIS
20	2018	Emamgholizadeh et al. [32]	Flows, Sediment	ANN, ANFIS, GEP
21	2019	Adnan et al. [44]	Flows, Sediment	ANFIS-FCM, DENFIS, MARS

Table A 2 Characteristics of the Gilgit River basin in the Upper Indus River.

River flow gauging station	Gilgit at Gilgit
Longitude	74° 18′ 25′′
Latitude	35° 55′ 35′′
Altitude of stream gauging station	1454 m a.s.l
Catchment drainage area	12095 km^2
Glacier-covered area	1326.7891 km^2 (source GLIMS)

Glacier cover percentage	10.01 %		
Mean elevation	3997 m a.s.l		
Area above 5000 m	10.1 %		
No. of meteorological stations having data for period 1981-2010	Observations monitored by Pakistan Meteorological Department (PMD)		
	Gilgit	Gupis	
	1460 m a.s.l	2156 m a.s.l	
No. of meteorological stations having data for period 1996-2010	Observations monitored by Water and Power Development Authority of Pakistan (WAPDA)		
	Ushkore	Yasin	Shendure
	3051 m a.s.l	3280 m a.s.l	3712 m a.s.l

Chapter 4- Prediction of sediment yields by using the hydroclimate and normalized difference vegetation index (NDVI) datasets with soft computing models

4.1 Abstract

The reliable predictions of sediment yield in data-based modelling depend upon the selection of suitable input combinations. These input combinations are critical to build the structures of the models, which influence the performance and results of the data-based models. Here, hydroclimate and biophysical inputs datasets, consisting of flows, rainfall, mean air temperature and Normalized Difference Vegetation Index (NDVI) were assessed. The best performing input combinations were assessed by using the four Artificial Neural Networks (ANNs) and three Adaptive Neuro-Fuzzy Logic Inference System (ANFIS) algorithms for the Brandu River basin, the sub basin of Upper Indus Basin (UIB), Pakistan. The results of best performing input networks of ANN and ANFIS were also compared with outputs of Sediment Rating Curves (SRC). The results reveal that by introducing the remotely sensed NDVI as biophysical parameters, in addition to hydroclimate parameters, cannot improve its model performance. The ANFIS with grid partitioning (GP) performed better only in testing phase with inputs networks of flows and rainfall. However, in overall comparison the ANN with Levenberg-Marquardt (LM) performed best with inputs of flows, rainfall and mean air temperatures for the period 1981-2010. The ANN-LM algorithm improved the accuracy of R^2 up to 28% compared to SRC. Here, we demonstrate that the effects of flows, rainfall and mean air temperature are more dominated factors than biophysical parameters of NDVI in sediment transports of Brandu River. These finding will be valuable for management of sediments and designing of future planned water infrastructures in Brandu River basin.

Keywords: Sediment yields; Input combinations; Normalized Difference Vegetation Index (NDVI); Daggar basin; Data based models

4.2 Introduction

The prediction of sediment yield is useful for planning and management of water resources, river ecosystems, operation and management of water reservoirs, design of useful life of water infrastructures and management of hydropower projects. The process of soil erosion and generation of sediment loads is a famous hot spot having global attention worldwide to manage the water resources and restore the natural river environment for its ecology. The sediment load generated due to soil erosion and flows process is changing due to changes in climate and land use pattern in catchments. The increase of population, rapid urbanization, deforestation, over grazing of animals and rapidly increase in human activities has affected the land cover. The changes in land use affect the soil erodibility, land surface frictions/roughness, gradient of catchment surface [1]. This changes in the vegetation and land cover ultimately affects the sediment yields. Similarly, the changes in climate also affects the sediment generation of the catchment. In the light

of land cover and climate changes it has become important to predict the sediment loads due to complex erosion process of sediment yields.

Over the past few decades, water resource engineers, hydrologist and sediment management experts have used the hydrological and databased models by using the inputs of flows and climatic data for predictions of sediment yields [2]. For prediction of sediment yields to estimate the sediments the methods range from databased models to the lumped or conceptual models and physical based models. Generally, the two categories of methods had been used i) conceptual/semi-distributed models ii) data-based models [3,4,5]. In semi-distributed conceptual models, the large amount of input datasets and numerous model parameters are required during calibrations to predict the sediment yields. However, the data-based black box models require the fewer amounts of input variables and model parameters to predict the amount of sediment yields. For this reason, the black-box models are more popular in simulation of sediment yields in comparison to the conceptual semi-distributed models [6]. In databased black-box models' artificial neural networks (ANNs) are famous due to its flexibility in building the mathematical structures between inputs and outputs parameters both for linear and non-linear process like sediment transports to predict the sediment loads [7].

In the previous years, the numerous applications of artificial intelligence (AI) models were carried out to compare their results with other methods for simulation of sediment yields. In these studies [2,8,9,10,11,12] the artificial neural networks results were compared with the other models, including tradition sediment rating curves (SRC), autoregressive integrated moving average (ARIMA), multiple linear regressions (MLR), semi distributed soil and water assessment (SWAT) models etc. Singh et al. [2] compared the results of semi distributed SWAT and ANN model to predict the sediment yields in Nagwa agriculture watershed. From their research the ANN model simulated the sediment yields with better results compared to the SWAT model. Pektas et al. [8] compared the results of ANN with MLR and ARIMA model for prediction of sediment yield. From this study ANN has shown better results than ARIMA and MLR models.

In addition to above discussed models the comparison of ANN with the other models such as adaptive neuro fuzzy logic inference system (ANFIS), support vector machine (SVM), genetic-algorithm based artificial intelligence (GA-AI) and other AI models were also carried out by the researchers in various studies to predict the sediment yields. The comparison of ANN model with ANFIS models in the study [12] shown that ANN is superior to the ANFIS for predicting the semimonthly sediment loads for Gedizer River in Turkey. Kaveh et al. [13] compared the results of ANFIS models by using the Levenberg-Marqaurdt, Hybrid and Back-Propagation learning algorithms to predict the sediment yields. Kaveh et al. [13] found that the ANFIS by using the Levenberg-Marqaurdt perform better than the Hybrid and Back-Propagation algorithm. Cobaner et al. [14] also compared the results ANN with ANFIS and SRC model and found that ANFIS is better in prediction of sediment yields than other models. The comparison of ANN, ANFIS and Gene Expression Programming (GEP) by Kisi et al. [15] also found that the GEP performs better than the ANN and ANFIS model for estimation of sediment loads. Yadac et al. [16] in the regional research compared the results of ANN with, SRC, GA-AI and SVM models for the Mahanadi River, India. This research showed that GA-AI is better than ANN, ANFIS and SRC models in prediction of sediment yields.

The major difference in the performance of these models which were used for sediment predictions in literature is due to the combination of differences in the model parameters as well their input variables. The studies [8,13] used the discharges and sediment loads as input variables recorded at gauging station with ANN, MLR, ARIMA and ANFIS models. Similarly, Kumar et al. [9] developed the input vectors consisting of the satellite rainfall datasets in addition to the flows and sediment load by using the ANN model for predicting the suspended sediments. The researchers [2,10,12,14,15] made the input networks with combination of the flows, sediment loads and rainfall datasets by using the ANN, ANFIS and GEP

algorithms to predict the sediments yields. Similarly, in few researchers [11,16] the input combinations of flows, sediment loads and climatic (rainfall and temperature) variables were used for simulation of sediment yields in the ANN, ANFIS and SVM models.

In the recent decade the physical characteristics of the catchment representing the of vegetation cover estimated from Normalized Difference Vegetation Index (NDVI) in addition to the discharges was used for Asian basins to improve the prediction of SRC model [17]. Similarly, Asadi et al. [18] used the NDVI as an input variable in addition to the hydro-climatic datasets with the ANN model to predict the discharges in rainfall-runoff modelling for two basins in Queensland, Australia. From the security of the literature and to best of author knowledge previously no study has been carried out to use the NDVI as input variable in addition to discharges and climatic datasets for prediction of sediment yields using AI models. In this study with the application of ANN model results were compared with the SRC, MLR, ANFIS embedded with grid partition ANFIS-GP, ANFIS embedded with subtractive clustering ANFIS-SC and ANFIS embedded with C-Means ANFIS-FCM by using the hydro-climatic and NDVI as input variable for Daggar the Sub-basin of Upper Indus River in Pakistan.

4.3 Material and Methodology

4.3.1 Data collection and study area

The present study is carried out of Brandu River basin situated in lower part of Upper Indus Basin (UIB). The Brandu River is the right tributary of Upper Indus River which joins the Indus River downstream of the Besham Qila i.e. the intake stream gauging station of Tarbela reservoir. The Figure 4.1 & Table 4.1 shows the location and characteristics of the Brandu River basin. The catchment area of Brandu River lies with latitudes ranging from 34° 25′ 00′′ to 34° 43′ 00′′ and longitudes 72° 12′ 00′′ to 72° 30′ 00′′ having its drainage area of 598 km^2. The elevation of the catchment ranges from 685-2801 m a.m. sea level. The mean basin elevation of the catchment is 1112 m. The Figure 4.2 shows the land use map of the Brandu basin. The agriculture, dense forests and sparse forests covers the 42%, 12% and 16% of the total catchment area respectively. Similarly, grass lands and bare soil/others cover the 28% and 2% of the total catchment area respectively. The Water and Development Authority (WAPDA) of Pakistan installed the gauging station in year 1969 to measure the discharges and suspended sediment concentrations (SSC) at an altitude of 700 m a.m. sea level of Brandu River near Daggar. Currently, there is no climatic station installed inside of the catchment. The Table 4.2 also shows the detailed information of the data collected during this study for the period 1981-2010.

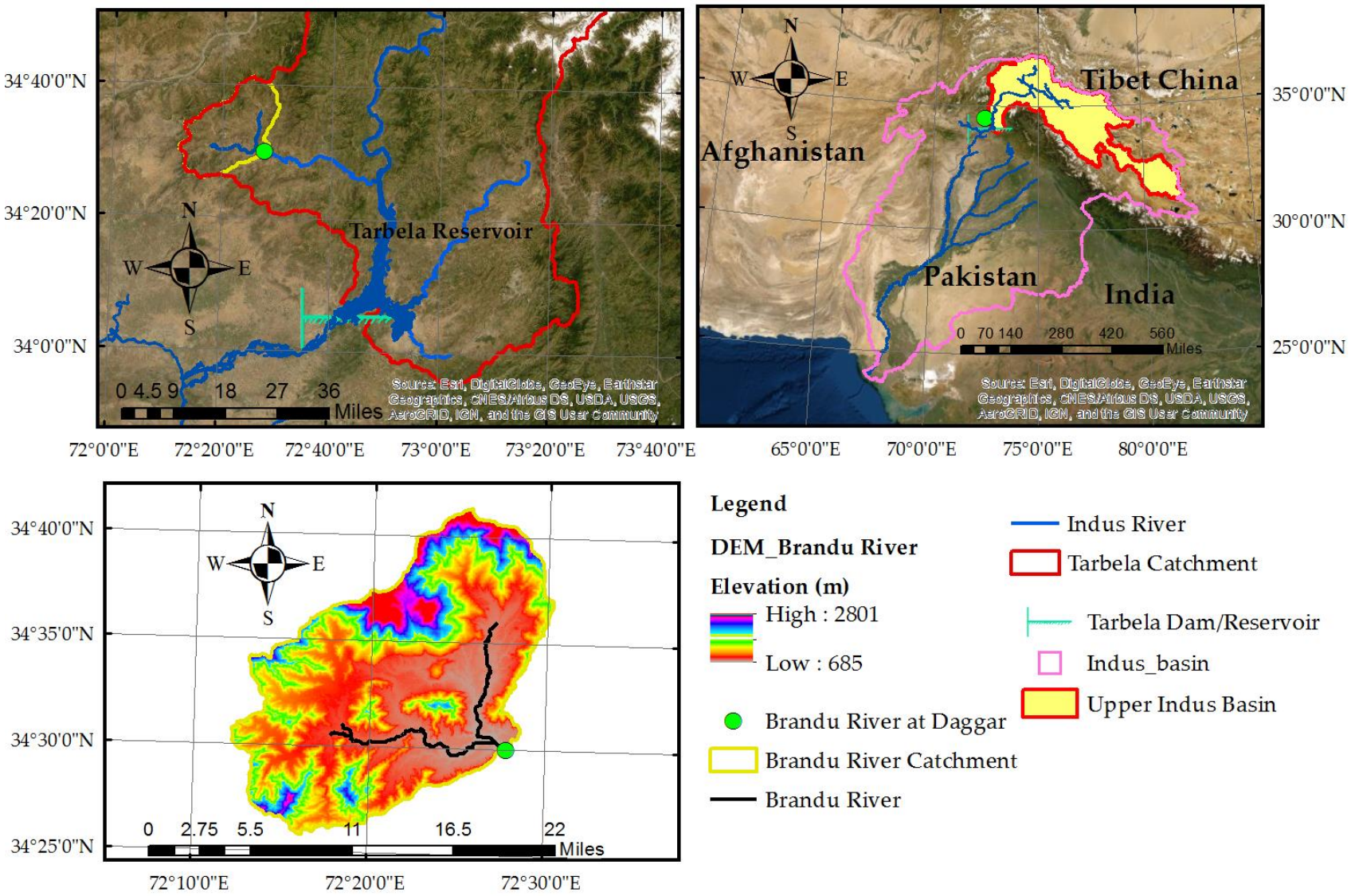

Figure 4. 1 Location of the Brandu River basin at the Daggar stream gauging station in the Upper Indus Basin (UIB) of Pakistan.

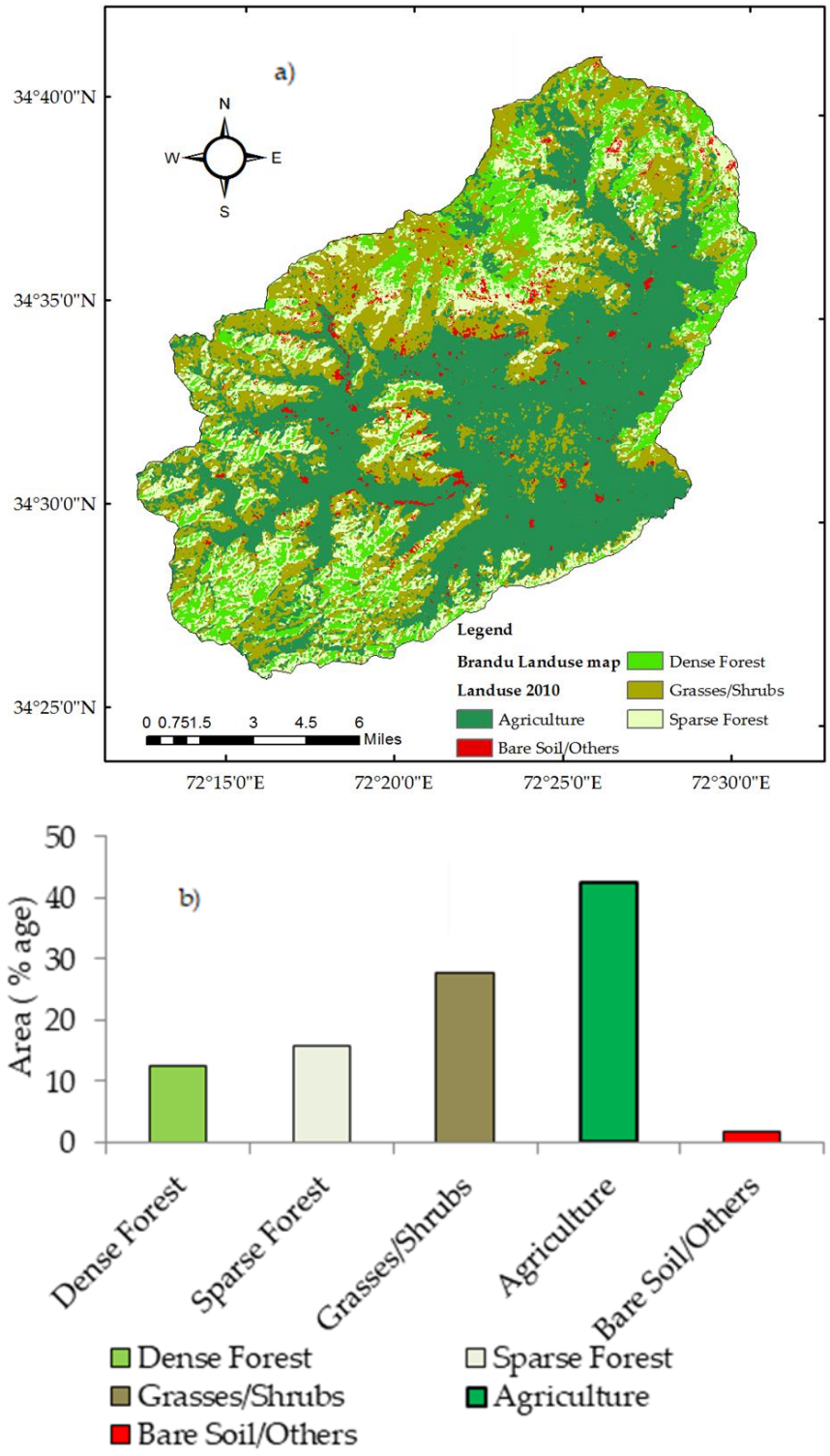

Figure 4. 2 Classification of the Landuse map of the Brandu River Basin for year 2010.

Table 4. 1 Characteristics of the Daggar River sub-basin of the Upper Indus River.

River flow gauging station	Brandu at Daggar
Longitude	72° 27′ 43′′
Latitude	34° 29′ 45′′
Altitude of stream gauging station	700 m
Catchment drainage area	598 km^2
Mean elevation	1112 m

The Figure 4.1 shows the hydrological characteristics of the catchment. The Brandu River basin is mainly the rainfall dominated basin of UIB. The mean monthly flows and SSC varies from 4.6-20.6 m^3/sec and 95-1726 mg/l respectively for the period 1981-2010. The mean annual flows and suspended sediment concentration (SSC) of Brandu River are 9.6 m^3/sec and 542 mg/l respectively during the period 1981-2010. Similarly, the mean basin total monthly rainfall and average temperature estimated from grid satellite data varies from 30-160 mm and 0.9-20.2 ºC respectively during the period 1981-2010. The mean basin total annual rainfall is approximately 1060 mm during the period 1981-2010. From the Figure 4.3, which shows that the basin flows and sediment yields of the basin mainly depends upon the seasonal spring and summer rainfall of the basin. The basin receives 74% of its annual rainfall starting from the springs (March) to the end of summer (October) season. This rainfall generates 92% and 87% contribution of annual flows and SSC during these two seasonal periods respectively. The Figure 4.3 also shows the monthly variation of normalized difference vegetation index (NDVI) with flows, SSC and rainfall. The value of mean monthly basin vegetation index also varies from 36% to 55% during the period 1981-2010. There are two peaks of the NDVI shown with the value of 47% and 55% during the months of April and August respectively due to higher monthly patterns of rainfall within the basin. The total 70% of the catchment area consists of agriculture and grass land majorly dependent upon the amounts of annual rainfall shows its importance in generation process of the amount of sediment yields and flows.

In this study in addition to the flows and SSC shown in the Table 4.2, the spatially distributed rainfall, mean temperature and normalized difference vegetation index (NDVI) datasets were used to predict the sediment yields of the basin. The grid climatic and NDVI datasets were extracted by using the SRTM 30 m DEM provided by (http://srtm.csi.cgiar.org/). The land use map of year 2010 of the Indus River is provided by The International Centre for Mountain Development (ICIMOD) (http://rds.icimod.org/Home/DataDetail?metadataId=28630). The DEM was used to extract the land use map for the study basin.

The Table 4.3 shows the Pearson correlation of the input and output variables used for this study. The cross correlation and partial auto correlation are generally used for lag times input combinations. However, these analyses cannot cover the non-linear relationship of input-output variables like sediment yields. Due to this reason various input combinations were scrutinized by examining the

test accuracy of the model outputs. The five better input combinations were used during this study for detailed model development as;

a. Q
b. Q, T
c. Q, P
d. Q, P, T
e. Q, P, T, NDVI

Where, Q = discharge [m^3/day], T = mean temperature [Cº], P = Rainfall [mm/day] and NDVI = Normalized difference vegetation index [fractions].

Table 4. 2 Collection of data used for prediction of suspended sediment yields of the Brandu River the Sub-basin of Upper Indus River.

Variable	Data Source	Period	Source
Q	Daily mean discharge [m^3 s^{-1}]	Daily, 1981–2010	Water and Power Development Authority (WAPDA), Pakistan
SSC	Suspended sediment concentration [mg l^{-1}]	Intermittent days per week 1981–2010	Water and Power Development Authority (WAPDA), Pakistan
NDVI	Normalized difference vegetation index in fractions ranging [0–1]	Weekly/bi monthly, basin avg. 1981–2010	https://ecocast.arc.nasa.gov/data/pub/gimms/3g.v0/
T	Daily mean, maximum & minimum air temperature [° C] on a 5x5 km grid	Daily, basin avg. 1981–2010	HI-AWARE project [43, 44]
P	Daily mean rainfall [mm day–1] on a 5x5 km grid	Daily, basin avg. 1981–2010	HI-AWARE project [43, 44]

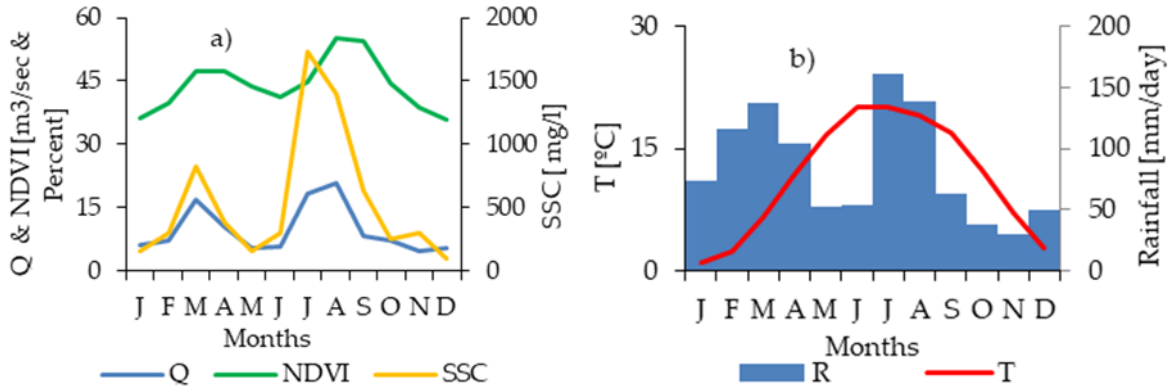

Figure 4. 3 Graphical presentations of (a) Discharges (Q), mean basin normalized difference vegetation index (NDVI) and suspended sediment concentrations (SSC) (b) mean basin rainfall (R) and mean basin average temperature (T) for Brand River basin

Table 4. 3 Relationship by using Pearson correlation coefficient for input variables of Gilgit Basin. Log Q: logarithm of water discharges; Log SSY: logarithm of sediment yields; SCA: snow covers area: T_{avg}: mean temperature; P: basin averaged effective rainfall; Evap: evapotranspiration.

	Q [m^3 day^{-1}]	Log SS_Y [tons day^{-1}]	NDVI [fractions]	T_{avg} [° C]	P [mm]
Q [m^3 day^{-1}]	1				
Log SS_Y [tons day^{-1}]	0.77	1			
NDVI [fractions]	0.43	0.38	1		
T_{avg} [° C]	0.12	0.31	0.45	1	
P [mm]	0.42	0.37	0.14	-0.08	1

Generally, the discharges are important to trigger the amount of sediments by channel erosion process. However, in addition to flows the rainfall, temperature and NDVI were also used with their different combinations. The rainfall triggers the hillslope erosion, gully erosions and mass wasting erosion. The temperature also controls the erosion process by indirect way in terms of leap area index etc. Similarly, as the basin is rain fed with most of its area covering the agriculture and grass land which could be represented by the NDVI values. The different values of NDVI affect the soil erosion process and transport capacity of flows with different friction losses over the periods. The dataset was divided into 83% and 17% for training and validation of the model respectively.

4.3.2 Artificial neural networks (ANN)

Artificial neural networks (ANNs) are soft computational models inspired from functions of brain nervous system. The development of ANN was originated with understanding of brain working to perform the tasks. From 1943-1949 McCulloch et al. and Hebb [19,20] started initially to design the neural model with ANN architectures called as ''postulate of learning'' for biological focused research purposes. The design of ANN during that was pure for biological research purposes rather than its focus with any computational ability. However, Rosenblatt et al. [21] expanded the work on neural model with introduction of perceptron learning theorem known as single layer feed forward neural network. Later on, Minsky at al. [22] explained the limitations of perceptron learning theorem with emphasizing on need of the extra computational layer in the model. In 1974 the backpropagation algorithm was developed during the Ph. D thesis by Werbos [23]. The significant development was made after 1980 by adding one more layer to single layer perceptron. This was known as multilayer perceptron learning algorithm. This multilayer perceptron learning algorithm gained the popularity by the research of Rumelhart et al. [24] in 1986.

Generally, ANN consists of three layers in a parallel system connected with the set of processing elements called as neurons functioning with the concept of brain nervous system of human body. These neurons or processing elements store the information and knowledge for computational purposes. The first layer of ANN is called input layer, second known as hidden (processing) layer and third layer is known as output layer. This system of parallel layers connected with number of neurons in each layer is known as Multilayer Perceptron (MLP). The Figure 4.4 further explains the basic architectures of the MLP ANN consisting of three layers. The literature [25, 26, 27, 28, 29, 30] further gives the explanation about the details of ANN model and its application in water sciences. The output layer generates the output for each network and then error between observed and network output is estimated. This output error is back-propagated for correction of weights in processing or hidden layer until the minimum errors between observed output and model output is optimized.

The performance of ANN model is dependent upon the number of neurons in hidden layer. The section of the number of neurons is important to avoid the over and under fittings of network. The optimum neurons should be in the range of $2\sqrt{N_1} + N_0$ where N1 and N0 are the number of input and output neurons respectively.

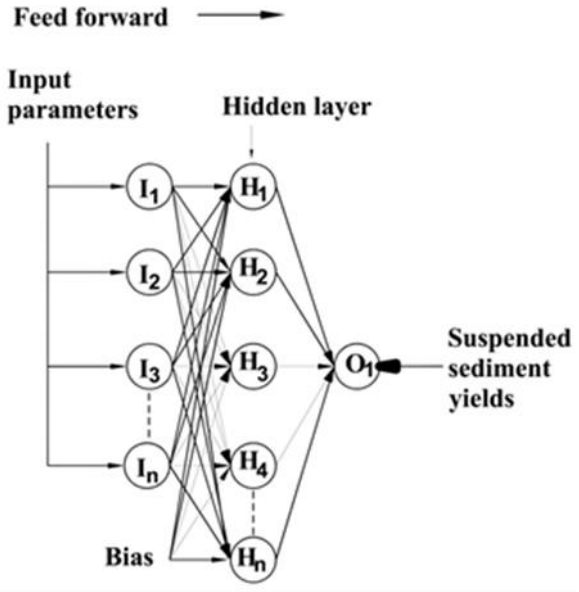

Figure 4. 4 Schematic diagram of ANN Model for prediction of sediment yields with one hidden layer.

In the present study ANN with (a) Levenberg-Marquardt (LM) (b) Bayesian Regularization (BR) (c) Gradient Descent (GD) (d) Scaled Conjugate Gradient (SGD) algorithms has been used to predict the sediment yields. The detailed information about the ANN could be found from the literature [31].

4.3.3 Adaptive neuro-fuzzy logic inference system (ANFIS)

The Adaptive neuro fuzzy logic inference system (ANFIS) is a novel architecture. It is the combinations of neural networks and fuzzy inference systems (FIS). The Figure 4.5 shows the basic [32] structure of ANFIS model. In ANFIS databased modelling the parameters of FIS are tuned up by using the neural network learning method. The ANFIS consist of a network structure which is connected with number of neurons. These neurons are characterized with fixed or adjustable parameters. The ANFIS translate the inputs parameters to the output values by fuzzy logic if-then rules with appropriate membership functions in ANN method. Three inference systems are classified as Tsukamoto's, Mamdani's and Sugeno's systems. The Mamdani's system [33] is mostly used in past. However, the Sugeno's system [34] is more efficient than other systems. In this study Sugeno's fuzzy logic structures has been used.

As an example, it's assumed that a FIS have two inputs x_1 and x_2 with target values of z. Here, inputs of discharge and NDVI can be supposed as x_1 and x2 with output z as sediment yield for a particular time t. Then in Sugeno's fuzzy logic structures typical rule set with two IF/THEN rules are expressed as:

Rule 1: IF x_1 is A_1 and x_2 is B_1, THEN $z_1 = f_1 = p_1 x_1 + q_1 x_{2+} r_1$ (1)

Rule2: IF x_1 is A_2 and x_2 is B_2, THEN $z_2 = f_2 = p_2 x_1 + q_2 x_{2+} r_2$ (2)

Where p_i, q_i and r_i are parameters corresponding to rule 1, Rule 2… Rule n.

The ANFIS model consists of five layers.

Layer 1

In first layer each node generates a membership grade for each input's variable. The output of i^{th} node with generalized bell membership function in first layer is expressed as:

$$Oi^1 = \mu_{Ai^{(x1)}} = \frac{1}{1+((x_1-c_i))/a_i)^{2Ni}} \quad (3)$$

Where, $\{a_i, c_i, N_i\}$ are the parameter sets for x_1 input in i^{th} node. These parameters change the shape of bell function in the range of 0-1.

Layer 2

The layer 2 is labeled with II in each node. In this layer every node multiplies the incoming signals coming from layer 1 as:

$$Oi^2 = wi = \mu_{Ai^{(x1)}} \times \mu_{Bi^{(x2)}} \quad , \quad i = 1, 2 \quad (4)$$

Layer 3

In layer 3 every node calculates the normalized firing strength as its relationship between firing strength of i^{th} rule to the sum of all rules:

$$Oi^3 = \bar{w} = \frac{w}{w_1+w_2} \quad i = 1, 2 \quad (5)$$

Layer 4

In layer 4 the sum of signals from second- and third-layers networks are calculated for each ith node towards the model output as:

$$Oi^4 = \bar{w}_i f_i = \bar{w}_i(p_i\, x_1 + q_i\, x_{2+} r_i) \quad i = 1, 2 \quad (6)$$

Here, $\bar{w}$ is the output from layer 3 in this equation.

Layer 5

Layer 5 calculates the overall output in the form of single node as the ANIFS model output against each target value as:

$$Oi^5 = \Sigma \bar{w}_i f_i = \frac{\Sigma \bar{w}_i f_i}{\Sigma \bar{w}_i} \quad i = 1, 2 \quad (7)$$

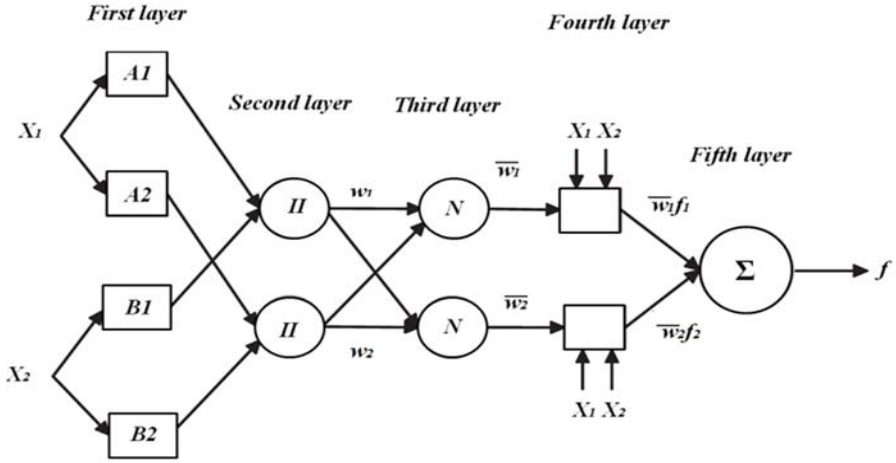

Figure 4. 5 Schematic diagram of ANFIS Model for prediction of sediment yields with two inputs.

This study used the hybrid learning method for determining model parameters of ANFIS. From the literature [35] the detail procedure and further information about ANFIS model can be found. For the current study three hybrid strategies of ANFIS model were used to produce the FIS. These strategies are named as grid partition (ANFIS-GP), subtractive clustering (ANFIS-SC) and fuzzy c-means clustering (ANFIS-FCM).

The ANFIS-GP is the combination of ANFIS and grid partition. The grid partition does the partition of the input linguistic variables by selecting appropriate combination of fuzzy numbers with its membership functions (MFs). In grid partition MFs are optimized according to input-output datasets starting from predefined number of MFs. The quantitative characteristics of datasets are divided into n partitions (n = 2, 3, 4…). In the current study eight MFs were used such as gaussmf, gauss2mf, trimf, trapmf, gbellmf, pimf, dsig, mf and psigmf. In AFNIS-GP model the number of rules has an exponential relationship with the number of input variables. The details about the ANFIS-GP can be found from the literature [32].

The ANFIS-SC model is the extended model derived from mountain clustering model [36]. It is combination of ANFIS model with subtractive clustering strategy. This model was later modified by Chiu [37]. The ANFIS-SC model has an advantage over mountain clustering method with the reduction of complex computations of mountain clustering. In ANFIS-SC model every data input combination is considered as potential cluster. The potential of each datasets is calculated by its distance from other data points in datasets. The value of influential radius is important to decide the number of clusters in the ANFIS-SC model. The smaller value of influential radius describes a greater number of clusters with more rules in comparison to its large value [38]. The critical value of influential radius during data space clustering procedure is determined by hit and trial methods. The detailed information and procedure of ANFIS-SC model can be found in the literature [39,40].

The ANFIS-FCM model was proposed [41, 42, 43, 44, 45] in the literature and enhanced by Zhang and Chen [46]. The ANFIS-FCM minimizes the errors by partitioning the X datasets into C clusters. This method reduced the errors regarding weighted distance of each data point xi towards all the centroids of the C clusters. After this the ANFIS-FCM model minimizes the objective function as:

$$Min\ J_{FCM} = \sum_{c=1}^{C}\sum_{i=1}^{N} {w^p}_{ic}\left\|x_{i-}\ v_c\right\|^2 \quad s.t.\sum_{c=1}^{C} w_{ic} = 1, i = 1,2,\dots,N \tag{8}$$

Where C, N, w_{ic}, v and x are number of clusters, number of data points, degree belongs to i^{th} data point of C^{ith} clusters data points and inputs data sets. The p (p > 1) entitles to the fuzzifier exponent. In ANFIS-FCM w_{ic} is calculated as:

$$w_{ic} = \frac{1}{\sum_{i=1}^{c}\left({d_{ic}}^2/{d_{ij}}^2\right)^{1/(p-1)}} \quad for\ i = 1,2,\dots N\ and\ c = 1,2,\dots C \tag{9}$$

In FCM model after initialization of centre vectors, centres are recomputed as:

$$v_c = \frac{\sum_{j=1}^{N} {w^p}_{Jc}\, x_j}{\sum_{j=1}^{N} {w^p}_{Jc}} \quad for\ c = 1,2,\dots N\ and\ 1 < p > N \tag{10}$$

The algorithm is run until convergence condition is completed.

4.3.4 Sediment rating curve (SRC)

The sediment rating curve is an empirical relationship of flows and sediment load or concentrations described as:

$$SSL_{(t)} = a \times {Q^b}_{(t)} \tag{11}$$

Where Q [m^3/day] is discharge, SSL [tons/day] both in log transformation form and a & b are the constants depends upon the characteristics of river and its catchments.

4.3.5 Performance measurement metrics for model evaluation

The performance of models was measured and assed using following statistics:

a. Pearson's correlation coefficient (R^2)

$$R^2 = \left(\frac{\sum_{i=1}^{N}(S_{i0} - \overline{S_{io}})(S_{is} - \overline{S_{is}})}{\sqrt{\sum_{i=1}^{N}(S_{i0} - \overline{S_{io}})^2 \sum_{i=1}^{N}(S_{is} - \overline{S_{is}})^2}}\right)^2 \tag{12}$$

Where *N* refers the data quantity, S_{io} is observed sediment and S_{is} is the simulated sediments and $\overline{S_{is}}$ is mean of simulated sediments.

b. Root mean square error (RMSE)

$$RMSE = \sqrt{\frac{1}{N}\sum_{i=1}^{N}((S_{io}) - (S_{is}))^2} \tag{13}$$

c. Nash-Sutcliffe efficiency (NSE)

$$NSE = 1 - \frac{\sum_{t=1}^{N}(S_{io} - S_{is})^2}{\sum_{t=1}^{N}(S_{is} - \overline{S_{is}})^2} \quad -\infty \leq NSE \leq 1 \qquad (14)$$

4.4 Results and Discussions

4.4.1 Relationships of NDVI between SSY, runoff and rainfall

The different distribution of land cover in the catchment has different size of impact on soil erosion process due to its variation of vegetative friction controlling the flows and eroding the sol in catchment. The Figure 4.6 shows the annual time series of flows, suspended sediment yields, normalized difference vegetation Index (NDVI) and rainfall since 1981-2010 in the Brandu River basin. The Figure 4.6 shows that the SSY is producing the similar pattern of trend as the flows, rainfall and partially NDVI both during wet and dry year period. However, normalized difference vegetation index (NDVI) is increasing after year 2000 opposite to the SSY, flows and rainfall trend. This increase in vegetation index is probably due to increase in the furrow agriculture area. The SSY is probably majorly controlled by the annual rainfall, flows generation and partially the land utilization for agriculture or vegetation in the catchment.

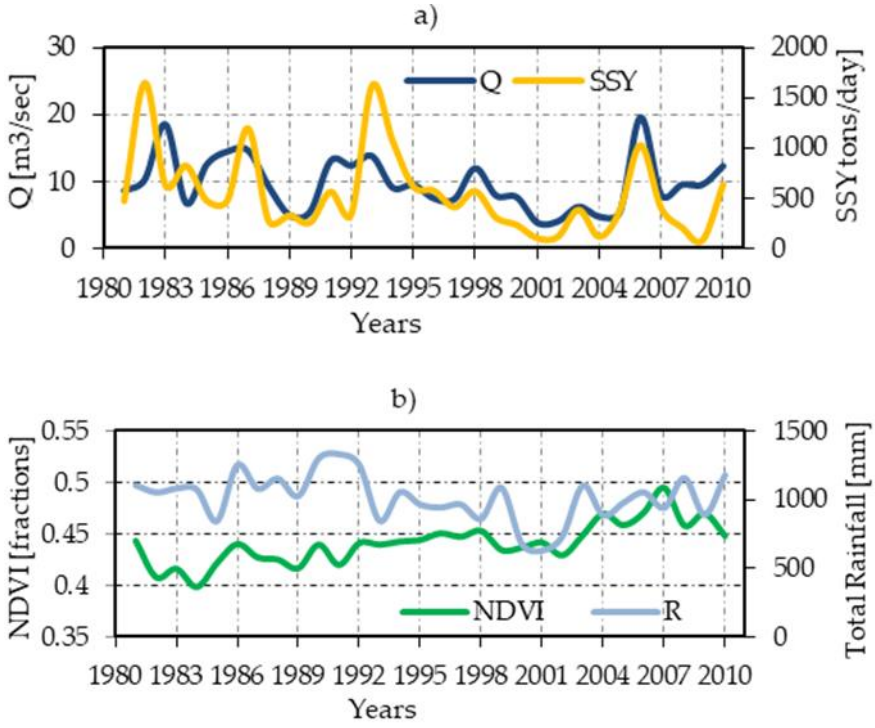

Figure 4. 6 Comparison among the annual flows (Q), suspended sediment yields (SSY), normalized difference vegetation Index (NDVI) and rainfall (mm) in the Brandu River basin.

4.4.2 ANN and ANFIS model results

In this study several input combinations were used to predict the sediment yields for Brandu River basin. The selection of input variable was decided with the best training and testing results of ANN and ANFIS networks. The Table 4.4 shows the results of the ANN models using four different feed forward back propogation alogithim for five bestl input combinations. The ANN model shows the better accuracies with input combinations of flows (Q), precipitation (P) and temperature (T) by using the Leveneberg-Marquardt (LM).

Similarly, Table 4.5 shows the training and test results of three ANFIS models embeded with grid partition (ANFIS-GP), subtractive clustering (ANFIS-SC) and fuzzy c-means clustering (ANFIS-FCM)

with five input combinations. The ANFIS model embeded with grid partition (ANFIS-GP) gives better results with input combinations of flows (Q) and precipitation (P).

Table 4. 4 Training and testing statistics of ANN model embedded with Levenberg-Marquardt (LM), Bayesian Regularization (BR), Gradient Descent (GD) and Scaled Conjugate Gradient (SCG) algorithms for Brandu River.

Learning method	Model inputs	Neurons	Transfer function		R^2		RMSE (tons/day)		NSE	
			Input	Output	Train	Test	Train	Test	Train	test
LM	Q	3	radbas	purelin	0.74	0.75	10,476	5,600	0.74	0.75
	Q, T	4	radbas	purelin	0.70	0.73	11,234	5,850	0.70	0.72
	Q, P	9	radbas	purelin	0.81	0.74	9,004	5,678	0.81	0.74
	Q, P, T	**13**	**radbas**	**tansig**	**0.90**	**0.77**	**6,472**	**5,573**	**0.90**	**0.75**
	Q, P, T, NDVI	5	logsig	purelin	0.88	0.73	6892	6564	0.88	0.65
BR	Q	8	radbas	purelin	0.82	0.69	8,638	8,364	0.82	0.67
	Q, T	4	logsig	tansig	0.89	0.70	6,716	6,131	0.89	0.7
	Q, P	4	radbas	purelin	0.84	0.69	8,166	6,219	0.84	0.69
	Q, P, T	5	logsig	purelin	0.89	0.74	6,829	5,773	0.89	0.73
	Q, P, T, NDVI	3	radbas	tansig	0.80	0.72	8963	6138	0.80	0.7
GD	Q	1	purelin	tansig	0.60	0.55	14,844	9,001	0.47	0.35
	Q, T	4	purelin	tansig	0.63	0.56	18,449	10,134	0.18	0.17
	Q, P	13	purelin	tansig	0.56	0.55	14,032	8,438	0.53	0.43
	Q, P, T	15	purelin	tansig	0.56	0.57	15,856	8,864	0.40	0.37
	Q, P, T, NDVI	20	purelin	tansig	0.54	0.54	14,162	7,797	0.52	0.51
SCG	Q	8	radbas	tansig	0.82	0.71	8,620	6,139	0.82	0.7
	Q, T	5	tansig	tansig	0.88	0.77	7,082	5,606	0.88	0.75
	Q, P	4	tansig	tansig	0.83	0.70	8,364	6,259	0.83	0.68
	Q, P, T	4	tansig	tansig	0.88	0.70	7,001	6,118	0.88	0.7
	Q, P, T, NDVI	4	tansig	tansig	0.88	0.63	6855	6,929	0.88	0.61

Table 4.4 shows that ANN-LM algorithm with the input combination of flows, precipitation and mean air temperature given minimum value of RMSE as 6,472 tons/day and 5,573 tons/day during training and testing period respectively. The optimum numbers of neurons were 13 with radbas and tansig as input and output transfer functions during this network respectively. Similarly, ANN-BR algorithmic also performed better with the input combination of flows, precipitation and mean air temperature. The minimum value of RMSE was 6,829 tons/day and 5,773 tons/day respectively during training and testing of the network. The optimum numbers of neurons were 5 having logsig and purelin as input and output transfer functions during this network. The ANN-GD performed better with input combination of flows and precipitation having RMSE of 14,032 tons/day and 8,438 tons/day during training and testing phase respectively. This network performed better at 13 optimum numbers of neurons with purelin and tansig as its input and output transfer functions. The ANN-SCG model performed better with input combinations of flows and mean air temperature showing the value of RMSE as 7,082 tons/day and 5,606 tons/day during training and testing of the

model respectively. This network selected 5 optimum numbers of neurons with tansig as its transfer functions both in input and output layers.

Table 4. 5 Training and testing statistics of AFIS model embedded with grid partition (GP), subtractive clustering (SC), fuzzy c-means (FCM) clustering algorithms and SRC model for Brandu River.

Learning method	Model inputs	Member Function	Transfer function	R^2		RMSE (tons/day)		NSE	
				Train	Test	Train	Test	Train	test
GP	Q	5	gaussmf	0.74	0.85	9,867	7,170	0.74	0.85
	Q, T	3	gaussmf	0.75	0.84	10,139	6,158	0.75	0.72
	Q, P	**2**	**gbellmf**	**0.71**	**0.85**	**10,865**	**4,603**	**0.71**	**0.84**
	Q, P, T	2	gaussmf	0.70	0.79	12,937	7,244	0.60	0.63
	Q, P, T, NDVI	2	dsigmf	0.70	0.86	12717	6533	0.60	0.80
SC	Q	0.14	radii	0.66	0.50	12,220	9,842	0.63	0.48
	Q, T	0.25	radii	0.64	0.69	12,120	6,437	0.64	0.67
	Q, P	0.11	radii	0.62	0.72	14,720	9,915	0.43	0.68
	Q, P, T	0.25	radii	0.62	0.76	13,571	8,623	0.52	0.76
	Q, P, T, NDVI	0.6	radii	0.56	0.58	13541	7748	0.56	0.6
FCM	Q	3	No.Clust.	0.77	0.71	12,918	6,800	0.77	0.71
	Q, T	5	No.Clust.	0.63	0.67	8,994	10,696	0.63	0.67
	Q, P	3	No.Clust.	0.63	0.67	12,330	6,803	0.63	0.67
	Q, P, T	7	No.Clust.	0.51	0.71	14,439	5,379	0.63	0.72
	Q, P, T, NDVI	9	No.Clust.	0.63	0.65	12,346	6,599	0.72	0.76
SRC	**Q**	**-**	**-**	**0.61**	**0.55**	**12,934**	**7,512**	**0.60**	**0.55**

Table 4.5 shows the results that the ANFIS-GP hybrid model performed better with input network of flows and precipitation having the RMSE of 10,865 tons/day and 4,603 tons/day during training and testing of network. This network was trained with 2 numbers of membership functions and gbellmf as its transfer function. The ANFIS-SC model shows the better results having flows and means air temperature as its model inputs. This model network shows the value of RMSE as 12,120 tons/day and 6,437 tons/day during the training and testing phase. This network performed better with influence radius of 0.25 as model parameter. Similarly, the ANN-FCM model performs better with only flow as input combination having RMSE of 12,918 tons/day and 6,800 tons/day during training and testing period. The model selected 3 optimum numbers of clusters during its best performance.

The Figure 4.7 also shows the RMSE statistics of ANN-LM, ANN- BR, ANN-GDS, ANN-SCG, ANFIS-GP, ANFIS-SC and ANFIS-FCM models for comparing the results with five input combinations during testing phase. The Figure 4.7 illustrates that the ANFIS-SC model performed better than other models during testing period. The ANFIS-SC model has shown the minimum value of RMSE with flows and precipitation as its input combination.

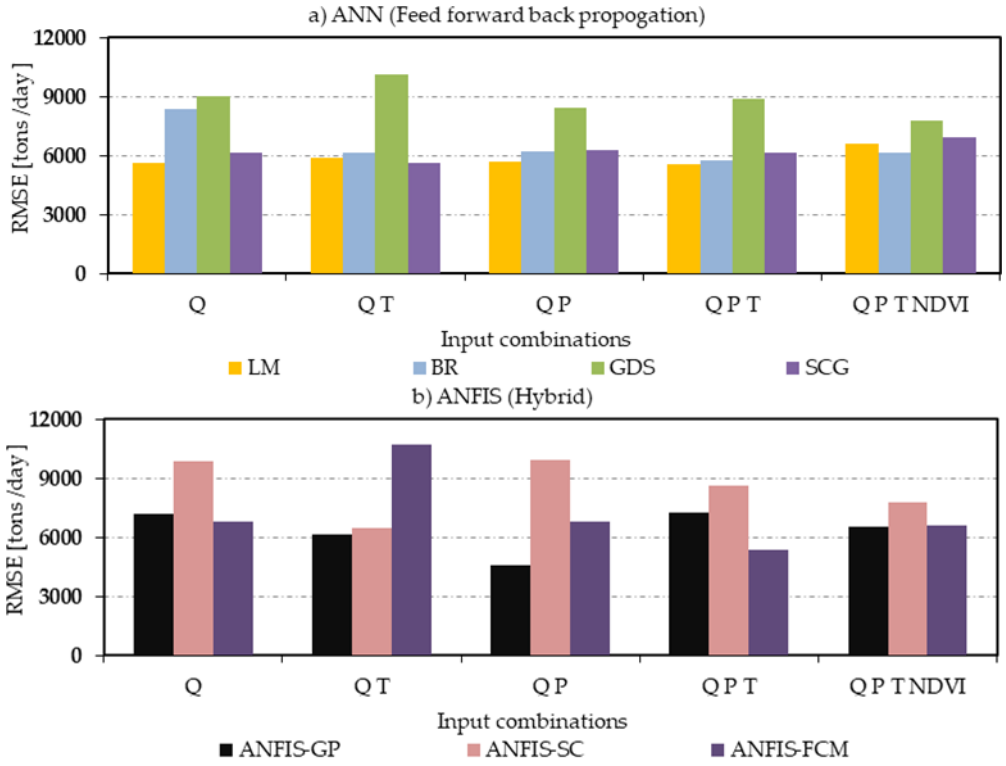

Figure 4. 7 Comparison of ANN-LM, ANN- BR, ANN-GDS, ANN-SCG, ANFIS-GP, ANFIS-SC and ANFIS-FCM models by RMSE statistics during testing period in the Brandu River basin.

4.4.3 SRC model results

The SRC equation obtained from 83% of datasets after optimization of over and under fitting of the model for training and testing of model is given as:

$$SSY = 3E\text{-}10 \times Q^{\wedge 2.0129} \quad (15)$$

Where SSY = tons/day and Q = m^3/day

From Table 4.5 the SRC shows the value of RMSE as 12,934 tons/day and 7,512 tons/day during training and testing phase respectively.

4.4.4 Discussion

The Figure 4.8 shows the monthly time series plot during testing period to compare the performance of best networks by using ANN, ANFIS and SRC modelling approaches. During the testing phase the ANFIS model embedded with grid partition (GP) performance better than all other models during the peak values of SSY. The ANFIS-GP simulates the SSY in very close pattern to the measured sediment loads at peak seasonal period starting from the month of June and ending in September. However, the ANFIS-GP overestimates the SSY during the spring months March-May. Similarly, the ANN-LM algorithm also simulated the SSY close to measured SSY during the months of June and July. During late winters in the months of Jan-Feb the ANFIS –GP and SRC model performs better

than ANN-LM algorithm. Generally, SRC underestimated the SSY during high peak months of sediment load generation period.

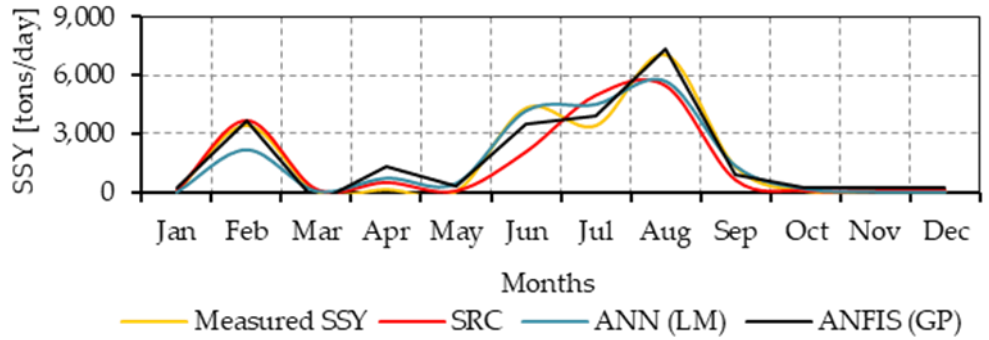

Figure 4. 8 Comparison of best performance of networks developed from the ANN, ANFIS and SRC models during testing period in the Brandu River basin.

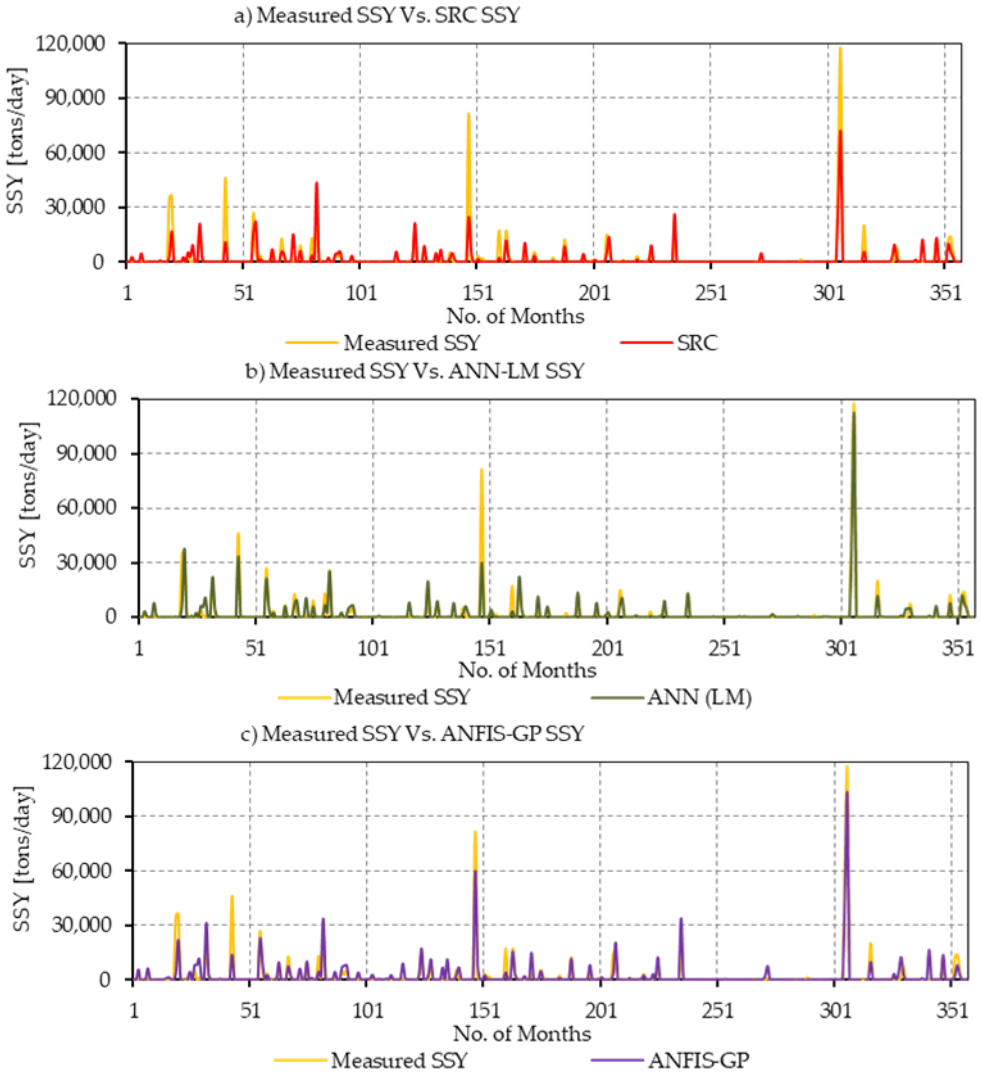

Figure 4. 9 Overall Comparison of the monthly measured SSY with the best outputs of SRC, ANN and ANFIS models at Brandu River since 1981-2010.

Similarly, the Figure 4.9 shows the overall comparison of the best performed SRC, ANN-LM, and ANFIS-GP with the measured sediment loads for whole month time series since 1981-2010. The ANN-LM and ANFIS-GP simulated the sediment loads very closed to measure SSY during almost all peak values. However, the SRC performance was less than ANN-LM and ANFIS-GP. The difference in the performance of these different models is due to difference in their model parameters, transfer functions as well as input combinations to build the network.

The Figure 4.10 shows the scatter plot of daily measured and simulated sediment loads for overall period since 1981-2010. The Scatter plot between measured SSY and simulated SSY of SRC model shows the value of correlation coefficient with R^2 as 0.60 for whole period since 1981-2010. Similarly, the scatter plot between measured SSY and ANN-LM modeled SSY loads show value of correlation coefficient with R^2 as 0.89 for the period 1981-2010. The scatter plot of measured SSY and simulated SSY of ANFIS-GP shows the R^2 value of correlation coefficient with R^2 as 0.72 for whole of the period since 1981-2010.

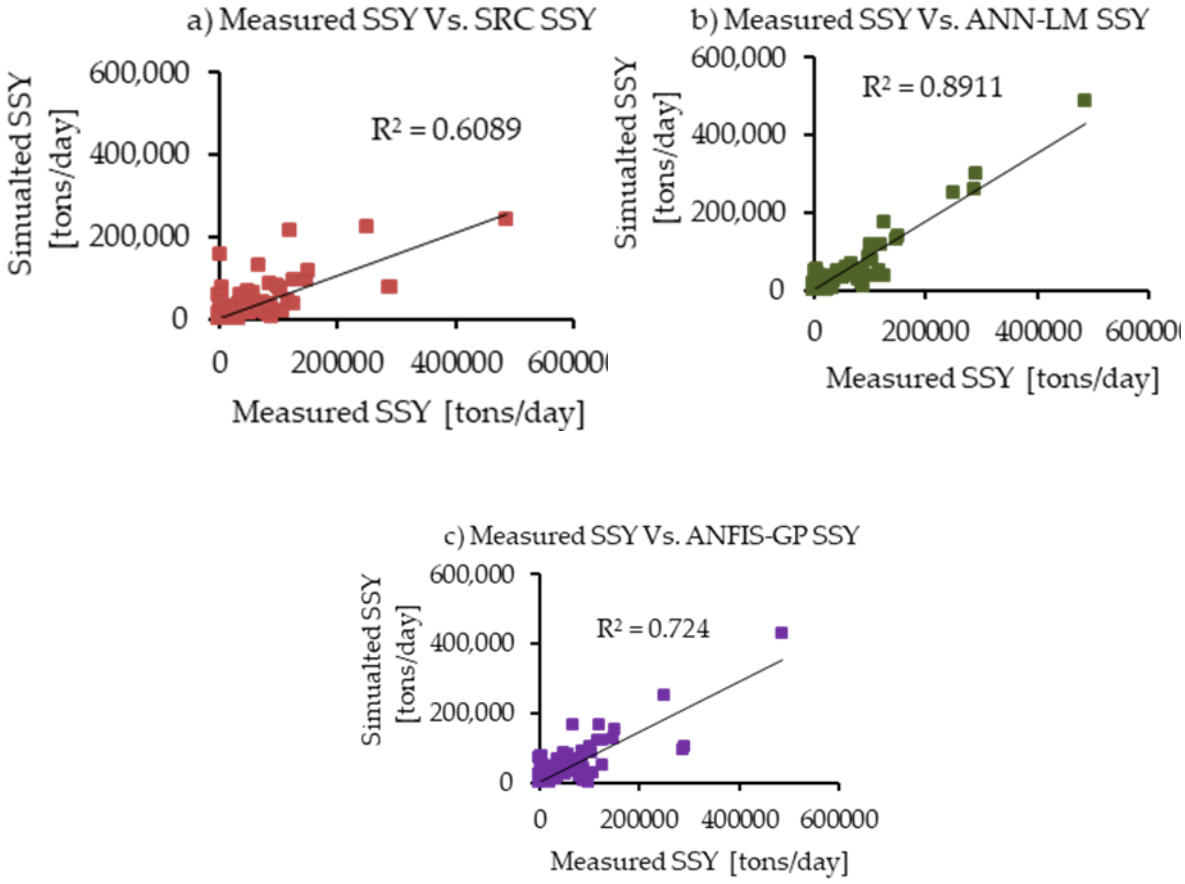

Figure 4. 10 Overall Comparison of the monthly measured SSY with the best outputs of SRC, ANN and ANFIS models at Brandu River since 1981-2010.

4.5 Conclusion

This study was formulated to develop the database sediment yield prediction model using the input of rainfall, temperature and NDVI for Brandu River catchment in Upper Indus Basin (UIB), Pakistan. The objective of study was to check the effectiveness of grid climatic inputs as rainfall and mean air temperature, along with NDVI as biophysical parameter in addition to stream flows to develop the

suitable modelling approach in Brandu River catchment. The selection of these input variables was decided based on the understanding made from hydrological and land use characteristics of the catchment. For this study the hydro-climatic and biophysical input of NDVI were used to test the applicability of ANN-LM, ANN-BR, ANN-GD, ANN-SCG, ANFIS-GP, ANFIS-SC and ANFIS-FCM databased models. From the results of this study it was concluded that prediction of daily SSY was not improved by using the biophysical NDVI in addition to hydro-climatic inputs. However, the ANFIS-GP performed best during testing period with input combination of flows and precipitation. For overall comparison between the four ANN, three ANFIS and one SRC modelling approach, the ANN-LM performed best with daily inputs of flows, precipitation and mean air temperature for the period 1981-2010 at Brandu River. The overall accuracy of R^2 was improved by 28% of SRC by using the ANN-LM model for whole period since 1981-2010 with input combinations of flows, precipitation and mean air temperature. Similarly, the ANFIS-GP model improved the accuracy of sediment rating curve R^2 by 11.5% since 1981-2010 with input combination of flows and precipitation. The performance of NDVI was poor probably due to the linear interpolation of by monthly NDVI to extract the daily values of NDVI or less domination factor of biophysical parameters or combination of both for sediment generation process. Further studies would be required to check the applicability of NDVI on monthly time scale as well as by using the other data-based model such as support vector machine (SVM), Multivariate adaptive regression splines (MARS) etc. for prediction of sediment loads. For development of reliable databased models, the preparation of suitable input variables and its high data quality is very important. In the present research availability of reliable high quality remotely sensed biophysical input of NDVI and hydro-climatic information could be its limited factors.

4.6 References

1. Wardrop, D.H.; Brooks, R.P. The Occurrence and Impact of Sedimentation in Central Pennsylvania Wetlands. Environmental Monitoring and Assessment 1998, 51, 119–130, doi:10.1023/A:1005958429834.
2. Singh, A.; Imtiyaz, M.; Isaac, R.K.; Denis, D.M. Comparison of soil and water assessment tool (SWAT) and multilayer perceptron (MLP) artificial neural network for predicting sediment yield in the Nagwa agricultural watershed in Jharkhand, India. Agricultural Water Management 2012, 104, 113–120, doi: 10.1016/j.agwat.2011.12.005.
3. Adnan, R.M.; Liang, Z.; El-Shafie, A.; Zounemat-Kermani, M.; Kisi, O. Prediction of Suspended Sediment Load Using Data-Driven Models. Water 2019, 11, doi:10.3390/w11102060.
4. Mustafa, M.R.; Rezaur, R.B.; Saiedi, S.; Isa, M.H. River Suspended Sediment Prediction Using Various Multilayer Perceptron Neural Network Training Algorithms—A Case Study in Malaysia. Water Resources Management 2012, 26, 1879–1897, doi:10.1007/s11269-012-9992-5.
5. Faiza Hallouz; Mohamed Meddi; Gil Mahé; Salaheddine Alirahmani; Abdelkader Keddar. Modeling of discharge and sediment transport through the SWAT model in the basin of Harraza (Northwest of Algeria). Water Science 2018, 32, 79–88, doi: 10.1016/j.wsj.2017.12.004.
6. Grayson, R.B.; Moore, I.D.; McMahon, T.A. Physically based hydrologic modeling: 1. A terrain-based model for investigative purposes. Water Resour. Res. 1992, 28, 2639–2658, doi:10.1029/92WR01258.
7. Tiwari, H.; Rai, S. Review of Information and soft computing techniques (ISCT) approaches in Water Resources Projects. In Managing Information Technology; DESIDOC: Delhi, India, 2015; pp. 89–94.

8. Pektas, A.O.; Cigizoglu, H.K. Long-range forecasting of suspended sediment. Hydrological Sciences Journal 2017, 62, 2415–2425, doi:10.1080/02626667.2017.1383607.
9. Kumar, D.; Pandey, A.; Sharma, N.; Flügel, W.-A. Modeling Suspended Sediment Using Artificial Neural Networks and TRMM-3B42 Version 7 Rainfall Dataset. J. Hydrol. Eng. 2015, 20, doi:10.1061/(ASCE)HE.1943-5584.0001082.
10. Melesse, A.M.; Ahmad, S.; McClain, M.E.; Wang, X.; Lim, Y.H. Suspended sediment load prediction of river systems: An artificial neural network approach. Agricultural Water Management 2011, 98, 855–866, doi: 10.1016/j.agwat.2010.12.012.
11. Yadav, A.; Chatterjee, S.; Equeenuddin, S.M. Prediction of suspended sediment yield by artificial neural network and traditional mathematical model in Mahanadi river basin, India. Sustain. Water Resour. Manag. 2018, 4, 745–759, doi:10.1007/s40899-017-0160-1.
12. Ulke, A.; Tayfur, G.; Ozkul, S. Predicting Suspended Sediment Loads and Missing Data for Gediz River, Turkey. J. Hydrol. Eng. 2009, 14, 954–965, doi:10.1061/(ASCE)HE.1943-5584.0000060.
13. Kaveh, K.; Duc Bui, M.; Rutschmann, P. A comparative study of three different learning algorithms applied to ANFIS for predicting daily suspended sediment concentration. International Journal of Sediment Research 2017, 32, 340–350, doi: 10.1016/j.ijsrc.2017.03.007.
14. Cobaner, M.; Unal, B.; Kisi, O. Suspended sediment concentration estimation by an adaptive neuro-fuzzy and neural network approaches using hydro-meteorological data. Journal of Hydrology 2009, 367, 52–61, doi: 10.1016/j.jhydrol.2008.12.024.
15. Kisi, O.; Shiri, J. River suspended sediment estimation by climatic variables implication: Comparative study among soft computing techniques. Computers & Geosciences 2012, 43, 73–82, doi: 10.1016/j.cageo.2012.02.007.
16. Yadav, A.; Chatterjee, S.; Equeenuddin, S.M. Suspended sediment yield estimation using genetic algorithm-based artificial intelligence models: case study of Mahanadi River, India. Hydrological Sciences Journal 2018, 63, 1162–1182, doi:10.1080/02626667.2018.1483581.
17. Wang, J.; Ishidaira, H.; Sun, W.; Ning, S. Development and interpretation of new sediment rating curve considering the effect of vegetation cover for Asian basins. ScientificWorldJournal. 2013, 2013, 154375, doi:10.1155/2013/154375.
18. Asadi, H.; Shahedi, K.; Jarihani, B.; Sidle, R. Rainfall-Runoff Modelling Using Hydrological Connectivity Index and Artificial Neural Network Approach. Water 2019, 11, 212, doi:10.3390/w11020212.
19. McCulloch, W.S.; Pitts, W. A logical calculus of the ideas immanent in nervous activity. The bulletin of mathematical biophysics 1943, 5, 115–133, doi:10.1007/BF02478259.
20. Hebb, D.O. The organization of behavior. A neuropsychological theory; John Wiley & Sons; London: Chapman & Hall: New York, 1949.
21. Rosenblatt, F. The perceptron: a probabilistic model for information storage and organization in the brain. Psychol. Rev. 1958, 65, 386–408, doi:10.1037/h0042519.
22. Minsky, M.; Papert, S. Perceptrons. An introduction to computational geometry / [M.L. Minsky, S. Papert]; MIT Press: Cambridge, Mass., 1969.
23. Werbos, P.J. Beyond regression, new tools for prediction and analysis in the behavioral sciences; Harvard University: S.l., 1974.

24. Rumelhart, D.E.; Hinton, G.E.; Williams, R.J. Learning representations by back-propagating errors. Nature 1986, 323, 533–536, doi:10.1038/323533a0.
25. Artificial Neural Networks in Hydrology. II: Hydrologic Applications. J. Hydrol. Eng. 2000, 5, 124–137, doi:10.1061/(ASCE)1084-0699(2000)5:2(124).
26. Haykin, S.S. Neural networks. A comprehensive foundation / Simon Haykin, 2nd ed.; Prentice Hall; London: Prentice-Hall International: Upper Saddle River, N.J., 1999, ISBN 0132733501.
27. Marquardt, D.W. An Algorithm for Least-Squares Estimation of Nonlinear Parameters. Journal of the Society for Industrial and Applied Mathematics 1963, 11, 431–441, doi:10.1137/0111030.
28. Rumelhart, D.E.; Hinton, G.E.; Williams, R.J. Learning Internal Representations by Error Propagation: Parallel Distributed Processing: Explorations in the Microstructure of Cognition, Vol. 1. In; Rumelhart, D.E., McClelland, J.L., PDP Research Group, C., Eds.; MIT Press: Cambridge, MA, USA, 1986; pp 318–362, ISBN 0-262-68053-X.
29. Minns, A.W.; Hall, M.J. Artificial neural networks as rainfall-runoff models. Hydrological Sciences Journal 1996, 41, 399–417, doi:10.1080/02626669609491511.
30. Nourani, V.; Baghanam, A.H.; Adamowski, J.; Gebremichael, M. Using self-organizing maps and wavelet transforms for space–time pre-processing of satellite precipitation and runoff data in neural network-based rainfall–runoff modeling. Journal of Hydrology 2013, 476, 228–243, doi: 10.1016/j.jhydrol.2012.10.054.
31. Haykin, S. Neural Networks: A Comprehensive Foundation, 2nd; Prentice Hall PTR: USA, 1998, ISBN 0132733501.
32. Jang, J.-S.R. ANFIS: adaptive-network-based fuzzy inference system. IEEE Trans. Syst., Man, Cybern. 1993, 23, 665–685, doi:10.1109/21.256541.
33. Mamdani, E.H.; Assilian, S. An experiment in linguistic synthesis with a fuzzy logic controller. International Journal of Man-Machine Studies 1975, 7, 1–13, doi:10.1016/S0020-7373(75)80002-2.
34. Takagi, T.; Sugeno, M. Fuzzy identification of systems and its applications to modeling and control. IEEE Trans. Syst., Man, Cybern. 1985, SMC-15, 116–132, doi:10.1109/TSMC.1985.6313399.
35. Abonyi, J.; Andersen, H.; Nagy, L.; Szeifert, F. Inverse fuzzy-process-model based direct adaptive control. Mathematics and Computers in Simulation 1999, 51, 119–132, doi:10.1016/S0378-4754(99)00142-1.
36. Yager, R.R.; Filev, D.P. Approximate clustering via the mountain method. IEEE Trans. Syst., Man, Cybern. 1994, 24, 1279–1284, doi:10.1109/21.299710.
37. Chiu, S. Extracting Fuzzy rules from Data for Function Approximation and Pattern Classification. Fuzzy Information Engineering: A Guided Tour of Applications 1997.
38. Chiu, S. Extracting fuzzy rules for pattern classification by cluster estimation. Proceedings of the Sixth International Fuzzy Systems Association World Congress, Sao Paulo, Brazil July 1995.
39. Chiu, S. Fuzzy Model Identification Based on Cluster Estimation. Journal of the Intelligent and Fuzzy Systems 1994, 2, 267–278, doi:10.3233/IFS-1994-2306.
40. Chiu, S. Extracting Fuzzy rules from Data for Function Approximation and Pattern Classification. Fuzzy Information Engineering: A Guided Tour of Applications 1997.
41. Cobaner, M. Evapotranspiration estimation by two different neuro-fuzzy inference systems. Journal of Hydrology 2011, 398, 292–302, doi: 10.1016/j.jhydrol.2010.12.030.

42. Bezdek, J.C.; Ehrlich, R.; Full, W. FCM: The fuzzy c-means clustering algorithm. Computers & Geosciences 1984, 10, 191–203, doi:10.1016/0098-3004(84)90020-7.
43. Jain, A.K.; Dubes, R.C. Algorithms for Clustering Data; Prentice-Hall, Inc: Upper Saddle River, NJ, USA, 1988, ISBN 0-13-022278-X.
44. Tsai, D.-M.; Lin, C.-C. Fuzzy C-means based clustering for linearly and nonlinearly separable data. Pattern Recognition 2011, 44, 1750–1760, doi: 10.1016/j.patcog.2011.02.009.
45. Taherdangkoo, M.; Bagheri, M.H. A powerful hybrid clustering method based on modified stem cells and Fuzzy C-means algorithms. Engineering Applications of Artificial Intelligence 2013, 26, 1493–1502, doi: 10.1016/j.engappai.2013.03.002.
46. Zhang, D.-Q.; Chen, S.-C. A novel kernelized fuzzy C-means algorithm with application in medical image segmentation. Artif. Intell. Med. 2004, 32, 37–50, doi: 10.1016/j.artmed.2004.01.012.

Chapter 5- Climate signaling in suspended sediment exports from Glacier and Snow Melts Sub-basins in the Upper Indus Basin (UIB)

5.1 Abstract

Exports of suspended sediments concentrations (SSC) during past decades from glaciers and snow dominated sub-basins in UIB is sensitive to the number of factors such as: changes of climate, activation-deactivation of sediment sources (proglacial area, hillslopes, gullies, river channel/banks etc.) and transport dynamics of sediment fluxes though fluvial river system. The present research outcome reports a non-significant slight decrease of annual SSC in Gilgit basin contrary to the increase of annual SSC in Astore basin of UIB during the period 1981-2010. The possible decrease of SSC in snow-glacier dominated Gilgit basin measured at the outlet of the basin is explored with an explanation of increase of mean air temperature and precipitations. Similarly, the increase of SSC in Astore basin is explained with the increase of mean air temperature and decrease of precipitations in snow fed dominated basin. The exports of sediments in both the basins is explained in context of changes in channel discharges (transport capacity, activation-deactivation of potential sources of sediment supplies due to changes of climate. The increase/decrease of SSC is due to erosions process of spatially distributed precipitations and temperature derived snow melts rate, snow cover fractions, effective rainfall and ice melts rate simulated with temperature index model. The erosion process due to snow melts, snow cover fractions, ice melts etc. are critical analyzed and explained. The results of Mann-Kendall Trend test show an increase of winter precipitations, snow melts, stream discharges and SSC due to warming of temperature in Gilgit basin as well in Astore basin. However, during late spring seasons the precipitations increased significantly in Gilgit basin contrary to its significantly reductions in Astore basin, which resulted in an increase of snow cover fractions in Gilgit and reductions of its in Astore basin respectively. In the Gilgit basin during summers the combined effect of Karakorum climate anomaly and increased snow cover area reduced the supplies of sediments at the outlet due to covering of exposed proglacial landscape, reduced debris flows and reduced snow melts from debris glaciers. However, in the Astore due to warming of mean air temperature, reduction of springs precipitations, increase of effective rainfall and reduction of early summer snow cover resulted in an increase of SSC. In the results the hydrological shift of glacier to the snow and snow to the rainfall dominations for transport of fine sediments has been noticed for Gilgit and Astore basin respectively. In conclusion its particular to include the relevancy of climate changes in UIB on stream discharges, sediment budgeting and its prediction in future

5.2 Introduction

Erosion of sediment yields are determined by four major factors (i) climate; (ii) land use; (iii) geology; and (iv) relief [1]. The climate changes, land use and earth surface evolution process respond to the denudation rates of drainage basins [2,3,4,5.6]. To understand the landscape evolution process in generation of orogenic erosions rates the knowledge about geological forcing, crustal thickness and glacier inheritance is important [7]. At global level the amount of discharges and basin relief characteristics are also strong factors to generate the sediment yields [8,9,10,11,12,13,14]. Khawaja F.A et al. [15] concluded that percentage of snow cover/ice cover (LCs) as a single independent variable explains 73.4% of the variance in sediment yields in Upper Indus Basin (UIB). He also furtherly explained that combination of percentage of snow cover/ice cover (LCs), climatic variables and relief represent the 98.5% variance of sediment yields in UIB. The glaciers of Himalayas covered with debris materials are evacuated from subglacial traction zone are primary source of sediment generations [16,17]. The amount of sediments generated depends upon long/short term storage and seasonal/diurnal variations of flow regime and seasonal influence of climate upon the glaciers [18,19,20]. Retrieval of glaciers [21,22,23] in UIB due to Karakorum Climate Anomaly [24,25] is reducing the summer sediment loads [26,27,28] along with less amount of seasonal discharges. Anthropogenic impacts on sediment yield is a recent consideration worldwide, and on global scale it covers the land cover/use changes due to deforestation, urbanization, increase of agriculture land, trapping the sediments in dams and hydro-power project etc. [29]. The anthropogenic activities impact the production of fine sediments in the basin [30,31]. Human activities are changing the amounts of sediment yields of the world's rivers by increasing the soil erodibility of river systems and decreasing the sediment fluxes to the coastal delta due to upstream retention of sediments in water reservoirs [29,32,33]. Moreover, Glazyrin et al. and Evans M. [2,34] highlighted the importance of seismic and tectonics activities, solid precipitations, glacier dominance, and catchment lithology.

The focus of present research work is on the dominating role of climatic factors [23,26,27,28] which start erosions process and transports the sediments in two selected snow/glacier dominated sub-basins in UIB environment. The premise of this work explains the impact of climate changes during past three decades on generations of sediment yields in alpine environment of UIB. The erosions process depends mainly on transport capacity of the channel and supply of sediments from its sources. The supply of sediments is dependent upon spatial location of sediments and process (glacial erosion, subglacial erosion, hillslope/sheet erosion, channel bed/bank erosion and mass wasting/landslides etc.) involved in transporting the sediment.

In this study the investigations looked at the specific erosion sources along with process-based perspective which depends upon the variations in hydroclimatic/land use (e.g. precipitation, snow cover, mean air temperature and runoff) conditions. The aim was to infer the effect of possible variation in hydroclimatic/land use parameters such as precipitations and its intensity, snow cover, increase/decrease of mean air temperature and flows on the sediment yields of the basin. Here, four major sediment sources were identifying; glacial erosion, hillslope/sheet erosion, river bed/bank erosion and landslides/mass wasting (rock falls, debris flows). Climatic and land use conditions such as precipitations, snow cover and mean air temperature activates these sources through different erosion process. At the base of glaciers, the abrasion of rocks/soil, bed rock fracture, and plucking

transport large amount of sediments to proglacial area during glacial erosion [35]. The subglacial part of glacier erosion covered with debris material evacuates the higher amount of sediments [16,17,36,37]. Moreover, the role of proglacial area during the spring/summer seasonal snow melts/ice melts and intense rainfall on snow free may entertain the erosion process, provided that the proglacial area is connected to river streams network [38]. The overland runoff and intensive rainfall erode the sediments as hillslope/sheet erosions from the permanently or partially frozen rock/soil [39]. During Autumns/Summer season intense rainfall may erode the sediments in the form of gully and rills where the sub catchments of UIB are largely snow free/bare soil. The rain storms trigger the mass wasting/landslides and debris flows and other mass movements [40,41]. Then other parameters in channel such as shear stresses, stream power and river morphology determine the channel sediment transport capacity and movements of sediments, hence this phenomenon transports the sediment to outlet of the catchment.

The investigations to find the linkages of precipitations, mean air temperature, area of snow cover variations and changes of flow dynamics in context of sediment transports of UIB is critical under current climate/snow cover changes. In some part of UIB due to Karakorum climate anomaly glaciers are either stable/expanding during past few decades [24,25]. In UIB together with stabilization or expansion of glaciers, an increase in the annual/seasonal snow cover area has been observed during past decades. [42,43,44,45,46,47].

The glacier and snow melts dominated Gilgit and Astore sub-basins of UIB lies in Hindukush and Western Himalayas respectively. Both the sub-basins drain into the main Indus River in the upstream of the Tarbela reservoir. The objective of this research is to explore the impact of climate warming/cooling on the dynamics of fine sediments transports in UIB. In this investigation the hydroclimatic forcing were conceptualized with the activation/deactivation of spatially distribution of sediment sources in Gilgit and Astore sub-basins.

In addition to flows as transport capacity of the channel, this study also considered the other four important hydroclimatic factors: (i) melting of ice (IM), evacuation of fine sediments and production of the glacial erosion through subglacial channel [16,17,18,19,48]; (ii) Snow cover fractions (SCF), impacts the amounts of ice melts through increase/decrease of albedo results in decrease/increase of ablation process and glacial basal velocity [38,49]; (iii) melting of snow (SM) from snow covered area, generates hillslope/sheet erosion in downstream as well as channel erosions [50]; (iv) effective rainfall (ER) i.e. liquid precipitation, activates hillslope/sheet erosion, landslides/mass wasting and channel erosion due to increase in upstream discharges [40,41]. The main objectives in this investigation are (a) estimation of ice melts (IM), snow melts (SM), snow cover fractions (SCF) and effective rainfall (ER) in both the sub-basins since 1981-2010 b) trend estimations for flows, suspended sediments, ice melts (IM), snow melts (SM), snow cover fractions (SCF) and effective rainfall (ER) (c) critical analysis of the possible reasoning for increase/decrease of sediments and flows trends in relation to four selected process.

5.3 Data Collection and Methodology

5.3.1 Study area and data collections

Two sub-basins of UIB, snow and glacier fed Gilgit sub-basin and mainly snow fed Astore sub-basin were selected to calibrate and validate the snow and ice melts of temperature-Index model. The characteristics of 12681 km^2 Gilgit River (snow and glacier fed) basin were also compared with the 4019 km^2 Astore River (snow-fed) basin shown in Figure 5.1. The snow and glacier melts from Hindukush and partially the glaciers of Karakorum ranges contribute to the Gilgit River sub-basin of UIB [46]. The Astore River sub-basin is north oriented snow-fed regime, lower and mid altitudes, compared to the south oriented Gilgit River sub-basin with high altitudes [45,46]. The Gilgit and Astore Rivers are both influenced by westerlies climate regime but slightly in a different pattern. The flows of Gilgit River mainly depend upon the westerlies winter snow falls that generates the high discharges in summer snow melts. Whereas the Astore River flows are driven by both the winter and spring rainfall at lower elevations. These rainfalls in Astore River catchment combines with winter snow falls by westerlies climate regime to generate the discharges in the basin. The discharges and rainfall regime of Gilgit and Astore basin are shown in Figure 5.2a. It shows that Astore basin is wetter than the Gilgit basin.

The Table 5.1 summarizes the difference between the features of Gilgit and Astore Rivers basins. The ASTER Global DIGITAL ELEVATION MODEL (ASTR-GDEM) of 30 m resolution was used to delineate the watershed area. The Gilgit and Astore basins differ in their relative distribution of ≤3300, 3301-4300, and >4300 m of altitudinal zones: 17%, 39% and 44% respectively, for Gilgit basin; 16%, 50% and 34% for Astore basin. Gilgit and Astore basins have 5-7% of its catchment area above 5000 m [46]. The elevation ranges of Gilgit and Astore basins vary from 1454-7048 m a.s.l and 1580-8058 m a.s.l respectively. The Gilgit and Astore basins area covered with glaciers area of 1327 km^2 (10.9%) and 328 km^2 (8.2%) respectively. The Table 5.2 shows the information of the data collected in current research for the period 1981-2010. The Gilgit and Astore mean basin grid precipitations are 670 mm/year and 670 mm/year respectively. In both the basin rainfall are strongly influenced by the orography, blowing and drifting of solid precipitations and terrain characteristics etc. The ranges of averaged basin mean temperatures of Gilgit and Astore catchments are -16.70 to 5.70 ºC and 16.70 to 4.47 ºC respectively (Fig. 5.2b). The Gilgit and Astore basins mean annual runoff are 291 and 241 m^3/sec respectively. The Gilgit basin is covered with 86% of its area with snows during winter which is depleted in summer's ablation period to the 12%. Similarly, The Astore basin is also covered with 90% of its area with snows during winter and reduces to 9% during summer's season.

Table 5.2 represents the datasets of variables collected, analyzed and simulated in this research. Daily flows and intermittent daily suspended sediment concentrations (SSC) for the period 1981-2010 was collected from the Water and Power Development Authority (WAPDA) of Pakistan. The grid data of precipitation and temperature of 5 × 5 km resolution determined in the HI-AWARE project for the Indus, Ganges, and Brahmaputra river basins were collected [51,52]. The Shuttle Radar Topography Mission's (SRTM) digital elevation model (DEM) data of 30-m resolution were applied as well. The mean basin precipitation data were extracted from the corrected rainfall data of the HI-AWARE project using DEM. Estimation of glacier areas was based on the glacier polygons of the Global Land

Ice Measurement (GLIMS) database. In this study, DEM is used to estimate the glacier area for each sub-basin from downloaded GLIMS polygons [53]. Snow cover maps derived from satellite imagery 8-day product MOD10A2 retrieved from Moderate Imaging Spectroradiometer (MODIS) 500 m resolutions were collected for the period 2000-2010. The procedure of previous literatures [46,43] to retrieve the snow cover area from snow cover product MOD10A2 was used to find snow cover fractions from by weekly MODIS images. The linearly interpolation between by weekly snow cover fractions was carried out to find the missing information of remaining days.

5.3.2 Methodology

The objectives of present work are to explore the impact of climate on dynamics of suspended sediments for Gilgit (glacier and snow-fed) and Astore (rainfall & snow) dominated basins during the period 1981-2010. The Table 5.2 describes the observed/simulated hydroclimatic and sediment transport variables. The Table 5.2 enlists the observed variables of discharges (Q), suspended sediment concentrations (SSC), mean basin precipitation (P) and mean basin temperatures (T); simulated spatially distributed snow cover fraction (SCF), snow melts (SM), ice melts (IM) and effective rainfall (ER). The Temperature-Index model consisting of snow and ice melt approach was used in the research. The interpolation of input datasets of precipitations and temperature on 250×250 m grid resolution was carried out by nearest neighbor interpolation approach. The analysis of variables enlisted in the Table 2 was carried out on monthly basis averaged over the basin. To detect and quantify the changes in suspended sediments and hydroclimatic variables, Mann Kendall Trend test and Sens slope was used for the time series period of 1981-2010. The Chapter 2 explains the detailed methodology of Mann Kendall Trend test and Sens Slope estimator.

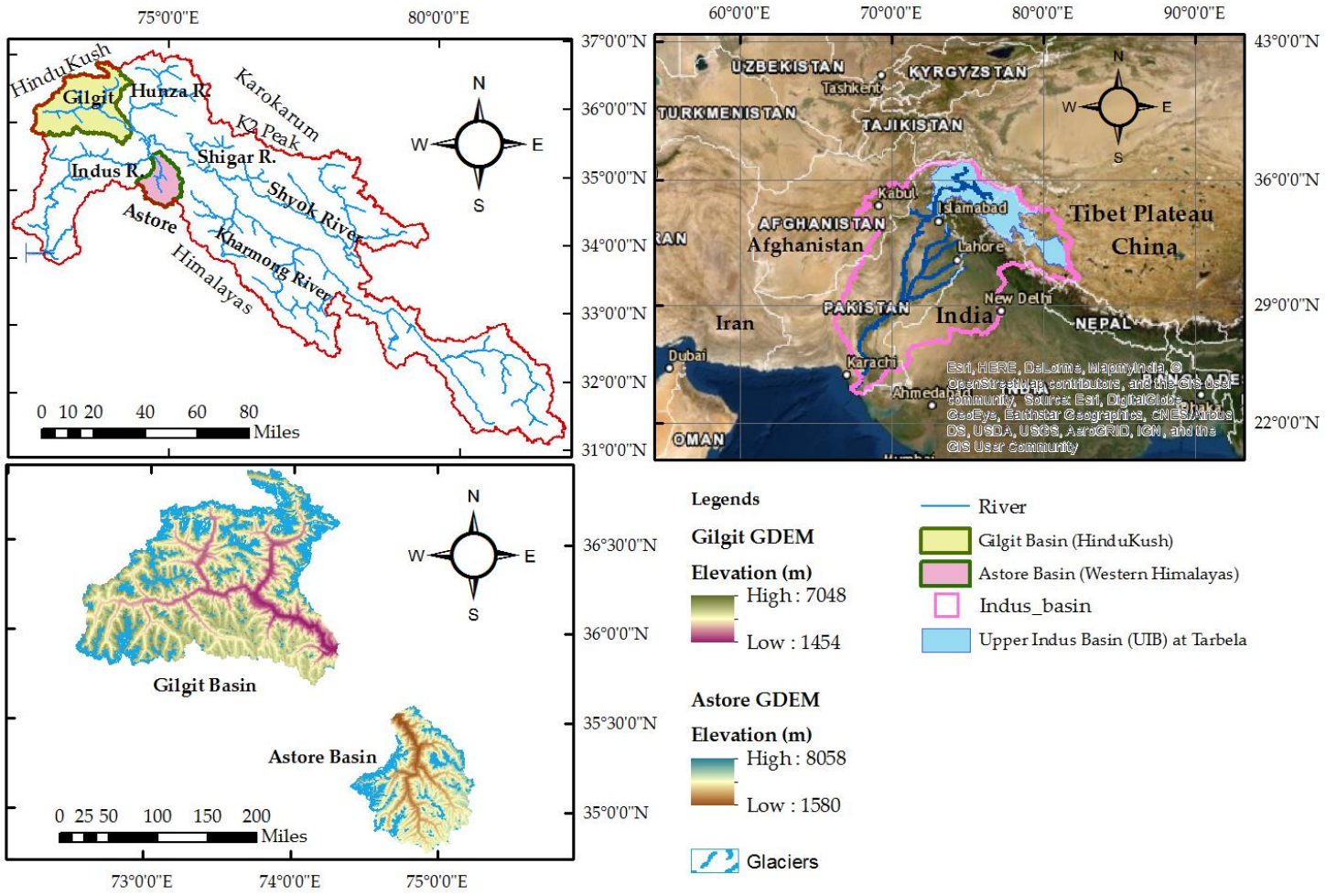

Figure 5. 1 Map of the Gilgit and Astore sub-basins of UIB with topography (GDEM 30 m resolutions), river networks and glacierized areas.

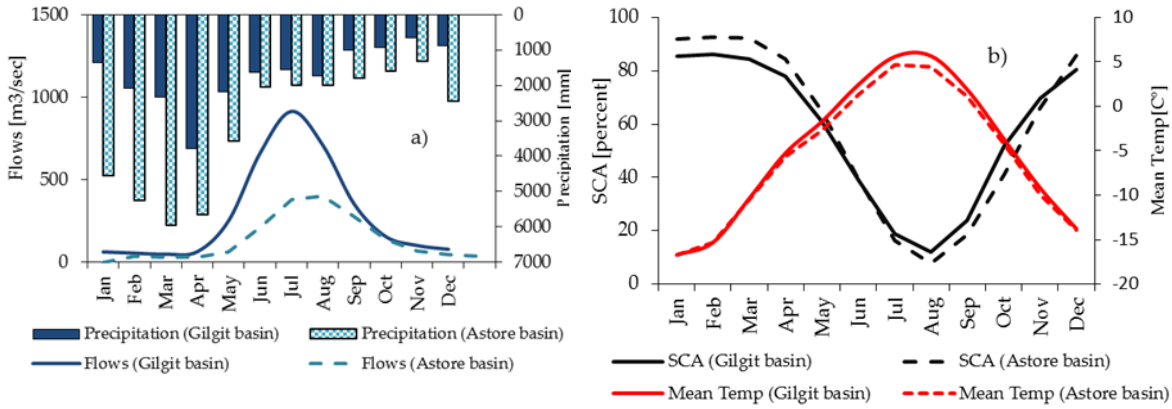

Figure 5. 2 Graphical presentations of (a) discharges (Q) and mean basin rainfall (R) (b) mean basin snow covered area (SCA), and mean basin temperature (T) for Gilgit and Astore sub-basins of UIB.

Table 5. 1 Characteristics of the Gilgit River basin in the Upper Indus River.

River flow gauging station	Gilgit at Gilgit
Longitude	74° 18′ 25′′
Latitude	35° 55′ 35′′
Elevation of stream gauging station	1454 m
Catchment drainage area	12681 km^2
Glacier-covered area	1327 km^2 (source GLIMS) [53]
Glacier cover percentage	10.90 %
Mean elevation	~ 4250 m [46]
River flow gauging station	Astore at Doyian
Longitude	74° 42′ 15′′
Latitude	35° 33′ 35′′
Elevation of stream gauging station	1580 m
Catchment drainage area	4019 km^2
Glacier-covered area	328 km^2 (source GLIMS) [53]
Glacier cover percentage	8.20 %
Mean elevation	~ 4100 m [46]

Table 5. 2 List of variables data collected, analyzed and simulated for Gilgi and Astore Sub-basins in UIB.

Variable	Data description	Period	Source
Q	Daily mean discharge [m^3 s^{-1}]	Daily, 1981–2010	Water and Power Development Authority (WAPDA), Pakistan
SSC	Suspended sediment concentration [mg l^{-1}]	Intermittent days per week 1981–2010	Water and Power Development Authority (WAPDA), Pakistan
SCF	Snow cover fractions ranging [0–1] extracted from MODIS satellite data	Basin avg. 2000–2010	https://nsidc.org/data/MOD10A2
T	Daily mean, maximum & minimum air temperature [° C] on a 5x5 km grid	Daily, basin avg. 1981–2010	HI-AWARE project [51, 52]
P	Daily mean rainfall [mm day–1] on a 5x5 km grid	Daily, basin avg. 1981–2010	HI-AWARE project [51, 52]
SCF (simulated)	Daily mean basin snow cover [fractions]	Daily, basin avg. 1981–2010	Temperature-Index model
SM	Daily snow melts rate [mm day–1]	Daily, basin avg. 1981–2010	Temperature-Index model
IM	Daily ice melts rates [mm day–1]	Daily, basin avg. 1981–2010	Temperature-Index model
ER	Daily mean basin effective rainfall [mm day–1]	Daily, basin avg. 1981–2010	Temperature-Index model

5.3.3 Temperature index-snow melt model

The temperature-Index (degree-day model) snow model is a simple spatially distributed model to simulate the snow melts. It requires lesser amount of data in comparison to the physical distributed hydrological models. The spatially distributed temperature index model is used successfully in pervious researches [54, 55] for large as well as small basins. In present modelling of snow melts the model has simulated the long-term snow melts and snow cover fractions after calibration and validation of the simulated snow cover fraction with the MODIS snow cover fractions. The model

was tested against MODIS snow cover and modelled snow cover for the period 2000-2007 and 2008-2010 in calibration and validation respectively.

The snow melts model account for snow accumulation and snow melts on spatial and temporal basis. In the Temp-Index snow melt model the grid precipitation P is first separated into snow and liquid rain form on daily time scale. The threshold temperature T_{RS} [°C], daily maximum temperature [°C] and daily minimum temperature [°C] separates the snow and liquid rainfall as:

$$\begin{cases} \text{Rain} = \text{R} = \text{C}_\text{p}\text{P} \\ \text{Snow} = \text{S} = (1 - \text{C}_\text{p})\text{P} \end{cases} \quad (1)$$

Where,

C_p is calculated as:

$$\begin{cases} \text{C}_\text{p} = 1 \text{ if } \text{T}_\text{min} > \text{T}_\text{RS} \\ \text{C}_\text{p} = 0 \text{ if } \text{T}_\text{max} \leq \text{T}_\text{RS} \\ \text{C}_\text{p} = \dfrac{\text{T}_\text{max} - \text{T}_\text{RS}}{\text{T}_\text{max} - \text{T}_\text{min}} \text{ if } \text{T}_\text{min} \leq \text{T}_\text{RS} < \text{T}_\text{max} \end{cases} \quad (2)$$

The precipitation is partitioned into snow and rainfall based on (a) daily minimum temperatures T_{min} (°C), daily maximum temperature T_{max} (°C) and rain-snow threshold temperature T_{RS} (°C). In equation 2 C_p is the factor calculated to find the percent of snow or rainfall in the basin for each grid cell.

Then daily rates of snow melt [mm day–1] is estimated as:

$$\begin{cases} \text{M}_\text{snow} = \text{K}_\text{snow}(\text{T}_\text{mean} - \text{T}_\text{SM}) \quad \text{if } \text{T}_\text{mean} > \text{T}_\text{SM} \\ \text{M}_\text{snow} = 0 \quad \text{if } \text{T}_\text{mean} > \text{T}_\text{SM} \end{cases} \quad (3)$$

Here the K_{snow} [mm day–1 °C] is the degree day factor for snow melts, T_{mean} [°C] is the mean daily air temperature and T_{SM} [°C] is the threshold temperature.

After the snow model simulations, the snow water equivalent or snow depth [mm] for each grid numbers of *i* is calculated as:

$$\text{SD}_\text{i}(\text{t}) = \text{SD}_\text{i}(\text{t} - 1) + \text{S}_\text{i}(\text{t}) - \text{M}_{\text{snow}_\text{i}}(\text{t}) \quad (4)$$

Finally the snow cover fraction SCF for *i = 1, 2, 3, 4,…., N* number of grids for the selected catchment is estimated for calibration and validation with the MODIS snow cover fraction as:

$$\text{SCF}\ (\text{t}) = \frac{1}{\text{N}} \sum_{\text{i}=1}^{\text{N}} \text{H}\ [\text{SD}_\text{i}(\text{t})] \quad (5)$$

Here, H = unit step function; when H = 0, SD = 0 and H = 1 then SD > 0. The area of integration N is the entire basin, sub-basins and elevation bands etc. The snow melts for the entire catchment are the arithmetic means of all grid melt rates [mm/day] averaged over the whole basin as;

$$\text{SM}\ (\text{t}) = \frac{1}{\text{N}} \sum_{\text{i}=1}^{\text{N}} SM_i\ (\text{t}) \quad (6)$$

The threshold temperature T_{RS} to define the type of precipitation into rain/snow and T_{SM} the threshold temperature for snow melt process depends upon numerous factors like boundary layer condition of atmosphere, temperature and air humidity etc. Depending upon the modelling approaches, region of study and altitudes of catchments the T_{RS} varies in the range -5 – 6 [°C] [56, 57]. The threshold snow/rainfall temperature T_{RS} for Gigit and Astore basins was selected -3 [°C] and -5 [°C] respectively. Similarly, the threshold temperature of snow melts T_{SM} was -4 [°C] and -6 [°C] for Gilgit and Astore basin.

5.3.4 Temperature Index-Ice melt model

The temperature index ice melts model simulates the ice melts similar to the snow melt model on spatial distributed grid cells that are covered with glaciers/ice. The model simulates the ice melts rates [mm/day] of each snow free glacier grids as;

$$\begin{cases} IM_i = K_{ice}(T_{mean} - T_{IM}) & \text{if } T_{mean} > T_{IM} \\ IM_i = 0 & \text{if } T_{mean} \leq T_{IM} \end{cases} \quad (7)$$

Here, *Tmean* [°C] = mean daily air temperature

T_{IM} [°C] = threshold daily temperature for onset of ice melt, and K_{ice} [mm day^{-1} °C^{-1}] = Ice melt factor

To estimate the total ice melts for whole catchment the ice melt rates of all number of grid cells are taken as arithmetic mean over all ice-covered grid cells in the basin as follow;

$$IM\,(t) = \frac{1}{N}\sum_{i=1}^{N} IM_i\,(t) \quad (8)$$

The threshold temperature of glacier melting T_{IM} for Gilgit and Astore basins was also set equals to threshold temperature of snow melts T_{SM}. Ice melts (IM) start when the glacier cells are snow free. The value of T_{IM} was also -4 [°C] and -6 [°C] for Gilgit and Astore basin.

5.3.5 Performance measurement metrics for model evaluation

The performance of snow melt model was measured using following statistics as;

Root mean square error (RMSE)

$$RMSE = \sqrt{\frac{1}{N}\sum_{i=1}^{N}((S_{io}) - (S_{is}))^{2}} \quad (9)$$

Nash-Sutcliffe efficiency (NSE)

$$NSE = 1 - \frac{\sum_{t=1}^{N}(S_{io} - S_{is})^2}{\sum_{t=1}^{N}(S_{is} - \overline{S_{is}})^2} \quad -\infty \leq NSE \leq 1 \quad (10)$$

Pearson's correlation coefficient (R^2)

$$R^2 = \left(\frac{\sum_{i=1}^{N}(S_{i0} - \overline{S_{io}})(S_{is} - \overline{S_{is}})}{\sqrt{\sum_{i=1}^{N}(S_{i0} - \overline{S_{io}})^2 \sum_{i=1}^{N}(S_{is} - \overline{S_{is}})^2}} \right)^2 \quad (11)$$

Here N refers the data quantity, S_{io} is observed values of output/snow cover fraction and S_{is} is the simulated values of output and $\overline{S_{is}}$ is mean of simulated values of output variable.

The calibration of ice-melt factor K_{ice} for both the basins is performed on basis of daily measured discharges during the months of ice melts (June-October) as well as during the whole year. Calibration is performed during the period 1981-2005 and validation covers the period 2006-2010.

The optimum a value of K_{ice} is found by calculated the mass balance error (MBE) for the period of glacier ablation as well as for annual period as;

$$\text{MBE}_{ablation/Annual} = 100 \times \frac{\sum_{i=1}^{n_y}(V^{Obs}{}_i - V^{sim}{}_i)}{\sum_{i=1}^{ny} V^{Obs}{}_i} \quad (12)$$

where,

n_y = number of calibration years, $V^{Obs}{}_i$ = observed discharge per volumes per unit area at the outlet [mm year^{-1}] and $V^{sim}{}_i$ = simulated discharge per volumes per unit area at the outlet [mm day^{-1}]

$$V^{Obs}{}_i = \sum_{\text{j=1}}^{\text{nd}} Q^{Obs}{}_j \quad (13)$$

$$V^{sim}{}_i = \sum_{\text{j=1}}^{\text{nd}} Q^{sim}{}_j = \sum_{\text{j=1}}^{\text{nd}} \left(R_j + SM_j + IM_j \right) \quad (14)$$

Here,

nd = number of observation of days during ablation period or whole year

$Q^{Obs}{}_j$ = daily observed discharge per unit area at the outlet of basin [mm day^{-1}]

$Q^{sim}{}_j$ = daily simulated discharge per unit area at the outlet of basin [mm day^{-1}]

R_j, SM_j and IM_j are daily rainfall, snow melts and ice melts over the grids of whole basin.

Rainfall and snows melts are estimated with snow melt model whereas ice melts are estimated with the ice melt model. In the current research does not cover the glacier evolution process, thickness of glacier ice due to expansion or retreat of glaciers, nor the glaciers ice discharges.

5.4 Results and Discussion

5.4.1 Simulation of snow melts and snow cover area

The model is calibrated and validate for the period 2000-2007 and 2008-2010 using snow and ice melts models for both the Gilgit and Atore basins. First the snow model was calibrated and validated based on the snow cover fractions of MODIS (SCF_{Mod}) and model simulated snow covers fraction (SCF_M). The snow model simulated the snow melts and snow-covered area in the catchments. Table 5.3 show the results of degree day factors for snow melts in both the basins. In the literature of regional researches [25, 58, 59, 60, 61, 62] the value of K_{snow} ranges from 3-7 [mm day^{-1} °C^{-1}] in Upper Indus basin (UIB). The Table 5.3 shows that value of K_{snow} of 3.1 and 4.2 [mm day–1 °C–1] in Gilgit and Astore basins lies within the ranges of past studies respectively. The difference between the value of K_{snow} in present and pervious research works is probably due to difference of their input datasets resolutions, length and period of calibrations

Table 5. 3 Results of performance measurement statistics during calibration (2000-2007) and validation (2008-2010) period of Temperature-Index snow model for simulations of snow melt and snow cover fraction.

Gilgit Basin k_{snow} = 3.1 [mm day–1 °C–1]		
	Calibration Period (2000-2007)	**Validation Period (2008-2010)**
R^2	0.90	0.90
NSE	0.72	0.70
RMSE	0.15	0.15
Astore Basin k_{snow} = 4.2 [mm day–1 °C–1]		
	Calibration Period (2000-2007)	**Validation Period (2008-2010)**
R^2	0.92	0.92
NSE	0.84	0.75
RMSE	0.13	0.15

The Table 5.3 shows the results of snow melts model during calibration and validation periods. The value of R_2 is found 0.90 and 0.92 during calibration as well as validation period of the Gilgit and Astore basins respectively. The results of performance measurements of R^2, NSE and RMSE shows that goodness of fit between the model and observed MODIS snow cover maps is more than 70% which is satisfactory in estimation of both the snow melts and snow cover area. Figure 5.3 shows the comparison between the MODIS snow cover fractions and snow model simulated snow cover fractions for both Gilgit and Astore basins.

The ice melt model was calibrated following the procedure of section 5.3.4. The value of degree day factor of ice melt K_{ice} was 7 [mm day–1 °C–1] and 9 [mm day–1 °C–1] of Gilgit and Astore basins respectively. Figure 5.4 shows the seasonal/annual patterns of observed flows and simulated snow

melts (SM), effective rainfall (R), ice melts (IM) after calibration and validation of temperature index model. Two goodness of fit measures (MBE_S) during ablation and (MBE_A) during whole year period were calculated for both the basins. The value of seasonal mass balance (MBE_S) varies from 10.2 to 13.4 percent. Similarly, the value of annual mass balance error (MBE_A) varies from 7 to 36%.

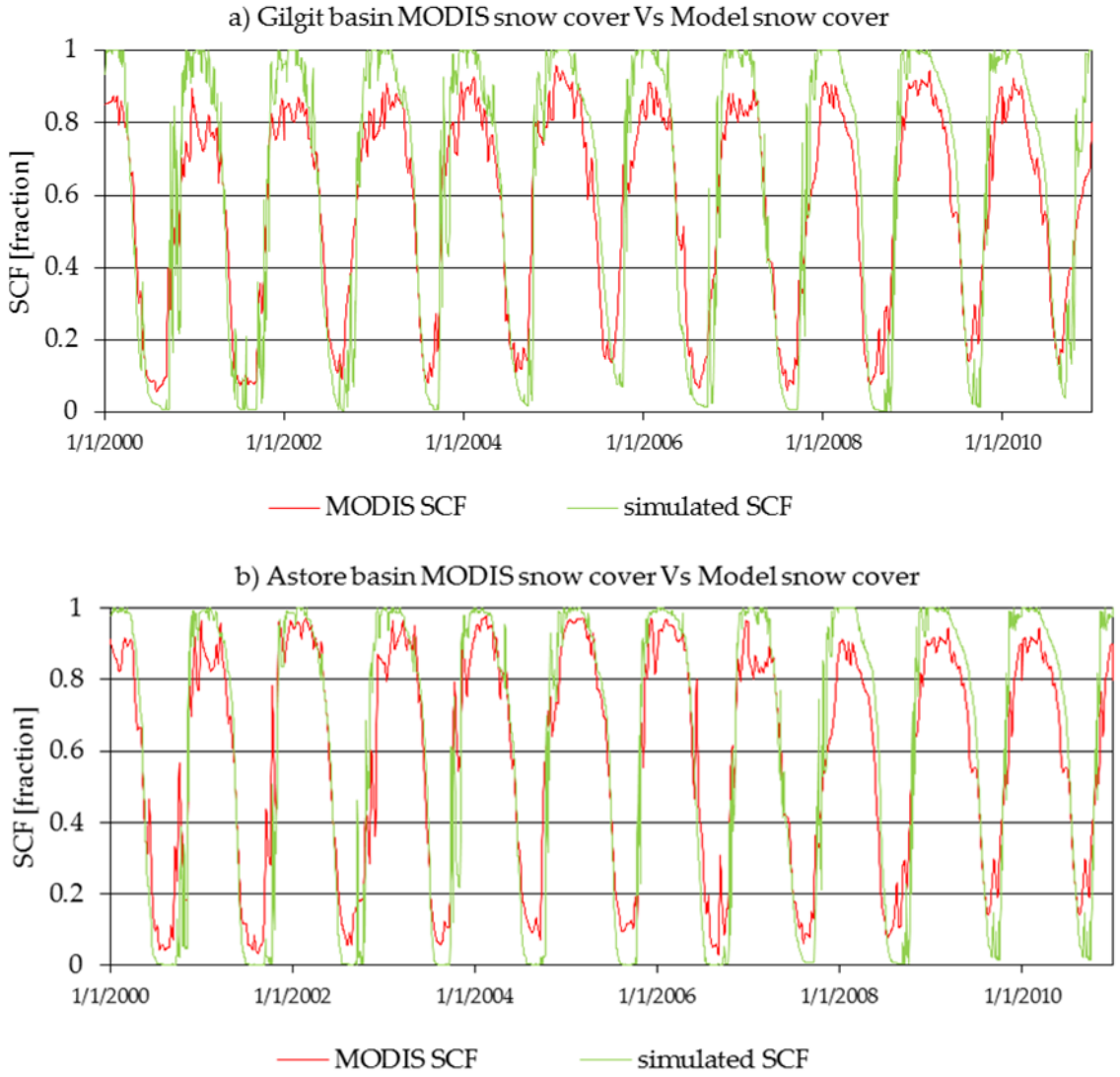

Figure 5. 3 Comparison between the MODIS observed snow cover fractions and temp-index snow model simulated snow cover fractions for Gilgit and Astore basins.

Table 5. 4 Results of goodness of fit measures: mass balance errors (MBE_S) computed during ablation period (June-October) and mass balance errors (MBE_A) during whole year for ice melt model calibrations.

	Gilgit Basin k_{ice} = 7 [mm day–1 °C–1]	
	Calibration Period (2000-2007)	Validation Period (2008-2010)
MBE_S(%)	10.2	10.5
MBE_A(%)	7.0	26.0
	Astore Basin k_{ice} = 9 [mm day–1 °C–1]	
	Calibration Period (2000-2007)	Validation Period (2008-2010)
MBE_S(%)	11.7	13.4
MBE_A(%)	36.0	22.0

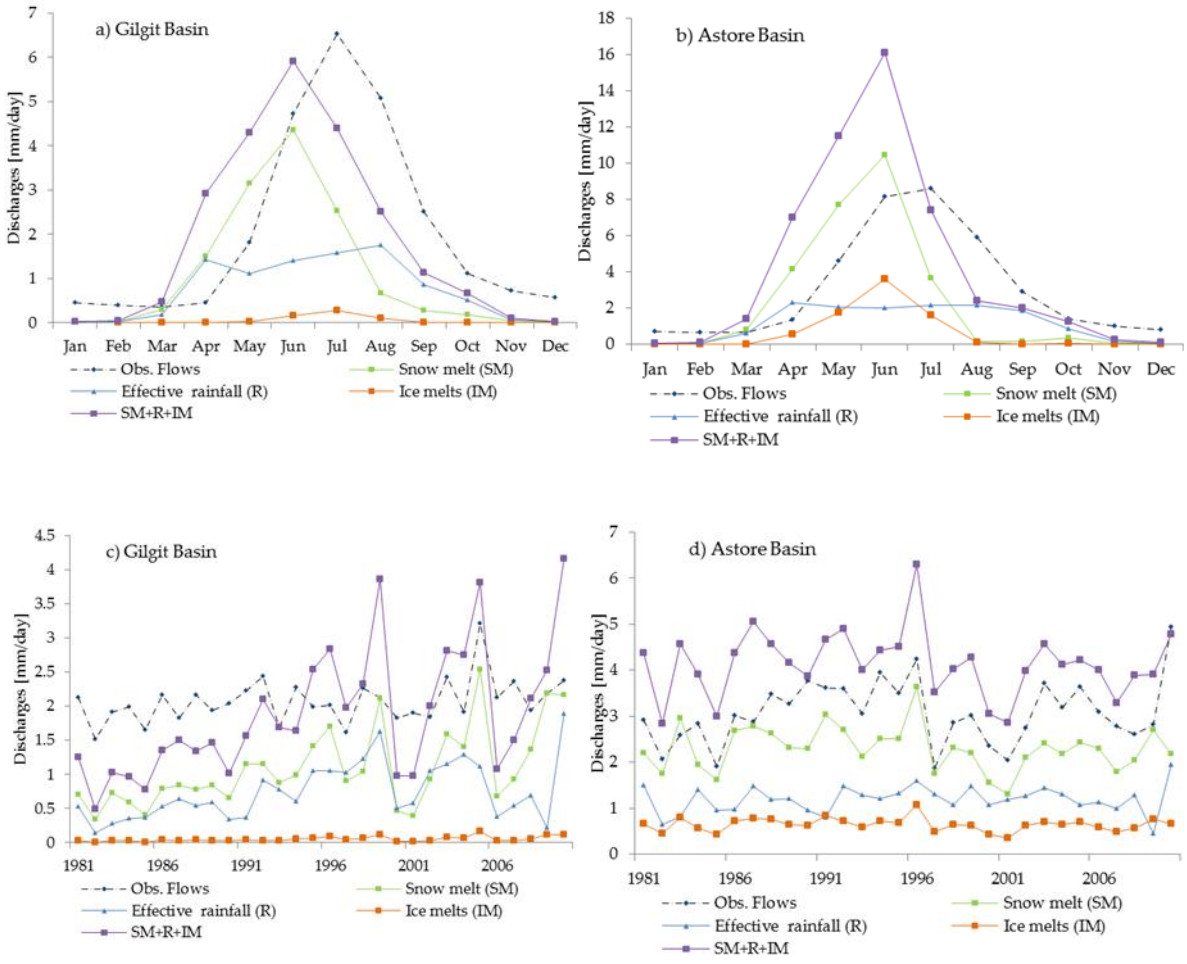

Figure 5. 4 Comparison of mean monthly/annual observed and simulated flows with different flow process for the period 1981-2010: (a) Gilgit basin (monthly) (b) Astore basin (monthly) (a) Gilgit basin (Annual) (b) Astore basin (Annual). Simulated SM+R+IM are the sum of snow melts (SM), effective rainfall (R) and ice melts (IM).

5.4.2 Effect of frequency of intermittent SSC Sampling

The cumulative distribution functions of measured flows, simulated snow cover fractions (SCF), snow melts (SM), ice melts (IM) and effective rainfall (ER) on continuous (all days) and intermittent (SSC daily measurements) frequency basis is shown in the Fig.5.5. Although during the intermittent days few extreme high and low events of SCF, SM, IM and ER may be missed in intermittent days, however the cumulative frequency distribution plot of both continuous and intermittent days are illustrated similar for Gilgit basin. Which implied that the intermittent samplings of SSC have ability to capture accurate and similar pattern of parameters measured/simulated on daily basis. It further supports that the conclusion about the statistical monthly/annual trends of flows, SSC, snow cover fractions, snow melts, ice melts and effective rainfall are not much influenced by the intermittent daily sampling of the SSC.

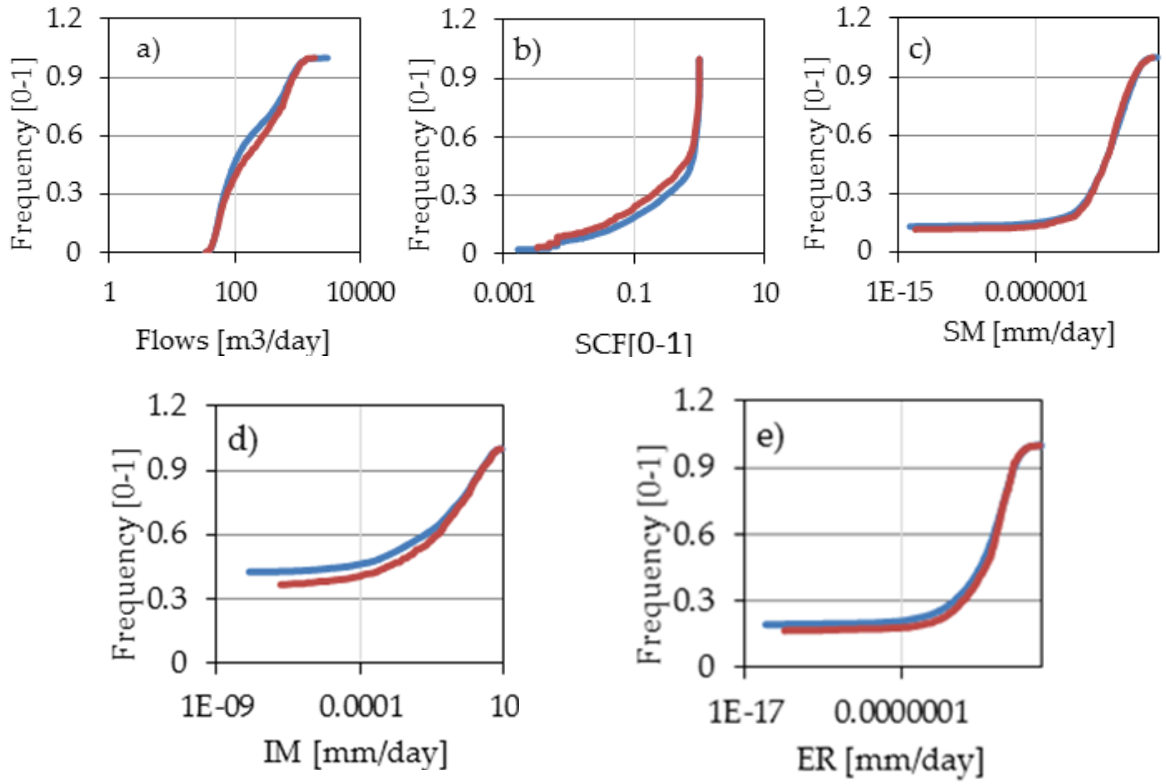

Figure 5. 5 Plots of Cumulative distribution functions of (a) measured flows, (b) snow cover fractions (SCF), (c) snow melts (SM), (d) ice melts (IM), and (e) effective rainfall (ER) on continuous (all days) and intermittent (SSC daily measurements) frequency of the Gilgit basin.

Note: line in blue colour represents continuous (all days) and line in red colour represents intermittent (SSC daily measurements) frequency.

5.4.3 Hydroclimatic changes and activation of sediment sources

The Figure 5.7 shows the warming of annual mean air temperature and basin annual rainfall in Gilgit basin during the period 1981-2010. The simultaneous increase in annual mean temperature and rainfall of Gilgit basin increases the annual flows contrary to the stable/decreasing trends of SSC. The warming trend of annual temperature in Gilgit basin is due to significantly increase of monthly temperature during the autumns and winters are mainly increasing (Oct-March), while changes during the late springs and summer are signalling cooling trends in Figure 5.8a.

Similarly, the Figure 5.8b also shows that the increase of annual precipitation in Gilgit basin is mainly due to the significant increase of monthly precipitation in winter and springs season (December-April) and partially due to increasing trend during summers.

The increase of mean annual flows is due to increase of summer flows shown in Figure 5.8d. The increase of effective rainfall and ice melts contributions is increasing the summer flows in Gilgit basin (Fig.5.8b, Fig.5.9c, Fig.5.9d). However contrary to the non-significant increase of flows during summer (June-Aug) the SSC are decreasing due to cooling of summer temperature, increase of snow cover fractions, increase of solid precipitations and decrease/no significant change in snow melts contributions basin (Fig.5.8c, Fig.5.9a, Fig.5.9b).

The precipitation and mean air temperature are the driving factors for snow melts, glacier melts and rainfall hydrological process. Both precipitation and mean air temperature are also much important for the relative contribution of effective rainfall and snow cover dynamics. The increase of snow cover during summer or late spring season, decrease of snow melts and cooling of summer mean air temperature called as Karakorum climate anomaly [24,25] are likely stabilizing or expanding the glacier over past three decades.

The increase of snow cover during summer season in Gilgit basin are probably covering the unstable proglacial landscape. The snow cover on the debris covered glaciers with high snow cover albedo can also decrease the snow melt and ice melts rates which are driving forces for glacial and snow melts erosions. Moreover, the cooling of summer mean air temperature could be reducing the flood risk imposed by glacial lakes and the probability of permafrost degradation. As the permafrost degradation decreases the slope stability resulting in the increase of erosion process [63,64,65].

The warming of winter temperature and precipitations is increasing the snow melts which ultimately increases the winter flows and SSC in Gilgit basin (Fig5.8, Fig.5.9a). During winter the significant increase of temperature is more dominated in generation of sediments and flows by increasing snow melts. The increase in snow melts during winter could activate the snow melts erosions and supply of discharges in channel. The increase in supply of channel discharges due to winter snow melts could increases the transport capacity of river to erode the seasonal glacial deposits as a wash loads.

The Figure 5.6a shows that the contribution of snow melts is more than effective rainfall and ice melts during winter, springs and early summers period in Gilgit basin. It also shows the importance of precipitation stored in the form of snow during winters and contributing then in the form of snow melts till the start of ablation period.

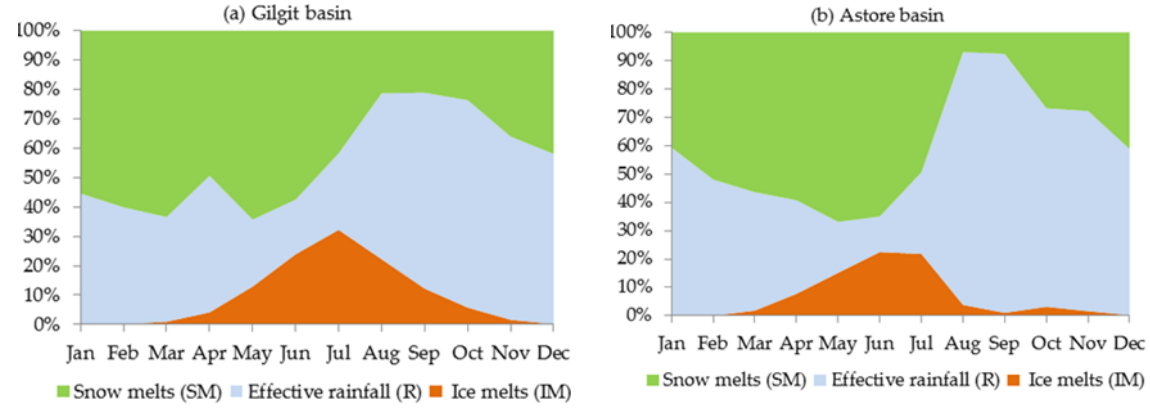

Figure 5. 6 Plots of Cumulative distribution functions of (a) measured flows, (b) snow cover fractions (SCF), (c) snow melts (SM), (d) ice melts (IM), and (e) effective rainfall (ER) on continuous (all days) and intermittent (SSC daily measurements) frequency of the Gilgit basin.

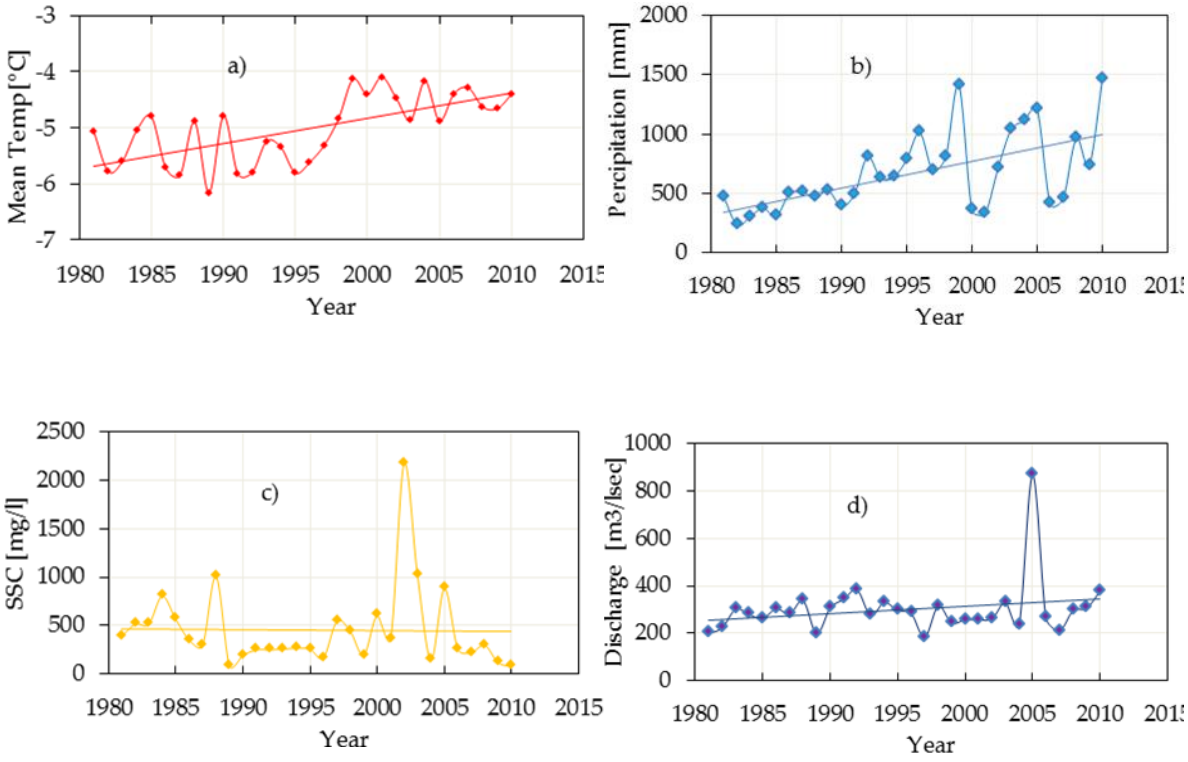

Figure 5. 7 Observed (a) mean basin air temperature (b) mean basin precipitations (c) suspended sediment concentrations (SSC) (d) measured discharge for the period 1981-2010 of Gilgit basin.

During summer the contribution of ice melts is also significant up to 30% in the month of July. During the months of late summers, the contribution of snow melts is more than summer effective rainfall. The Effective rainfall is more dominated factor in flow generation process during the autumn season (Sep-Nov) when precipitations contribute in the liquid form rather than snow due to again increase

of air temperature (Fig.5.6, Fig.5.8a). So, the increase in SSC during autumns season could be due to increase in the amount of precipitation in liquid form on snow free area of Gilgit catchment.

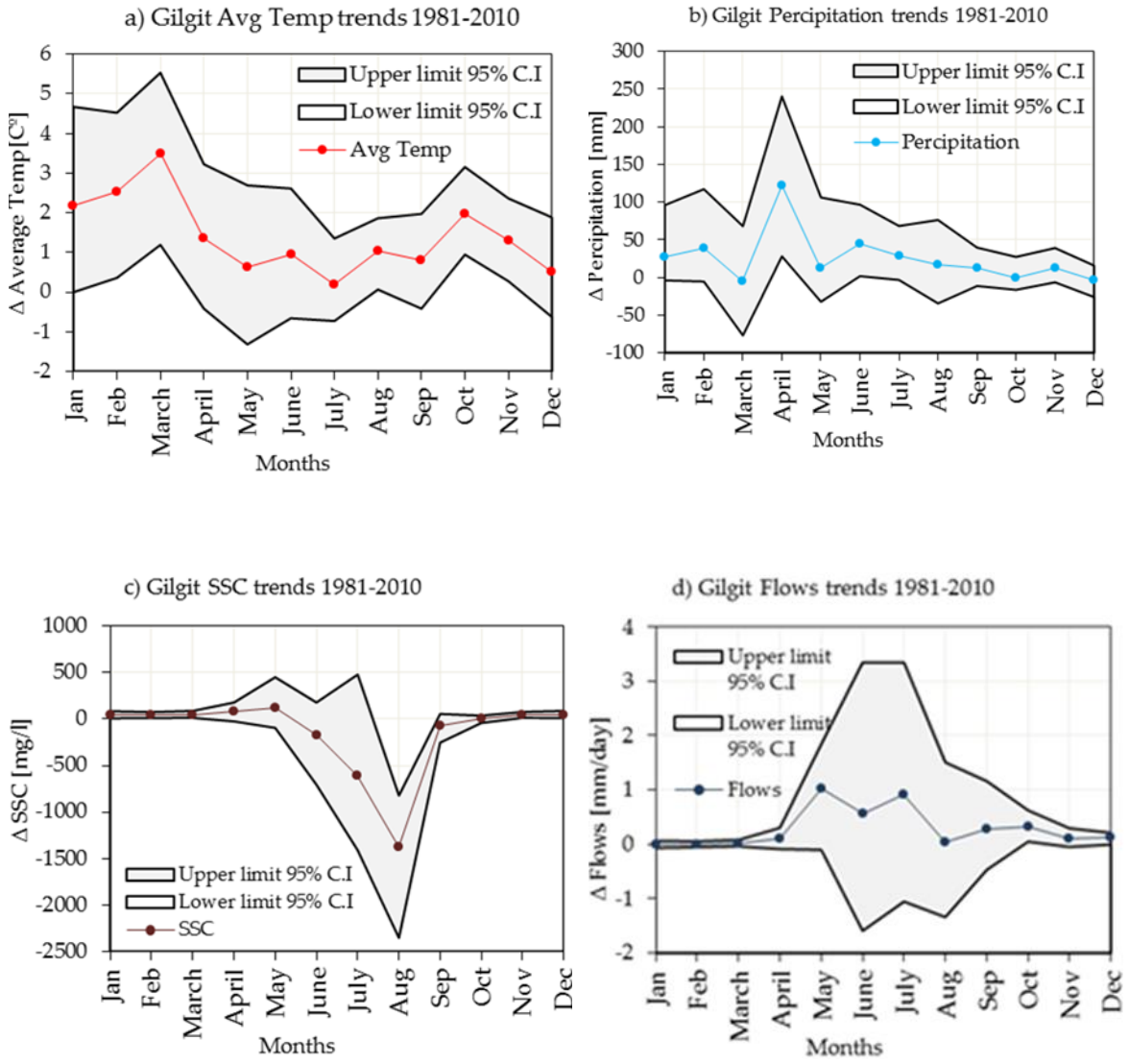

Figure 5. 8 Observed (a) mean basin air temperature (b) mean basin precipitations (c) suspended sediment concentrations (SSC) (d) measured discharge for the period 1981-2010 of Gilgit basin.

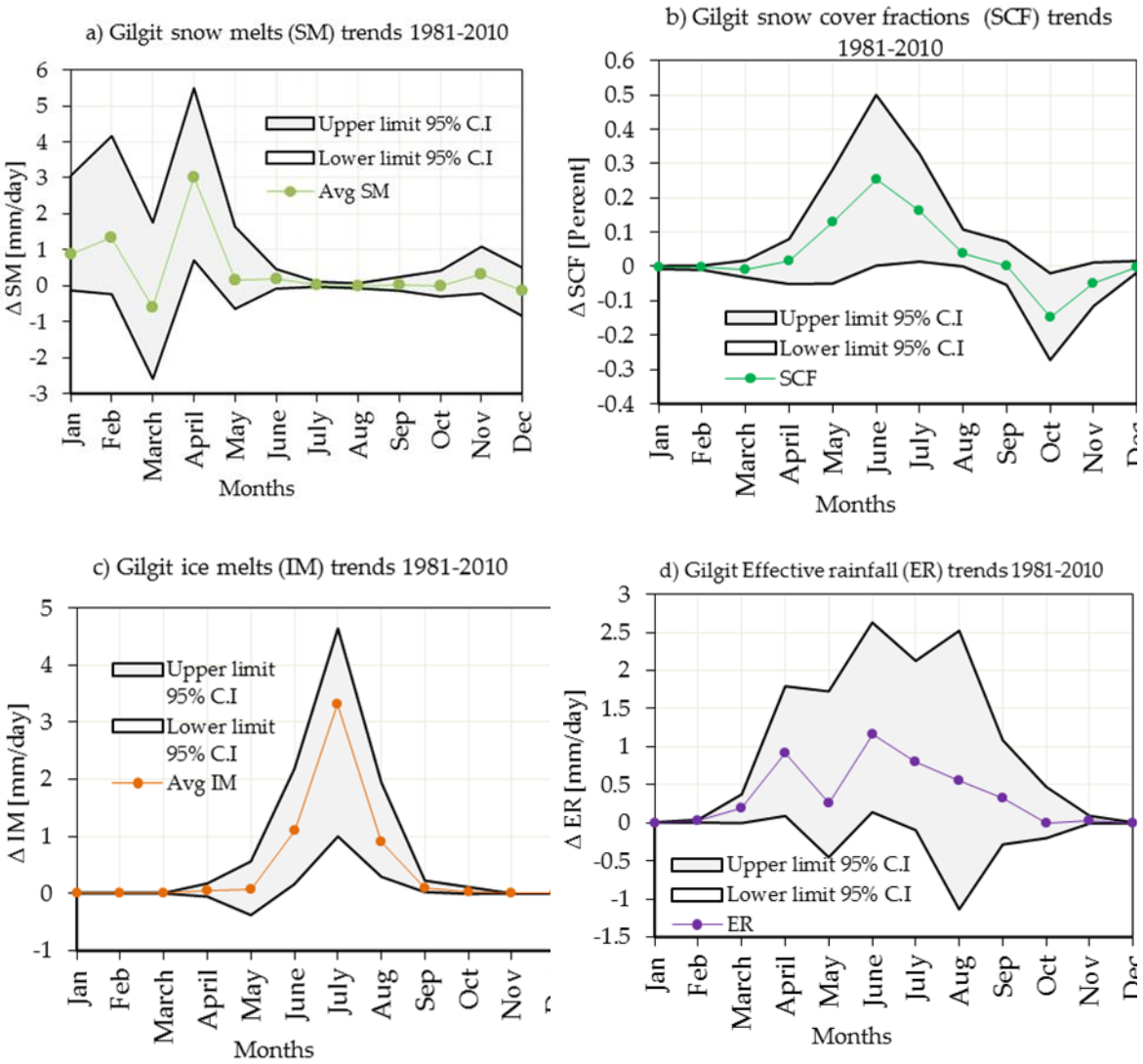

Figure 5. 9 Monthly changes in (a) mean basin snow melts (SM) (b) mean basin snow cover fractions (SCF) (c) mean basin ice melts (IM) (d) mean basin effective rainfall (ER) for the period 1981-2010 of Gilgit basin.

The Figure 5.10 shows the warming of annual mean air temperature but decrease of basin annual rainfall in Astore basin during the period 1981-2010. The simultaneous increase in annual mean temperature of Astore basin increases the annual flows as well as annual SSC. The warming trend during annual temperature in Astore basin reveals that monthly temperature during the autumns and winters (Oct-Mar) are mainly increasing, while changes during the late springs and summer are signalling cooling trends shown in Figure 5.11a. However, the decrease of annual precipitation in Astore basin is mainly due to the significant decrease of monthly precipitation in spring season (March-May) shown in Figure 5.11b. As shown in the Figure 5.2 the months of springs (March-May) have major rainfall contribution in total annual rainfall of Astore basin. The significant decrease of spring rainfall during this period is an important factor contributing the stream flows during early summers (Fig. 5.11b). The non-significant increase of mean annual flows in Astore catchment is due to increase of springs snow melts, ice melts and effective rainfall contribution in annual flows (Fig. 5.10, Fig.5.11 d, Fig. 5.12a, Fig. 5.12c, Fig. 5.12 d). As the precipitations in winter increases the winter snow cover accumulation also increases during winter. With the start of spring seasons an increase of spring temperature increases the snow melts from winter snows accumulation rapidly beside the decrease of springs rainfall which can increase the annual flows of Astor River. The decrease in the snow cover during spring and early summers in Astore basin is probably due to the reduction of spring/early-summer precipitations.

The increase of annual SSC is probably due to increase in monthly SSC during winter, late springs and early summers. The warming of mean air temperature during winter is significant increasing the flows, snow melts and SSC (Fig. 5.11a, Fig. 5.11c, Fig. 5.11d, Fig. 5.12a). The increase of SSC during springs (March-April) coincides with the increase of Astore River flows, snow melts and effective rainfall (Fig.5.11 c, Fig. 5.12a, Fig. 5.12c, Fig. 5.12 d). Similarly, the reduction of snow cover fraction during early summer seasons implies an increase in the contribution of effective rainfall on snow free area to erode the sediments in Astor basin (Fig. 5.12b & 5.12d). Moreover, the reduction in snow cover albedo during spring and summer due to lesser amount of seasonal precipitations could be exposing the paraglacial unstable landscape, which are high source of sediment erosions activated by snow melts, glacier melts and effective rainfall [66,67]. During autumn season (Sep-Oct) the slightly increase in the SSC also coincide with slightly increase of seasonal precipitation, effective rainfall and reduction of snow fractions (Fig. 5.11b, Fig. 5.11 b, Fig. 5.12b, Fig. 5.12d). Reduction of snow cover during autumn season (Sep-Oct) implies more precipitation occurs in the liquid form to generate the erosions. Similarly, increase of rainfall during autumns could increase the hillslope erosions, activation of mass wasting, enhance of channel and bank erosions [40,41]

The Figure 5.6b shows that the contribution of effective rainfall is more dominated factor during autumn and partially during winter season in flow generation process. However, the contribution of snow melts is more than effective rainfall and ice melts during springs and summers season in Astore basin. It also shows the importance of springs snow cover fractions, spring solid/liquid precipitations and snow melts contribution as dominating factor in springs discharges. The contribution of ice melts is less during the summers in comparison to the snow melts. The effective rainfall has lesser contribution during summer season than ice melts.

The signalling of climate in context of sediment dynamics is important for future climate projections. Under the challenges of large uncertainty for future climate changes and its projections the current results depict the important consideration of increase of mean annual air temperature and mean annual precipitations for future climate change models in Gilgit basin. The results of this research further highlight the shift of snow dominated characteristics of Astore basin to the rainfall-dominated hydrological regime. This shift of hydrological regime interpreted from the hydroclimatic trends of Astore catchment is resulting in the reduction summer flows, increase of winter snow melts, reduction of spring precipitations and significant reduction of springs snow covers fraction. In contrast to shift of these hydrological regimes the changes and prediction of sediment fluxes in future could be highly unrealistic, less reliable using the future climate change model. The sediment estimation/predictions are uncertain due to complex process of sediment transport, feedback of different hydrological process, inherent stochastic in sediment transport and mobilization of sediment from its source.

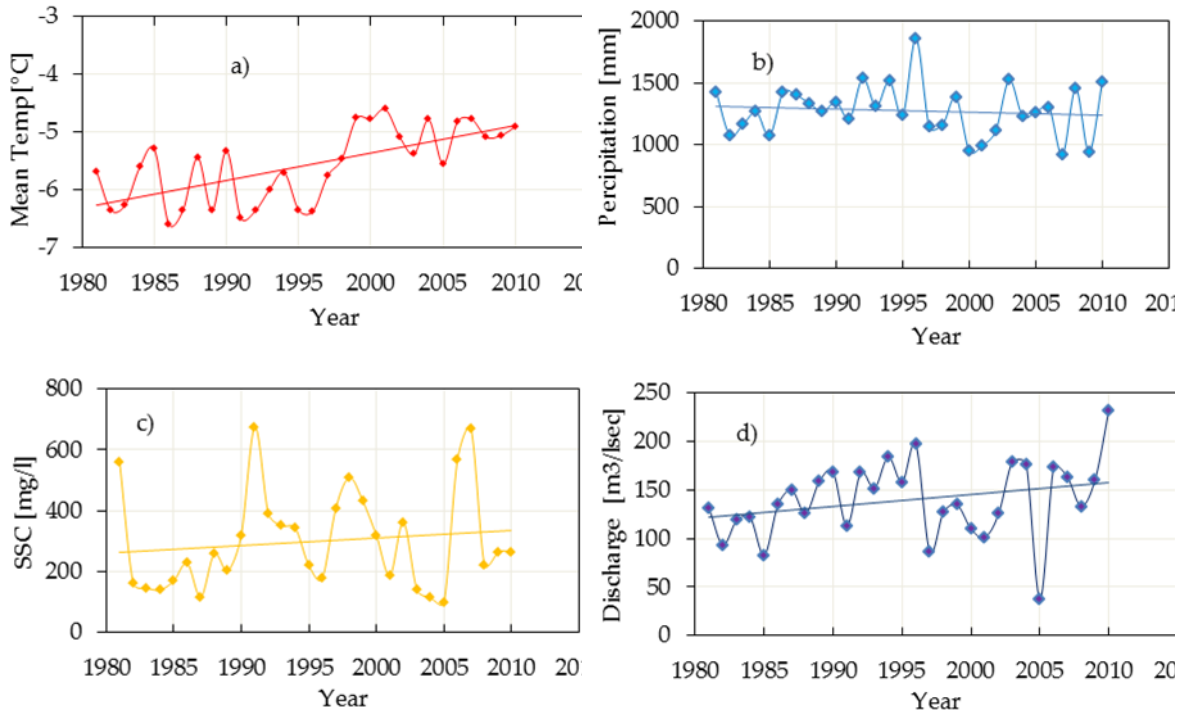

Figure 5. 10 Observed (a) basin mean temperature (b) mean basin precipitations (c) suspended sediment concentrations (SSC) (d) measured discharge for the period 1981-2010 of Astore basin.

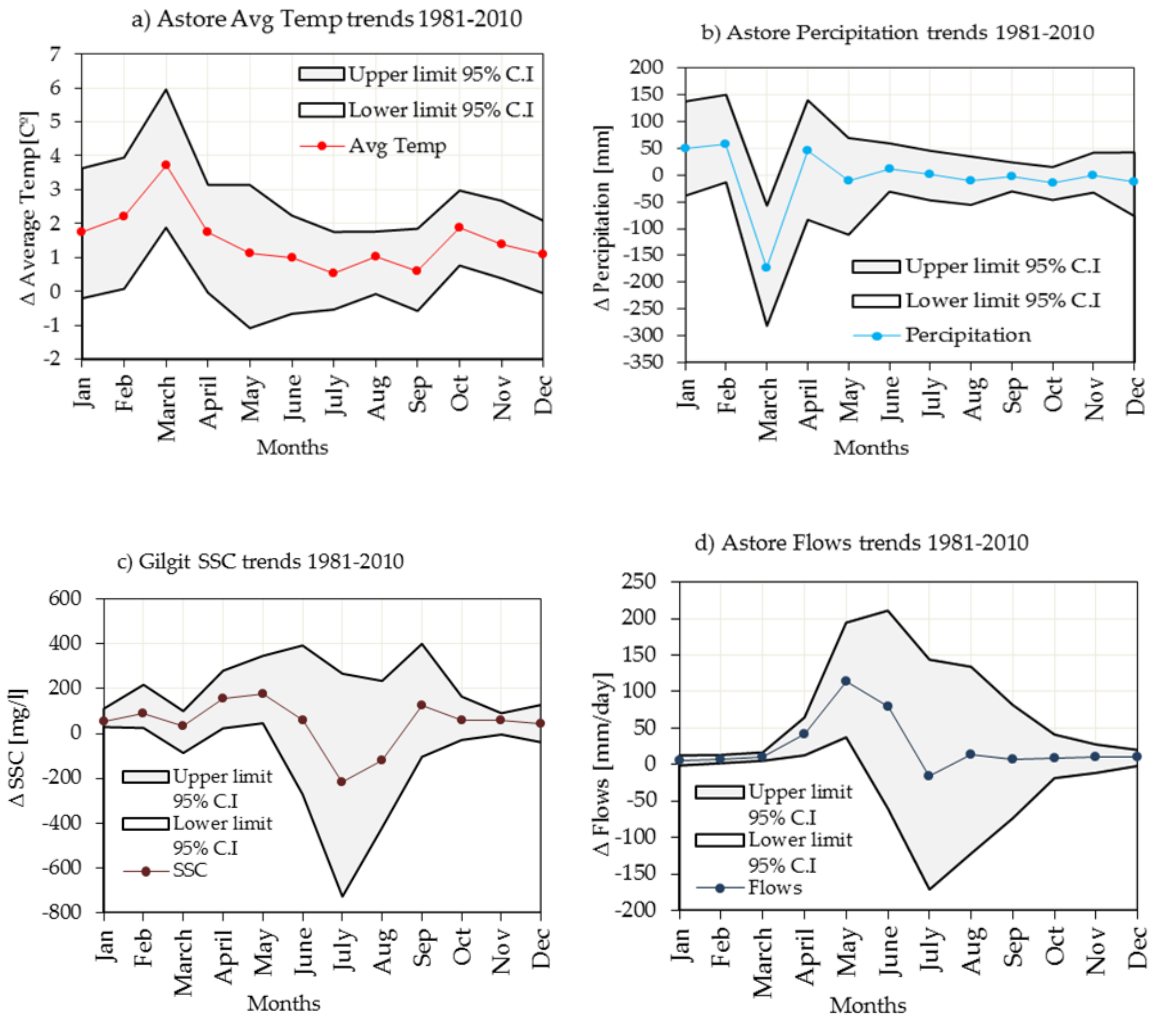

Figure 5. 11 Observed (a) mean basin air temperature (b) mean basin precipitations (c) suspended sediment concentrations (SSC) (d) measured discharge for the period 1981-2010 of Astore basin.

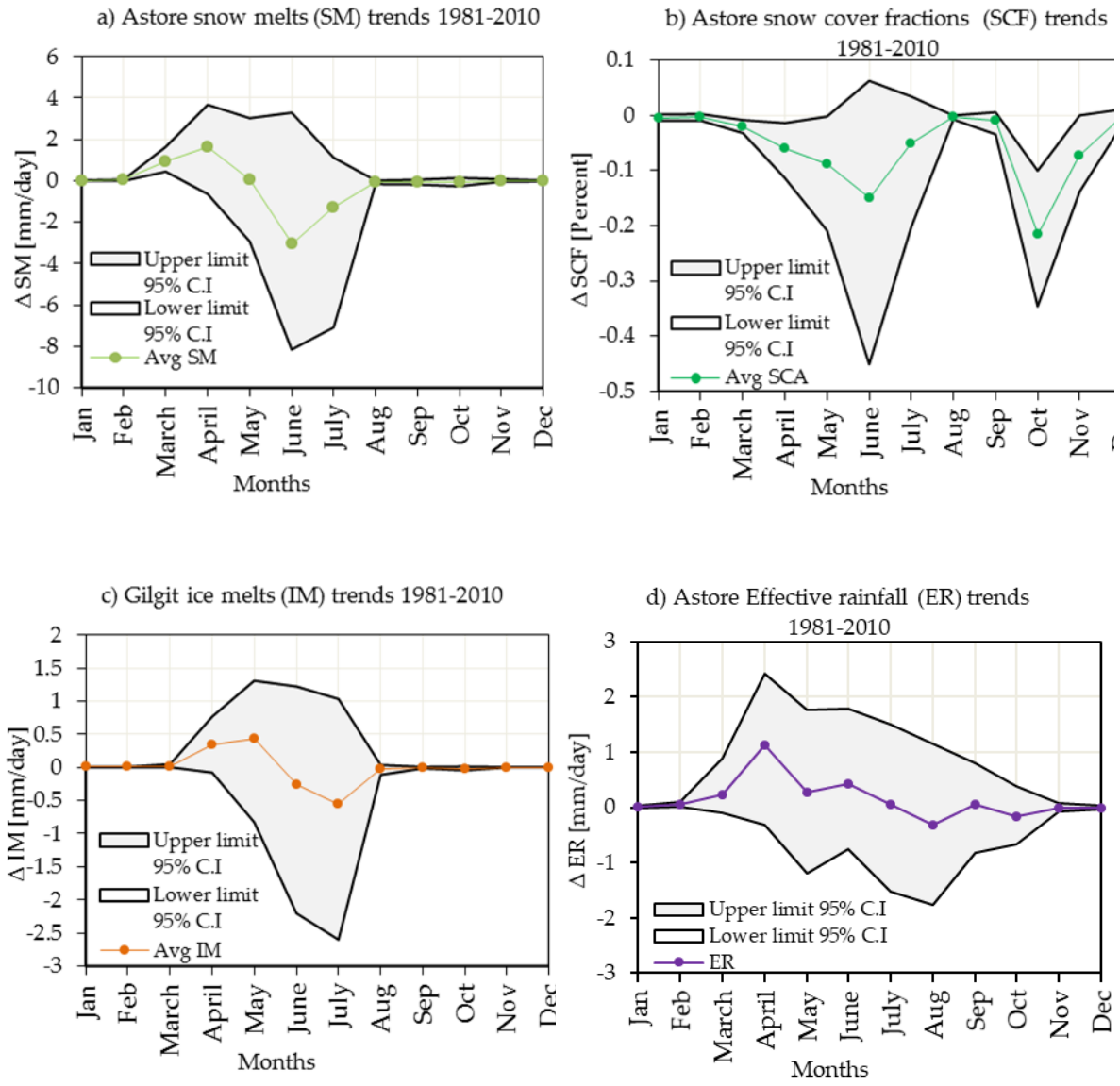

Figure 5. 12 Monthly changes in (a) mean basin snow melts (SM) (b) mean basin snow cover fractions (SCF) (c) mean basin ice melts (IM) (d) mean basin effective rainfall (ER) for the period 1981-2010 of Astore basin.

5.5 Conclusions

The main focus of current research was to analyse the changes/trends of hydroclimatic variables and suspended sediments of the Gilgit basin (Hindukush range) and Astore basin (Western Himalayas) during the period 1981-2010. In addition, the non-significant decrease of annual suspended sediments in Gilgit and increase of annual sediment in Astore basin suggested a causal linkage between the transport dynamics of fine sediments and climatic changes. Four important factors highlighted as: (a) warming mean annual air temperature (b) increase/decrease of mean basin precipitations (c) increase/decrease of snow cover albedo and (d) enhanced SSC has a linkage in the form of an increase transport capacity and activation/deactivation of sediment sources to increase/decrease the sediment supplies. The results of present research conclude that transport capacity of the channel due to discharges is not sufficient to explain the decrease/increase of annual suspended sediment concentrations (SSC). The conclusion of analysis is that reduction/increase of annual precipitation under the warmer climate impacts the transport dynamics of fine sediments through activation/deactivation of sediment sources influencing the sediment production and transport in the catchment.

To understand the phenomena of sediment supplies, the present research work analysed the three sediment fluxes as: (1) sediment erosions due to snow melts in the form of hillslope/gully and channel/stream erosions (2) sediment erosions due to erosivity of effective rainfalls over snow free landscape in the form of hillslope erosion, channel bank erosions and erosion from landslides/mass wasting (3) sediment transports due to glacier melts. The changes in snow and ice melt rates together with snow cover fractions and amounts of rainfalls were also analysed to understand the changes in SSC during the period 1981-2010.

The results of this work show that the changes in mean annual precipitations and mean annual air temperatures during the period 19821-2010 does not clearly show the evident similar pattern of change in the SSC. However, the increase/decrease of monthly snow covers, snow melts, ice melts and effective rainfall clearly shows the relevant pattern of changes in monthly flows and SSC. The increase of winter precipitations of both Gilgit and Astore basin are evident along with increasing snow melts, SSC and winter flows. However, the spring precipitations increases in Gilgit basin contrary to the significant reduction of spring precipitations in Astore basin. Here, the clear evident was also found about the increase of snow cover fractions in late springs/early summers in Gilgit basin contrary to the Astore basin. Which was probably due to the reduction in seasonal precipitations and decrease/increase of effective rainfall. These changes in snow cover dynamics, snow melts rates and seasonal precipitations link with the changes in SSC. The changes of monthly mean air temperature are alike to the changes in SSC in both of the basins during whole of the year. It was assessed that the changes of monthly/seasonal SSC in Gilgit basins are altered due to combined effect of changes in monthly/seasonal precipitations and monthly/seasonal mean air temperatures in Gilgit basin. The increase of winter and spring precipitations along with warming/cooling trend of climate, increase of snow cover fractions during summer is altering the hydrological regime and sediment erosion process over the year in Gilgit basin. The increased springs/early summer precipitations along with the increase of snow cover fractions during summers is in accordance with the reduction of SSC during summers in Gilgit basin. This shows the relevancy of snow melts, snow

cover and ice melts in transports of sediments in Gilgit basin. Contrary to the Gilgit basin the spring precipitations in Astore basin has been reduced significantly along with the reductions of snow cover fractions, increase of effective rainfall and reduction of SSC. Which implies that the hydrological regime of Astore basin is shifted from the snow-dominated basins to the rainfall dominated basins. Contrary to the Gilgit basin the amounts of seasonal/annual precipitations in Astore basin are more dominated than ice melt rates and mean air temperature in altering the sediment dynamics and hydrological regimes.

In the Gilgit basin the changes in sediments are not consistent with the changes of flows and channel transport capacity, the main emphasise of current research is to understand the sediment productions and its transports due to different hydrological process (SM, IM, SCF and ER) responsible for activation/deactivation of sediments in the catchments in addition to sediment transports in the channel. Due to constraints of the hydrological modelling and limitations of the data inputs incurrent study it is difficult to conclude that in which directions sediment flux will be changed in future. However, a more reliable Glacio-hydrological modelling can show a better understanding of process-based understanding connecting the hydrological changes, sediment transport and present/future climate changes for both the Gilgit and Astore basins.

5.6 References

1. Meade, R.H. Suspended sediment in the Amazon River and its tributaries in Brazil during 1982-84; Open-File Report 85-492, 1985. http://pubs.er.usgs.gov/publication/ofr85492.
2. Glazyrin, G.; Tashmetov, H.K. Sediment yield alteration of mountain rivers and climate change in central Asia. Effects of Scale on Interpretation and Management of Sediment and Water Quality, Osterkamp WR (ed). 1995, IAHS Publication No. 226. IAHS Press: Wallingford; 187–190.
3. Tucker, G.E.; Slingerland, R. Drainage basin responses to climate change. Water Resour. Res. 1997, 33, 2031–2047, doi:10.1029/97WR00409.
4. Walling, D.E. Linking land use, erosion and sediment yields in river basins. Hydrobiologia 1999, 410, 223–240, doi:10.1023/A:1003825813091.
5. van Rompaey, A.J.J.; Govers, G.; Puttemans, C. Modelling land use changes and their impact on soil erosion and sediment supply to rivers. Earth Surf. Process. Landforms 2002, 27, 481–494, doi:10.1002/esp.335.
6. Church, M.; Slaymaker, O. Disequilibrium of Holocene sediment yield in glaciated British Columbia. Nature 1989, 337, 452–454, doi:10.1038/337452a0.
7. Molnar, P.; England, P. Late Cenozoic uplift of mountain ranges and global climate change: chicken or egg? Nature 1990, 346, 29–34, doi:10.1038/346029a0.
8. Jansen, I.M.L.; Painter, R.B. Predicting sediment yield from climate and topography. Journal of Hydrology 1974, 21, 371–380, doi:10.1016/S0022-1694(74)80006-5.
9. Pinet, P.; Souriau, M. Continental erosion and large-scale relief. Tectonics 1988, 7, 563–582, doi:10.1029/TC007i003p00563.

10. Summerfield, M.A.; Hulton, N.J. Natural controls of fluvial denudation rates in major world drainage basins. J. Geophys. Res. 1994, 99, 13871–13883, doi:10.1029/94JB00715.
11. Ludwig, W.; Probst, J.-L. River sediment discharge to the oceans; present-day controls and global budgets. American Journal of Science 1998, 298, 265–295, doi:10.2475/ajs.298.4.265.
12. Hovius, N. Controls on sediment supply by large rivers. Relative Role of Eustasy, Climate, and Tectonism in Continental Rocks; SEPM (Society for Sedimentary Geology), 1998; pp 2–16, ISBN 1-56576-042-5.
13. Syvitski, J.P.M.; Milliman, J.D. Geology, Geography, and Humans Battle for Dominance over the Delivery of Fluvial Sediment to the Coastal Ocean. The Journal of Geology 2007, 115, 1–19, doi:10.1086/509246.
14. Milliman, J.D.; Syvitski, J.P.M. Geomorphic/Tectonic Control of Sediment Discharge to the Ocean: The Importance of Small Mountainous Rivers. The Journal of Geology 1992, 100, 525–544, doi:10.1086/629606.
15. Faran Ali, K.; Boer, D.H. de. Factors controlling specific sediment yield in the upper Indus River basin, northern Pakistan. Hydrol. Process. 2008, 22, 3102–3114, doi:10.1002/hyp.6896.
16. Arora, M.; Kumar, R.; Kumar, N.; Malhotra, J. Assessment of suspended sediment concentration and load from a large Himalayan glacier. Hydrology Research 2014, 45, 292–306, doi:10.2166/nh.2013.129.
17. Haritashya, U.K.; Singh, P.; Kumar, N.; Gupta, R.P. Suspended sediment from the Gangotri Glacier: Quantification, variability and associations with discharge and air temperature. Journal of Hydrology 2006, 321, 116–130, doi:10.1016/j.jhydrol.2005.07.037.
18. Jansson, P.; Hock, R.; Schneider, T. The concept of glacier storage: a review. Journal of Hydrology 2003, 282, 116–129, doi:10.1016/S0022-1694(03)00258-0.
19. Orwin, J.F.; Lamoureux, S.F.; Warburton, J.; Beylich, A. A framework for characterizing fluvial sediment fluxes from source to sink in cold environments. Geografiska Annaler: Series A, Physical Geography 2010, 92, 155–176, doi:10.1111/j.1468-0459.2010.00387.x.
20. Orwin, J.F.; Smart, C.C. Short-term spatial and temporal patterns of suspended sediment transfer in proglacial channels, small River Glacier, Canada. Hydrol. Process. 2004, 18, 1521–1542, doi:10.1002/hyp.1402.
21. Gardelle, J.; Berthier, E.; Arnaud, Y. Slight mass gain of Karakoram glaciers in the early twenty-first century. Nature Geosci 2012, 5, 322–325, doi:10.1038/ngeo1450.
22. Forsythe, N.; Fowler, H.J.; Li, X.-F.; Blenkinsop, S.; Pritchard, D. Karakoram temperature and glacial melt driven by regional atmospheric circulation variability. Nature Clim Change 2017, 7, 664–670, doi:10.1038/nclimate3361.
23. Ali, K.F.; De Boer, D.H. Spatial patterns and variation of suspended sediment yield in the upper Indus River basin, northern Pakistan. Journal of Hydrology 2007, 334, 368–387, doi:10.1016/j.jhydrol.2006.10.013.

24. Hewitt, K. The Karakoram Anomaly? Glacier Expansion and the 'Elevation Effect,' Karakoram Himalaya. Mountain Research and Development 2005, 25, 332–340, doi:10.1659/0276-4741(2005)025[0332:TKAGEA]2.0.CO;2.
25. Lutz, A.F.; Immerzeel, W.W.; Kraaijenbrink, P.D.A.; Shrestha, A.B.; Bierkens, M.F.P. Climate Change Impacts on the Upper Indus Hydrology: Sources, Shifts and Extremes. PLoS ONE 2016, 11, e0165630, doi:10.1371/journal.pone.0165630.
26. Ateeq-Ur-Rehman, S.; Bui, M.; Rutschmann, P. Variability and Trend Detection in the Sediment Load of the Upper Indus River. Water 2018, 10, 16, doi:10.3390/w10010016.
27. Tarar, Z.; Ahmad, S.; Ahmad, I.; Majid, Z. Detection of Sediment Trends Using Wavelet Transforms in the Upper Indus River. Water 2018, 10, 918, doi:10.3390/w10070918.
28. Ul Hussan, W.; Khurram Shahzad, M.; Seidel, F.; Costa, A.; Nestmann, F. Comparative Assessment of Spatial Variability and Trends of Flows and Sediments under the Impact of Climate Change in the Upper Indus Basin. Water 2020, 12, 730, doi:10.3390/w12030730.
29. Syvitski, J.P.M.; Vörösmarty, C.J.; Kettner, A.J.; Green, P. Impact of humans on the flux of terrestrial sediment to the global coastal ocean. Science 2005, 308, 376–380, doi:10.1126/science.1109454.
30. Foster, G.C.; Dearing, J.A.; Jones, R.T.; Crook, D.S.; Siddle, D.J.; Harvey, A.M.; James, P.A.; Appleby, P.G.; Thompson, R.; Nicholson, J.; et al. Meteorological and land use controls on past and present hydro-geomorphic processes in the pre-alpine environment: an integrated lake-catchment study at the Petit Lac d'Annecy, France. Hydrol. Process. 2003, 17, 3287–3305, doi:10.1002/hyp.1387.
31. Wieckowska-Lüth, M.; Kirleis, W.; Doerfler, W. Holocene history of landscape development in the catchment of Lake Skogstjern, southeastern Norway, based on a high-resolution multi-proxy record. The Holocene 2017, 27, 1928–1947, doi:10.1177/0959683617715691.
32. Meybeck, M. Global analysis of river systems: from Earth system controls to Anthropocene syndromes. Philos. Trans. R. Soc. Lond. ,. B,. Biol. Sci. 2003, 358, 1935–1955, doi:10.1098/rstb.2003.1379.
33. Walling, D.E.; Fang, D. Recent trends in the suspended sediment loads of the world's rivers. Global and Planetary Change 2003, 39, 111–126, doi:10.1016/S0921-8181(03)00020-1.
34. Evans, M. Temporal and Spatial Representativeness of Alpine Sediment Yields: Cascade Mountains, British Columbia. Earth Surf. Process. Landforms 1997, 22, 287–295, doi:10.1002/(SICI)1096-9837(199703)22:3<287:AID-ESP757>3.0.CO;2-V.
35. Boulton, G.S. Processes and Patterns of Glacial Erosion. In Glacial Geomorphology; Coates, D.R., Ed.; Springer Netherlands: Dordrecht, 1982; pp 41–87, ISBN 978-94-011-6493-1.
36. Allouche, O.; Tsoar, A.; Kadmon, R. Assessing the accuracy of species distribution models: prevalence, kappa and the true skill statistic (TSS). Journal of Applied Ecology $V 43 2006, 43, 1223–1232, doi:10.1111/j.1365-2664.2006.01214.x.

37. Collins, D. Sediment transport from glacierized basins in the Karakoram mountains. Erosion and Sediment Yield: Global and Regional Perspectives (Proceedings of the Exeter Symposium, July 1996), IAHS Alpine Glacier Project, Department of Geography, University of Manchester, Manchester Ml 3 9PL, UK. 1996, 236.
38. Lane, S.N.; Bakker, M.; Gabbud, C.; Micheletti, N.; Saugy, J.-N. Sediment export, transient landscape response and catchment-scale connectivity following rapid climate warming and Alpine glacier recession. Geomorphology 2017, 277, 210–227, doi:10.1016/j.geomorph.2016.02.015.
39. Quinton, W.L.; Carey, S.K. Towards an energy-based runoff generation theory for tundra landscapes. Hydrol. Process. 2008, 22, 4649–4653, doi:10.1002/hyp.7164.
40. Bennett, G.L.; Molnar, P.; Eisenbeiss, H.; McArdell, B.W. Erosional power in the Swiss Alps: characterization of slope failure in the Illgraben. Earth Surf. Process. Landforms 2012, 37, 1627–1640, doi:10.1002/esp.3263.
41. Wulf, H.; Bookhagen, B.; Scherler, D. Climatic and geologic controls on suspended sediment flux in the Sutlej River Valley, western Himalaya. Hydrol. Earth Syst. Sci. 2012, 16, 2193–2217, doi:10.5194/hess-16-2193-2012.
42. Bilal, H.; Chamhuri, S.; Mokhtar, M.B.; Kanniah, K.D. Recent snow cover variation in the Upper Indus Basin of Gilgit Baltistan, Hindukush Karakoram Himalaya. J. Mt. Sci. 2019, 16, 296–308, doi:10.1007/s11629-018-5201-3.
43. Atif, I.; Iqbal, J.; Mahboob, M. Investigating Snow Cover and Hydrometeorological Trends in Contrasting Hydrological Regimes of the Upper Indus Basin. Atmosphere 2018, 9, 162, doi:10.3390/atmos9050162.
44. Tahir, A.A.; Chevallier, P.; Arnaud, Y.; Ahmad, B. Snow cover dynamics and hydrological regime of the Hunza River basin, Karakoram Range, Northern Pakistan. Hydrol. Earth Syst. Sci. 2011, 15, 2275–2290, doi:10.5194/hess-15-2275-2011.
45. Tahir, A.A.; Chevallier, P.; Arnaud, Y.; Ashraf, M.; Bhatti, M.T. Snow cover trend and hydrological characteristics of the Astore River basin (Western Himalayas) and its comparison to the Hunza basin (Karakoram region). Sci. Total Environ. 2015, 505, 748–761, doi:10.1016/j.scitotenv.2014.10.065.
46. Tahir, A.A.; Adamowski, J.F.; Chevallier, P.; Haq, A.U.; Terzago, S. Comparative assessment of spatiotemporal snow cover changes and hydrological behavior of the Gilgit, Astore and Hunza River basins (Hindukush–Karakoram–Himalaya region, Pakistan). Meteorol Atmos Phys 2016, 128, 793–811, doi:10.1007/s00703-016-0440-6.
47. Hasson, S.; Lucarini, V.; Khan, M.R.; Petitta, M.; Bolch, T.; Gioli, G. Early 21st century snow cover state over the western river basins of the Indus River system. Hydrol. Earth Syst. Sci. 2014, 18, 4077–4100, doi:10.5194/hess-18-4077-2014.

48. Swift, D.A.; Nienow, P.W.; Hoey, T.B. Basal sediment evacuation by subglacial meltwater: suspended sediment transport from Haut Glacier d'Arolla, Switzerland. Earth Surf. Process. Landforms 2005, 30, 867–883, doi:10.1002/esp.1197.
49. Herman, F.; Beyssac, O.; Brughelli, M.; Lane, S.N.; Leprince, S.; Adatte, T.; Lin, J.Y.Y.; Avouac, J.-P.; Cox, S.C. Erosion by an Alpine glacier. Science 2015, 350, 193–195, doi:10.1126/science.aab2386.
50. Lenzi, M.A.; Marchi, L. Suspended sediment load during floods in a small stream of the Dolomites (northeastern Italy). CATENA 2000, 39, 267–282, doi:10.1016/S0341-8162(00)00079-5.
51. Immerzeel, W.W.; Wanders, N.; Lutz, A.F.; Shea, J.M.; Bierkens, M.F.P. Reconciling high-altitude precipitation in the upper Indus basin with glacier mass balances and runoff. Hydrol. Earth Syst. Sci. 2015, 19, 4673–4687, doi:10.5194/hess-19-4673-2015.
52. Lutz, A.F.; Immerzeel, W.W. HI-AWARE Reference Component 1. Climate Dataset for the Indus, Ganges and Brahmaputra River Basins. FutureWater Rep. 2015, 146. Available online:https://www.futurewater.eu/wpcontent/uploads/2015/10/Report_IGB_historical_climate_dataset.pdf (accessed on 06.03.2018).
53. GLIMS, and National Snow and Ice Data Center. GLIMS Glacier Database. Glaciers in the Karakorum Mountain Region; National Snow and Ice Data Center: Boulder, CO, USA, 2012, doi:10.7265/N5V98602.
54. Hock, R. Temperature index melt modelling in mountain areas. Journal of Hydrology 2003, 282, 104–115, doi:10.1016/S0022-1694(03)00257-9.
55. Costa, A.; Molnar, P.; Stutenbecker, L.; Bakker, M.; Silva, T.A.; Schlunegger, F.; Lane, S.N.; Loizeau, J.-L.; Girardclos, S. Temperature signal in suspended sediment export from an Alpine catchment. Hydrol. Earth Syst. Sci. 2018, 22, 509–528, doi:10.5194/hess-22-509-2018.
56. Collins, W.; Rasch, P.; Boville, B.; McCaa, J.; Williamson, D.; Kiehl, J.; Briegleb, B.; Bitz, C.; Lin, S.-J.; Zhang, M.; et al. Description of the NCAR Community Atmosphere Model (CAM 3.0), 2004.
57. Auer, A.H. The Rain versus Snow Threshold Temperatures. Weatherwise 1974, 27, 67, doi:10.1080/00431672.1974.9931684.
58. Tahir, A.A.; Chevallier, P.; Arnaud, Y.; Neppel, L.; Ahmad, B. Modeling snowmelt-runoff under climate scenarios in the Hunza River basin, Karakoram Range, Northern Pakistan. Journal of Hydrology 2011, 409, 104–117, doi:10.1016/j.jhydrol.2011.08.035.
59. Tahir, A.A.; Hakeem, S.A.; Hu, T.; Hayat, H.; Yasir, M. Simulation of snowmelt-runoff under climate change scenarios in a data-scarce mountain environment. International Journal of Digital Earth 2019, 12, 910–930, doi:10.1080/17538947.2017.1371254.

60. Hayat, H.; Akbar, T.A.; Tahir, A.A.; Hassan, Q.K.; Dewan, A.; Irshad, M. Simulating Current and Future River-Flows in the Karakoram and Himalayan Regions of Pakistan Using Snowmelt-Runoff Model and RCP Scenarios. Water 2019, 11, 761, doi:10.3390/w11040761.
61. Adnan, M.; Nabi, G.; Kang, S.; Zhang, G.; Adnan, R.M.; Anjum, M.N.; Iqbal, M.; Ali, A.F. Snowmelt Runoff Modelling under Projected Climate Change Patterns in the Gilgit River Basin of Northern Pakistan. Pol. J. Environ. Stud. 2017, 26, 525–542, doi:10.15244/pjoes/66719.
62. Adnan, M.; Nabi, G.; Saleem Poomee, M.; Ashraf, A. Snowmelt runoff prediction under changing climate in the Himalayan cryosphere: A case of Gilgit River Basin. Geoscience Frontiers 2017, 8, 941–949, doi:10.1016/j.gsf.2016.08.008.
63. Cheng, G.; Wu, T. Responses of permafrost to climate change and their environmental significance, Qinghai-Tibet Plateau. J. Geophys. Res. 2007, 112, 169, doi:10.1029/2006JF000631.
64. Lawrence, D.M.; Slater, A.G. A projection of severe near-surface permafrost degradation during the 21st century. Geophys. Res. Lett. 2005, 32, 241, doi:10.1029/2005GL025080.
65. Zhao, L.; Ping, C.-L.; Yang, D.; Cheng, G.; Ding, Y.; Liu, S. Changes of climate and seasonally frozen ground over the past 30 years in Qinghai Xizang (Tibetan) Plateau, China. Global and Planetary Change 2004, 43, 19–31, doi:10.1016/j.gloplacha.2004.02.003.
66. Shekhar, M.S.; Chand, H.; Kumar, S.; Srinivasan, K.; Ganju, A. Climate-change studies in the western Himalaya. Ann. Glaciol. 2010, 51, 105–112, doi:10.3189/172756410791386508.
67. Meigs, A.; Krugh, W.C.; Davis, K.; Bank, G. Ultra-rapid landscape response and sediment yield following glacier retreat, Icy Bay, southern Alaska. Geomorphology 2006, 78, 207–221, doi:10.1016/j.geomorph.2006.01.029.

Chapter 6- Conclusion and Recommendations

6.1 Conclusions

The present research focuses on the assessment of climate changes on generation process of suspended sediments and development of a suitable data-based modelling approach for sediment predictions by introducing the innovative input combination of snow cover fractions and normalized difference vegetative index (NDVI) in addition to the hydroclimatic datasets in alluvial river of UIB in the Pakistan. Estimation of suspended sediments with the measured data collected from the field is very expensive, time consuming and required a lot of resources especially in the Alpine mountain environments of UIB. The availability of remotely sensed data from satellites such as air temperature, precipitation, snow cover fraction and NDVI as biophysical parameter provide the opportunity to check the applicability of suitable modelling framework to quantify and predict the sediment loads. The methodological framework in present research was divided into four different objectives to assess the changes and prediction of suspended sediments: (1) Comparative Assessment of Spatial Variability and Trends of Flows and Sediments Under the Impact of Climate Change in The Upper Indus Basin (2) Application of soft computing models with input vectors of snow cover area in addition to hydro-climatic data to predict the sediment loads (3) Prediction of sediment yields by using the hydroclimate and normalized difference vegetation index (NDVI) datasets with soft computing models (4) Climate signaling in suspended sediment exports from Glacier and Snow Melts Sub-basins in the Upper Indus Basin (UIB). The conclusion drawn from this research are summarized as:

- Assessment of climate changes flows and suspended sediments in UIB

The upper Indus River comprises the catchment area of 172,000 km^2 upstream of Tarbela reservoir in Pakistan. The sediment transport of alluvial river in UIB depends upon the discharges originating from glacier and snow melts in higher mountains and rainfall contributions in lower part of the catchment. The difference in physiography, climate and hydrological process generate the different sediments concentrations in each sub-basin. To assess the climate change and spatial pattern of flows and SSC in UIB an effort has been made in this work. The assessment of trends of climate changes on flows and SSC in this research work concludes that the annual flows and sediments in lower part of main Indus River at Besham Qila i.e. upstream of Tarbela dam are in a balanced state during the period 1981-2010. However, the annual SSC in the upper snow- and glacier-dominated Hindukush and Karakorum basins were decreased during this period. Similarly, in the upper snow and rainfed basin of Western and Central Himalayas the annual SSC are increased. The SSC during summers in upper snow-and glacier-dominated Hindukush and Karakorum basins has significantly reduced due to its Karakorum climate anomaly. However, during the months of winter season the flows and SSC were significantly increased due to warming of mean air temperature in the glacier- and snow-dominated basins. In lower part of UIB, Indus at Daggar and Gorband the SSC and flows are

decreased due to significant reduction of rainfalls during spring, autumn and summer seasons. On the main Indus River at Kachura the SSC during the winter and spring season SSC has increased with increase of its discharges which might be eroding the seasonal deposits of glaciers in alluvial channel. The deposition in this area during summers could be explained with absence of any significant discharges responsible to transport the suspended solids in natural morpho dynamic process of River sediment transports.

- Applicability of soft computing models with input vectors of snow cover area in addition to hydro-climatic data to predict the sediment loads

In the case of prediction of sediment loads in Gilgit basin, an ANN, ANFIS and MARS modelling approach was developed using the hydroclimatic and generated snow cover fractions using temperature index snow melt model. The results of these data-based model demonstrate the capability of these models to generate better results than tradition sediment rating curve. Combining the inputs of snow cover fraction in addition to discharge and climate parameters the performance of the models was significantly improved. It can be concluded that in snow and glacier dominated basins like Gilgit the inputs of snow cover fractions can improve the results of the data-based models in addition to hydroclimatic variables.

It was also demonstrated that the measured peak sediment yields can also be predicted accurately using ANN, ANFI-FM and MARS models. The relative accuracy of the ANFIS-FCM, ANN and MARS models were less than the other models against the peak measured sediment values. Over all, the ANFIS-FCM model was successful to predict the sediment loads in glacier and snow melt dominated basins like Gilgit basin. These findings can be useful for the hydrologists to use this model to estimate the sediment loads during extreme flood events in glacier and snow dominated basins.

- Applicability of prediction models with the normalized difference vegetation index (NDVI) as biophysical parameter in addition to hydroclimatic input datasets

The attempt has been made to investigate the applicability of ANN-LM, ANN-BR, ANN-GD, ANN-SCG, ANFIS-GP, ANFIS-SC and ANFIS-FCM databased models to predict the suspended sediment loads by introducing the normalized difference vegetation index (NDVI) as biophysical parameters with flows and climate parameters in rainfall and irrigated Brandu basin of UIB. These input parameters with various combinations were tried using data-based models to check and compare the effectiveness of biophysical/ and rainfall/temperature parameter in addition to daily discharges for prediction of the sediment load. It was found that the performance of NDVI representing biophysical and land cover feature of the catchment has less performance in its all combinations with other parameters such as discharges and climate. During testing period ANFIS-GP model performance was better with inputs of flows and precipitation. It shows that the rainfall is the second parameter dominated after transport capacity of the channel due to its increased discharges. Rainfall is more important than the NDVI for prediction of sediment load in this catchment. From the overall comparison of between all the models ANN-LM model performed best both during training and testing period. The ANN-LM improved the accuracy of model up to 28% compared to the results of sediment rating curve (SRC).

- Climate signaling in export of suspended sediment exports in glacier and snow melt basins

For better understanding of sediment exports the present research analyzed the phenomena of sediment supplies and its sources activated/deactivated due to (1) snow melts in the form of hillslope/gully and channel/stream erosions (2) erosivity of effective rainfalls over snow free landscape in the form of hillslope erosion, channel bank erosions and erosion from landslides/mass wasting (3) glacier melts. The results of two sub-basins Gilgit (glacier and snow-fed) and Astore (snow-rainfall) shown that the increase of winter precipitation and warming of mean air temperature increased the winter snow melts rates. The increased of snow melts further enhanced the river discharges and significantly increased sediment loads in both Gilgit and Astore basin due to stream/channel erosion and hill/gully erosions. In Gilgit basin the significantly increase of late spring and early summers precipitations with cooling of summer temperature significantly increased the snow cover area during summer season and resulted in reduction of sediment supplies. It can also be interpreted as that the increased snow cover during summer reduces the supply of sediments by covering the exposed landscape of proglacial area and debris cover with high albedo of snows. Which can also reduce the melt rates contributions from the debris glacier to wash the sediment loads in the channel.

In Astore basin the results shown a significant reduction of precipitation during the spring and summer season reduced the snow cover area and increased the role of effective rainfall to erode the sediments on largely snow free area in the catchment. It can also be concluded that in Gilgit basin the seasonal precipitation and seasonal mean air temperature both are important in exports of sediment. However, in Astore basin the role of seasonal precipitation is more obvious than mean air temperature for altering the sediment dynamics and hydrological regimes.

6.2 Significance of the research

The present scientific research has resulted in advancement of knowledge of proposing the framework for prediction of sediment yields using the remotely sensed datasets of snow cover maps and normalized difference vegetation Index (NDVI) in addition to the hydroclimatic data sets for sparsely distributed gauged basins. This frame work for prediction of SSC with data-based modelling approach is robust, accurate and dependent upon the freely and easily available global remote sensing datasets to the research community, which offer the opportunity to apply it for other similar sparsely distributed River basins of the world with its similar catchment hydrology, challenges of scare data availability and economical method to accurately predict and quantify the sediments at the outlet of the basin.

This scientific work presented by assessment of climate changes on flows and sediment yields in UIB provided the better practical understanding and technical contribution in assessment of changes of sediment yields due to climate. Introducing the snow cover and NDVI as biophysical factor for prediction of sediments using data-based models has given the satisfactory results. Simulation of snow melts, ice melts, snow cover and effective rainfall etc. helped to figure out the dominated flow process, which enhanced the better understanding of the sediment erosion and its transport dynamics due to these different flow process in the catchment.

Identification of spatial patterns of sediments, application of multi data values extracted from the satellite imagery and processed in Arc-GIS environment for sediment predictions using artificial intelligence models in addition to flows as an input provided a cost effective, robust and efficient approach to study and estimate the sediments yields.

This methodology is thus useful to understand the erosion processes in Alpine catchments like UIB, and also provide an economical way for estimation of sediments for better planning, management of sediments and design/operations of water infrastructures in future.

The results of this research are useful of ensuring the water demands for agriculture, drinking and hydropower generation purposes in an increasing population of Karakorum Hindukush and Himalayas mountainous area. It can also help in sustainable development of water resources and envisaging the remedial water management strategies to reduce the risks of climate vulnerability, food security and livelihood of the people.

6.3 Recommendation of Future Work

This research has some limitations and provide some suggestion to improve the data gaps and future research in these areas:

1. Application of long-term real time daily snow cover and NDVI datasets for prediction of sediment and flows
2. Improving the frequency of sediment measurements in the field and installation of climatic stations in sparsely distributed UIB especially at higher mountains with elevations more than 3000 m. am. sea level.
3. Modelling the snow and ice melts using spatially distributed physical models with more detailed and correct information of climate in the basin for better assessment of variations in sediments yields and discharges due to climate changes.
4. Extending the research work introducing the NDVI as biophysical factor to assess the sediment yields and flows in lower Indus basins as well in the catchments of Tsunami Tree project using other data-based algorithms such Support Vector Machine and Deep Learning etc.
5. Application of extended framework using the inputs of snow cover, snow melts and ice melts etc. to predict the sediments using machine learning in other sparsely distributed catchments of the world.

List of Symbols

UIB	Upper Indus basin
SSC	Suspended sediment concentrations
SRC	Sediment rating curves
ANN	Artificial neural networks
SSL	Suspended sediment loads
USLE	Universal soil loss equation
MUSLE	Modified universal soil loss equation
AI	Artificial intelligence
ANFIS	Artificial neuro fuzzy logic inference system
SVM	Support vector machine
MARS	Multiple adaptive regression splines
GP	Grid partition
SC	Subtractive clustering
FCM	Fuzzy C-Means
NDVI	Normalized difference vegetation index
LCs	Land cover of snow
GDP	Gross domestic product
Q–TSS	Discharge–total suspended solids
T–Q	Time–discharge
TFPW	Trend-free pre-whitening
WAPDA	Water and Power Development Authority
SWHP	Surface Water Hydrology Project
PMD	Pakistan Meteorological Department
SRTM	Shuttle Radar Topography Mission's
DEM	Digital elevation model
GLIMS	Global Land Ice Measurement
WK	Western Karakorum
HK	Hindukusch
CH	Central Himalayas
EK	Eastern Karakorum
CK	Central Karakorum
NWH	North Western Himalayas
SNHT	Standard normal homogeneity test
BR Statistics	Buishand's range
Min.	Minimum
Max.	Maximum
Std.	Standard Deviation
CV	Coefficient of variations

Cs	Coefficient of skewness
CK	Coefficient of kurtosis
DJF	December, January, February
MAM	March, April, May
JJA	June, July, August
SON	September, October, November
MLR	Multiple linear regression
WANN	Wavelet artificial neural network
WLSVM	Wavelet based least square support vector machine
SVR	Support vector regression
T	Mean basin temperature
Q	Discharge
SCA	Snow covered area
R	Rainfall
Evap	Evapotranspiration
MODIS	Moderate Resolution Imaging Spectroradiometer
NSIDC	National Snow and Ice Data Center
TRS	Threshold temperature for snow/ice
Cp	Constant of precipitation
MLP	Multilayer Perceptron
FFBP	Feed forward back propagation
FIS	Fuzzy inference systems
MFs	Membership functions
BF	Basis-functions
GCV	Generalized cross validation
SSY	Suspended sediment yields
R^2	Coefficient of determination
NSE	Nash–Sutcliffe efficiency
RMSE	Root mean squared error
ARIMA	Autoregressive integrated moving average
SWAT	Soil and water assessment
GA-AI	Genetic-algorithm based artificial intelligence
GEP	Gene Expression Programming
ICIMOD	International Centre for Mountain Development
BR	Bayesian Regularization
GD	Gradient Descent
SCG	Scaled Conjugate Gradient
IM	Melting of ice/Ice melts
SCF	Snow cover fractions
SM	Melting of snow/Snow melts
ER	Effective rainfall
ASTER-GDEM	ASTER global digital elevation model
P	Precipitation

SCF_{Mod}	Snow cover fractions of MODIS
SCFM	Snow cover fractions of simulated model
MBE_S	Mass balance error during ablation seasons
MBE_A	Mass balance error during whole year